Self-assembly of Biodegradable Polymers from the Macro to the Nanoscale: Processing, Structure and Biodegradation

Mario Iván Peñas Núñez

PhD Thesis

Advisors

Dr. Rebeca Hernández Velasco (ICTP-CSIC)

Prof. Alejandro Jesús Müller Sánchez

Department of Polymers and Advanced Materials: Physics, Chemistry and Technology, University of the Basque Country UPV/EHU

Donostia/San Sebastián, 2024

eman ta zabal zazu

Universidad del País Vasco

Euskal Herriko Unibertsitatea

Self-assembly of Biodegradable Polymers from the Macro to the Nanoscale: Processing, Structure and Biodegradation

Mario Iván Peñas Núñez

Advisors

Dr. Rebeca Hernández Velasco (ICTP-CSIC)

Prof. Alejandro Jesús Müller Sánchez

Dept. of Polymeric Nanomaterials and Biomaterials, Institute of Polymer Science and Technology, ICTP-CSIC

Dept. of Polymers and Advanced Materials: Physics, Chemistry and Technology, University of the Basque Country UPV/EHU

Donostia/San Sebastián, 2024

Agradecimientos

Después de una larga etapa que comenzó en Madrid y culmina ahora en San Sebastián, termino una fase vital que me ha resultado francamente provechosa en lo profesional, y en lo personal. Todo esto no habría sido posible sin la ayuda y el apoyo brindados por todas esas personas a las que quiero agradecer.

En primer lugar, me gustaría agradecer a mis directores, la Dra. Rebeca Hernández y el Prof. Alejandro J. Müller, por la oportunidad de realizar esta tesis doctoral en sus respectivos grupos de investigación, y por todo el apoyo y consejos brindados a lo largo de esta etapa formativa. También me gustaría destacar la predisposición y útiles consejos, académicos y personales, que amablemente me brindó la Prof. Carmen Mijangos durante mi periodo en Madrid y en sus estancias estivales en San Sebastián.

A la Universidad del País Vasco (UPV/EHU) y POLYMAT y a todas las personas que me ayudaron para poder comenzar en Madrid y realizar mi estancia en Bélgica, así como al Instituto de Ciencia y Tecnología de Polímeros (ICTP-CSIC) por acogerme. Por supuesto, este proyecto de tesis no habría sido posible sin el apoyo económico de las distintas instituciones, comenzando por el contrato FPI (PRE2018-086104) y los numerosos proyectos financiados por el Ministerio de Ciencia e Innovación, las ayudas del Gobierno Vasco y el proyecto BIODEST. Asimismo, agradecer al sincrotrón ALBA (BL11) por la financiación para las medidas SAXS/WAXS, así como a Marc Malfois, Juan Carlos Martínez y Cristián Huck por el apoyo técnico.

No me puedo olvidar de todas aquellas personas que me han ayudado para que este proyecto salga a la luz. Durante mi estancia en Madrid, me gustaría destacar la ayuda que de un modo u otro me han prestado, comenzando por la Prof. Evis Penott, por su ayuda y consejo al comienzo de mi tesis, Iban Amenabar (CIC NanoGUNE, San Sebastián), Aurora Nogales, Esther Rebollar y Tiberio Ezquerra (IEM-CSIC y IQFR-CSIC, Madrid), Araceli Flores, Pilar Posadas, David Gómez, y todos aquellos investigadores que me ayudaron en el

ICTP-CSIC. Tampoco puedo olvidarme de Roberto y su diligencia a la hora de gestionar el día a día, micrófono en mano. También al grupo de Biomateriales y HEMPOL, por la amabilidad con la que me permitieron utilizar sus equipos. De esta bonita etapa por Madrid me quedo con todas las relaciones establecidas con otros compañeros, como Dani, Yeral, Raúl, Víctor, Eli, Cristina, y muchos otros con los que he coincidido en congresos y otros acontecimientos.

No puedo acabar sin agradecer a todos los que han formado parte de mi grupo en Madrid (Nanostructured Polymers and Gels Group –NanoPoly&Gels–, ICTP-CSIC), empezando por el sempiterno Luis, el cual me ha acompañado en numerosas tardes de discusiones científicas; Laia, que tan bien me orientó al comienzo de mi etapa predoctoral; Álex, con el que hemos compartido tan buenos momentos "tridimensionales"; Jorge, por su ayuda en nuestra pelea personal con los geles; Edward, por la perfecta sintonía con la que trabajamos; Alexis, por los buenos momentos en Barcelona; Adrián, por los consejos y la pasión científica que transmite; Elena, Gabi, Arkaitz y Celia, por su compañía y ayuda; y en último lugar, Miryam, por ser el nexo entre Madrid y San Sebastián, la cual me ha brindado muchísima ayuda con su pasión y dedicación.

Chronologically speaking, I would like to thank Prof. Jean-Marie Raquez and his group at the University of Mons (Belgium), and specially Dr. Rosica Mincheva, for the opportunity and support to develop my work with them. Those months in Mons I learnt many novel techniques, such as atmospheric plasma, and this opportunity allowed me to know a new country, and meet new people and friends. Me gustaría dedicar una mención especial a Gaby y Kathe por su desinteresada hospitalidad y amistad esos tres meses, al igual que a Connie.

De mi periodo en San Sebastián me gustaría agradecer en primer lugar a la Dra. Agurtzane Múgica y la Dra. Manoli Zubitur por toda la ayuda recibida, así como al resto de personas que han puesto su granito de arena para ayudarme para que esta tesis saliera adelante. Itxaso Calafel, Nora Aramburu, Itziar Otaegi, Gonzalo Guerrica, Robert Aguirresarobe, Mercedes Fernández, Amaia Iturrospe,

por su paciencia, y al resto de profesores y personal de UPV/EHU y POLYMAT. También me gustaría dedicar una pequeña mención a Antxon Martínez de Ilarduya (UPC, Barcelona), y a Ana Beloqui, por enseñarme cómo funcionan las enzimas, así como a su grupo por brindarme toda la ayuda que necesité y las charlas inesperadas. Por supuesto, a todos aquellos con los que he podido establecer bonitas relaciones de amistad y colaboración.

A mi grupo de Análisis Térmico, por la ayuda y las charlas y la buena compañía: Eider, por su compañía todo este tiempo y los viajes al ALBA; Jorge, por su ayuda con DSC y la alegría mexicana que trasmite; Ainhoa y su ayuda con el procesado y las eternas charlas; Juan y su advocación al sol y el buen tiempo; Nico, Sebas, Maryam y Nico, por su compañía en las comidas; María, Valentina, Andrómeda y toda la buena *familia italiana*; el dúo Ricardo y Riccardo; Pablo y sus impresiones; Yilong and our discussions with Jorge; Fateme, Ali, Mª Virginia, Leire, y a todos los visitantes, por hacer de mi estancia un lugar mejor.

Tengo muchísimo que agradecer a mi familia, especialmente a mis padres y mis hermanos, por todo el apoyo y consejos, y por estar ahí cuando les he necesitado. Sin todo ese sacrificio, especialmente por parte de mis padres, esta tesis doctoral no habría podido salir a la luz.

Por último, a mis amigos de toda la vida, Bea, MJ, Selena, Yeray, Amaia, Asli, y todos los demás, por el apoyo constante a lo largo de estos años y los grandes momentos vividos, y a aquellos que conocí en Madrid gracias a una pequeña gran comunidad online: Korey, Javi, Manu, y al resto de la tropa, por los buenos momentos y los viajes que me han brindado estos años. Y por supuesto, agradecer a mi pareja y compañía en esta vida, por estar ahí en todo momento, desde que empecé esta etapa predoctoral, pero también por estar ahí desde mis comienzos químicos. Mil gracias.

Grupo NanoPoly&Gels en ICTP-CSIC (Madrid), octubre 2019.

Parte del LPCM de la Universidad de Mons (Bélgica), febrero 2022.

Grupo AMP en UPV/EHU y POLYMAT (San Sebastián), junio 2023.

Index

List of Abbreviations

2θ	Scattering angle
ΔH_m	Melting enthalpy
ΔH_m^0	Equilibrium melting enthalpy
$Đ$	Dispersity index (M_w/M_n ratio)
ε	Molar absorption coefficient
ε_b	Elongation at break
λ	X-ray wavelength
$\emptyset$	Weight fraction
τ	Rate of denaturation of the enzyme
v_d	Rate of degradation
C	Concentration
CO_2P	Carbon dioxide permeability
E	Young's modulus/elastic modulus
E'	Storage modulus
G'	Storage modulus (rheology)
G''	Loss modulus (rheology)
H	Hardness
M_c	Critical molecular weight for entanglements
M_n	Number average molecular weight
m_t	Weight loss of the sample
M_w	Weight average molecular weight
O_2P	Oxygen permeability
pH	Potential/power of hydrogen (refers to acidity/basicity of an aqueous solution, in logarithmic scale)
pK_a	Acid dissociation constant (K_a) in logarithmic scale
q	Scattering vector

R_g	Radius of giration
t	Time (degradation time)
T_c	Crystallization temperature
$T_{gel\text{-}sol}$	Gel-sol phase transition temperature
T_m	Melting temperature
$T_{sol\text{-}gel}$	Sol-gel phase transition temperature
$T_{sol\text{-}gel\text{-}sol}$	Sol-gel-sol phase transition temperature
U	Enzymatic activity
W	Weight
X_c	Degree of crystallinity
^{1}H-NMR	Proton Nuclear Magnetic Resonance
AF	Abaca fiber
AFM	Atomic Force Microscopy
Alg	Alginate
AlgEmbLi	Alginate-embedded lipase
ASTM	American Society for Testing and Materials
ATR	Attenuated Total Reflectance
BC	*Burkholderia cepacia*
BD	1,4-butanediol
BS	Butylene succinate
BSA	Bovine serum albumin
C25A	Cloisite® 25A
CalB	*Candida antarctica* lipase B
CAGR	Compound annual growth rate
CF	Cotton fiber
CGM	Corn gluten meal
Chi	Chitosan
CL	ε-caprolactone

CM	Canola meal
CNC	Cellulose nanocrystals
DBM	Dense-branching morphology
DCM	Dicholoromethane
DES	Diethyl succinate
DLA	Diffusion-limited aggregation
DMAz	Dimethylazelate
DMS	Dimethyl succinate
DSC	Differential Scanning Calorimetry
DTMOP	Di(trimethylolpropane)
eROP	Enzymatic ring-opening polymerization
Et_2O	Diethyl ether
Et_3B	Triethylborane
EtOAc	Ethyl acetate
EVOH	Ethylene vinyl alcohol
EU	European Union
FHT	Fluorohectorite
FTIR	Fourier-Transform Infrared spectroscopy
GIWAXS	Grazing-Incidence X-ray Scattering at Wide Angle
GPC	Gel Permeation Chromatography
HA	Hydroxyapatite
HDPE	High-density polyethylene
HMDI	Hexamethylene diisocyanate
INF	Isora nanofibers
ISO	International Standardization Organization
JF	Jute fiber
KFP	Konjac fly powders
LbL	Layer-by-layer

LCP	Liquid crystal polymer
LDPE	Low-density polyethylene
MALDI-TOF	Matrix-Assisted Laser Desorption/Ionization with Time-Of-Flight detector
MCC	Microcrystalline cellulose
MDI	Methylene diphenyl diisocyanate
MeOH	Methanol
MMT	Montmorillonite
Nano-FTIR	Fourier-Transform Infrared nanospectroscopy
NCC	Nanocrystalline cellulose
NFC	Nanofibrillated cellulose
NPs	Nanoparticles
NR	Natural rubber
OMLS	Organically modified layered silicate
OMMT	Organically modified montmorillonite
OPMF	Oil palm mesocarp fibers
PAN	Polyacrylonitrile
PBA	Poly(butylene adipate)
PBAT	Poly(butylene adipate-*co*-terephthalate)
PBF	Poly(butylene fumarate)
PBMS	Poly(butylene 2-methylsuccinate)
PBS	Poly(butylene succinate)
PBSA	Poly(butylene succinate-*co*-adipate)
PBSu	Poly(butylene succinate)
PBT	Poly(butylene terephthalate)
PcBS	Poly(*cis*-butene succinate)
PCL	Poly(ε-caprolactone)
PDLA	Poly(*D*-lactic acid)

PDMS	Polydimethylsiloxane
PE	Polyethylene
PEG	Poly(ethylene glycol)
PEI	Polyethyleneimine
PEMA	Poly(ethyl methacrylate)
PEO	Poly(ethylene oxide)
PET	Poly(ethylene terephthalate)
PGA	Poly(glycolide)
PHA	Polyhydroxyalkanoates
PHB	Polyhydroxybutyrate
PHBV	Poly(3-hydroxybutyrate-*co*-3-hydroxyvalerate)
PHS	Poly(hexamethylene succinate)
PLA	Poly(lactic acid)
PLLA	Poly(*L*-lactic acid)
PLOM	Polarized light optical microscopy
Plur	Pluronic
PMMA	Poly(methyl methacrylate)
PMP	Polymethylpentene
pNP	*p*-nitrophenol
pNPB	*p*-nitrophenyl butyrate
pNPP	*p*-nitrophenyl palmitate
PP	Polypropylene
PPC	Polysaccharide polyelectrolyte complexes
PPO	Poly(propylene oxide)
PPS	Poly(propylene succinate)
PRHB	Poly((R)-3-hydroxybutyrate)
PS	Polystyrene
PSF	Pistachio shell flour

PTFE	Polytetrafluoroethylene
PTMS	Poly(tetramethylene succinate)
PTMSP	Poly(1-trimethylsilyl-1-propyne)
PVA	Polyvinyl alcohol
PVC	Polyvinyl chloride
PVDC	Polyvinylidene chloride
PVDF	Polyvinylidene fluoride
rCell	Recycled cellulose
RGB	Red green blue
RHF	Rice husk flour
RI	Refractive index
RT	Room temperature
RWP	Rubberwood powders
SA	Succinic acid
SAP	Saponite
SAXS	Small Angle X-ray Scattering
SEC	Size Exclusion Chromatography
SEM	Scanning Electron Microscopy
SG	Switchgrass
SM	Soy meal
SNC	Starch nanocrystals
SRF	Sugarcane rind fiber
ROP	Ring-opening polymerization
s-SNOM	Scattering-type Scanning Near-field Optical Microscopy
t-BuP_1	Tert-butyliminotris(dimethylamino)phosphorane
t-BuP_2	1-tert-butyl-2,2,4,4,4-pentakis(dimethylamino)2λ5,4λ5catenadi(phosphazene)

TFAA	Trifluoroacetic acid
THF	Tetrahydrofuran
TMOP	Trimethylolpropane
TNBT	Titanium (IV) butoxide
TTIP	Titanium (IV) isopropoxide
ULDPE	Ultra-low-density polyethylene
USD	United States dollar
UV	Ultraviolet
UVA	Ultraviolet A
UV-Vis	Ultraviolet-Visible spectroscopy
WAXS	Wide Angle X-ray Scattering
WCA	Water Contact Angle
WF	Wood flour
PBS-*co*-PBF	Poly(butylene succinate-*co*-butylene fumarate)
PBS-*ran*-PBA	Poly(butylene succinate-*ran*-butylene adipate)
PBS-*ran*-PBAz	Poly(butylene succinate-*ran*-butylene azelate)
PBS-*ran*-PBEPS	Poly(butylene succinate-*ran*-2-butyl-2-ethyl-propylene succinate)
PBS-*ran*-PBF	Poly(butylene succinate-*ran*-butylene fumarate)
PBS-*ran*-PBF-*ran*-PBA	Poly(butylene succinate-*ran*-butylene fumarate-*ran*-butylene adipate)
PBS-*ran*-PBFur	Poly(butylene succinate-*ran*-butylene furanoate)
PBS-*ran*-PBMS	Poly(butylene succinate-*ran*-butylene 2-methylsuccinate)
PBS-*ran*-PBT	Poly(butylene succinate-*ran*-butylene terephthalate)
PBS-*ran*-PcBS	Poly(butylene succinate-*ran*-*cis*-butene succinate)
PBS-*ran*-PCL	Poly(butylene succinate-*ran*-ε-caprolactone)
PBS-*ran*-PDMSu	Poly(butylene succinate-*ran*-decamethylene succinate)
PBS-*ran*-PHS	Poly(butylene succinate-*ran*-hexamethylene succinate)

PBS-*ran*-PIS	Poly(butylene succinate-*ran*-isosorbide succinate)
PBS-*ran*-PNS	Poly(butylene succinate-*ran*-neopenthyl succinate)
PBS-*ran*-PPS	Poly(butylene succinate-*ran*-propylene succinate)
PBS-*ran*-PTDGS	Poly(butylene succinate-*ran*-thiodiethylene glycol succinate)
PCL-*b*-PEO-*b*-PCL	Linear poly(ε-caprolactone-*block*-ethylene oxide-*block*-ε-caprolactone)
$(PEO\text{-}b\text{-}PCL)_3$	3-arm star poly(ethylene oxide-*block*-ε-caprolactone)
$(PEO\text{-}b\text{-}PCL)_4$	4-arm star poly(ethylene oxide-*block*-ε-caprolactone)

Summary

The present thesis studies the assembly of semicrystalline biopolyesters in bulk and in solution, with a special focus on poly(butylene succinate) (PBS) and poly(ε-caprolactone) (PCL). Both approaches –with the preparation of nanostructured films and gels in the assembly in solution, and blends in the assembly in bulk– have been extensively studied, establishing the relationship between the morphology/crystalline structure and their properties. Among biopolyesters, poly(lactic acid) (PLA) is the mostly employed one; other less-used materials are poly(butylene adipate-*co*-terephthalate) (PBAT), PCL and PBS. All of them are fully biodegradable, and can also be bio-based polymers through enzymatic synthesis. PLA, PBAT, and PCL have been exhaustively explored in recent years; however, less information regarding PBS can be found. This reason encouraged the evaluation of the state of the art on biopolyesters, with a focus on PBS. In the introductory part, the mechanical and crystalline behavior, barrier properties, and biodegradation of PBS-based materials are presented.

The first part of the original results of this thesis concerns the preparation of ultrathin nanostructured films with semicrystalline structure from organic solutions of PBS, PCL, and a random copolyester PBS-*ran*-PCL, and the characterization of the resulting morphology and structure. These films were prepared through sequential dip-coating on a silicon substrate into three different organic solutions, resulting in varying compositions of PBS and PCL, which were dependent on the initial concentration and the number of dipping steps. The results showed a partial dissolution of the film, as the solvent was able to dissolve all the three components, giving rise to a final composition (spherulitic/axialitic morphology) which was always richer in the last deposited layer component.

The assembly of biopolyesters and polysaccharides is presented in the second part, where the mechanical behavior and enzymatic biodegradation of PBS films with multilayer alginate/chitosan (Alg/Chi) coatings was studied. Firstly, an indepth study of the enzymatic degradation of PBS was done. The degradation rate of PBS films coated with Alg/Chi was lower the higher the number of layers, constituting an effective barrier to the diffusion of the enzyme. This modulation of

the enzymatic degradation of biopolyesters films was further explored with the preparation of self-degradable PBS films with enzyme embedded alginate particles through melt-extrusion, paving the way for the employment of this innovative procedure despite the minor degradation observed. Blends obtained from PLA, PBAT, and PBS were also prepared in the same way, producing novel materials that allowed the evaluation of the degradation mechanisms of these three biopolyesters. The results obtained evidence the importance of selecting the most appropriate enzyme for each polymer, exposing the need to explore enzymes capable of degrading all blend components.

The final part of this research deals with the preparation of hydrogels from linear triblock and 3- and 4-arm star block copolymers consisting of poly(ethylene oxide) (PEO) and semicrystalline blocks of PCL, synthesized by a combined ring-opening polymerization and organic catalyst switch strategy. Hydrogels from the linear copolymers underwent a temperature-dependent sol-gel-sol transition, behaving as a solution at room temperature (RT) and transforming into a non-flowing gel upon heating. On the other hand, hydrogels from the 4-arm star copolymers showed a single gel-sol transition with no flow at RT, making them suitable for 3D printing. Additionally, the crystalline organization of the PEO and PCL blocks within the hydrogels was evaluated through DSC and SAXS/WAXS, and compared with bulk materials. Results evidenced a clear structural organization in the hydrogels related to the crystallization of the PCL blocks, and unexpectedly, the presence of PEO block crystals was also perceived. Hence, remarkable double crystalline hydrogels were obtained for the first time.

The materials generated in this thesis and prepared through the assembly of different biopolyesters evidenced improved properties in terms of mechanical behavior and enzymatic biodegradation, which were closely related to their crystalline structure and morphology. The results obtained in this work have demonstrated the possibilities of employing them in sustainable applications (e.g., as biodegradable films for agricultural applications) or for biomedical purposes, with the preparation of biomaterials inks.

Resumen

La presente tesis estudia el ensamblaje de biopoliésteres semicristalinos en masa y en solución, destacando el polibutilén succinato (PBS) y la poli(ε-caprolactona) (PCL). Ambos enfoques –preparación de películas y geles nanoestructurados por ensamblaje en solución, y mezclas por ensamblaje en masa– han sido ampliamente estudiados, estableciendo la relación entre la morfología/estructura cristalina y sus propiedades. De entre todos los biopoliésteres, el ácido poliláctico (PLA) es el más utilizado; otros materiales son el polibutilén adipato-*co*-tereftalato (PBAT), PCL y PBS. Todos ellos son biodegradables y también pueden ser polímeros de base biológica mediante síntesis enzimática. El PLA, PBAT y PCL han sido explorados exhaustivamente en los últimos años; sin embargo, hay poca información sobre el PBS. Ello motivó la evaluación del estado del arte sobre biopoliésteres, con énfasis en PBS. En la parte introductoria se presenta el comportamiento mecánico y cristalino, las propiedades barrera, así como la biodegradación de materiales basados en PBS.

La primera parte de los resultados originales de esta tesis se ocupa de la preparación de películas nanoestructuradas ultrafinas a partir de soluciones orgánicas de PBS, PCL, y un copoliéster aleatorio PBS-*ran*-PCL y la caracterización de la morfología y estructura. Las películas se obtuvieron por recubrimiento por inmersión de un sustrato de silicio en disoluciones de los tres polímeros, resultando en composiciones variables de PBS y PCL, dependientes de la concentración inicial y del número de pasos. Se observó una disolución parcial de las capas, ya que el disolvente podía disolver los tres componentes, dando lugar a una composición final (morfología esferulítica/axialítica) enriquecida en el componente de la última capa depositada.

El ensamblaje de biopoliésteres y polisacáridos se presenta en la segunda parte, donde se estudió el comportamiento mecánico y la degradación enzimática de películas de PBS con recubrimientos multicapa de alginato/quitosano (Alg/Chi). Primeramente, se hizo un estudio en profundidad de la degradación enzimática de PBS. La degradación de películas de PBS recubiertas era menor cuanto mayor era el número de capas, constituyendo una barrera eficaz a la

difusión de la enzima. Esta modulación de la degradación enzimática en biopoliésteres se exploró más a fondo en películas de PBS autodegradables preparadas por co-extrusión con partículas de alginato y enzima, allanando el camino para el empleo de este procedimiento a pesar de la baja degradación apreciada. También se prepararon mezclas a partir de PLA, PBAT, y PBS, generando nuevos materiales que permitieron ahondar en el estudio de sus mecanismos de degradación. Estos resultados evidencian la importancia de seleccionar la enzima más adecuada para cada polímero, exponiendo la necesidad de explorar enzimas capaces de degradar todos los componentes de una mezcla.

La parte final de esta investigación trata sobre la preparación de hidrogeles a partir de copolímeros lineales tribloque y en estrella de 3 y 4 brazos compuestos por polióxido de etileno (PEO) y PCL, sintetizados mediante polimerización por apertura de anillo y una estrategia de intercambio de catalizador orgánico. Los hidrogeles de los copolímeros lineales mostraron una transición sol-gel-sol dependiente de la temperatura, comportándose como una solución a temperatura ambiente y transformándose en gel al calentarse. Por otro lado, los hidrogeles de los copolímeros estrella de 4 brazos mostraron una única transición gel-sol sin fluir a temperatura ambiente, haciéndolos adecuados para impresión 3D. Además, la organización cristalina de los bloques de PEO y PCL en los hidrogeles se estudió por DSC y SAXS/WAXS, evidenciando una organización estructural en los hidrogeles relacionada con la cristalización de los bloques de PCL e, inesperadamente, se observó la presencia de cristales de PEO. De este modo se obtuvieron por primera vez hidrogeles doblemente cristalinos.

Los materiales generados en esta tesis y preparados mediante el ensamblaje de diferentes biopoliésteres mostraron mejores propiedades en términos de comportamiento mecánico y biodegradación enzimática, estrechamente relacionadas con su estructura cristalina y morfología. Los resultados obtenidos en este trabajo han demostrado las posibilidades de emplearlos en aplicaciones sostenibles, como películas biodegradables para aplicaciones agrícolas, o con fines biomédicos, con la preparación de tintas de biomateriales.

Chapter 1

General Introduction and Objectives

1.1. Introduction

Currently, many research efforts within the field of polymers are aimed at designing and developing polymeric materials under environmental sustainability criteria with the aim of reducing dependence on petroleum raw materials and eliminating plastic waste. In fact, in 2018 the EU Commission published the document "A European Strategy for Plastics in a Circular Economy" in which it proposes as a challenge for the year 2030 *Transform the way in which plastic products are designed, produced, used and recycled in the EU* and more recently in the "The Plastics Transition" strategy issued by Plastics Europe aimed to establish a roadmap for plastics in Europe to be circular and have net-zero emissions by 2050.[1,2] One of the strategies to address this challenge is the design of new materials from biodegradable polymers, including petroleum derivatives such as polyesters –poly(lactic acid) (PLA), poly(ε-caprolactone) (PCL), poly(butylene succinate) (PBS) and their copolyesters and blends, among others– as well as the use of polymers obtained from renewable sources, among which those extracted from biomass, polysaccharides or proteins (agropolymers) stand out.[3,4] Taking into consideration the high importance of focusing polymers towards zero-waste materials, the biodegradation of biopolymers and its comprehension becomes an area of intensive research nowadays.[5,6]

The development of new polymeric materials obtained through combination of biopolyesters, such as PCL or PLA with polysaccharides such as potato starch, has been carried out mainly by formulating mixtures through reactive extrusion processes in the melt.[7] As an example, the MATER-BI company (https://www.novamont.com/eng/mater-bi) commercially manufactures compostable bags based on mixtures of PCL (or PLA) and potato starch, among other biodegradable products. When this type of polyesters with a hydrophobic character are combined with hydrophilic polymers or components, obtaining homogeneous materials constitutes a research challenge that requires the development of strategies to avoid thermal degradation of the natural polymer in

the melt, improve the interfacial adhesion properties or covalent cross-linking to obtain final materials with good mechanical properties.

In these regards, the present PhD project aims to develop novel strategies for the assembly of biopolymers in solution (layer-by-layer assembly and gelation) through combination of biopolyesters and polymers from the biomass (polysaccharides) with the aim of improving and/or modulating the bulk properties of the final materials such as mechanical properties or biodegradability among others.

The first part of this PhD project studies the structure and properties relationship of biopolyesters thin films prepared through a dip-coating deposition and their combination with biobased polysaccharidic coatings manufactured through layer-by-layer methodology. To that aim, as a first step, a fundamental study was carried out aimed to understand the nanostructural organization of thin films produced through dip-coating starting from organic solutions of PCL, PBS and random copolymers PBS-*ran*-PCL synthesized in the group of Prof. Alejandro J. Müller.[8–13] The combination of advanced characterization techniques such as Grazing-Incidence X-ray Scattering at Wide Angle (GIWAXS) and Scattering-type Scanning Near-field Optical Microscopy (s-SNOM) and Fourier Transform Infrared nanospectroscopy (nano-FTIR) allows for the characterization of the structure and chemical organization of the thin films at the nanoscale.

Then, a procedure for coating of PBS films with layers of alginate and chitosan assembled through spray-coating assembly has been implemented. Biobased coatings have been employed before as barriers for modulation of drug release[14,15] and for tuning of barrier properties in packaging materials. In the present thesis, biobased coatings have been employed as a means to modulate enzymatic degradation and the process has been monitored through weight loss degradation measurements and modelled according to a modified Michaelis-Menten model. After the analysis of enzymatic degradation of PBS in bulk and coated films, such study was extended to the study of enzymatic degradation of

poly(lactic acid) (PLA), poly(butylene adipate-*co*-terephthalate) (PBAT) and their blends with PBS. The materials were provided by the group of Prof. Supakij Suttiruengwong in Silpakorn University (Thailand). Because of their mechanical properties and ability to be processed, they are material candidates for the replacement of conventional plastics, for instance in the packaging area.[16] The aim in here is to implement a preparation method for achieving self-degradation of the biopolymers and their blends through embedding of enzymes within biopolymers formulations able to be processed through extrusion. Few examples of this approach exist in literature, and such approach has been pioneered by Carbios as a means to obtain home-compostable PLA through trapping ‘‘active” enzymes within bioplastics such as PLA.[17]

Finally, since the pioneering works of Bae *et al.*,[18,19] many works have been published regarding self-assembly in solution and as gels of biodegradable amphiphilic block copolymers, and specifically, those constituted of blocks of poly(ethylenoxide) (PEO) and PCL (as diblocks, triblocks and random copolymers),[20] however, the influence of the crystallization over the gelation is an aspect that has been poorly understood in literature. In this PhD thesis, the objectives have been enlarged to undertake the study of fundamental aspects of gelation and its relation to the crystalline structure of the blocks in model linear and star block copolymers of PEO and PCL. In addition, a proof-of-concept of their applicability as sacrificial (biodegradable) biomaterial inks for applications in 3D (bio)printing. The linear and star block copolymers under study in this thesis have been synthesized by the group of Prof. Nikos Hadjichristidis in King Abdullah University of Science and Technology (Saudi Arabia), using a ring opening polymerization strategy which is explained in the experimental part.

Therefore, in Chapter 1, a general introduction and objectives of this doctoral research are presented. Chapter 2 provides a general overview on current investigation about biodegradable biopolyesters, including general properties of PBS and PCL, self-assembly of block copolymers with crystallizable blocks, PCL and PEO and biodegradation of biopolyesters focused on enzymatic degradation.

Chapter 3 aims to study the nanostructural organization of thin films formed through assembly of PBS, PCL and their random copolymers through advanced characterization techniques such as Grazing-Incidence X-ray Scattering at Wide Angle (GIWAXS) and Scattering-type Scanning Near-field Optical Microscopy (s-SNOM) and Fourier Transform Infrared nanospectroscopy (nano-FTIR). Chapters 4 and 5 are focused on biodegradation studies of PBS films and their blends and propose novel strategies to modulate enzymatic degradation through polysaccharidic coatings and self-degradation. Chapter 6 shows the results corresponding to the study of self-assembly of block copolymers with crystallizable blocks, PCL and PEO into polymer hydrogels. To finish, Chapter 7 reports the final remarks of this doctoral research along with the list of the publications and conference contributions derived from this thesis.

The current thesis has been carried out in the framework of the research project MAT2017-83014-C2 (1 and 2) coordinated between the Advanced Multiphasic Polymers Group from the University of the Basque Country (UPV/EHU) and POLYMAT (IP: Alejandro J. Müller), in Donostia/San Sebastián and the Nanostructured Polymers and Gels group (IP: Rebeca Hernández) in Madrid, which is part of the Institute of Polymer Science and Technology from the Spanish National Research Council (ICTP-CSIC). During the first period of this thesis (approximately 2 years), the experimental work was carried out at the ICTP-CSIC, whereas for the second period, the experimental work was carried out at UPV/EHU and POLYMAT. Further fruitful collaborations were established with Prof. Jean-Marie Raquez and his group at the University of Mons (Belgium), through a 3-months internship. The work developed during this internship let us delve in the enzymatic biodegradation of PBS, explored in Chapters 4 and 5.

1.2. Objectives

1.2.1. General objective

The main objective of the present work is the design of novel strategies for the assembly of semicrystalline biopolyesters, mainly PBS and PCL, and their copolymers with crystallizable blocks in the bulk and in solution. Assembly in solution will result in the formation of nanostructured films and gels whereas assembly in the bulk will give rise to blends. For the three systems under study, the relation between the resulting morphology and crystalline structure and the influence on properties such as mechanical properties and enzymatic biodegradation will be established.

Hence, three main systems are studied:

i) Nanostructured films formed through multilayer assembly of semicrystalline biopolyesters;

ii) semicrystalline biopolyesters and their blends and biobased coatings;

iii) polymer hydrogels formed through self-assembly of copolymers with crystallizable blocks.

1.2.2. Specific objectives

i) Nanostructured films formed through multilayer assembly of semicrystalline biopolyesters (PBS, PCL and PBS-*ran*-PCL)

- Optimization of the processing parameters to obtain nanostructured thin films through dip-coating procedure
- Determination of the composition of the thin films
- Analysis of the morphology and crystallinity of the resulting thin films

- Nanoscale chemical characterization by s-SNOM and nano-FTIR techniques

ii) semicrystalline biopolyesters and their blends and biobased coatings: PBS, PLA, PBAT and their blends and coatings with alginate and chitosan

- Preparation of biobased coated PBS films through spray-assisted LbL procedure
- Analysis of the morphology and nanomechanical properties of biobased coatings
- Establishment of experimental protocols for the determination of enzymatic degradation in solution
- Optimization of the processing parameters for the preparation of enzyme-embedded extruded films
- Analysis of the mechanism for enzymatic degradation of biopolyesters, coated films and their blends through combination of different experimental techniques

iii) polymer hydrogels formed through self-assembly of copolymers with crystallizable blocks: triblock copolymers of PEO and PCL (linear and star copolymers)

- Establisment of phase diagrams (concentration-temperature) through inverted vial tests combined with rheological measurements
- Analysis of the crystalline organization of the PCL and the PEO blocks in the bulk and in the gels by synchrotron SAXS and WAXS combined with DSC results
- Evaluation of the performance of the hydrogels and sacrificial (bio)material inks in direct ink printing

1.3. References

1. Plastics Europe, The Plastics Transition. *Changing Plastics for Good* **2023**, *1*, 1–21. DOI: 10.1191/0960327102ht283ed.

2. European Commission, A European Strategy for Plastics in a Circular Economy. *Communication from the Commission to the European Parliament, the Council, the European Economic and Social Committee and the Committee of the Regions* **2018**, *028*, 1–23.

3. Zhu, Y.; Romain, C.; Williams, C. K., Sustainable polymers from renewable resources. *Nature* **2016**, *540* (7633), 354–362. DOI: 10.1038/nature21001.

4. Rosenboom, J. G.; Langer, R.; Traverso, G., Bioplastics for a circular economy. *Nature Reviews Materials* **2022**, *7*, 117–137. DOI: 10.1038/s41578-021-00407-8.

5. Samir, A.; Ashour, F. H.; Hakim, A. A. A.; Bassyouni, M., Recent advances in biodegradable polymers for sustainable applications. *npj Materials Degradation* **2022**, *6* (68), 1–28. DOI: 10.1038/s41529-022-00277-7.

6. Polman, E. M. N.; Gruter, G. J. M.; Parsons, J. R.; Tietema, A., Comparison of the aerobic biodegradation of biopolymers and the corresponding bioplastics: A review. *Science of the Total Environment* **2021**, *753*, 141953. DOI: 10.1016/j.scitotenv.2020.141953.

7. Imre, B.; Pukánszky, B., Compatibilization in bio-based and biodegradable polymer blends. In: *European Polymer Journal*. **2013**, 1215–1233. DOI: 10.1016/j.eurpolymj.2013.01.019.

8. Ciulik, C.; Safari, M.; Martínez de Ilarduya, A.; Morales-Huerta, J. C.; Iturrospe, A.; Arbe, A.; Müller, A. J.; Muñoz-Guerra, S., Poly(butylene succinate-ran-ε-caprolactone) copolyesters: Enzymatic synthesis and crystalline isodimorphic character. *European Polymer Journal* **2017**, *95*, 795–808. DOI: 10.1016/j.eurpolymj.2017.05.002.

9. Safari, M.; Martínez De Ilarduya, A.; Mugica, A.; Zubitur, M.; Muñoz-Guerra, S.; Müller, A. J., Tuning the Thermal Properties and Morphology of Isodimorphic Poly[(butylene succinate)-ran-(ε-caprolactone)] Copolyesters by Changing Composition, Molecular Weight, and Thermal History. *Macromolecules* **2018**, *51* (23), 9589–9601. DOI: 10.1021/acs.macromol.8b01742.

10. Safari, M.; Leon Boigues, L.; Shi, G.; Maiz, J.; Liu, G.; Wang, D.; Mijangos, C.; Müller, A. J., Effect of Nanoconfinement on the Isodimorphic Crystallization of Poly(butylene succinate- ran-caprolactone) Random Copolymers. *Macromolecules* **2020**, *53* (15), 6486–6497. DOI: 10.1021/acs.macromol.0c01081.

11. Safari, M.; Pérez-Camargo, R. A.; Ballester-Bayarri, L.; Liu, G.; Mugica, A.; Zubitur, M.; Wang, D.; Müller, A. J., Biodegradable binary blends of poly (butylene succinate) or poly (ε-caprolactone) with poly (butylene succinate-ran-ε-caprolactone) copolymers: Crystallization behavior. *Polymer* **2022**, *256*, 125206. DOI: 10.1016/j.polymer.2022.125206.

12. Safari, M.; Otaegi, I.; Aramburu, N.; Guerrica-Echevarria, G.; De Ilarduya, A. M.; Sardon, H.; Müller, A. J., Synthesis, structure, crystallization and mechanical properties of isodimorphic PBS-ran-PCL copolyesters. *Polymers* **2021**, *13* (14), 2263. DOI: 10.3390/polym13142263.

13. Safari, M.; Mugica, A.; Zubitur, M.; de Ilarduya, A. M.; Muñoz-Guerra, S.; Müller, A. J., Controlling the isothermal crystallization of isodimorphic PBS-ran-PCL random copolymers by varying composition and supercooling. *Polymers* **2020**, *12* (1), 17. DOI: 10.3390/polym12010017.

14. Criado-Gonzalez, M.; Mijangos, C.; Hernández, R., Polyelectrolyte multilayer films based on natural polymers: From fundamentals to Bio-Applications. *Polymers* **2021**, *13* (14), 2254. DOI: 10.3390/polym13142254.

15. Criado-Gonzalez, M.; Fernandez-Gutierrez, M.; San Roman, J.; Mijangos, C.; Hernández, R., Local and controlled release of tamoxifen from multi (layer-by-layer) alginate/chitosan complex systems. *Carbohydrate Polymers* **2019**, *206*, 428–434. DOI: 10.1016/j.carbpol.2018.11.007.

16. Chuakhao, S.; Torres Rodríguez, J.; Lapnonkawow, S.; Kannan, G.; Müller, A. J.; Suttiruengwong, S., Formulating PBS/PLA/PBAT blends for biodegradable, compostable packaging: The crucial roles of PBS content and reactive extrusion. *Journal of Polymers and the Environment* **2023**, *XXXX* (XXX), XXX–XXX. **Manuscript submitted for publication**.

17. Dubois, P., Reactive Extrusion (REx): Using Chemistry and Engineering to Solve the Problem of Ocean Plastics. *Engineering* **2022**, *14*, 15–18. DOI: 10.1016/j.eng.2021.12.009.

18. Bae, S. J.; Suh, J. M.; Sohn, Y. S.; Bae, Y. H.; Kim, S. W.; Jeong, B., Thermogelling poly(caprolactone-b-ethylene glycol-b-caprolactone) aqueous solutions. *Macromolecules* **2005**, *38* (12), 5260–5265. DOI: https://doi.org/10.1021/ma050489m.

19. Bae, S. J.; Joo, M. K.; Jeong, Y.; Kim, S. W.; Lee, W. K.; Sohn, Y. S.; Jeong, B., Gelation behavior of poly(ethylene glycol) and polycaprolactone triblock and multiblock copolymer aqueous solutions. *Macromolecules* **2006**, *39* (14), 4873–4879. DOI: 10.1021/ma060153s.

20. Shi, J.; Yu, L.; Ding, J., PEG-based thermosensitive and biodegradable hydrogels. *Acta Biomaterialia* **2021**, *128*, 42–59. DOI: 10.1016/j.actbio.2021.04.009.

Chapter 2

State of the Art on Biopolyesters

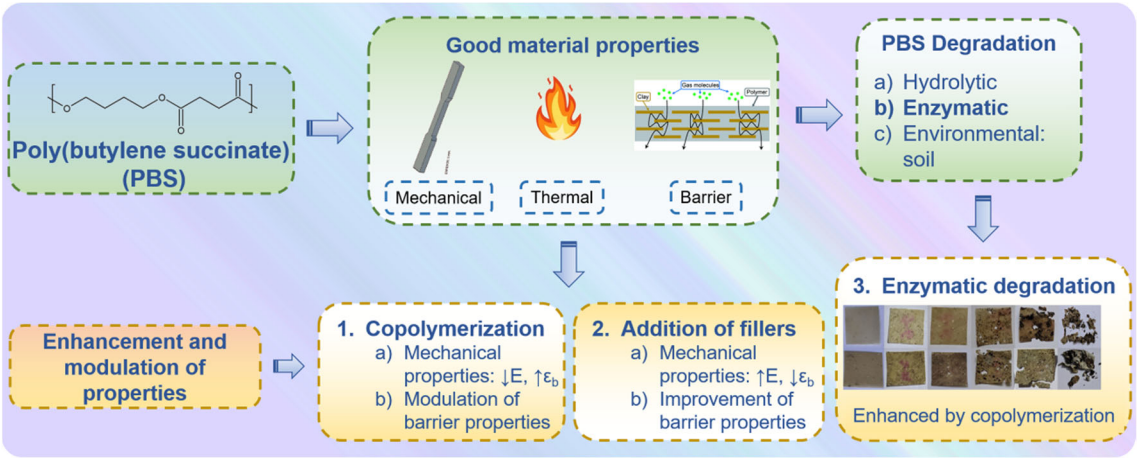

2.1. Brief Introduction to Crystalline Biopolyesters

Plastic consumption has undergone an incredible increase over the last decades, reaching a record of 400 million tons produced in 2022 worldwide, with a rise of 9.5 % with respect to 2018,[1] with a deceleration period in 2019-2020 due to the COVID-19 pandemic.[2] Since the 1950s, worldwide plastic production has increased by a factor of more than 200, with a compound annual growth rate (CAGR) of 8.4 %.[3–5] As plastic production increases, plastic waste follows a similar increment. This fact is a significant problem, as most plastic materials are single-use products, which implies that they end up in the environment, such as landfills, or directly in the oceans, remaining there for many years. Over the last decades, research on biodegradable polymers has exponentially increased, motivated by the need to diminish human impact on the environment and reduce global plastic pollution, which is also related to the emission of greenhouse gases.[6] Plastic wastes produced within the last seven decades have reached the astonishing amount of 6300 million tons,[3,7] setting up plastic pollution in the spotlight as a highly concerning problem to be solved with haste. Among the multiple applications, packaging leads plastic wastes production, with almost 150 million tons in 2015, of which less than 4 % were recycled.[4] Additionally, the more concerning fact is that about 1-5 % of all plastics end up in marine environments, as around 80 % of oceanic wastes come from landfills.[8] The direct consequence of this is the production of microplastics, which cause important damage in the terrestrial and marine wildlife,[6] while also affecting human beings, not only producing health issues, but also damaging tourism, fishing, and shipping industries.[9] Although the COVID-19 pandemic has slightly diminished the total production of plastics, the problem of wastes has increased for all the single-use plastic products required in this pandemic situation, such as masks, face shields, gloves, and other personal protective equipments.[4] Within this context, research on biodegradable polymers, defined as those “whose chemical and physical characteristics undergo deterioration and completely degrade when exposed to microorganisms, aerobic and anaerobic processes”, has attracted increasing

attention.[10] Although the bio-based plastic capacities have shown an increasing trend in the past years, circular plastics (i.e., recycled and bio-based plastics) production is still ~10 % of the world plastic production.[2] Among them, global bioplastics production was 2.22 million tonnes in 2022 (0.5 % of the total plastic production), with almost a half of it devoted to packaging. Plastic industries are making the effort to reduce the use of fossil-based materials, as evidenced by the forecasted production data for bioplastics, with an exponential increase up to 7.43 million tonnes in 2028 and a CAGR of 14 % for the 2022-2027 period (3-4 % for the overall growth of polymers).[11,12]

In this thesis, apart from PBS, other aliphatic polyesters: poly(ε-caprolactone) (PCL) and poly(lactic acid) –or polylactide– (PLA); as well as poly(butylene adipate-*co*-terephthalate) (PBAT), a common aliphatic/aromatic copolyester are also investigated. These biopolyesters (i.e., PCL, PLA and PBAT) are fully biodegradable polyesters, which can be obtained either from fossil-based derivatives, or from renewable resources, as in the case of poly(butylene succinate) (PBS).[13] PCL is an aliphatic biopolyester, which can be obtained from cyclic ε-caprolactone via ring-opening polymerization (ROP), generally with petroleum-based raw materials, although it is possible to produce bio-based PCL from 5-hydroxymethyl furfural.[14] Commonly employed for packaging and drug delivery, PCL can be blended or copolymerised with other polymers to enhance its properties, increasing its usage. PLA is typically produced through polycondensation of lactic acid, which can be obtained via a bio-based procedure from the fermentation of sugars or through ROP of lactide (the cyclic dimer of lactic acid). The excellent optical properties and its low price compared with other biopolymers make PLA the most price-competitive synthetic bioplastic.[4] The biocompatility of PLA-based materials make them suitable for biomedical applications. Finally, PBAT is obtained from fossil-based raw materials (as PCL), through direct esterification or ester exchange polymerization of its three monomers: adipic acid, terephthalic acid, and 1,4-butanediol. Its good mechanical and barrier properties (comparable to low density polyethylene, LDPE), together with the easy thermal-processing make PBAT a commonly employed biopolymer

in agriculture for the production of mulching films, which can degrade in soil in ~9 months.[4,15] The main characteristics and properties of these biopolyesters, as well as PBS, are included in Table 2.1.

Table 2.1. Thermal and mechanical properties, and main characteristics of the studied biopolyesters.

Parameters	PBS	PCL	PLA	PBAT	Ref.
T_g (ºC)	-32	-60	61	-29	[16,17]
T_m (ºC)	115	57	169	110-115	[16,17]
X_c (%)	31	38	1	9	[17–19]
E (MPa)	580	220	2230	56	[17–19]
ε_b (%)	8	110	3	680	[17–19]
Price (USD/kg)	4.5	n.a.	2-3	4.1	[4]
Global production (kton/year)	20	n.a.	676	100	[12]
Main applications	Packaging, biomedicine, agriculture	Packaging, biomedicine, agriculture, commodities	Packaging, biomedicine, agriculture, automotive	Packaging, biomedicine, agriculture	[20,21]

Despite the fact that PCL, PLA and PBAT have also been studied within this thesis, PBS constitutes the main focus in this research. Considering the limited amount of information available in the literature about this biopolyester in comparison to other biopolyesters, the current chapter will present a comprehensive review of recent investigations on PBS. Poly(butylene succinate) (PBS or PBSu), also known as poly(tetramethylene succinate) (PTMS), is an aliphatic polyester that can be included in fossil-based biodegradable polymers. However, many advances have been made in preparing 100 % bio-based PBS (Bio-PBS) produced from bio-based 1,4-butanediol.[22] Among the group of bioplastics, polyhydroxyalkanoates (PHA), which can be produced in aqueous environments by the actions of different microorganisms,[6] present many advantages that make these materials suitable for many applications, such as packaging, biomedical devices, electronics, and agricultural purposes, among

others.[23] Notwithstanding the higher production of PBS compared to PHA (4.3 vs. 1.2 % of total bioplastics production in 2019),[24] as well as the higher cost of PHA against PBS (USD 4000–15,000/t of PHA vs. USD 2000–5000/t of PBS),[23,25,26] make PBS a more suitable candidate to be used for commercial purposes in the field of biodegradable plastics. Furthermore, a drop in price for Bio-PBS by almost half is expected, a move from USD 4400/t to prices of USD 2700/t.[27]

PBS presents interesting physicochemical properties; it is biodegradable and nontoxic, making this polymer a good candidate for various biomedical applications, packaging, agriculture, and others. In an extensive review by Gigli *et al.*, the main biomedical applications of PBS are summarized, including its employment as scaffolds for tissue engineering or matrixes for drug delivery.[21] In agriculture, PBS has been investigated to develop biodegradable polymeric mulch films to reduce plastic accumulation in soil.[28] PBS has also been studied for the fabrication of soft packaging because, in comparison to poly(lactic acid) (PLA), PBS is more flexible with a higher value of elongation at break, and presents similar good barrier properties to oxygen and water vapor.[29] Despite extensive research on PBS and its potential applications, the widespread employment of this polymer is still limited due to its relatively high cost. Hence, many strategies are being developed to, on the one hand, lower the cost of PBS and, on the other hand, modify the mechanical, physicochemical, and thermal properties of PBS to adjust degradation times and meet specific requirements for selected applications. Such approaches include the formation of blends, the synthesis of copolymers, and the addition of filler materials to prepare composite materials.[30] Over the last few years, many reviews have provided a thorough analysis of the thermal, mechanical, and biodegradation properties of PBS in comparison to other biodegradable polyesters,[31] in PBS composites and nanocomposites with incorporated natural fillers,[5] and in blends with other polymers, most notably with PLA.[32] It is important to remark that, even if the blending of PBS with synthetic and natural polymers constitutes one of the most straightforward routes to modulate PBS properties, PBS-based blends are often immiscible, leading to phase separation and hence poor mechanical properties. One alternative is using compatibilizers or

crosslinkers in the blend, aiming to improve phase mixing in the blends. However, such a strategy might compromise the degradability of the material.[33] In this regard, a recent study has shown the employment of a PBS-based copolymer as an effective compatibilizer in a compostable ternary blend made of PBS, random PBS-based copolymers, and plasticized wheat flour.[34]

For PBS, random copolymerization constitutes a common strategy for combining the desired properties of two different homopolymers. In PBS copolyesters, the comonomer composition strongly influences the crystallization behavior, which in turn affects their biodegradation, thermal, and mechanical properties.[14] It follows that a thorough investigation of the crystallinity behavior of PBS copolymers as a function of the comonomer composition is necessary to design PBS-based materials with the physical and biodegradation properties required for specific applications. In the current Chapter, we summarize and quantitatively compare the results corresponding to PBS copolyesters synthesized in our group and other research groups to determine, on the one hand, the influence of different synthetic routes on the resulting molecular weight of PBS copolyesters and, on the other hand, the impact of the comonomer content on the crystallization behavior and resulting mechanical properties of the selected PBS copolyesters, including a series of biodegradable PBS-*ran*-PCL synthesized and characterized in our group.[35] Such analysis is extended to PBS composite films, for which the effect of the incorporation of the selected fillers on the mechanical and barrier properties is analyzed. In a recent study from our group, authors presented the peculiar rheological properties for these PBS-*ran*-PCL copolymers, and their applications such as hot melt adhesives.[36] Moreover, a thorough analysis of experimental protocols aimed to determine the biodegradation of PBS and its copolyesters is provided, with emphasis on PBS enzymatic degradation. Finally, future perspectives for the design of PBS-based materials with tailored properties are discussed.

2.2. Poly(butylene succinate) (PBS)

2.2.1. Synthesis of PBS

Poly(butylene succinate) is obtained from two monomers: succinic acid (SA) and 1,4-butanediol (BD). SA can be obtained through the hydrogenation of fossil-derived maleic acid (anhydride) or 1,4-butanediol. BD is produced through the hydrogenation of 1,4-butynediol, previously obtained from acetylene and formaldehyde. This monomer (i.e., BD) can also be obtained through the hydrogenation of methyl maleate ester derived from maleic anhydride. In order to move to greener production methods, SA can be prepared through fermentation, whereas it is possible to obtain the BD monomer from a genetically modified organism.[37,38] The polymerization routes for the production of PBS can be divided into two categories: petroleum-based synthesis and bio-based polymerization. The petroleum-based synthesis relies on polycondensation reactions, generating higher molecular weight than the bio-based polymerization. However, the latter is based on enzymes as catalysts of the reaction, representing a greener alternative. The description of the experimental methodology for each of the polymerization routes is provided below.

a. Petroleum-based synthesis: transesterification polymerization: melt, chain extender, and solution

The petroleum-based synthesis is based on transesterification polymerization (shown in Scheme 2.1), carried out in the melt or in solution. Through these methods, PBS of intermediate and high molecular weight can be obtained.

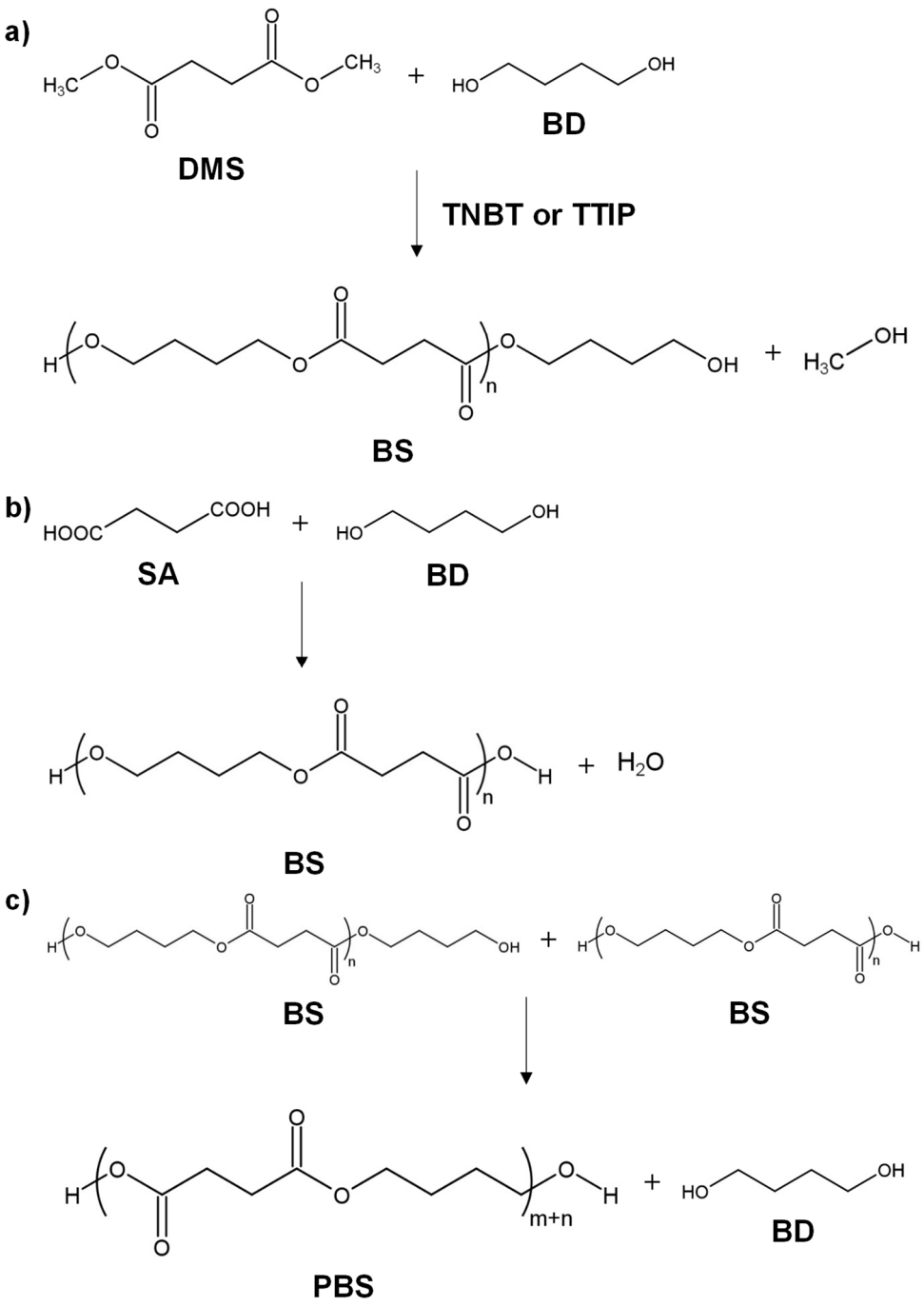

Scheme 2.1. Transesterification polymerization of PBS: **a)** transesterification step, **b)** direct polymerization step, and **c)** polycondensation step.

Intermediate molecular weight, e.g., the number average molecular weight, M_n ~60,000 g/mol and the weight average molecular weight, M_w ~100,000 g/mol,[39,40] obtained through a transesterification polymerization carried out in the melt. This polymerization employs dimethyl succinate (DMS) and BD as monomers, in stoichiometric relation or with an excess of BD below 10 mol%. Titanium (IV) butoxide (TNBT) or titanium (IV) isopropoxide (TTIP) are

commonly used as catalysts of the reaction (Figure 2.1).[41] Before the reaction process, the reactor is filled with nitrogen at room temperature to remove air and avoid oxidation during the transesterification step. After that, the reaction system is heated at a temperature ranging from 150 to 190 ºC, with constant stirring and under a nitrogen atmosphere to start the transesterification reaction (Scheme 2.1a). Then, a distillation step is needed to discard most of the methanol and water produced during the reaction. In a second stage, polycondensation (Scheme 2.1c) is carried out under vacuum at a higher temperature to remove the BD formed in the reaction and polymerize the oligomers to the polymer.[42] A second option for petroleum-based syntheses is the direct polymerization (Scheme 2.1b) of both monomeric units (SA and BD), starrom dicarboxylic acids and alkyl diols. High molecular weight can be obtained by using a chain-extension step. Direct polymerization can be carried out in the melt or in solution. In the melt, the polymerization consists of two steps: first, the esterification reaction occurs at temperatures from 150 to 200 ºC, under atmospheric pressure, or in a low vacuum. In the second step, the polycondensation is carried out under a high vacuum at a higher temperature (220–240 ºC) for deglycolization. It is important to note that both steps should be done under a nitrogen atmosphere to avoid oxidation.[43]

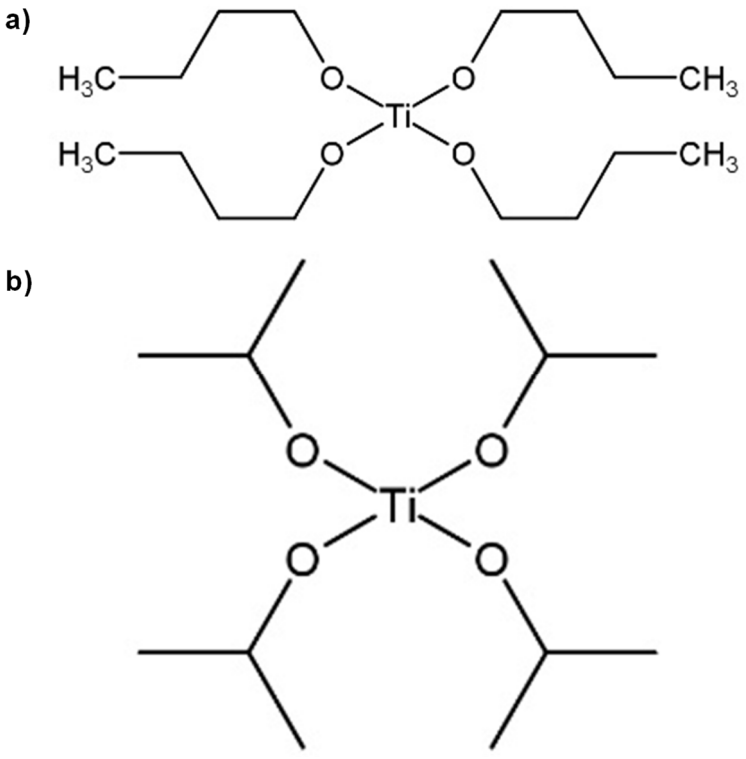

Figure 2.1. Chemical structures of two different catalysts employed in the transesterification step: **a)** titanium (IV) butoxide (TNBT), and **b)** titanium (IV) isopropoxide (TTIP).

For high-M_w PBS production, an extra chain-extension step (Scheme 2.2) is added to the melt condensation polymerization, achieving M_n ~80,000 g/mol and M_w ~250,000 g/mol. Some authors have reported even higher values: M_n ~180,000 g/mol and M_w ~450,000 g/mol,[44] ~500,000 g/mol,[45] or up to M_w ~1,000,000 g/mol.[46] These values are supported by Showa Denko, which commercially produced high-M_w PBS (Bionolle) with a chain extender (hexamethylene diisocyanate, HMDI), reaching M_n ~200,000 g/mol and M_w ~300,000 g/mol (see Scheme 2.2). A chain extender with two functional groups can react with the terminal –OH or –COOH of PBS. The reaction conditions for the chain extension are not as critical as the direct melt polycondensation. Therefore, the chain extender incorporation decreases the biosafety and could affect the biodegradability of PBS, which might prevent the employment of the so-obtained PBS in food packaging. Many chain extenders have been investigated, e.g., isocyanate,[40] oxazoline,[47] anhydride, biscaprolactamate,[48] silazane,[49] and epoxy compound.[45] Diisocyanate and anhydride are suitable for extending the –OH of the PBS, whereas oxazoline and epoxy compounds are used to extend the –COOH groups of PBS.[41]

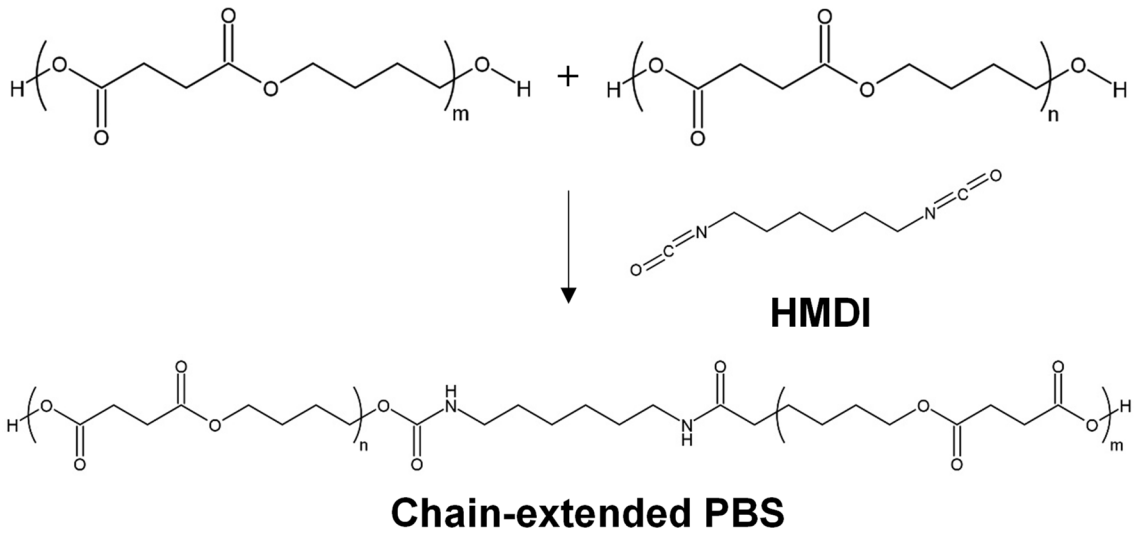

Scheme 2.2. Chain-extension step with hexamethylene diisocyanate (HMDI) to produce high-M_w PBS.

In the polymerization from solution, the monomers are dissolved in a solvent, such as xylene or decahydronaphthalene. This procedure improves the removal of the small molecular materials formed in the reaction process. Both reactions, esterification, and polycondensation proceed at lower temperatures, which avoids the oxidation of PBS, although the reaction time increases.[41] Regarding the molecular weight obtained, M_n ~120,000 g/mol and M_w ~280,000 g/mol can be achieved,[50] although lower values are also obtained.[51]

b. Bio-based polymerization: enzymatic synthesis

This method is relatively recent with respect to petroleum-based synthesis and presents the advantages of milder reaction conditions and the absence of residual metals and metal salts. *Candida antarctica* lipase B (CalB) is usually employed as a catalyst in synthesizing PBS from the monophasic reaction mixtures of diethyl succinate (DES) and 1,4-butanediol (see Scheme 2.3). In this case, the reaction temperature dramatically affects the molecular weight of the polymer. In general, reaction temperatures are below 100 ºC, with reaction times of 24 hours. Another remarkable result obtained from this procedure is the narrow dispersity index of the PBS obtained. However, the molecular weight is low compared to other polymerization methods.[52] Debuissy *et al.*, reported a "green" enzymatic procedure to obtain PBS starting from telechelic hydroxylated poly((R)-3-hydroxybutyrate) (PHB-diol) oligomers and employing CalB and BD in a single-step process. The same authors also described another procedure for this enzymatic synthesis, where the main difference is that the PHB-diol oligomers were introduced after 24 hours of the CalB-catalyzed reaction.[53] Cyclic butylene succinate oligomers have also been obtained through enzymatic ring-opening polymerization (eROP) employing CalB as the catalyst at temperatures below 100 ºC. The obtained oligomers presented low molecular weight: 4700 g/mol and 6100 g/mol for M_n and M_w, respectively.[54]

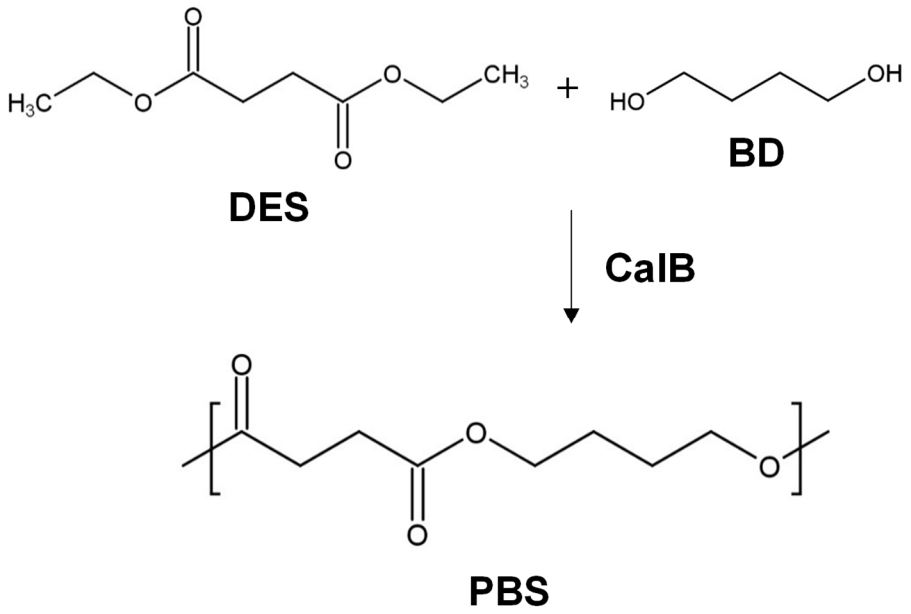

Scheme 2.3. Enzymatic synthesis of PBS by the employment of CalB.

2.2.2. PBS copolyesters

This section illustrates the effect of the preparation conditions of selected PBS-based copolyesters on (a) the molecular weight and (b) the general trends found in the literature on the effect of comonomer content on the crystallization behavior and mechanical properties. All the results are plotted as a function of the PBS content.

a. Influence of the preparation conditions on the molecular weight

PBS copolyesters are obtained through the same experimental procedures, transesterification, or enzymatic synthesis described for the PBS homopolymer in Section 2.2.1. Figure 2.2 shows the variation of M_w with the PBS composition for representative PBS copolymers synthesized previously by some of us and reported in the literature, such as PBS-*ran*-ε-caprolactone (PBS-*ran*-PCL), PBS-*ran*-butylene adipate (PBS-*ran*-PBA), and PBS-*ran*-butylene azelate (PBS-*ran*-PBAz).

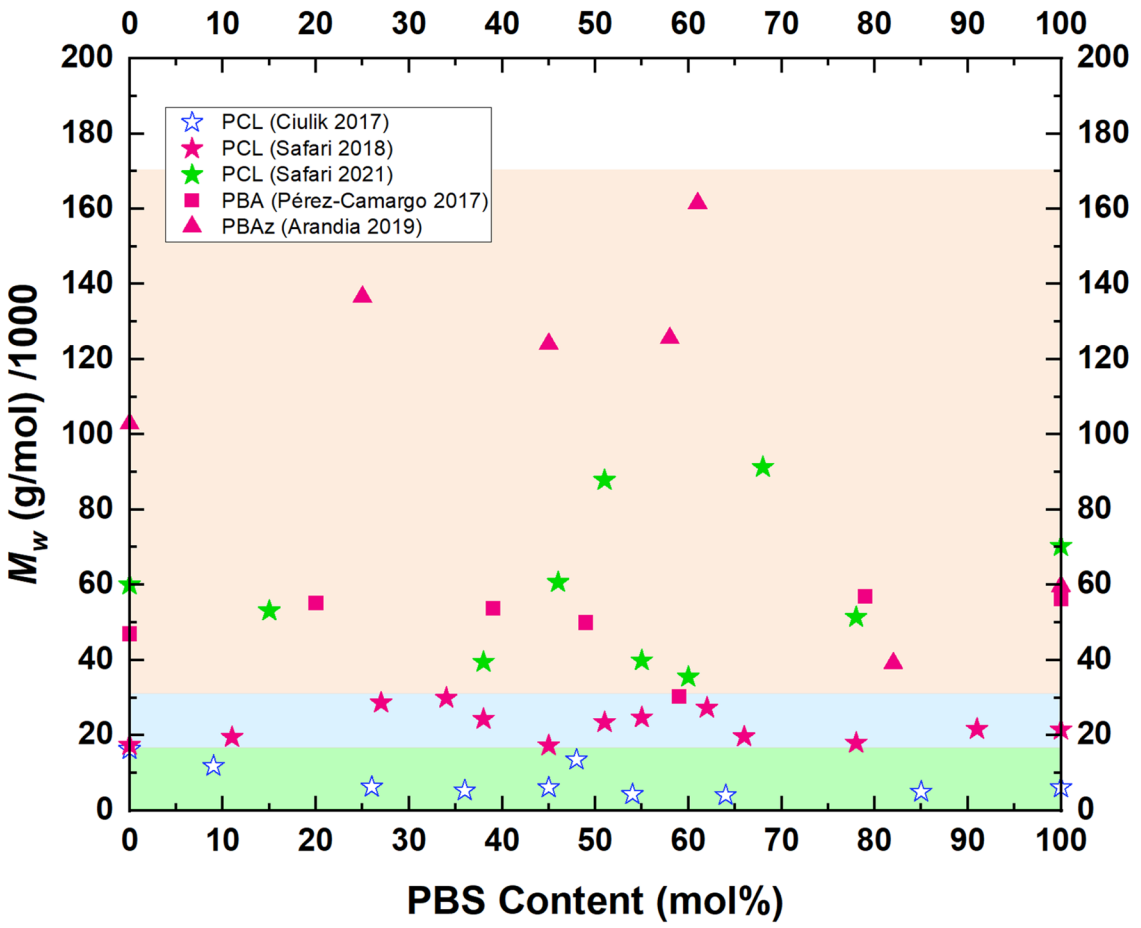

Figure 2.2. Variation of the weight average molecular weight (M_w) with PBS composition. The different comonomers are indicated in the legend. The green area corresponds to low-M_w copolymers (obtained by enzymatic synthesis), the blue covers intermediate-M_w copolymers, and the orange region indicates high-M_w copolymers. Data taken from Refs.[35,54–57]

b. Enzymatic synthesis for PBS-based copolyesters

As can be observed in Figure 2.2, the use of enzymatic synthesis to prepare PBS-*ran*-PCL copolyesters results in polymers with lower M_w than those obtained for PBS-*ran*-PCL copolyesters synthesized by transesterification synthesis. The experimental procedure followed for the synthesis of PBS-*ran*-PCL through transesterification is similar to that followed for the synthesis of PBS-*ran*-PBA and PBS-*ran*-PBAz copolyesters.

Different polymerization pathways were followed for obtaining PBS-*ran*-PCL copolyesters, giving rise to a wide range of molecular weights. For the lowest M_w copolyesters (4000-14,000 g/mol), an enzymatic synthesis was performed,

starting from dimethyl succinate and 1,4-butanediol, at a mild mixing temperature (below 100 ºC) to obtain cyclic BS oligomers. Later on, the enzyme (immobilized CalB) was added to the reaction medium (in a ratio of 1:1 to the reactants). The cyclization reaction was maintained for 48 h under nitrogen flow. The preparation methodology continued with the dispersion of the reaction mixture in chloroform and the recovery of the enzyme by filtration. The copolyesters were finally obtained by mixing the cyclic reactants (BS and CL) with CalB (50 % w/w relative to the total mass of reactants) at 130 ºC for 24 h under a nitrogen flow, and finished with the dispersion in chloroform and recovery of the enzyme, as in the previous step for the obtaining of cyclic BS oligomers.[54]

c. Transesterification/ROP reaction

Safari *et al.* synthesized PBS-*ran*-PCL copolyesters with different M_w ranges following a transesterification/ROP reaction and a polycondensation step, mixing dimethyl succinate, 1,4-butanediol, and ε-caprolactone at different ratios. The first reaction was conducted at 160 ºC for 4 h, and later on, the polycondensation step was performed at 190 ºC at a high vacuum, in the case of the medium M_w copolymers (17,000-30,000 g/mol).[55] For the high M_w copolyesters (35,000-91,000 g/mol), the polycondensation step lasted longer (6 h instead of 4 h) and was carried out at higher temperatures (220 ºC instead of 190 ºC).[35]

PBS-*ran*-PBA copolyesters were synthesized following a two-stage melt polycondensation reaction (polycondensation and postpolycondensation) starting from a bio-based SA (obtained by fermentation of glucose), BD, and adipic acid (AA). For the esterification step, the reaction temperature was kept at 200 ºC. Later on, TTIP catalyst was introduced into the reactor (210 ºC, with argon flux). For the second step (postpolycondensation), the temperature was slowly raised to 230 ºC, and reduced pressure was employed to avoid uncontrolled foaming and to minimize oligomer evaporation. This procedure led to copolymers with M_w in the range 30,000-57,000 g/mol and a polydispersity index of 1.6-2.0, as observed in Figure 2.2.[56] Similarly, a two-stage melt polycondensation has been employed to

synthesize PBS-*ran*-PBAz copolyesters with some modifications: esterification of dimethylazelate (DMAz), SA, and BD was carried out at 200 ºC at atmospheric pressure employing TNBT as the catalyst. The polycondensation step was carried out at reduced pressure, and for this step, the temperature was raised to 250 ºC. The M_w of the so-obtained copolymers were in the 40,000-160,000 g/mol range, improving the latter in the case of the copolymers in comparison with the homopolymers.er authors have followed a similar procedure to synthesize PBS-*ran*-PBAz copolyesters, giving rise to lower M_w than the one observed in Figure 2.2, due to milder synthesis conditions.[58]

d. Crystallization behavior in PBS copolyesters as determined by DSC

PBS is a promising material since it combines good thermal and mechanical properties with easy processability and relatively low cost. PBS possesses a relatively high melting temperature (110 ºC) and a low glass transition temperature (-25 ºC) crucial for applications. Its mechanical properties are comparable to commodity nonbiodegradable polymers, like polyethylene (PE) and polypropylene (PP). PBS is fully biodegradable, but its high crystallinity slows down its degradation rate and induces low barrier properties. Thus, to overcome these disadvantages and tailor the final properties of the PBS, its chain structure is modified, mainly to decrease its crystallinity, either by adding additives or a second phase, e.g., copolymerization. In this way, the range of applications of the PBS-based materials is broadened, and its price is reduced.[59–61]

Different strategies have been used to tailor the properties of PBS, such as blending with other polymers, incorporating natural fibers, nanofillers, or through copolymerization, as block and random copolymers. Here, for brevity, we will focus on the thermal behavior of the PBS-based random copolymers.

In general, the random copolymerization allows achieving final properties in between those of the parent components. From a crystallization point of view, different crystallization modalities, namely (a) comonomer exclusion, (b) isomorphism, and (c) isodimorphism, have been reported and recently reviewed.[62]

Further details of the different crystallization modes can be found elsewhere.[62,63] Briefly, if we consider a PA-*ran*-PB copolymer, three scenarios can occur: (a) Total Comonomer Exclusion: In the PA-rich phase, B comonomers are totally excluded from the PA crystals, and vice versa. Such excluded B or A comonomers will hinder the crystallization of the PA- or PB-rich crystals, respectively. Therefore, only the PA- and PB-rich phases can crystallize with low B or A comonomer content, e.g., 20 % of the randomly distributed co-units along the chain are enough to inhibit the crystallization completely;[62] (b) Isomorphism: The PA-*ran*-PB copolymer can crystallize in a single phase due to the total inclusion (cocrystallization) of the respective comonomer (isomorphism); (c) Isodimorphism: In between cases (a) and (b), the PA-rich phase allows a partial inclusion of B comonomers and vice versa, making possible the crystallization in all the composition range. For isodimorphic random copolymers, when the melting point (T_m) is plotted as a function of the comonomer content, as in Figure 2.3, a clear pseudo-eutectic behavior is typically obtained. Considering Figure 2.3 as an example, to the left of the pseudo-eutectic point or region, the PA-rich phase crystallizes with some inclusion of B comonomers; thus, structurally, the copolymer crystallizes with a PA unit cell with distortions, i.e., expansion or shrinkage of the unit cell, caused by the inclusion of B comonomers in the crystal lattice. The opposite, i.e., the PB unit cell with A comonomers inclusion, occurs at the right side of the pseudo-eutectic point or region. In some cases, it has been demonstrated that both PA- and PB-rich phases can be formed at the pseudo-eutectic point.

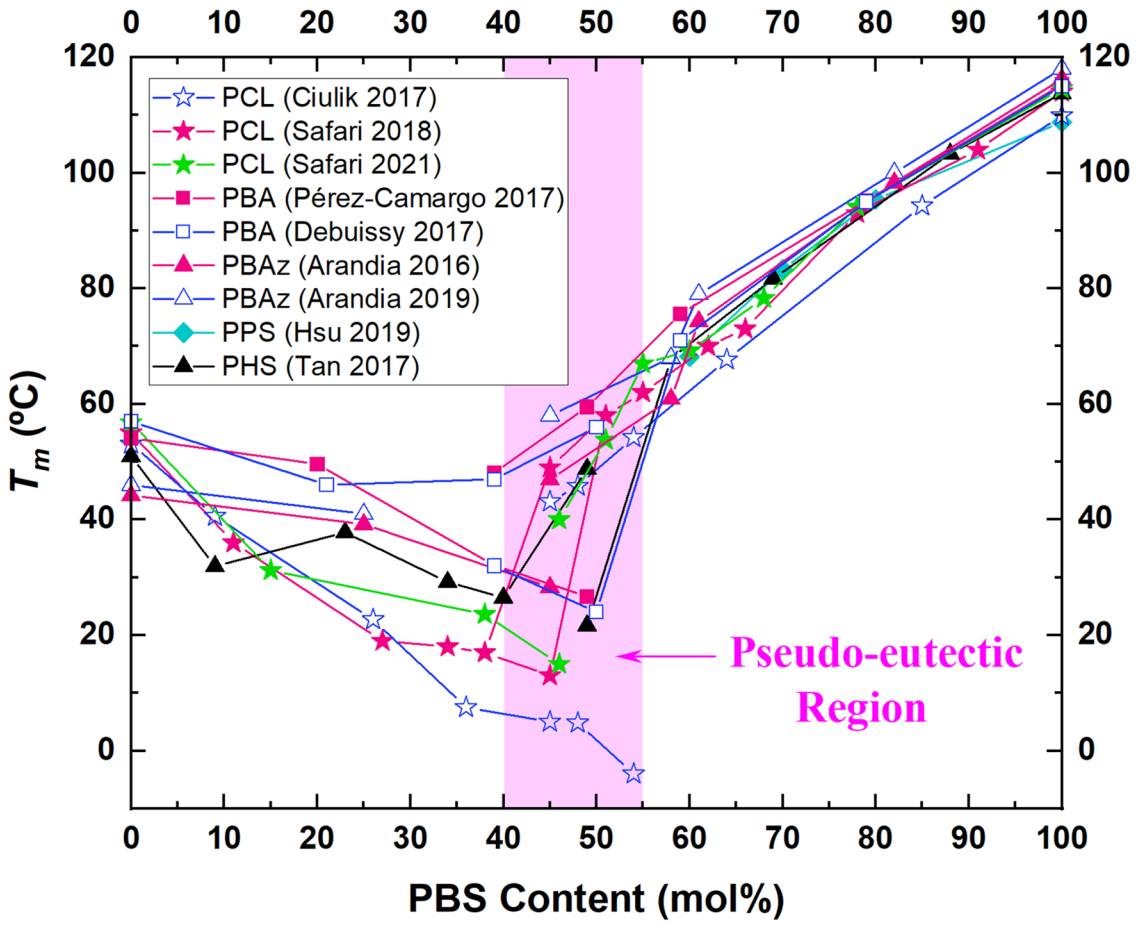

Figure 2.3. Variation of the melting temperature as a function of the PBS composition for selected copolyesters. Pseudo-eutectic points can be observed in the shaded region. Taken from Refs.[35,54–57,60,64–66]

Figure 2.3 shows that, typically, the PBS-based copolymers display an isodimorphic behavior, exhibiting a clear pseudo-eutectic point. The determination of the position of the pseudo-eutectic point is still unclear; however, it seems that it depends on the crystallization ability of the material.[67–69] The PBS possesses a symmetrical chemical structure, adopting an all-*trans* conformation within its unit cell, facilitating the formation of a highly ordered crystalline structure.[68] This provides a high melting point to the PBS and a more stabilized crystalline structure than other copolyesters. In general, those polymers that can form isodimorphic copolymers with PBS are characterized by a strong crystallization ability.[68] Thus, the PBS-based copolymers display a pseudo-eutectic point or region around 50 %, as the PBS-*ran*-PBAz,[57,64,70,71] PBS-*ran*-PBA,[56,59] and PBS-*ran*-PCL[35,54,55,72,73] studied by our group and shown in Figure 2.3. In these random copolymers, the

pseudo-eutectic point or region displays the crystallization of both crystalline phases.

Pérez-Camargo *et al.*[56,59,62] found that for 50:50 PBS-*ran*-PBA copolymers, the "double-crystallization" behavior depends on the cooling rate. Similar results are also reported by Arandia *et al.*[57,64,70,71] in 58:42 PBS-*ran*-PBAz copolymers and Safari *et al.*[35,54,55,72,73] in 45:55 PBS-*ran*-PCL copolymers of different M_w. In these systems, a slow cooling rate, e.g., 5 ºC/min, is favored for the crystallization of the PBS-rich phase, which has ample time (note that the crystallization of the PBS occurs first) to develop spherulites with a relatively high degree of crystallinity. This forces the second component, i.e., PBA, PBAz, or PCL, to crystallize in the confined interlamellar spaces of the PBS-rich crystalline lamellae. However, such confinement effect at slow cooling rates hinders the crystallization of the second phase.

In contrast, at faster cooling rates, e.g., 50 ºC/min, the PBS-rich phase in 58:42 PBS-*ran*-PBAz crystallizes during cooling but develops a lower degree of crystallinity. This gives a chance to the PBAz to crystallize during the fast cooling within the interlamellar regions of the PBS spherulitic templates.[70] For 50:50 PBS-*ran*-PBA and 45:55 PBS-*ran*-PCL copolymers, the rapid cooling inhibits the crystallization during the cooling of the PBS, allowing the PBA- or PCL-rich phases to develop crystallinity. In the subsequent heating, both crystalline phases displayed a sequential cold-crystallization and melting. The PBS crystallizes and melts at higher temperatures than the other phase, either PBA or PCL; for more details, see the following publications.[56,62] In the 40:60 PBS-*ran*-PBA, it was found that only favorable thermodynamic conditions, e.g., slow cooling rates, allow the crystallization of the minority PBS phase. In contrast, the PBA phase is the only one able to crystallize without these conditions.[56,74] Similarly, under isothermal tests, a low crystallization temperature, T_c, favored the formation of both PBA- and PBS-rich phases, while at high T_c a PBS-rich phase was the only one formed. Safari *et al.* reported similar behavior in 45:55 PBS-*ran*-PCL copolymers. It is important to remark that Safari *et al.*[35] studied the PBS-*ran*-PCL

copolymers in a wide range of M_w, obtaining a pseudo-eutectic behavior in all the cases, and similar trends due to the M_w are above the critical molecular weight for entanglements (M_c). In a more recent contribution, Pérez-Camargo *et al.*[59] found that comonomer inclusion depends on the crystallization conditions. The fast crystallization, i.e., nonisothermal test, favored the BA inclusion inside the PBS crystals, whereas slow crystallization (i.e., isothermal test) strongly limits it. Intermediate crystallization, i.e., a combination of nonisothermal and isothermal tests, generated in a successive self-nucleation and annealing test, causes an intermediate situation.

Figure 2.3 shows that most of the PBS-based copolymers possess similar behaviors; however, there are exceptions, e.g., comonomer exclusion and isomorphism, and below, these cases are briefly described.

e. Pseudo-eutectic point at different content, comonomer exclusion, and isomorphism in PBS-based copolymers

The pseudo-eutectic point at a PBS content of around 50 % for PBS-based copolymers has its exceptions, as found by Yu *et al.*[68] These authors studied PBS-*ran*-*cis*-butene succinate, PBS-*ran*-PcBS, copolymers with a pseudo-eutectic point located at 20 % of PBS content. This means that the PBS mainly dominates the copolymer crystallization. This behavior was surprising since the PBS and the PcBS have the same chain length and similar monomer size, but the PcBS possesses one *cis* double bond in the alkyl unit, generating such a particular behavior. The authors attributed the "atypical" pseudo-eutectic behavior for PBS-based copolymers to the different crystallization abilities. The *cis*-isomer in the PcBS introduces "kinks" into the main chain. This difficulty in forming crystals as perfect as the PBS (i.e., all-*trans* configuration, which generated a more stabilized crystalline structure) resulted in a weaker crystallization ability.

In the PBS-*ran*-propylene succinate (PBS-*ran*-PPS) copolymers, prepared by Papageorgiou and Bikiaris,[75] and more recently by Debuissy *et al.*,[76] the very slow crystallization kinetics of the PPS limited the copolymer crystallization to the PBS-

rich phase. Such very slow crystallization is caused by the odd chain length of the 1,3-propanediol group.[77] For the as-received samples directly obtained from the synthesis, the WAXS experiments at RT reveal that the PBS-*ran*-PPS copolymers display PBS unit cells even when it is in the minority phase (i.e., 40 %). In contrast, the PPS-rich unit cell is only present with a PPS content from 80 to 90 %.[75,78] The behavior dramatically changes when the initial thermal history is erased, revealing a more complex trend. After erasing the thermal history and cooling the sample from the melt, only the PBS-rich compositions can crystallize, while the PPS-rich compositions cannot crystalize, as shown in Figure 2.3. After crystallization from the melt, such behavior is similar to a comonomer exclusion case. Similar findings were reported by Papageorgiou and Bikiaris.[75]

The isomorphic behavior, which is not commonly reported, has been found in PBS-based copolymers. The PBS-*ran*-butylene fumarate (PBS-*ran*-PBF) copolymers can form isomorphic copolymers.[79] Ye *et al.*[79] found that T_m increased linearly with the PBF content, the melting enthalpies hardly changed, and all the copolymers displayed similar crystal structures. These authors attributed the isomorphism to the match of all-*trans* conformation adopted by PBS and PBF comonomers. Similar behavior was also found by Zheng *et al.*[80] in multiblock copolymers of PBS-*co*-PBF. In the following contribution, Ye *et al.* found that in random terpolyester PBS-*ran*-PBF-*ran*-PBA,[81] the PBS and the PBF can cocrystallize in an isomorphic mode, despite the presence of the PBA comonomer. Such isomorphism was even found recently in PBS/PBF blends.[82] In this case, the isomorphism is located in the PBS-rich blends due to the strong hydrogen bonding ability of fumarate units.[82]

f. Influence of the comonomer content in the crystallinity

Figure 2.4 plots the degree of crystallinity (X_c) as a function of the comonomer content. X_c is calculated according to Equation 2.1, which is applicable in copolymers.

$$X_c = \frac{\Delta H_m}{\Delta H_m^0 \cdot \emptyset} \qquad \text{(Eq. 2.1)}$$

ΔH_m and ΔH_m^0 are the melting enthalpy and the equilibrium melting enthalpy of the phase under consideration and $\emptyset$ is the weight fraction of the phase under consideration. In general, the extent of X_c depression is related to the easiness of comonomer cocrystallization. As Müller *et al.*[62] pointed out, the decrease of the X_c with the comonomer inclusion indicates that the co-units represent defects for the crystal. For instance, for comonomer exclusion, a strong depression of X_c with the composition is expected since the excluded comonomer decreases the length of the crystallizable sequence (by limiting the number of second comonomer units) included in the crystalline lattice. In contrast, for the isomorphic copolymer, it is reported that X_c remains unchanged or even increases with comonomer content,[79] as the comonomer does not represent an interruption for the crystallizable sequences. In the case of isodimorphic copolymers, as shown Figure 2.4, a pseudo-eutectic behavior of the X_c vs. comonomer content is often obtained due to the partial inclusion of comonomer units.

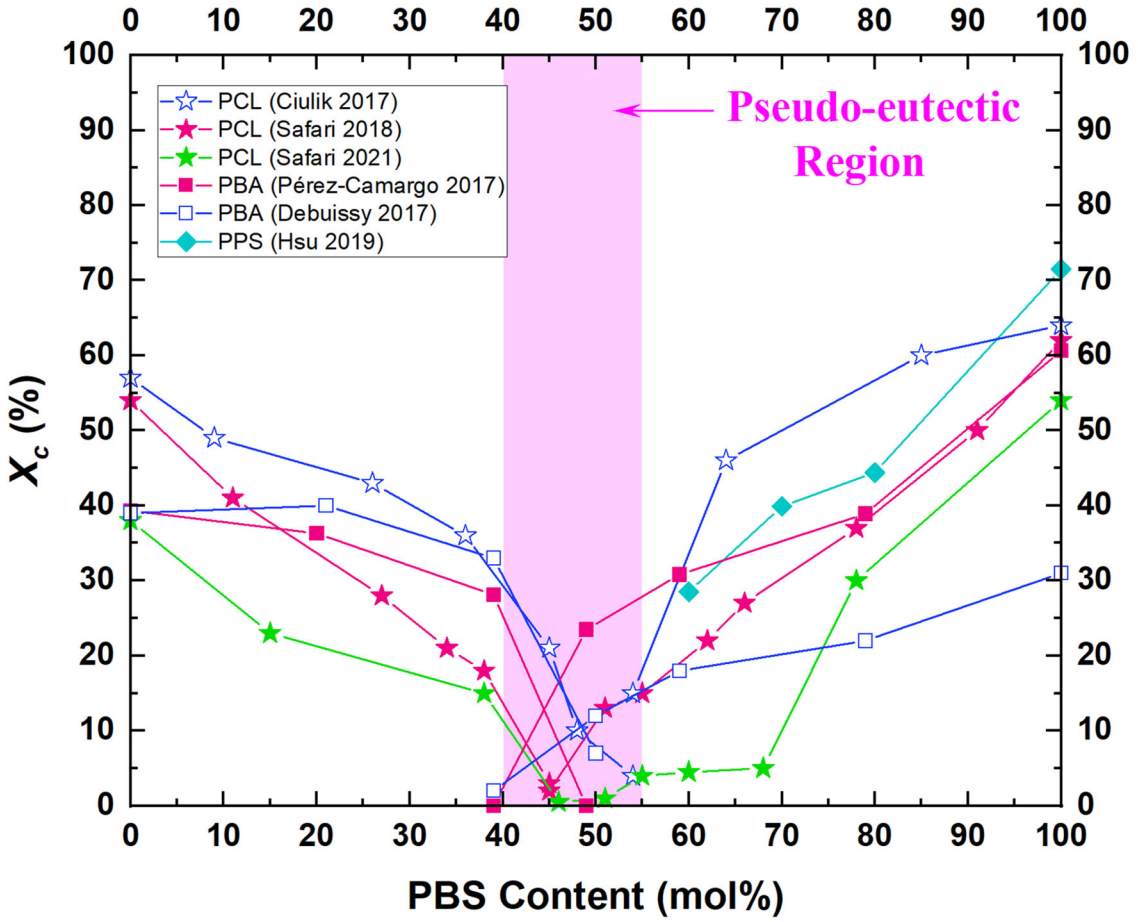

Figure 2.4. Variation of the degree of crystallinity as a function of the PBS composition for selected copolyesters. Pseudo-eutectic points can be observed in the shaded region. Data taken from Refs.[35,54–56,65,66]

As summary, Figures 2.3 and 2.4 show that in PBS-based copolymers, the second phase (i.e., second comonomer) tailors the temperature of the use of the copolymer as well as the crystallinity. Such behavior influences these copolymers' mechanical properties and degradation, as shown in the following sections.

g. Effect of comonomer content on mechanical properties

PBS presents a lower Young's modulus value compared to other common polyesters, such as polyethylene terephthalate (PET) or polylactic acid (PLA), and similar values for elongation at break to low-density polyethylene (LDPE), polypropylene (PP), or polycaprolactone (PCL).[38] The mechanical properties range of values commonly reported, for PBS in the literature is: Young's modulus of 0.5-1 GPa,[83–86] a tensile strength of 30-50 MPa, and elongations at break varying

from values below 5 % up to 500 %.[87–94] The mechanical properties-molecular weight dependence has also been studied in the literature. It has been found that at higher M_w values, the elongation at break increases, which ranges from 355 % (high M_w) to 25 % (low M_w). Similarly, the tensile strength slightly increases with M_w.[41]

Figures 2.5a and 2.5b show, respectively, Young's modulus (E) and the elongation at break (ε_b) obtained from the stress–strain curves of selected PBS-based copolymers plotted against the PBS content of the copolymers.

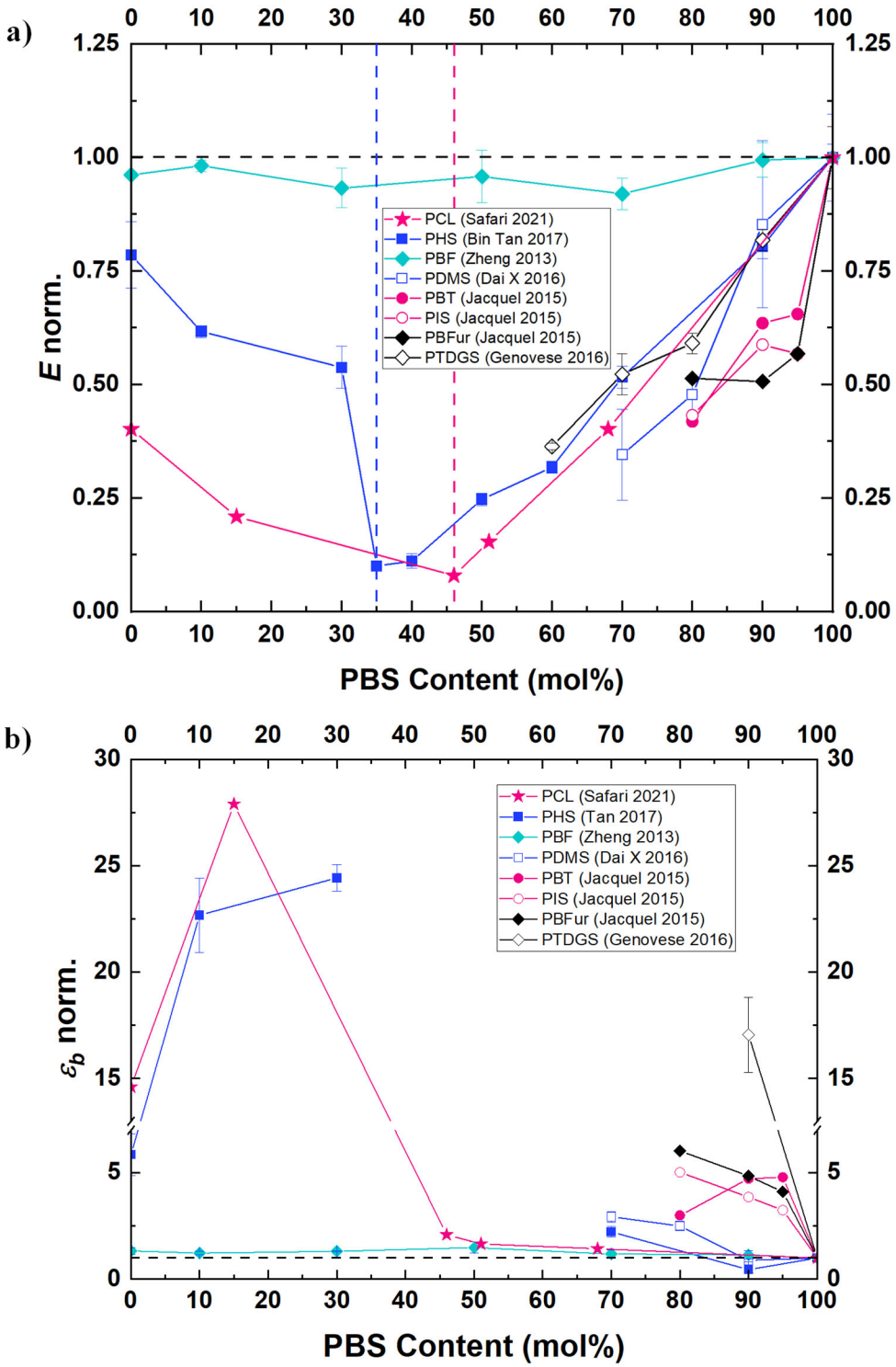

Figure 2.5. a) Variation of the normalized elastic moduli (E) with PBS composition for different copolymers, and **b)** variation of the normalized elongation at break (ε_b) with PBS composition for different copolymers. For a better comparison, the values have been normalized to those of neat PBS. Dashed colored vertical lines reflect a minimum in the elastic moduli, in agreement with the composition of the pseudo-eutectic point observed in the T_m vs. the composition graph (Figure 2.3). Data taken from Refs.[35,60,80,95–97]

Generally speaking, for the PBS homopolymer, introducing a comonomer results in a decrease in the Young's modulus and an increase in the elongation at break values. Going into detail on the results for each particular copolymer shown in Figure 2.5a, the variation of the Young's modulus with PBS content has been determined for the whole range of BS compositions for PBS-*ran*-PCL and PBS-*ran*-PHS copolyesters. For these two copolymers, the variation of *E* is clearly dependent on the composition range, exhibiting a pseudo-eutectic behavior, registering the minimum properties at the pseudo-eutectic point, i.e., at 45 % and 35 mol% PBS for PBS-*ran*-PCL[35] and PBS-*ran*-PHS,[60] respectively. This is in line with the variation of the T_m and X_c values as a function of the PBS content (Figures 2.3 and 2.4, respectively). As expected, these results show a direct correlation of the mechanical properties on X_c. The PBS-*co*-PBF multiblock copolymers show a different trend, since the *E* values remain practically unchanged with the PBS content. This particular trend is caused by the isomorphic-like behavior reported for the PBS-*co*-PBF system. Moreover, the PBS and PBF have similar elastic moduli values.[80]

For the other copolymers, shown in Figure 2.5a, PBS-*ran*-decamethylene succinate (PBS-*ran*-PDMSu),[95] PBS-*ran*-butylene terephthalate (PBS-*ran*-PBT), PBS-*ran*-isosorbide succinate (PBS-*ran*-PIS) and PBS-*ran*-butylene furanoate (PBS-*ran*-PBFur),[96] and PBS-*ran*-thiodiethylene glycol succinate (PBS-*ran*-PTDGS),[97] the variation of *E* with the PBS composition has only been determined for the BS-rich composition range (at compositions higher than ~60 mol% PBS) and show a linear decrease of *E* with the introduction of the comonomer in the PBS-rich compositions. A corresponding increase in the values of the elongation at break is depicted in Figure 2.5b for these same copolymers. It is important to note that, in the case of PBS-*ran*-PTDGS, the elongation at break increases up to 35 times at 80 mol% PBS with respect to the PBS homopolymer. Such a result is promising for using this copolyester in soft packaging applications.[97]

2.2.3. PBS nanocomposites: modulation of mechanical properties

The incorporation of organic and inorganic fillers to produce nanocomposites are common routes for the modulation of mechanical properties and directly impacts the barrier properties of PBS. Figure 2.6 shows representative results corresponding to the variation of the mechanical properties, elastic moduli, and elongation at break of PBS nanocomposites as a function of filler content. Here, we have selected PBS/nanoclays nanocomposites, which incorporate organo-modified montmorillonite (CLOISITE® 25A, C25A) and other examples of PBS nanocomposites, such as those incorporating zinc oxide nanoparticles (ZnO), hydroxyapatite nanoparticles (HA), or cellulose nanocrystals (CNC).

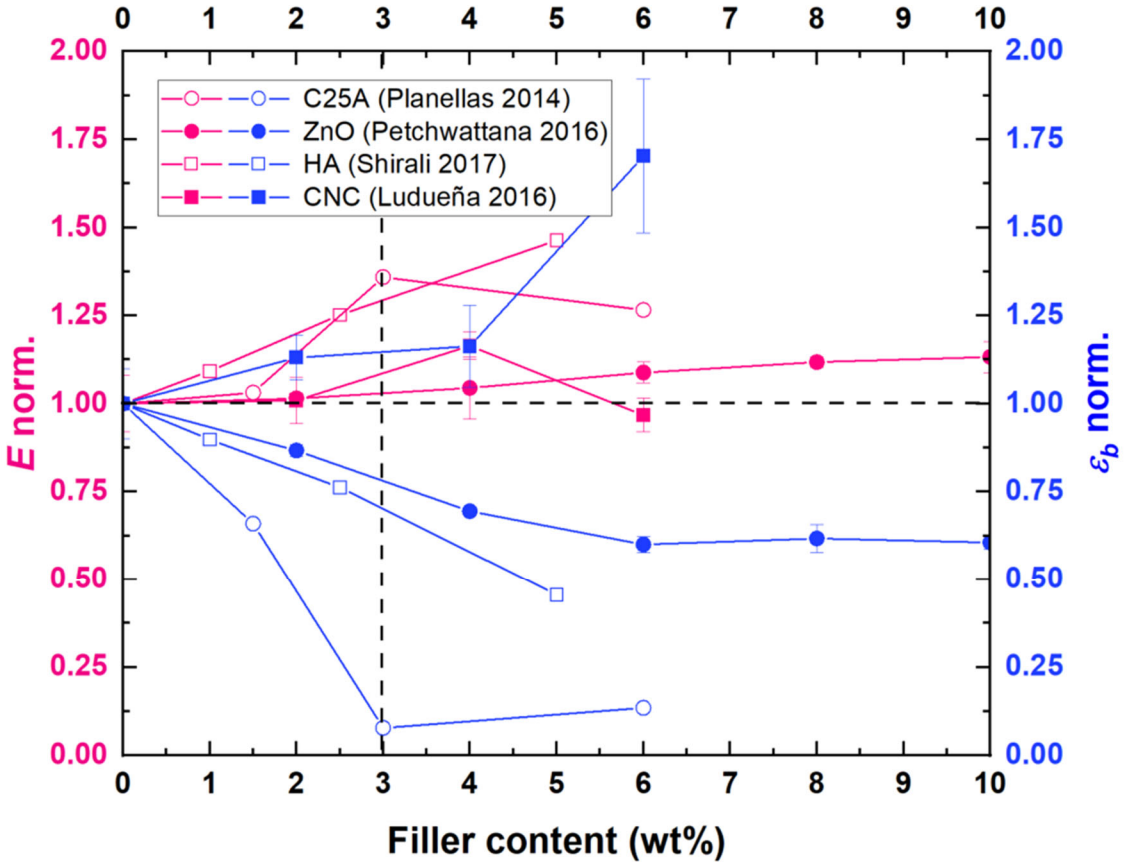

Figure 2.6. Variation of the elastic moduli (E) and elongation at break (ε_b) with filler content. For a better comparison, both parameters have been normalized to that of neat PBS. The dashed black line corresponds to a "critical" filler content. Data taken from Refs.[88,90,91,98]

As shown in Figure 2.6, PBS/nanoclays nanocomposites such PBS/C25A increased their elastic moduli up to 1.25 times at 3 wt% nanofiller. Then, above this concentration, a decrease of the elastic moduli is observed, ascribed to the clay degradation during processing.[91] Several reviews on the development of PBS nanocomposites, through the incorporation of clays and nanoclays as fillers, show different preparation routes, including in situ intercalation, solution casting, melt intercalation, transesterification, and master batch.[99] The types of clays commonly employed for the formation of PBS nanocomposites are mainly constituted by the family of 2:1 phyllosilicates: montmorillonite (MMT), saponite (SAP), and fluorohectorite (FHT).[100]

Figure 2.6 also shows the results corresponding to PBS nanocomposites prepared by incorporating inorganic nanoparticles, like zinc oxide (ZnO) and hydroxyapatite (HA). Incorporating ZnO nanoparticles (100 nm average size) gives rise to a slight increase in the elastic moduli for PBS nanocomposite films up to a ZnO concentration of 10 wt% and a decrease of the values corresponding to the elongation at break. The rigidity of the ZnO nanoparticles, the restriction of the chain entanglement, and the rearrangement of crystallized PBS chains induced by the nanoparticles explained the results found for these PBS nanocomposites.[88] The incorporation of hydroxyapatite nanoparticles also increases the values of the elastic moduli up to 1.5 times at an HA concentration of 5 wt%.[98]

Finally, the incorporation of bionanofillers constitutes an important field of research nowadays due to the possibility of preparing fully biodegradable polymer nanocomposites. As an example, Figure 2.6 shows the variation of the mechanical properties for PBS ternary nanocomposites obtained through the mixing of PBS, poly(ethylene glycol) (PEG), and cellulose nanocrystals (CNC) in a weight ratio of 80:20 in PBS:PEG, and increasing amounts of CNC (2, 4 and 6 wt%). PBS/PEG/CNC nanocomposites showed a slight increase of the elastic moduli up to CNC contents of 4 wt%. Above this content, the elastic moduli decreased compared to the pristine PBS because of the poor dispersion of the CNC within the PBS matrix.[90] Other bionanofillers that have been employed to modify the

mechanical properties of PBS are isora nanofibers (INF) extracted from *Helicteres isora* by thermo-mechano-chemical treatments,[101] wood flour (WF),[102] oil palm mesocarp fibers (OPMF),[86] or konjac fly powders (KFP),[103] among others.

In summary, the general trend found for PBS nanocomposites is that incorporating nanofillers, even at a low content (less than 6 wt% filler), results in an increase of the elastic moduli and a decrease of the elongation a break. However, many factors play a key role, such as the degree of dispersion, the crystallinity or the orientation of the nanoparticles, and the interactions between the polymer matrix and the nanoparticles, which are necessary to propagate the stress through the nanocomposite. That is why each particular PBS nanocomposite has to be studied separately to extract proper conclusions on the variation of the mechanical properties with the nanofiller content.

2.2.4. Barrier properties

The study of barrier properties in the materials field is an important step for their evaluation for food packaging applications and food-related categories.[104,105] It is also important for other applications such as coatings for many different substrates[106] or mulching films that can be employed to protect crops in agriculture.[20,30,107] This type of study must consider both gas and liquid barrier properties, as packages should protect the food from both external gases and liquids. Moreover, the shelf life of the product is also affected by these permeants, water vapor being one of the most relevant.[108] Regarding the liquid barrier properties, the most commonly studied one is water,[109,110] although other liquids have also been studied, such as acetic acid, ethanol, or isooctane, among others.[111]

Nevertheless, having a material that accomplishes the required gas barrier properties is a must, as food needs to be preserved under certain atmospheric conditions. Thus, novel materials should be designed to fulfill all the requirements for food packaging in terms of gas permeability. For this purpose, the most abundant gases in the atmosphere are commonly studied (e.g., water vapor, oxygen, carbon dioxide, and nitrogen).[112] Some reports have also included helium,

argon, methane or hydrogen, or vapors such as methanol or dimethyl carbonate.[113,114] It is crucial to have the oxygen levels under control, as high values could accelerate the enzymatic degradation of the food, whereas too low levels could lead to tissue deterioration. Carbon dioxide is related to antimicrobial properties, whereas nitrogen is used to complete the inside atmosphere of the package, being inert to food and protecting the film from breaking.[115]

The most studied and commonly used materials for food packaging are synthetic polymers (e.g., PET, PP, and PE), although PLA has already become one of the most important alternatives to these "commodities" among biodegradable polymers.[116,117] Nonetheless, PBS is promising due to its good processing conditions and its wide range of thermomechanical properties. It also shows similar/enhanced barrier properties compared to PLA, positioning PBS as a real alternative in the field of biodegradable polymeric packages.

Figure 2.7a shows an overview of the gas barrier properties (O_2 and CO_2) corresponding to several polymers. As it can be appreciated, gas permeabilities of polymeric materials cover a wide range of values, starting from the extremely low values of polyacrylonitrile (PAN) or a liquid crystal polymer (LCP) from Vectra, which present triple bonds or aromatic rings in their structures, to the very high values for silicones, such as polydimethylsiloxane (PDMS) or poly(1-trimethylsilyl-1-propyne) (PTMSP). When expressing the permeabilities in Barrers (1 $Barrer = 10^{-10} \cdot cm^3_{STP} \cdot cm^{-2} \cdot s^{-1} \cdot cm \cdot cm \cdot Hg^{-1}$, where cm^3_{STP} stands for standard cubic centimeter, representing the number of moles of gas that would occupy 1 cm^3 at standard temperature and pressure), a common unit used to express gas permeability, a range over 10 orders of magnitude can be achieved. In the previous expression, $cm^3_{STP} \cdot cm^{-2} \cdot s^{-1}$ denotes the gas flux through the material, cm comes from the thickness of the film, and $cm \cdot Hg^{-1}$ stands for pressure drop across the material.

Within the group of "commodities" (nonbiodegradable polymers) commonly employed in food packaging, or in other applications where gas permeabilities play

an important role (e.g., mulching films for crops protection), we can see that some of them present excellent barrier properties (PVDC), good barrier properties (PET, PVC, and Nylon 6), or average barrier properties (HDPE, LDPE, and PP). In the field of biodegradable polymers, few polymers show excellent barrier properties: chitosan and ethylene vinyl alcohol (EVOH) are two examples.[104] Within the group of biopolymers with good barrier properties, we can find PLA, PCL, PHB, PHBV, or collagen, among others.[118] Regarding PBS, it shows slightly enhanced barrier properties compared to those mentioned above, which leaves PBS in an advantaged place towards barrier properties within biodegradable polymers, and similar barrier properties to those of PVA[109,119] (see Figure 2.7b).

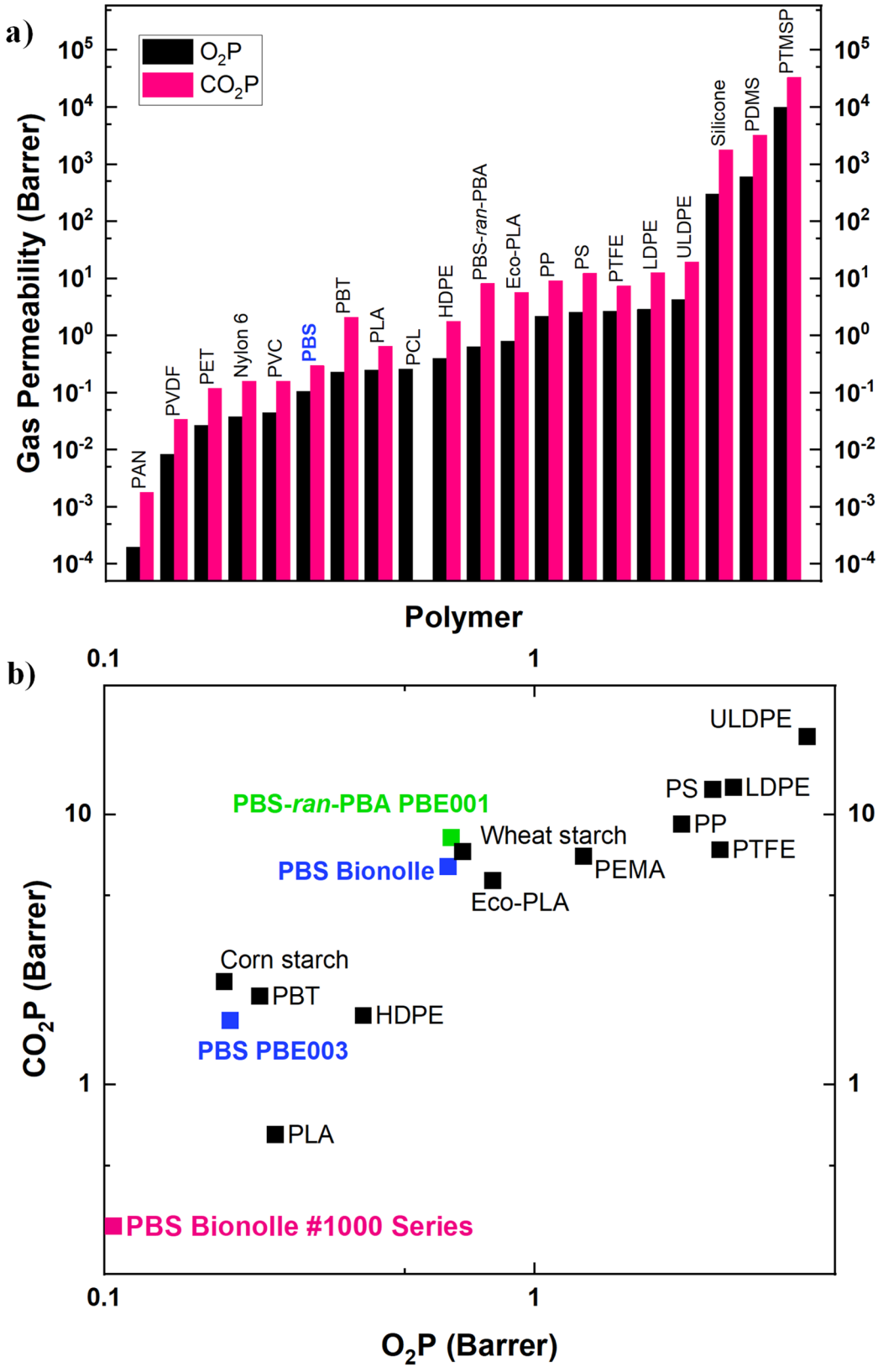

Figure 2.7. Gas barrier properties (*O_2P* and *CO_2P*) for several commercial polymers and biopolymers: **a)** bar chart for a general overview, and **b)** plot for intermediate permeabilities (PBS region). Note that both axes are presented in decimal logarithm form. Data taken from Refs.[106,109,111,113,114,117,120–130]

a. PBS-based copolymers

One possibility of modulation of PBS barrier properties is the copolymerization of PBS with different comonomers. A comparison of the permeability of PBS, PBS-*ran*-PBA, and PLA to oxygen and carbon dioxide showed a higher permeability of the three polymers to CO_2 compared to oxygen, as can be observed in Figure 2.7a. Among these three polyesters, PBS-*ran*-PBA showed improved barrier properties to both gases with respect to PLA, while PBS showed a lower permeability for oxygen but higher to CO_2. These results are quite promising for PBS, turning it into an alternative to PLA, one of the most employed polymers for biodegradable packaging films.[111] Other authors showed that PLA/PBS-*ran*-PBA[131] and PLA/PBS[130] (80/20) multilayer blend films achieved similar barrier properties to those of PLA and PBS, and much better than neat PBS-*ran*-PBA.

Genovese *et al.* studied the influence in oxygen and carbon dioxide permeabilities (i.e., O_2P and CO_2P) of different poly(butylene succinate-*ran*-thiodiethylene glycol succinate) (PBS-*ran*-PTDGS) copolymers. It was found that the barrier properties to both gases were improved when compared to a commercial PLA. When compared to the PBS homopolymer, PBS-*ran*-PTDGS copolymers showed a similar performance towards oxygen, with a reduction of up to ~25 % in the oxygen transmission rate. Therefore, these materials present a similar or even better barrier to oxygen than the PBS homopolymer. However, the incorporation of thioether linkages resulted in a worsening of the barrier properties of PBS towards carbon dioxide, with transmission rates that doubled those of the PBS homopolymer. This behavior was not due to a decrease in crystallinity, but was explained by the lower chain mobility induced by the higher M_w in the copolymers. Notwithstanding, the PBS-*ran*-PTDGS copolymer with 30 mol% thiodiethylene glycol units exhibited the best barrier properties of the whole series, with a better behavior towards oxygen and a similar performance towards carbon dioxide compared to PBS, making it a potential candidate for food packaging applications.[97]

Duan *et al.* synthesized two different sugar-based PBS copolymers, employing two cyclic alditols: isosorbide and 2,3-*O*-isopropylidene-L-threitol. Results showed that isosorbide copolymers presented a ~60 % diminishment in oxygen permeability compared to the PBS homopolymer, whereas the threitol-based copolymers reduced the O_2P by more than 35 % when compared to PBS.[132]

The opposite behavior was found when PBS was copolymerized with neopentyl glycol and 2-butyl-2-ethyl-propanediol, leading to worse barrier properties than the PBS homopolymer. PBS-*ran*-neopenthyl succinate (PBS-*ran*-PNS) and PBS-*ran*-2-butyl-2-ethyl-propylene succinate (PBS-*ran*-PBEPS) showed a significant increase in gas transmission rates with respect to PBS: more than a ~300 % increase for CO_2, ~700 % increase in the case of O_2, and ~800 % increase for N_2 for the PBS-*ran*-PBEPS copolymers; whereas for the PBS-*ran*-PNS copolymer, the gas transmission rates doubled when compared to neat PBS. According to the authors, this behavior was due to a reduction in the crystallinity degree, as gas molecules find it easier to diffuse through the amorphous regions.[115] Despite this, some of these copolymers presented similar or even better barrier properties to those of LDPE, commonly employed in flexible food packages.

b. PBS-based nanocomposites

Besides the variation of mechanical properties, the incorporation of nanofillers within the PBS matrix (and their copolyesters matrices) is a strategy widely employed for the modulation of the barrier properties of this biopolyester. This is a promising approach for enhanced materials for food packaging applications. The reason for this improvement is the physical hindrance to gas molecules due to the presence of fillers in the polymer matrix.[133]

The reinforcement of PBS with nanocrystalline cellulose (NCC) and nanoclays enhances the barrier properties of this biopolyester.[110] The study of Xu *et al.* based on PBS nanocomposites with NCC fillers showed a large improvement in gas barrier properties. With a low amount of NCC (3 wt%), the gas transmission rates were reduced to ~40 and ~60 % for water vapor and oxygen, respectively.

Furthermore, the addition of 4 wt% of a compatibilizer (methylene diphenyl diisocyanate, MDI) to the PBS with 3 wt% of NCC resulted in a higher reduction of water vapor and oxygen transmission rates to ~63 and ~97 %, respectively, compared to the PBS homopolymer.[87] In another example, with PBS-*ran*-PBA nanocomposites prepared by adding unmodified nanoclays (5 wt%), the O_2P of the PBS-*ran*-PBA was reduced by ~35 %. A further reduction of the O_2P to values of ~50 % was obtained with the organic modification of the nanoclays (5 wt%) due to better compatibility with the PBS-*ran*-PBA matrix, which improved the dispersion of the modified clays.[122] Cloisite 30B, an organically modified montmorillonite (OMMT), was studied in PBS/PLA blends (50/50) to improve the PBS barrier properties. A linear relationship between the cloisite content and oxygen/water vapor permeability was found, showing a decrease of ~50 % for both gases with 7 wt% of the OMMT,[134] in a similar way as for the PLA/PBS-*ran*-PBA and PLA/PBS clay nanocomposites,[135] whereas other authors reported a lower reduction of O_2P in PLA/PBS blends (80/20 w/w) with Cloisite 30B.[123] A similar reduction was achieved for PBS nanocomposites with organically modified layered silicate (OMLS),[120,136] and organomodified beidellite clay nanocomposites.[137] For PBS-*ran*-PBA nanocomposites with native montmorillonite and OMMT, the gas permeabilities drop between 60 and 70 % in water-injection-extruded PBS-*ran*-PBA/Cloisite 30B nanocomposites.[121]

Similarly, Petchwattana *et al.* reported that the incorporation of ZnO into PBS films led to a considerable reduction of the gas permeability, as the transmission rates were reduced between ~25 and ~30 % for water vapor and oxygen, respectively, for the PBS nanocomposite with a 10 wt% of ZnO.[88] The addition of 2 wt% graphene nanoplatelets to PBS involved a ~35 and ~40 % reduction of oxygen and water vapor permeabilities, respectively, which was attributed to an increased tortuosity due to the presence of the filler.[128]

The compatibility between banana starch nanocrystals (SNC) and PBS was evaluated for its application as bionanocomposites for packaging films. Both water vapor and oxygen transmission rates were improved with the incorporation of the

modified SNC to PBS, achieving better barrier properties with higher nanocrystals content (9 wt%). These parameters were reduced by ~50 and ~60 % for water vapor and oxygen, respectively.[138]

Considering PBS/PLA blends (60/40), the study of the influence in barrier properties of two different types of zeolites (5A and 13X) showed that both zeolite nanocomposites achieve lower O_2P (~60 % reduction) and CO_2P (~40 % reduction) when compared to the PBS/PLA blend. This behavior is attributed to the tortuosity and the porosity of zeolites, as O_2 and CO_2 molecules are smaller than the zeolite pores. On the other hand, the water vapor permeability increased by ~60 % because of the highly polar nature of zeolites.[139]

As we have seen within this section, PBS barrier properties can also be modulated by copolymerization with different monomers or by preparing PBS nanocomposites. In PBS copolymers, barrier properties may be enhanced or worsened depending on the nature of the second monomer. The preparation of PBS nanocomposites commonly leads to less permeable materials, as the presence of fillers induces a more tortuous pathway for gas molecules.[100,109,110,140–143] Although results may differ from one study to another, the general trend has shown that polymeric nanocomposites, and particularly PBS nanocomposites, present better barrier properties than PBS. The aforementioned ways of modulation, linked to the good barrier properties inherent to PBS, compared to other biodegradable polymers (see Figure 2.7b), make it a potential candidate within this polymer category for certain applications where barrier properties must be taken into consideration, such as food packaging.

2.3. Biodegradation of Biopolyesters

Research on biodegradable polymers has become more and more important over the last few years. Nowadays, wastes and landfill accumulation are an increasing concern worldwide, and biodegradable polymers emerge as a promising alternative for its reduction.[144,145] The situation is especially dramatic regarding plastic waste into the oceans, where plastic fragments within the range of a few micrometers to several centimeters end up in the ocean and cause significant damage to the local wildlife and the ecosystems.[6,146,147]

PBS, as already mentioned in this Chapter, is a biodegradable polyester that can effectively decompose into water and carbon dioxide (CO_2). PBS can be included in the fossil-based biodegradable polymers, although many advances have been made in the field of bio-based PBS (Section 2.2.1). Because of this, PBS and many of its copolymers can be biodegraded (i.e., naturally occurring enzymes and microorganisms) despite its monomers (SA and BD) being mainly produced from petroleum derivatives. Several reviews can be found in the literature that discuss the most common biodegradation routes for biodegradable polymers, such as PCL, PLA, or PHA.[43,148] Nevertheless, less information regarding PBS biodegradation is available, as research is still ongoing. PBS degradation methods include hydrolytic degradation, enzymatic degradation, and biodegradation in environmental conditions, such as burial, activated sludge, and compost.[41]

2.3.1. Hydrolytic degradation

One of the most common mechanisms of polymer degradation is hydrolytic degradation. In this case (and in the case of enzymatic degradation), the degradation rate depends on PBS crystallinity. Hydrolytic degradation occurs faster in the lower density amorphous regions, facilitating water penetration. This phenomenon causes an increase in the overall degree of crystallinity due to the faster degradation of amorphous domains (that can crystallize once degraded) compared to the more crystalline ones.[149] Some authors report no variation in weight for PBS when exposed to hydrolytic degradation,[150] while others report low

weight loss.[151,152] One study reported a ~31 wt% weight loss for PBS after 24 weeks of hydrolytic degradation at 37 ºC. This result could be explained due to the relatively low crystallinity (~56 %, as determined by DSC) of the PBS used.[153] The pH of the media is also an important parameter that must be taken into account. Morales-Huerta *et al.* reported a 10 wt% weight loss for hydrolytic degradation at pH = 7.4 after 30 days, whereas the weight loss increased to values higher than 25 wt% for a pH = 2.0 media.[154]

As can be deduced from different studies, PBS can be effectively degraded by the hydrolysis of the ester bonds, achieving different results depending on many different parameters involved, such as the synthesis method, molecular weight, crystallinity, or the experimental conditions of the biodegradation assays.

2.3.2. Enzymatic degradation

So far, enzymatic degradation is regarded as one of the most attractive and effective methods for the biodegradation of biopolyesters. The main reason is the presence of labile ester bonds in the chemical structures of biopolyesters, where enzymes can attack.[20] Then, the enzymatic degradation process usually starts with the attachment of the enzyme on the surface, and hydrolysis proceeds via surface erosion. Among all the different types and families of enzymes that can effectively biodegrade PBS and its copolymers, some examples are included in this Chapter. Table 2.2 shows various enzymes and different experimental conditions for PBS enzymatic biodegradation.

Table 2.2. Classification of enzymes by families for different PBS enzymatic degradation studies.

Family	Enzyme	Substrate	Experimental conditions	Results (weight loss)	Ref.
Cutinase	*Fusarium solani*	PBS films 30·10·0.1 mm^3	pH = 8.0 at 40 ºC, 20 µg/mL	100 wt% in 6 h	155
Cutinase	*Pichia pastoris*	PBS films 30·10·0.5 mm^3	pH = 7.4 at 37 ºC, 0.15 mg/mL	100 wt% in 12 h	156
Cutinase	*Fusarium solani*	PBS films 30·10·0.1 mm^3	pH = 7.4 at 37 ºC, 10 mg/mL	98.4 wt% in 12 h	157
Cutinase	*Fusarium solani*	PBS films 30·10·0.5 mm^3	pH = 7.2 at 37 ºC, 18 U/mL	~100 wt% in 26 h	158
Lipase	*Candida antarctica* (CalB)	PBS films 30·10·0.5 mm^3	pH = 7.2 at 45 ºC, 18 U/mL	95.1 wt% in 26 h	158
Lipase	*Candida rugosa*	PBS films 10·10·0.5 mm^3	pH = 7.4 at 30 ºC, 0.1 mg/mL	2 wt% after 7 weeks	159
Lipase	*Pseudomonas cepacia*	PBS films 20·30·0.3 mm^3	pH = 8.0 at 40 ºC, 0.06 mg/mL	2 wt% after 90 h	160
Lipase	*Candida antarctica* (CalB) N435	PBS films 30·10 mm^2	pH = 7.4 at 37 ºC, 1.2 mg/mL	1.8 wt% after 90 h	161
Lipase	Porcine pancreas	PBS films 30·10 mm^2	pH = 7.4 at 37 ºC, 0.8 mg/mL	0.9 wt% after 90 h	161
Lipase	*Pseudomonas cepacia*	PBS films 10·10·0.1 mm^3	pH = 6.86 at 45 ºC, 0.22 mg/mL	4.6 wt% after 50 h	162
Lipase	Porcine pancreas	PBS discs 10·10·0.2 mm^3	pH = 7.4 at 37 ºC, 1 mg/mL	21 wt% after 30 days	154
Lipase	*Pseudomonas fluorescens*	PBS films 10·10·0.2 mm^3	pH = 7.3 at 37 ºC, 2 mg/mL	No visible degradation after 300 h	163

Lipase	*Pseudomonas cepacia*	PBS films $10 \cdot 10 \cdot 0.1$ mm^3	pH = 6.86 at 45 ºC, 0.53 mg/mL	100 wt% after 288 h	80

Enzymatic degradation assays for biopolyesters and PBS are commonly carried out at physiological temperature (i.e., 37 ºC).[154,157,160] However, it has been demonstrated that this degradation method is favored at a temperature close to T_m (the PBS melting temperature is above 100 ºC).[164] Some authors have reported low weight loss values for PBS homopolymer at different experimental conditions, reaching a 3.5 wt% weight loss after 12 days in the presence of *P. cepacia* lipase,[164] or even lower.[159,161] The low degree of degradation obtained could be attributed to the high crystallinity of this polymer compared to other aliphatic polyesters.[164] Other studies carried out under different experimental conditions report much higher degradation rates. For example, for enzymatic degradation assays employing cutinases, weight losses reach almost 100 wt% in just 12 hours,[157] as seen in Table 2.2. An interesting study developed by Shi *et al.* showed the influence of two different enzymes (*Fusarium solani* cutinase and *Candida antarctica* lipase B, CalB) in the degradation rate of PBS. They found that the PBS degradation rate was much faster by the action of cutinase. PBS degraded in the presence of cutinase reached ~50 wt% in 4 hours, whereas those degraded in the presence of lipase reached ~20 wt% over the same time. For both cases, a nearly total decomposition was achieved after 26 hours.[158]

Figure 2.8 shows the results corresponding to different biodegradation studies where the weight loss of PBS in the presence of lipase from *P. cepacia* has been reported. As can be observed in Figure 2.8, only one study shows a relatively high weight loss of PBS with this enzyme (>40 wt% in 100 hours).[80] For the rest, the weight loss reached after several hours in contact with *P. cepacia* is very low (<6 wt%), which could be attributed, in part, to the low concentration of the enzyme employed for some of the studies.[160,162,165]

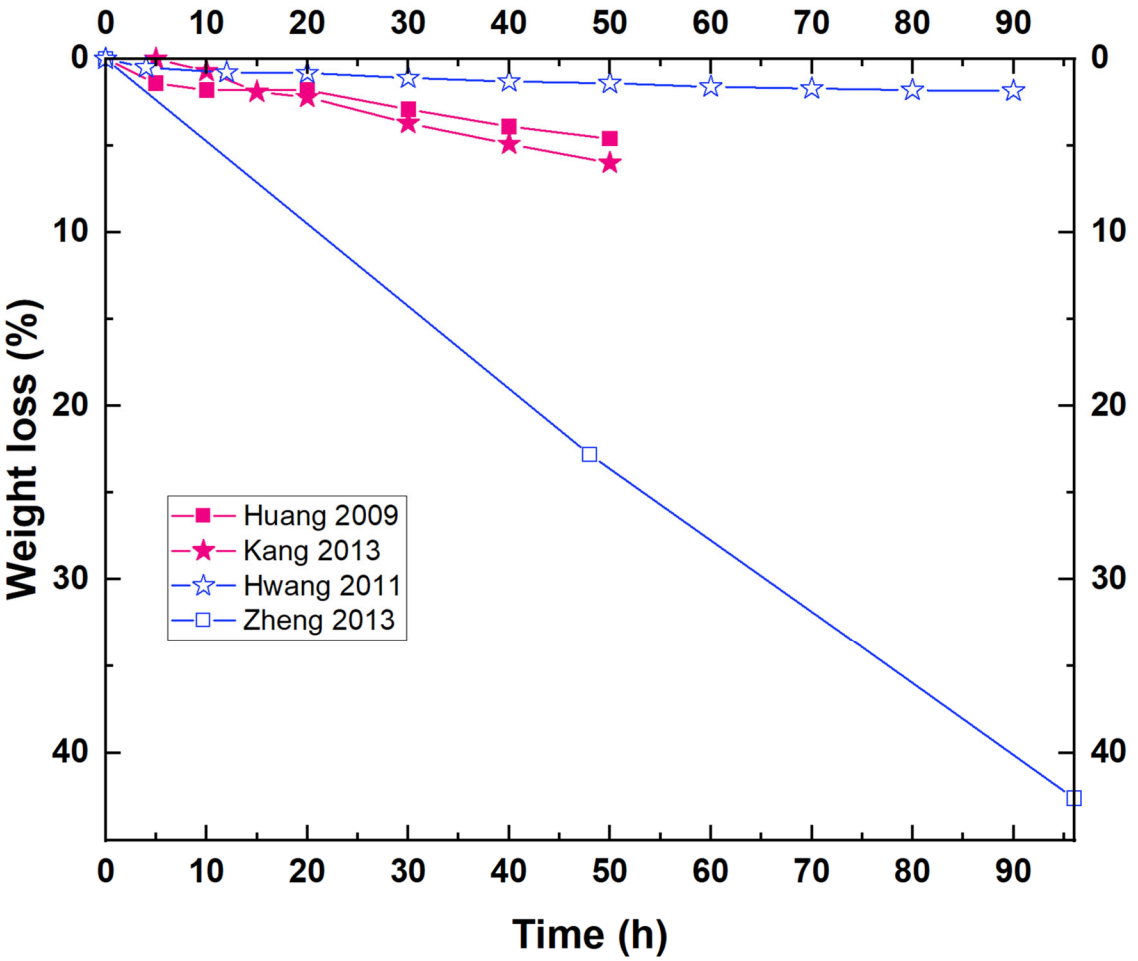

Figure 2.8. Weight loss curves corresponding to various enzymatic degradation studies of PBS by the action of a lipase from *P. cepacia*. Experimental conditions differ from one study to another, although the same enzyme is used. Data taken from Refs.[80,160,162,165]

2.3.3. PBS-based copolymers: hydrolytic and enzymatic degradation

In the case of PBS copolymers, different (and opposite) results are reported depending on the nature of the second comonomer. For instance, the biodegradability of aromatic polyesters is less favored than in the case of aliphatic polyesters such as PBS.[154] Thus, incorporating a second comonomer in the structure of PBS could favor or prevent the degradation of the polyester, attending to the nature of the second constituent.

Hydrolytic and enzymatic degradation of PBS-*ran*-PBFur copolyesters have been determined by placing 60:40 and 40:60 copolymers in a pH = 2.0 or pH = 7.4 medium at 37 ºC.[154] Firstly, the enzymatic degradation was more effective than

hydrolysis, reaching 15-20 wt% vs. 3-5 wt% weight losses for the latter (hydrolysis) after 30 days. Furthermore, the behavior of the copolyesters was more similar to that of PBS in the case of enzymatic degradation. Regarding the acidic medium, the results were in between enzymatic and hydrolytic degradation, but far away from those obtained for the PBS homopolymer, as the homopolymer achieved a 30 wt% weight loss, compared to the 10-15 wt% of the copolymers.

Han *et al.* studied the enzymatic degradation behavior for different poly(butylene succinate-*ran*-butylene 2-methylsuccinate) (PBS-*ran*-PBMS) copolyesters, reporting higher degradation rates for those copolymers with a higher PBMS content. Considering the copolymer with 20 mol% in PBMS, the hydrolytic degradation (without the enzyme) showed a negligible weight loss compared to that of the enzymatic degradation (amano lipase from *Pseudomonas fluorescens*), achieving a 30 wt% weight loss in 300 hours.[163]

The copolymerization of PBS with salicylic acid was studied as an attempt to produce polymer films with potential applications in agricultural applications. Enzymatic degradation assays carried out in the presence of CalB showed very low degradation after 20 days (~1.5 wt% for neat PBS); however, the addition of salicylic acid increased this value up to ~3.5 wt%.[166]

In the case of the enzymatic hydrolysis of PBS and PBS-*ran*-PBA copolymers in the presence of *Candida cylindracea* lipase,[167] the highest degradation was obtained for the copolyesters containing 25 and 50 mol% of butylene succinate, reaching 20 and 30 wt% weight loss values, respectively, after 90 hours. It is necessary to remark that the enzymatic degradation is not affected by the molecular weight; hence, similar results are obtained for low M_w (~6300 g/mol) and high M_w (~29,000 g/mol).[168]

2.3.4. Biodegradation in environmental conditions

Although enzymatic hydrolysis (laboratory conditions) has shown satisfactory results for PBS biodegradation, this biopolyester commonly degrades

in environmental conditions.[169] The study of the biodegradation of PBS under environmental conditions will give an idea for the implementation of PBS in agricultural applications such as mulching films.[61,108,170] PE films are commonly employed for this application, being an effective method for promoting plant growth during the cold seasons (i.e., spring and autumn). The problem here is the recyclability of the PE film due to the contamination caused to the soil itself, so a biodegradable film is required, and PBS is a suitable candidate to solve this issue.[171]

The experiments for this type of biodegradation are usually carried out following different standards from international organizations (ISO, ASTM, and EU). Because of this, the definition of more experimental parameters is required as compared to enzymatic and hydrolytic assays. As the conditions and parameters differ from one study to another (as well as the soil employed for the tests and the microorganisms content in the soil), biodegradation in environmental conditions covers a wide range of variable results.[172] Below we summarize the representative results corresponding to biodegradation studies carried out under environmental conditions for PBS homopolymer and copolymers, with special focus on PBS composites with biofillers (PBS-based biocomposites).

a. PBS homopolymer and PBS-based copolymers

PBS biodegradation in environmental conditions usually takes more time as compared to enzymatic/hydrolytic PBS degradation. Kim *et al.* reported a low degradation of PBS when exposed to environmental degradation (<8 wt% weight loss after 120 days).[173] Similar trends have been obtained by Huang *et al.* (<3 wt% weight loss in 100 days)[174] and other reports.[145] However, the study of PBS biodegradation in a controlled compost at 58 ºC (based on ISO 14855-2) showed that PBS powder biodegradation reached 60 wt% weight loss in 40 days and increased to 80 wt% in less than 80 days. These results are highly promising, opening a path for the establishment of experimental protocols to determine the environmental biodegradation of this aliphatic polyester.[144] These outstanding

results are explained as the PBS was tested in powder form, which differs from the tensile specimens commonly used to determine environmental biodegradation.

The biodegradation of PBS and PBS-*ran*-PBA copolymers subjected to different environments, as biodegradation in compost, soil, and artificial weathering, has been reported. For the artificial weathering, both polymers were submitted to UVA radiation and artificial rain, whereas in soil and compost experiments, no radiation was employed. For the first assay, a ~30 wt% weight loss was achieved for PBS in 24 weeks (~50 wt% in the case of the PBS-*ran*-PBA copolymer). In contrast, biodegradation in soil and artificial weathering showed negligible degradation for PBS, while PBS-*ran*-PBA presented a ~20 wt% weight loss for the biodegradation in soil experiment and negligible for artificial weathering.[107] In another study, the biodegradation of PBS-*ran*-PBFur copolymers in compost at 58 ºC showed the best results for the 20 mol% of furanoate composition, achieving an almost 100 % of degradation in 80 days.[96]

b. PBS-based biocomposites

The presence of fillers in PBS biocomposites has been widely studied to modulate the degradation in environmental conditions, as in the case of other types of degradation and thermomechanical and barrier properties, as we have seen in previous sections. Special cases are natural fillers, that, in addition to being easily biodegraded, can potentially increase the degradation rate of PBS. Table 2.3 includes several examples of biodegradation studies carried out under environmental conditions for different PBS-based biocomposites. Among all the examples presented in this table, some interesting results will be commented on below. As a general idea to consider, the trend shows that PBS-based biocomposites degrade faster than neat PBS.

Table 2.3. Different biodegradation studies of PBS and PBS biocomposites carried out in environmental conditions.

Filler	Content (wt%)	Experimental conditions	Results (Weight loss)	Ref.
Rubberwood powders (RWP)	0-40	60 days, no UV radiation, water control each 48 h	< 1 wt% (PBS) 2-10 wt% (PBS/RWP)	145
Rice husk flour (RHF) and wood flour (WF)	0-40	4 months	7 wt% (PBS) 8-12 wt% (PBS/RHF and PBS/WF)	173
Sugarcane rind fiber (SRF)	0-15	100 days, natural soil in cropland, water control each 24 h	2.5 wt% (PBS) 10-20 wt% (PBS/SRF)	174
Microcrystalline cellulose (MCC) and nanofibrillated cellulose (NFC)	0-40	75 days, simulated compost, 58 ºC, pH = 5.7-6.3, 50 wt% water content	100 wt% in 75-80 days (PBS) 100 wt% in 65-70 days (PBS/MCC and PBS/NFC)	175
Cotton fiber (CF)	0-40	Based on ISO 14855-2 100 days, 58 ºC, 10 mL/min air flow	~60 wt% (PBS) ~90 wt% (PBS/CF)	176
Rice husk flour (RHF)	0-40	Based on ASTM D 6003-96 80 days, 30 ºC, pH = 7, 50-60 wt% water content	~12 wt% (PBS) 13-18 wt% (PBS/RHF)	177

Jute fiber (JF)	0-30	180 days, compost soil, 30 ºC, constant water control	31.4 wt% (PBS) 47.3-62.5 wt% (PBS/JF)	178
Abaca fiber (AF)	10	180 days, black soil and leaf mold for gardening, 25-30 ºC, water control each 48 h	~30 wt% (PBS) ~50 wt% (PBS/AF)	179
Soy, canola, and corn gluten meals (SM, CM, CGM) and switchgrass (SG)	25	Based on ASTM D6400 200 days, 3 month-old compost, 58 ºC, pH = 7-8, 50-55 wt% water content	~95 wt% (PBS) ~85 wt% (PBS/SG) 90-95 wt% (PBS/SM, PBS/CM and PBS/CGM)	180
Organically modified montmorillonite (OMMT)	0-10	180 days, natural compost, 30 ºC, pH = 7.46, 60-70 wt% water content	~9 wt% (PBS) ~3.5-5 wt% (PBS/OMMT)	181
Nanofibrillated cellulose (NFC) and recycled cellulose (rCell)	0-15 (PBS/NFC) 0-50 (PBS/rCell)	80 days, 58 ºC, pH = 5.7-6.5, >50 wt% water content	~80 wt% (PBS) ~85-92 wt% (PBS/NFC) 100 wt% in 70 days (PBS/rCell)	182,183
Pistachio shell flour (PSF)	0-30	Based on ISO 20200 112 days, compost, 58 ºC, 55 % relative humidity	~18 wt% (PBS) ~14-17.5 wt% (PBS/PSF)	184

Although the experimental conditions differ from one study to another, it has been observed that cellulose fillers (micro- or nano-sized) achieve one of the best results for PBS degradation. Platnieks *et al.* have studied many different PBS/cellulose-based composite films: microcrystalline cellulose (MCC),[175] nanofibrillated cellulose (NFC),[161,168] and recycled cellulose from TetraPak®.[183] The experimental conditions were similar for all the studies, employing a simulated compost under aerobic conditions at 58 ºC, with a slightly acidic medium (pH = 5.7-6.5) and a water content of 50 % or higher. The authors found that, although almost every sample was completely disintegrated within 75-80 days, PBS-biocomposites degraded 5-10 days earlier than neat PBS films. In general, the degradation rate was faster at higher filler content. However, for the PBS/rCell biocomposite with the highest content in rCell, the degradation rate was faster in the early stages of the assay, whereas it slowed down during the course of the experiment (see Figure 2.9a-c). If we compare the results corresponding to the PBS biocomposites with high filler content (i.e., 40 wt%), it was found that the PBS/MCC composite degraded faster than the other two biocomposites (i.e., PBS/NFC and PBS/rCell) which present a similar behavior, being much faster than the biodegradation of neat PBS (see Figure 2.9d).

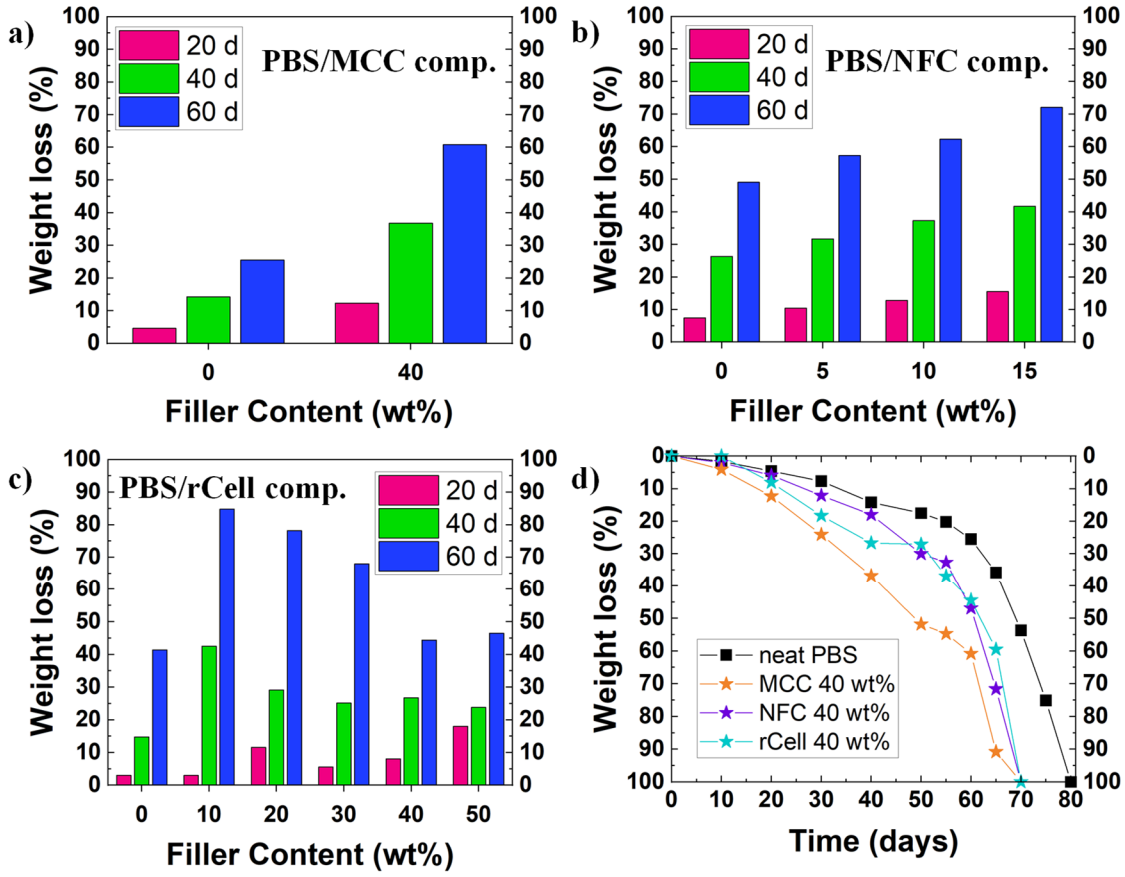

Figure 2.9. Biodegradation in environmental conditions for several PBS/cellulose-based biocomposites: influence of filler content in weight loss for: **a)** PBS/MCC composites, **b)** PBS/NFC composites, and **c)** PBS/rCell composites. **d)** Variation of biodegradation rates for PBS and the three PBS/cellulose-based biocomposites. In Figures 2.9a-c, weight losses at 20, 40, and 60 days are represented. Data taken from Refs.[175,182,183]

Other PBS biocomposites include rubberwood powder (RWP) from sawdust wastes as a natural filler (lignocellulosic nature). The environmental degradation of these PBS/RWP biocomposites was studied, showing a ~10 wt% weight loss after 60 days of soil burial testing. This behavior was attributed to the decrease in the crystallinity of the PBS biocomposites with the increasing content of RWP.[145] In another example, the biodegradation of the PBS biocomposites with rice husk flour (RHF) and wood flour (WF) in soil burial testing showed a 10 wt% degradation for the RHF composites after 120 days.[173] In both cases, the weight loss was directly related to the biocomposite content, increasing with the filler content.

In this section, we have discussed the biodegradation of PBS and PBS-based materials in environmental conditions, which could lead to the employment of this biopolyester as mulching films for agricultural purposes. As has been commented on within this section, PBS presents a slower degradation rate when subjected to environmental conditions than enzymatic and hydrolysis conditions. However, its effective disintegration in the environment opens the door to many interesting applications where the material should not remain in the environment but needs to be usable for a certain period of time, as for the aforementioned agricultural uses such as plastic mulching films.[20]

2.4. Conclusions and Future Perspectives

This Chapter focused on reviewing the current strategies to modulate the thermo-mechanical, barrier, and biodegradation properties of PBS. The modulation of the high crystallization and low degradation rates are desired for the commercial applications of PBS. With this aim, we revised the random copolymerization of PBS. PBS random copolyesters displayed a rich crystallization behavior since they can crystallize in three crystallization modes: isomorphism, comonomer exclusion, and isodimorphism. Independently of the crystallization mode, the PBS-rich compositions can crystallize, in most cases with a depression of the transition temperatures and the crystallinity. These thermal properties depression, on the one hand, extends the applications of PBS copolymers to a broad range of final use temperatures, and, on the other hand, represents the desired reduction of the high crystallinity of PBS, which influences its mechanical properties and degradation, among others. As a result, PBS-based copolymers are promising materials, as copolymerization is an excellent route to tune the properties of PBS.

The modulation of the mechanical and barrier properties can also be achieved by using fillers (micro- and nanosized particles) as additives, creating composite materials based on PBS. Currently, in this revision, we have found that several fillers are being investigated to tailor the PBS properties, including inorganic and organic fillers with bio-based nanofillers. One of the most investigated bio-based nanofillers is cellulose nanowhiskers due to the possibility of achieving fully biodegradable composite materials. The mechanical and barrier properties improvements are generally attained at a low filler content. Nevertheless, the design of composite PBS materials and the study of the resulting properties must be done on a one-by-one case because the final performance depends on many variables (filler dimensionality, interaction between the polymer matrix and the filler, and many others).

This Chapter highlights the wide variety of existing methodologies in the literature to measure PBS degradation through different routes (hydrolytic, enzymatic, and soil). Enzymatic degradation constitutes one of the most promising routes to biodegrade this polymer. However, the results reported in the literature are highly influenced by the type and concentration of the enzyme employed in the experiments and the experimental conditions (i.e., temperature), making it difficult to establish common trends in the enzymatic degradation of PBS. It is then foreseeable and necessary to develop standard protocols or set up general experimental methodologies to measure enzymatic PBS degradation to support the rapid development of PBS and its copolymers.

Future research is needed to continue tailoring PBS properties. From a synthesis point of view, implementing sustainable and efficient polymerization routes from bio-based monomers will be required. In this line, "green catalysts" (i.e., enzymes, revised in this contribution) emerge as a strong alternative, intending to achieve high-M_w PBS with comparable properties to those obtained from traditional polycondensation routes. For the modulation of PBS properties, investigating the structure–properties relationship of PBS and PBS-based materials and its relation to processing is necessary in aiming to design commercial applications for this biopolyester. The modulation strategies should strive to achieve the desired changes, e.g., decreasing the crystallinity, without affecting the biodegradable character of the PBS.

2.5. References

1. Plastics Europe, G. M. R.; GmbH, C. M. & S., Plastics - the fast Facts 2023. *Plastics Europe* **2023**, *1* (October).

2. Europe, P., Plastics – the Facts 2022. *Plastic Europe* **2022**, *1* (October), 1–80.

3. Geyer, R.; Jambeck, J. R.; Law, K. L., Production, use, and fate of all plastics ever made. *Science Advances* **2017**, *3* (7), 19–24. DOI: 10.1126/sciadv.1700782.

4. Rosenboom, J.-G.; Langer, R.; Traverso, G., Bioplastics for a circular economy. *Nature Reviews Materials* **2022**, *7*, 117–137. DOI: 10.1038/s41578-021-00407-8.

5. Rafiqah, S. A.; Khalina, A.; Harmaen, A. S.; Tawakkal, I. A.; Zaman, K.; Asim, M.; Nurrazi, M. N.; Lee, C. H., A review on properties and application of bio-based poly(butylene succinate). *Polymers* **2021**, *13* (9), 1436. DOI: 10.3390/polym13091436.

6. Chen, G. Q.; Patel, M. K., Plastics derived from biological sources: Present and future: A technical and environmental review. *Chemical Reviews* **2012**, *112* (4), 2082–2099. DOI: 10.1021/cr200162d.

7. Chinthapalli, R.; Skoczinski, P.; Carus, M.; Baltus, W.; De Guzman, D.; Käb, H.; Raschka, A.; Ravenstijn, J., Biobased Building Blocks and Polymers - Global Capacities, Production and Trends, 2018-2023. *Industrial Biotechnology* **2019**, *15* (4), 237–241. DOI: 10.1089/ind.2019.29179.rch.

8. Jambeck, J. R.; Ji, Q.; Zhang, Y.-G.; Liu, D.; Grossnickle, D. M.; Luo, Z.-X., Plastic waste inputs from land into the ocean. *Science* **2015**, *347* (6223), 764–768. DOI: 10.1126/science.1260879.

9. ten Brink, P.; Schweitzer, J.-P.; Watkins, E.; Janssens, C.; De Smet, M.; Leslie, H.; Galgani, F., Circular economy measures to keep plastics and their value in the economy, avoid waste and reduce marine litter. *Economics Discussion Papers* **2018**, *3* (January), 15.

10. Abhilash, M.; Thomas, D., Biopolymers for Biocomposites and Chemical Sensor Applications. In: *Biopolymer Composites in Electronics*. (Elsevier Inc.) **2017**, 405–435. DOI: 10.1016/B978-0-12-809261-3.00015-2.

11. Skoczinski, P.; Carus, M.; Tweddle, G.; Ruiz, P.; Guzman, D. de; Ravenstijn, J.; Käb, H.; Hark, N.; Dammer, L.; Raschka, A., Bio-based Building Blocks and Polymers: Global Capacities, Production and Trends 2022–2027. *Industrial Biotechnology* **2023**, *02* (February), 1–28. DOI: 10.52548/CMZD8323.

12. European Bioplastics, Bioplastics Market Development Update 2023. **2023**, *1* (December), 1–2.

13. Bianchi, M.; Dorigato, A.; Morreale, M.; Pegoretti, A., Evaluation of the Physical and Shape Memory Properties of Fully Biodegradable Poly(lactic acid) (PLA)/Poly(butylene adipate terephthalate) (PBAT) Blends. *Polymers* **2023**, *15* (4), 881. DOI: 10.3390/polym15040881.

14. Zhang, Q.; Song, M.; Xu, Y.; Wang, W.; Wang, Z.; Zhang, L., Bio-based polyesters: Recent progress and future prospects. *Progress in Polymer Science* **2021**, *120*, 101430. DOI: 10.1016/j.progpolymsci.2021.101430.

15. Akhir, M. A. M.; Zubir, S. A.; Mariatti, J., Effect of different starch contents on physical, morphological, mechanical, barrier, and biodegradation properties of tapioca starch and poly(butylene adipate-co-terephthalate) blend film. *Polymers for Advanced Technologies* **2023**, *34* (2), 717–730. DOI: 10.1002/pat.5922.

16. Weng, Y. X.; Jin, Y. J.; Meng, Q. Y.; Wang, L.; Zhang, M.; Wang, Y. Z., Biodegradation behavior of poly(butylene adipate-co-terephthalate) (PBAT), poly(lactic acid) (PLA), and their blend under soil conditions. *Polymer Testing* **2013**, *32* (5), 918–926. DOI: 10.1016/j.polymertesting.2013.05.001.

17. Safari, M.; Otaegi, I.; Aramburu, N.; Guerrica-Echevarria, G.; De Ilarduya, A. M.; Sardon, H.; Müller, A. J., Synthesis, structure, crystallization and mechanical properties of isodimorphic PBS-ran-PCL copolyesters. *Polymers* **2021**, *13* (14), 2263. DOI: 10.3390/polym13142263.

18. Botta, L.; Titone, V.; Mistretta, M. C.; La Mantia, F. P.; Modica, A.; Bruno, M.; Sottile, F.; Lopresti, F., PBAT based composites reinforced with microcrystalline cellulose obtained from softwood almond shells. *Polymers* **2021**, *13* (16), 2643. DOI: 10.3390/polym13162643.

19. Li, W.; Sun, C.; Li, C.; Xu, Y.; Tan, H.; Zhang, Y., Preparation of effective ultraviolet shielding poly (lactic acid)/poly (butylene adipate-co-terephthalate) degradable composite film using co-precipitation and hot-pressing method. *International Journal of Biological Macromolecules* **2021**, *191* (August), 540–547. DOI: 10.1016/j.ijbiomac.2021.09.097.

20. Satti, S. M.; Shah, A. A., Polyester-based biodegradable plastics: an approach towards sustainable development. *Letters in Applied Microbiology* **2020**, *70* (6), 413–430. DOI: 10.1111/lam.13287.

21. Gigli, M.; Fabbri, M.; Lotti, N.; Gamberini, R.; Rimini, B.; Munari, A., Poly(butylene succinate)-based polyesters for biomedical applications: A review in memory of our beloved colleague and friend Dr. Lara Finelli. *European Polymer Journal* **2016**, *75*, 431–460. DOI: 10.1016/j.eurpolymj.2016.01.016.

22. Zini, E.; Scandola, M., Green Composites: An Overview. *Polymer Composites* **2011**, *32* (2), 1905–1915. DOI: 10.1002/pc.21224.

23. Saratale, R. G.; Cho, S. K.; Saratale, G. D.; Kadam, A. A.; Ghodake, G. S.; Kumar, M.; Bharagava, R. N.; Kumar, G.; Kim, D. S.; Mulla, S. I.; Shin, H. S., A comprehensive overview and recent advances on polyhydroxyalkanoates (PHA) production using various organic waste streams. *Bioresource Technology* **2021**, *325* (January), 124685. DOI: 10.1016/j.biortech.2021.124685.

24. European Bioplastics, Bioplastics market data 2019. Global production capacities of bioplastics 2019-2024. **2020**, *1* (February), 1–4.

25. Ratshoshi, B. K.; Farzad, S.; Görgens, J. F., Techno-economic assessment of polylactic acid and polybutylene succinate production in an integrated sugarcane biorefinery. *Biofuels, Bioproducts and Biorefining* **2021**, *15* (6), 1871–1887. DOI: 10.1002/bbb.2287.

26. Ioannidou, S. M.; Ladakis, D.; Moutousidi, E.; Dheskali, E.; Kookos, I. K.; Câmara-Salim, I.; Moreira, M. T.; Koutinas, A., Techno-economic risk assessment, life cycle analysis and life cycle costing for poly(butylene succinate) and poly(lactic acid) production using renewable resources. *Science of the Total Environment* **2022**, *806*, 150594. DOI: 10.1016/j.scitotenv.2021.150594.

27. Ni, Y.; Richter, G. M.; Mwabonje, O. N.; Qi, A.; Patel, M. K.; Woods, J., Novel integrated agricultural land management approach provides sustainable biomass feedstocks for bioplastics and supports the UK's "net-zero" target. *Environmental Research Letters* **2021**, *16* (1), 014023. DOI: 10.1088/1748-9326/abcf79.

28. Sander, M., Biodegradation of Polymeric Mulch Films in Agricultural Soils: Concepts, Knowledge Gaps, and Future Research Directions. *Environmental Science & Technology* **2019**, *53* (5), 2304–2315. DOI: 10.1021/ACS.EST.8B05208.

29. Wu, F.; Misra, M.; Mohanty, A. K., Challenges and new opportunities on barrier performance of biodegradable polymers for sustainable packaging. *Progress in Polymer Science* **2021**, *117*, 101395. DOI: 10.1016/j.progpolymsci.2021.101395.

30. Platnieks, O.; Gaidukovs, S.; Kumar Thakur, V.; Barkane, A.; Beluns, S., Bio-Based Poly (Butylene Succinate): Recent Progress, Challenges and Future Opportunities. *European Polymer Journal* **2021**, *161* (September), 110855. DOI: 10.1016/j.eurpolymj.2021.110855.

31. Larrañaga, A.; Lizundia, E., A review on the thermomechanical properties and biodegradation behaviour of polyesters. *European Polymer Journal* **2019**, *121*, 109296. DOI: 10.1016/j.eurpolymj.2019.109296.

32. Su, S.; Kopitzky, R.; Tolga, S.; Kabasci, S., Polylactide (PLA) and Its Blends with Poly(butylene succinate) (PBS): A Brief Review. *Polymers* **2019**, *11* (7), 1193. DOI: 10.3390/polym11071193.

33. Sionkowska, A., Current research on the blends of natural and synthetic polymers as new biomaterials: Review. *Progress in Polymer Science* **2011**, *36* (9), 1254–1276. DOI: 10.1016/j.progpolymsci.2011.05.003.

34. Soccio, M.; Dominici, F.; Quattrosoldi, S.; Luzi, F.; Munari, A.; Torre, L.; Lotti, N.; Puglia, D., PBS-based green copolymer as efficient compatibilizer in Thermoplastic inedible Wheat Flour/Poly (Butylene Succinate) Blends. *Biomacromolecules* **2020**, *21* (8), 3254–3269. DOI: 10.1021/acs.biomac.0c00701.

35. Safari, M.; Otaegi, I.; Aramburu, N.; Guerrica-Echevarria, G.; Martínez de Ilarduya, A.; Sardon, H.; Müller, A. J., Synthesis, structure, crystallization and mechanical properties of isodimorphic PBS-ran-PCL copolyesters. *Polymers* **2021**, *13* (14), 2263. DOI: 10.3390/polym13142263.

36. Sandoval, A. J.; Fernández, M. M.; Candal, M. V.; Safari, M.; Santamaria, A.; Müller, A. J., Rheology and Tack Properties of Biodegradable Isodimorphic Poly(butylene succinate)-Ran-Poly(ε-caprolactone) Random Copolyesters and Their Potential Use as Adhesives. *Polymers* **2022**, *14* (February), 623. DOI: 10.3390/polym14030623.

37. Burk, M. J.; Van Dien, S. J.; Burgard, A.; Niu, W., Compositions and methods for the biosynthesis of 1,4-butanediol and its precursors. *US8067214 B2* **2011**.

38. Díaz, A.; Katsarava, R.; Puiggalí, J., Synthesis, properties and applications of biodegradable polymers derived from diols and dicarboxylic acids: from polyesters to poly(ester amide)s. *International Journal of Molecular Sciences* **2014**, *15* (5), 7064–7123. DOI: 10.3390/ijms15057064.

39. Tserki, V.; Matzinos, P.; Pavlidou, E.; Vachliotis, D.; Panayiotou, C., Biodegradable aliphatic polyesters. Part I. Properties and biodegradation of poly(butylene succinate-co-butylene adipate). *Polymer Degradation and Stability* **2006**, *91* (2), 367–376. DOI: 10.1016/j.polymdegradstab.2005.04.035.

40. Tserki, V.; Matzinos, P.; Pavlidou, E.; Panayiotou, C., Biodegradable aliphatic polyesters. Part II. Synthesis and characterization of chain extended poly(butylene succinate-co-butylene adipate). *Polymer Degradation and Stability* **2006**, *91* (2), 377–384. DOI: 10.1016/j.polymdegradstab.2005.04.036.

41. Xu, J.; Guo, B.-H., Microbial succinic acid, its polymer poly(butylene succinate), and applications. In: *Plastics from Bacteria: Natural Functions and Applications*. (Springer-Verlag) **2010**, 347–388. DOI: 10.1007/978-3-642-03287.

42. Xu, J.; Guo, B. H., Poly(butylene succinate) and its copolymers: Research, development and industrialization. *Biotechnology Journal* **2010**, *5* (11), 1149–1163. DOI: 10.1002/biot.201000136.

43. Luyt, A. S.; Malik, S. S., Can biodegradable plastics solve plastic solid waste accumulation? In: *Plastics to Energy: Fuel, Chemicals, and Sustainability Implications*. (Elsevier Inc.) **2019**, 403–423. DOI: 10.1016/B978-0-12-813140-4.00016-9.

44. Zhu, Q. Y.; He, Y. S.; Zeng, J. B.; Huang, Q.; Wang, Y. Z., Synthesis and characterization of a novel multiblock copolyester containing poly(ethylene succinate) and poly(butylene succinate). *Materials Chemistry and Physics* **2011**, *130* (3), 943–949. DOI: 10.1016/j.matchemphys.2011.08.012.

45. Zhou, H.; Wang, X.; Du, Z.; Li, H.; Yu, K., Preparation and characterization of chain extended poly(butylene succinate) foams. *Polymer Engineering and Science* **2015**, *55* (5), 988–994. DOI: 10.1002/pen.23964.

46. Fujimaki, T., Processability and properties of aliphatic polyesters, "BIONOLLE", synthesized by polycondensation reaction. *Polymer Degradation and Stability* **1998**, *59* (1–3), 209–214. DOI: 10.1016/s0141-3910(97)00220-6.

47. Huang, C. Q.; Luo, S. Y.; Xu, S. Y.; Zhao, J. B.; Jiang, S. L.; Yang, W. T., Catalyzed chain extension of poly(butylene adipate) and poly(butylene succinate) with 2,2'-(1,4-phenylene)-bis(2-oxazoline). *Journal of Applied Polymer Science* **2010**, *115* (3), 1555–1565. DOI: 10.1002/app.31160.

48. Zhao, J. B.; Li, K. Y.; Yang, W. T., Chain extension of polybutylene adipate and polybutylene succinate with adipoyl- and terephthaloyl-biscaprolactamate. *Journal of Applied Polymer Science* **2007**, *106* (1), 590–598. DOI: 10.1002/app.26635.

49. Zhao, J. B.; Wu, X. F.; Yang, W. T., Synthesis of aliphatic polyesters by a chain-extending reaction with octamethylcyclotetrasilazane and hexaphenylcyclotrisilazane as chain extenders. *Journal of Applied Polymer Science* **2004**, *92* (5), 3333–3337. DOI: 10.1002/app.20330.

50. Ishii, M.; Okazaki, M.; Shibasaki, Y.; Ueda, M.; Teranishi, T., Convenient synthesis of aliphatic polyesters by distannoxane-catalyzed polycondensation. *Biomacromolecules* **2001**, *2* (4), 1267–1270. DOI: 10.1021/bm015576a.

51. Zhu, C.; Zhang, Z.; Liu, Q.; Wang, Z.; Jin, J., Synthesis and Biodegradation of Aliphatic Polyesters from Dicarboxylic Acids and Diols. *Journal of Applied Polymer Science* **2003**, *90*, 982–990. DOI: 10.1002/app.12722.

52. Azim, H.; Dekhterman, A.; Jiang, Z.; Gross, R. A., Candida antarctica lipase B-catalyzed synthesis of poly(butylene succinate): Shorter chain building blocks also work. *Biomacromolecules* **2006**, *7* (11), 3093–3097. DOI: 10.1021/bm060574h.

53. Debuissy, T.; Pollet, E.; Avérous, L., Enzymatic Synthesis of a Bio-Based Copolyester from Poly(butylene succinate) and Poly((R)-3-hydroxybutyrate): Study of Reaction Parameters on the Transesterification Rate. *Biomacromolecules* **2016**, *17* (12), 4054–4063. DOI: 10.1021/acs.biomac.6b01494.

54. Ciulik, C.; Safari, M.; Martínez de Ilarduya, A.; Morales-Huerta, J. C.; Iturrospe, A.; Arbe, A.; Müller, A. J.; Muñoz-Guerra, S., Poly(butylene succinate-ran-ε-caprolactone) copolyesters: Enzymatic synthesis and crystalline isodimorphic character. *European Polymer Journal* **2017**, *95*, 795–808. DOI: 10.1016/j.eurpolymj.2017.05.002.

55. Safari, M.; Martínez De Ilarduya, A.; Mugica, A.; Zubitur, M.; Muñoz-Guerra, S.; Müller, A. J., Tuning the Thermal Properties and Morphology of Isodimorphic Poly[(butylene succinate)-ran-(ε-caprolactone)] Copolyesters by Changing Composition, Molecular Weight, and Thermal History. *Macromolecules* **2018**, *51* (23), 9589–9601. DOI: 10.1021/acs.macromol.8b01742.

56. Pérez-Camargo, R. A.; Fernández-D'Arlas, B.; Cavallo, D.; Debuissy, T.; Pollet, E.; Avérous, L.; Müller, A. J., Tailoring the structure, morphology, and crystallization of isodimorphic poly(butylene succinate-ran-butylene adipate) random copolymers by changing composition and thermal history. *Macromolecules* **2017**, *50* (2), 597–608. DOI: 10.1021/acs.macromol.6b02457.

57. Arandia, I.; Zaldua, N.; Maiz, J.; Pérez-Camargo, R. A.; Mugica, A.; Zubitur, M.; Mincheva, R.; Dubois, P.; Müller, A. J., Tailoring the isothermal crystallization kinetics of isodimorphic poly(butylene succinate-ran-butylene azelate) random copolymers by changing composition. *Polymer* **2019**, *183*, 121863. DOI: 10.1016/j.polymer.2019.121863.

58. Díaz, A.; Franco, L.; Puiggalí, J., Study on the crystallization of poly(butylene azelate-co-butylene succinate) copolymers. *Thermochimica Acta* **2014**, *575*, 45–54. DOI: 10.1016/j.tca.2013.10.013.

59. Pérez-Camargo, R. A.; Liu, G.; Cavallo, D.; Wang, D.; Müller, A. J., Effect of the crystallization conditions on the exclusion/inclusion balance in biodegradable poly(butylene succinate-ran-butylene adipate) copolymers. *Biomacromolecules* **2020**, *21*, 3420–3435. DOI: 10.1021/acs.biomac.0c00847.

60. Tan, B.; Bi, S.; Emery, K.; Sobkowicz, M. J., Bio-based poly(butylene succinate-co-hexamethylene succinate) copolyesters with tunable thermal and mechanical properties. *European Polymer Journal* **2017**, *86*, 162–172. DOI: 10.1016/j.eurpolymj.2016.11.017.

61. Sisti, L.; Totaro, G.; Marchese, P., PBS makes its entrance into the family of biobased plastics. In: *Biodegradable and Biobased Polymers for Environmental and Biomedical Applications*. (Scrivener Publishing) **2016**, 225–286. DOI: 10.1002/9781119117360.ch7.

62. Pérez-Camargo, R. A.; Arandia, I.; Safari, M.; Cavallo, D.; Lotti, N.; Soccio, M.; Müller, A. J., Crystallization of isodimorphic aliphatic random copolyesters: Pseudo-eutectic behavior and double-crystalline materials. *European Polymer Journal* **2018**, *101*, 233–247. DOI: 10.1016/j.eurpolymj.2018.02.037.

63. Pan, P.; Inoue, Y., Polymorphism and isomorphism in biodegradable polyesters. *Progress in Polymer Science* **2009**, *34* (7), 605–640. DOI: 10.1016/j.progpolymsci.2009.01.003.

64. Arandia, I.; Mugica, A.; Zubitur, M.; Iturrospe, A.; Arbe, A.; Liu, G.; Wang, D.; Mincheva, R.; Dubois, P.; Müller, A. J., Application of SSA thermal fractionation and X-ray diffraction to elucidate comonomer inclusion or exclusion from the crystalline phases in poly(butylene succinate-ran-butylene azelate) random copolymers. *Journal of Polymer Science, Part B: Polymer Physics* **2016**, *54* (22), 2346–2358. DOI: 10.1002/polb.24146.

65. Debuissy, T.; Pollet, E.; Avérous, L., Synthesis and characterization of biobased poly(butylene succinate-ran-butylene adipate). Analysis of the composition-dependent physicochemical properties. *European Polymer Journal* **2017**, *87*, 84–98. DOI: 10.1016/j.eurpolymj.2016.12.012.

66. Hsu, K. H.; Chen, C. W.; Wang, L. Y.; Chan, H. W.; He, C. L.; Cho, C. J.; Rwei, S. P.; Kuo, C. C., Bio-based thermoplastic poly(butylene succinate-co-propylene succinate) copolyesters: Effect of glycerol on thermal and mechanical properties. *Soft Matter* **2019**, *15* (47), 9710–9720. DOI: 10.1039/c9sm01958h.

67. Yu, Y.; Wei, Z.; Liu, Y.; Hua, Z.; Leng, X.; Li, Y., Effect of chain length of comonomeric diols on competition and miscibility of isodimorphism: A comparative study of poly(butylene glutarate-co-butylene azelate) and poly(octylene glutarate-co-octylene azelate). *European Polymer Journal* **2018**, *105*, 274–285. DOI: 10.1016/j.eurpolymj.2018.06.006.

68. Yu, Y.; Wei, Z.; Zheng, L.; Jin, C.; Leng, X.; Li, Y., Competition and miscibility of isodimorphism and their effects on band spherulites and mechanical properties of poly(butylene succinate-co-cis-butene succinate) unsaturated aliphatic copolyesters. *Polymer* **2018**, *150*, 52–63. DOI: 10.1016/j.polymer.2018.07.024.

69. Yu, Y.; Wei, Z.; Zhou, C.; Zheng, L.; Leng, X.; Li, Y., Miscibility and competition of cocrystallization behavior of poly(hexamethylene dicarboxylate)s aliphatic copolyesters: Effect of chain length of aliphatic diacids. *European Polymer Journal* **2017**, *92*, 71–85. DOI: 10.1016/j.eurpolymj.2017.04.036.

70. Arandia, I.; Mugica, A.; Zubitur, M.; Arbe, A.; Liu, G.; Wang, D.; Mincheva, R.; Dubois, P.; Müller, A. J., How composition determines the properties of isodimorphic poly(butylene succinate-ran-butylene azelate) random biobased copolymers: From single to double crystalline random copolymers. *Macromolecules* **2015**, *48* (1), 43–57. DOI: 10.1021/ma5023567.

71. Arandia, I.; Mugica, A.; Zubitur, M.; Mincheva, R.; Dubois, P.; Müller, A. J.; Alegría, A., The Complex Amorphous Phase in Poly(butylene succinate-ran-butylene azelate) Isodimorphic Copolyesters. *Macromolecules* **2017**, *50* (4), 1569–1578. DOI: 10.1021/acs.macromol.6b02713.

72. Safari, M.; Leon Boigues, L.; Shi, G.; Maiz, J.; Liu, G.; Wang, D.; Mijangos, C.; Müller, A. J., Effect of Nanoconfinement on the Isodimorphic Crystallization of Poly(butylene succinate- ran-caprolactone) Random Copolymers. *Macromolecules* **2020**, *53* (15), 6486–6497. DOI: 10.1021/acs.macromol.0c01081.

73. Safari, M.; Mugica, A.; Zubitur, M.; Martínez De Ilarduya, A.; Muñoz-Guerra, S.; Müller, A. J., Controlling the Isothermal Crystallization of Isodimorphic PBS-ran-PCL Random Copolymers by Varying Composition and Supercooling. *Polymers* **2020**, *12* (1), 17. DOI: 10.3390/polym12010017.

74. Schäfer, M.; Yuan, S.; Petzold, A.; Pérez-Camargo, R. A.; Müller, A. J.; Thurn-Albrecht, T.; Saalwächter, K.; Schmidt-Rohr, K., Asymmetric Co-unit Inclusion in Statistical Copolyesters. *Macromolecules* **2021**, *54* (2), 835–845. DOI: 10.1021/acs.macromol.0c01965.

75. Papageorgiou, G. Z.; Bikiaris, D. N., Synthesis, cocrystallization, and enzymatic degradation of novel poly(butylene-co-propylene succinate) copolymers. *Biomacromolecules* **2007**, *8* (8), 2437–2449. DOI: 10.1021/bm0703113.

76. Debuissy, T.; Sangwan, P.; Pollet, E.; Avérous, L., Study on the structure-properties relationship of biodegradable and biobased aliphatic copolyesters based on 1,3-propanediol, 1,4-butanediol, succinic and adipic acids. *Polymer* **2017**, *122*, 105–116. DOI: 10.1016/j.polymer.2017.06.045.

77. Kluge, M.; Bikiaris, D. N.; Robert, T., Enhancing the properties of poly(propylene succinate) by the incorporation of crystallizable symmetrical amido diols. *European Polymer Journal* **2019**, *120*, 109195. DOI: 10.1016/j.eurpolymj.2019.08.022.

78. Debuissy, T.; Pollet, E.; Avérous, L., Synthesis and characterization of biobased poly(butylene succinate-ran-butylene adipate). Analysis of the composition-dependent physicochemical properties. *European Polymer Journal* **2017**, *87*, 84–98. DOI: 10.1016/j.eurpolymj.2016.12.012.

79. Ye, H. M.; Wang, R. D.; Liu, J.; Xu, J.; Guo, B. H., Isomorphism in poly(butylene succinate-co-butylene fumarate) and its application as polymeric nucleating agent for poly(butylene succinate). *Macromolecules* **2012**, *45* (14), 5667–5675. DOI: 10.1021/ma300685f.

80. Zheng, L.; Wang, Z.; Wu, S.; Li, C.; Zhang, D.; Xiao, Y., Novel poly(butylene fumarate) and poly(butylene succinate) multiblock copolymers bearing reactive carbon-carbon double bonds: Synthesis, characterization, cocrystallization, and properties. *Industrial & Engineering Chemistry Research* **2013**, *52* (18), 6147–6155. DOI: 10.1021/ie303573d.

81. Wei, X. W.; Huang, G.; Wang, J.; Meng, X.; Zhou, Q.; Ye, H. M., Tailoring crystallization of random terpolyester: Combination of isodimorphism and isomorphism. *Macromolecules* **2020**, *53* (20), 8918–8927. DOI: 10.1021/acs.macromol.0c01689.

82. Wei, X. W.; Yang, L. L.; Li, Y.; Meng, X.; Cai, L. H.; Zhou, Q.; Ye, H. M., Asymmetrical formation of isomorphism in the crystalline/crystalline blend of poly(butylene succinate) and poly(butylene fumarate). *Polymer* **2021**, *235*, 124282. DOI: 10.1016/j.polymer.2021.124282.

83. Poussard, L.; Mecheri, A.; Mariage, J.; Barakat, I.; Bonnaud, L.; Raquez, J. M.; Dubois, P., Synthesis of oligo(butylene succinate)-based polyurethanes: Influence of the chemical structure on thermal and mechanical properties. *Journal of Renewable Materials* **2014**, *2* (1), 13–22. DOI: 10.7569/JRM.2013.634132.

84. Jamaluddin, N.; Razaina, M. T.; Ishak, Z. . M., Mechanical and Morphology Behaviours of Polybutylene (succinate)/Thermoplastic Polyurethaneblend. *Procedia Chemistry* **2016**, *19*, 426–432. DOI: 10.1016/j.proche.2016.03.034.

85. Kim, T.; Jeon, H.; Jegal, J.; Kim, J. H.; Yang, H.; Park, J.; Oh, D. X.; Hwang, S. Y., Trans crystallization behavior and strong reinforcement effect of cellulose nanocrystals on reinforced poly(butylene succinate) nanocomposites. *RSC Advances* **2018**, *8* (28), 15389–15398. DOI: 10.1039/c8ra01868e.

86. Then, Y. Y.; Ibrahim, N. A.; Zainuddin, N.; Chieng, B. W.; Ariffin, H.; Zin Wan Yunus, W. M., Effect of 3-aminopropyltrimethoxysilane on chemically modified oil palm mesocarp fiber/poly(butylene succinate) biocomposite. *BioResources* **2015**, *10* (2), 3577–3601. DOI: 10.15376/biores.10.2.3577-3601.

87. Xu, J.; Manepalli, P. H.; Zhu, L.; Narayan-Sarathy, S.; Alavi, S., Morphological, barrier and mechanical properties of films from poly(butylene succinate) reinforced with nanocrystalline cellulose and chitin whiskers using melt extrusion. *Journal of Polymer Research* **2019**, *26* (8), 1–10. DOI: 10.1007/s10965-019-1783-8.

88. Petchwattana, N.; Covavisaruch, S.; Wibooranawong, S.; Naknaen, P., Antimicrobial food packaging prepared from poly(butylene succinate) and zinc oxide. *Measurement: Journal of the International Measurement Confederation* **2016**, *93*, 442–448. DOI: 10.1016/j.measurement.2016.07.048.

89. Zainal Abidin, A. S.; Yusoh, K.; Jamari, S. S.; Abdullah, A. H.; Ismail, Z., Surface functionalization of graphene oxide with octadecylamine for improved thermal and mechanical properties in polybutylene succinate nanocomposite. *Polymer Bulletin* **2018**, *75* (8), 3499–3522. DOI: 10.1007/s00289-017-2217-6.

90. Ludueña, L. N.; Fortunati, E.; Morán, J. I.; Alvarez, V. A.; Cyras, V. P.; Puglia, D.; Manfredi, L. B.; Pracella, M., Preparation and characterization of polybutylene-succinate/poly(ethylene-glycol)/cellulose nanocrystals ternary composites. *Journal of Applied Polymer Science* **2016**, *133* (15), 43302. DOI: 10.1002/app.43302.

91. Planellas, M.; Sacristán, M.; Rey, L.; Olmo, C.; Aymamí, J.; Casas, M. T.; Del Valle, L. J.; Franco, L.; Puiggalí, J., Micro-molding with ultrasonic vibration energy: New method to disperse nanoclays in polymer matrices. *Ultrasonics Sonochemistry* **2014**, *21* (4), 1557–1569. DOI: 10.1016/j.ultsonch.2013.12.027.

92. Henke, L.; Zarrinbakhsh, N.; Endres, H. J.; Misra, M.; Mohanty, A. K., Biodegradable and Bio-based Green Blends from Carbon Dioxide-Derived Bioplastic and Poly(Butylene Succinate). *Journal of Polymers and the Environment* **2016**, *25* (2), 499–509. DOI: 10.1007/s10924-016-0828-x.

93. Phua, Y. J.; Chow, W. S.; Mohd Ishak, Z. A., Reactive processing of maleic anhydride-grafted poly(butylene succinate) and the compatibilizing effect on poly(butylene succinate) nanocomposites. *Express Polymer Letters* **2013**, *7* (4), 340–354. DOI: 10.3144/expresspolymlett.2013.31.

94. He, L.; Song, F.; Li, D. F.; Zhao, X.; Wang, X. L.; Wang, Y. Z., Strong and Tough Polylactic Acid Based Composites Enabled by Simultaneous Reinforcement and Interfacial Compatibilization of Microfibrillated Cellulose. *ACS Sustainable Chemistry and Engineering* **2020**, *8* (3), 1573–1582. DOI: 10.1021/acssuschemeng.9b06308.

95. Dai, X.; Qiu, Z., Synthesis and properties of novel biodegradable poly(butylene succinate-co-decamethylene succinate) copolyesters from renewable resources. *Polymer Degradation and Stability* **2016**, *134*, 305–310. DOI: 10.1016/j.polymdegradstab.2016.11.004.

96. Jacquel, N.; Saint-Loup, R.; Pascault, J. P.; Rousseau, A.; Fenouillot, F., Bio-based alternatives in the synthesis of aliphatic-aromatic polyesters dedicated to biodegradable film applications. *Polymer* **2015**, *59*, 234–242. DOI: 10.1016/j.polymer.2014.12.021.

97. Genovese, L.; Lotti, N.; Gazzano, M.; Siracusa, V.; Dalla Rosa, M.; Munari, A., Novel biodegradable aliphatic copolyesters based on poly(butylene succinate) containing thioether-linkages for sustainable food packaging applications. *Polymer Degradation and Stability* **2016**, *132*, 191–201. DOI: 10.1016/j.polymdegradstab.2016.02.022.

98. Shirali, H.; Rafizadeh, M.; Afshar Taromi, F.; Jabbari, E., Fabrication of in situ polymerized poly(butylene succinate-co-ethylene terephthalate)/hydroxyapatite nanocomposite to fibrous scaffolds for enhancement of osteogenesis. *Journal of Biomedical Materials Research - Part A* **2017**, *105* (9), 2622–2631. DOI: 10.1002/jbm.a.36115.

99. Ojijo, V.; Sinha Ray, S., Processing strategies in bionanocomposites. *Progress in Polymer Science* **2013**, *38* (10–11), 1543–1589. DOI: 10.1016/j.progpolymsci.2013.05.011.

100. Ojijo, V.; Sinha Ray, S., Nano-biocomposites based on synthetic aliphatic polyesters and nanoclay. *Progress in Materials Science* **2014**, *62* (2014), 1–57. DOI: 10.1016/j.pmatsci.2014.01.001.

101. Joy, J.; Jose, C.; Varanasi, S. B.; Mathew, L. P.; Thomas, S.; Pilla, S., Preparation and characterization of poly(butylene succinate) bionanocomposites reinforced with cellulose nanofiber extracted from Helicteres isora plant. *Journal of Renewable Materials* **2016**, *4* (5), 351–364. DOI: 10.7569/JRM.2016.634128.

102. Saeed, U.; Nawaz, M. A.; Al-Turaif, H. A., Wood flour reinforced biodegradable PBS/PLA composites. *Journal of Composite Materials* **2018**, *52* (19), 2641–2650. DOI: 10.1177/0021998317752227.

103. Chen, Z.; Gan, L.; Chang, P. R.; Liu, C.; Huang, J.; Gao, S., Cost Reduction and Mechanical Enhancement of Biopolyesters Using an Agricultural Byproduct from Konjac Glucomannan Processing. *ACS Sustainable Chemistry and Engineering* **2017**, *5* (8), 6498–6506. DOI: 10.1021/acssuschemeng.7b00615.

104. Brody, A. L., Packaging of Foods. *Encyclopedia of Food Microbiology: Second Edition* **2014**, *2*, 1017–1027. DOI: 10.1016/B978-0-12-384730-0.00244-5.

105. Li, S. L.; Wu, F.; Yang, Y.; Wang, Y. Z.; Zeng, J. B., Synthesis, characterization and isothermal crystallization behavior of poly(butylene succinate)-b-poly(diethylene glycol succinate) multiblock copolymers. *Polymers for Advanced Technologies* **2015**, *26* (8), 1003–1013. DOI: 10.1002/pat.3519.

106. Robeson, L. M., Polymer Membranes. In: *Polymer Science: A Comprehensive Reference*. (Elsevier B.V.) **2012**, 325–347. DOI: 10.1016/B978-0-444-53349-4.00211-9.

107. Puchalski, M.; Szparaga, G.; Biela, T.; Gutowska, A.; Sztajnowski, S.; Krucińska, I., Molecular and supramolecular changes in polybutylene succinate (PBS) and polybutylene succinate adipate (PBSA) copolymer during degradation in various environmental conditions. *Polymers* **2018**, *10* (3), 1–12. DOI: 10.3390/polym10030251.

108. Ayu, R. S.; Khalina, A.; Harmaen, A. S.; Zaman, K.; Mohd Nurrazi, N.; Isma, T.; Lee, C. H., Effect of empty fruit brunch reinforcement in polybutylene-succinate/modified tapioca starch blend for agricultural mulch films. *Scientific Reports* **2020**, *10* (1), 1166. DOI: 10.1038/s41598-020-58278-y.

109. Lagarón, J.-M., Multifunctional and nanoreinforced polymers for food packaging. In: *Multifunctional and Nanoreinforced Polymers for Food Packaging*. (Woodhead Publishing Limited) **2011**, 1–28. DOI: 10.1533/9780857092786.1.

110. Nazrin, A.; Sapuan, S. M.; Zuhri, M. Y. M.; Ilyas, R. A.; Syafiq, R.; Sherwani, S. F. K., Nanocellulose Reinforced Thermoplastic Starch (TPS), Polylactic Acid (PLA), and Polybutylene Succinate (PBS) for Food Packaging Applications. *Frontiers in Chemistry* **2020**, *8*, 213. DOI: 10.3389/fchem.2020.00213.

111. Siracusa, V.; Lotti, N.; Munari, A.; Dalla Rosa, M., Poly(butylene succinate) and poly(butylene succinate-co-adipate) for food packaging applications: Gas barrier properties after stressed treatments. *Polymer Degradation and Stability* **2015**, *119*, 35–45. DOI: 10.1016/j.polymdegradstab.2015.04.026.

112. Giacinti Baschetti, M.; Minelli, M., Test methods for the characterization of gas and vapor permeability in polymers for food packaging application: A review. *Polymer Testing* **2020**, *89*, 106606. DOI: 10.1016/j.polymertesting.2020.106606.

113. Massey, L. K., Permeability properties of plastics and elastomers: A guide to packaging and barrier materials. (Plastics Design Library) **2003**, 1–585. DOI: 10.1016/s0168-3659(03)00333-x.

114. Číhal, P.; Vopička, O.; Lanč, M.; Kludský, M.; Velas, J.; Hrdlička, Z.; Michalcová, A.; Dendisová, M.; Friess, K., Poly(butylene succinate)-cellulose triacetate blends: permeation, pervaporation, sorption and physical structure. *Polymer Testing* **2018**, *65*, 468–479. DOI: 10.1016/j.polymertesting.2017.12.026.

115. Guidotti, G.; Soccio, M.; Siracusa, V.; Gazzano, M.; Salatelli, E.; Munari, A.; Lotti, N., Novel random PBS-based copolymers containing aliphatic side chains for sustainable flexible food packaging. *Polymers* **2017**, *9* (12), 724. DOI: 10.3390/polym9120724.

116. Siracusa, V.; Rocculi, P.; Romani, S.; Rosa, M. D., Biodegradable polymers for food packaging: a review. *Trends in Food Science and Technology* **2008**, *19* (12), 634–643. DOI: 10.1016/j.tifs.2008.07.003.

117. Siracusa, V.; Blanco, I.; Romani, S.; Tylewicz, U.; Rocculi, P.; Rosa, M. D., Poly(lactic acid)-modified films for food packaging application: Physical, mechanical, and barrier behavior. *Journal of Applied Polymer Science* **2012**, *125* (S2), E390–E401. DOI: 10.1002/app.36829.

118. McHugh, T. H.; Krochta, J. M., Sorbitol-vs Glycerol-Plasticized Whey Protein Edible Films: Integrated Oxygen Permeability and Tensile Property Evaluation. *Journal of Agricultural and Food Chemistry* **1994**, *42* (4), 841–845. DOI: 10.1021/jf00040a001.

119. Rudnik, E., Properties and Applications. In: *Compostable Polymer Materials: Second Edition*. (Elsevier) **2019**, 49–98. DOI: 10.1016/B978-0-08-099438-3.00003-3.

120. Okamoto, K.; Ray, S. S.; Okamoto, M., New poly(butylene succinate)/layered silicate nanocomposites. II. Effect of organically modified layered silicates on structure, properties, melt rheology, and biodegradability. *Journal of Polymer Science, Part B: Polymer Physics* **2003**, *41* (24), 3160–3172. DOI: 10.1002/polb.10708.

121. Charlon, S.; Follain, N.; Dargent, E.; Soulestin, J.; Sclavons, M.; Marais, S., Poly[(butylene succinate)-co-(butylene adipate)]-Montmorillonite Nanocomposites Prepared by Water-Assisted Extrusion: Role of the Dispersion Level and of the Structure-Microstructure on the Enhanced Barrier Properties. *Journal of Physical Chemistry C* **2016**, *120* (24), 13234–13248. DOI: 10.1021/acs.jpcc.6b00339.

122. Dean, K. M.; Pas, S. J.; Yu, L.; Ammala, A.; Hill, A. J.; Wu, D. Y., Formation of Highly Oriented Biodegradable Polybutylene Succinate Adipate Nanocomposites: Effects of Cation Structures on Morphology, Free Volume, and Properties. *Journal of Applied Polymer Science* **2009**, *113*, 3716–3724. DOI: 10.1002/app.

123. Bhatia, A.; Gupta, R. K.; Bhattacharya, S. N.; Choi, H. J., Effect of clay on thermal, mechanical and gas barrier properties of biodegradable poly(lactic acid)/poly(butylene succinate) (PLA/PBS) nanocomposites. *International Polymer Processing* **2009**, *25* (1), 5–14. DOI: 10.3139/217.2214.

124. Petersen, K.; Nielsen, P. V.; Olsen, M. B., Physical and mechanical properties of biobased materials - Starch, polylactate and polyhydroxybutyrate. *Starch/Staerke* **2001**, *53* (8), 356–361. DOI: 10.1002/1521-379X(200108)53:8<356::AID-STAR356>3.0.CO;2-7.

125. Olabarrieta, I.; Forsström, D.; Gedde, U. W.; Hedenqvist, M. S., Transport properties of chitosan and whey blended with poly(ε-caprolactone) assessed by standard permeability measurements and microcalorimetry. *Polymer* **2001**, *42* (9), 4401–4408. DOI: 10.1016/S0032-3861(00)00680-7.

126. Bastarrachea, L.; Dhawan, S.; Sablani, S. S., Engineering Properties of Polymeric-Based Antimicrobial Films for Food Packaging. *Food Engineering Reviews* **2011**, *3* (2), 79–93. DOI: 10.1007/s12393-011-9034-8.

127. Xu, Y.; Zhang, S.; Wang, P.; Wang, J., Synthesis of poly(butylene succinate) phosphorus-containing ionomers for versatile crystallization and improved thermal conductivity. *Polymer* **2018**, *154*, 258–271. DOI: 10.1016/j.polymer.2018.09.025.

128. Cosquer, R.; Pruvost, S.; Gouanvé, F., Improvement of barrier properties of biodegradable polybutylene succinate/graphene nanoplatelets nanocomposites prepared by melt process. *Membranes* **2021**, *11* (2), 151. DOI: 10.3390/membranes11020151.

129. Xie, L.; Xu, H.; Chen, J. Bin; Zhang, Z. J.; Hsiao, B. S.; Zhong, G. J.; Chen, J.; Li, Z. M., From nanofibrillar to nanolaminar poly(butylene succinate): Paving the way to robust barrier and mechanical properties for full-biodegradable poly(lactic acid) films. *ACS Applied Materials and Interfaces* **2015**, *7* (15), 8023–8032. DOI: 10.1021/acsami.5b00294.

130. Messin, T.; Marais, S.; Follain, N.; Guinault, A.; Gaucher, V.; Delpouve, N.; Sollogoub, C., Biodegradable PLA/PBS multinanolayer membrane with enhanced barrier performances. *Journal of Membrane Science* **2020**, *598*, 1–11. DOI: 10.1016/j.memsci.2019.117777.

131. Messin, T.; Follain, N.; Guinault, A.; Sollogoub, C.; Gaucher, V.; Delpouve, N.; Marais, S., Structure and Barrier Properties of Multinanolayered Biodegradable PLA/PBSA Films: Confinement Effect via Forced Assembly Coextrusion. *ACS Applied Materials and Interfaces* **2017**, *9* (34), 29101–29112. DOI: 10.1021/acsami.7b08404.

132. Duan, R. T.; He, Q. X.; Dong, X.; Li, D. F.; Wang, X. L.; Wang, Y. Z., Renewable sugar-based diols with different rigid structure: comparable investigation on improving poly(butylene succinate) performance. *ACS Sustainable Chemistry and Engineering* **2016**, *4* (1), 350–362. DOI: 10.1021/acssuschemeng.5b01335.

133. Attallah, O. A.; Mojicevic, M.; Lanzagorta Garcia, E.; Azeem, M.; Chen, Y.; Asmawi, S.; Fournet, M. B., Macro and micro routes to high performance bioplastics: bioplastic biodegradability and mechanical and barrier properties. *Polymers* **2021**, *13*, 2155. DOI: 10.3390/polym13132155.

134. Risse, S.; Tighzert, L.; Berzin, F.; Vergnes, B., Microstructure, rheological behavior, and properties of poly(lactic acid)/poly(butylene succinate)/organoclay nanocomposites. *Journal of Applied Polymer Science* **2014**, *131* (12), 40364. DOI: 10.1002/app.40364.

135. Salehiyan, R.; Ray, S. S., Influence of Nanoclay Localization on Structure–Property Relationships of Polylactide-Based Biodegradable Blend Nanocomposites. *Macromolecular Materials and Engineering* **2018**, *303* (7), 1800134. DOI: 10.1002/mame.201800134.

136. Ray, S. S.; Okamoto, K.; Okamoto, M., Structure-property relationship in biodegradable poly(butylene succinate)/layered silicate nanocomposites. *Macromolecules* **2003**, *36* (7), 2355–2367. DOI: 10.1021/ma021728y.

137. Ilsouk, M.; Raihane, M.; Rhouta, B.; Meri, R. M.; Zicans, J.; Vecstaudža, J.; Lahcini, M., The relationship of structure, thermal and water vapor permeability barrier properties of poly(butylene succinate)/organomodified beidellite clay bionanocomposites prepared by in situ polycondensation. *RSC Advances* **2020**, *10* (61), 37314–37326. DOI: 10.1039/d0ra07521c.

138. Saeng-on, J.; Aht-Ong, D., Compatibility of banana starch nanocrystals/poly(butylene succinate) bio-nanocomposite packaging films. *Journal of Applied Polymer Science* **2018**, *135* (43), 46836. DOI: 10.1002/app.46836.

139. Preedanorawut, R.; Threepopnatkul, P.; Sittatrakul, A., Effect of zeolite types on properties of polybutylene succinate/polylactic acid films. *IOP Conference Series: Materials Science and Engineering* **2020**, *773* (1), 012026. DOI: 10.1088/1757-899X/773/1/012026.

140. Gain, O.; Espuche, E.; Pollet, E.; Alexandre, M.; Dubois, P., Gas barrier properties of poly(ε-caprolactone)/clay nanocomposites: Influence of the morphology and polymer/clay interactions. *Journal of Polymer Science, Part B: Polymer Physics* **2005**, *43* (2), 205–214. DOI: 10.1002/polb.20316.

141. Follain, N.; Belbekhouche, S.; Bras, J.; Siqueira, G.; Chappey, C.; Marais, S.; Dufresne, A., Tunable gas barrier properties of filled-PCL film by forming percolating cellulose network. *Colloids and Surfaces A* **2018**, *545*, 26–30. DOI: 10.1016/j.colsurfa.2018.02.040.

142. Mao, L.; Wu, H.; Liu, Y.; Yao, J.; Bai, Y., Enhanced mechanical and gas barrier properties of poly(ε-caprolactone) nanocomposites filled with tannic acid-Fe(III) functionalized high aspect ratio layered double hydroxides. *Materials Chemistry and Physics* **2018**, *211*, 501–509. DOI: 10.1016/j.matchemphys.2018.03.008.

143. Mohamed, R. M.; Yusoh, K., A Review on the Recent Research of Polycaprolactone (PCL). *Advanced Materials Research* **2015**, *1134*, 249–255. DOI: 10.4028/www.scientific.net/amr.1134.249.

144. Kunioka, M.; Ninomiya, F.; Funabashi, M., Biodegradation of poly(butylene succinate) powder in a controlled compost at 58°C evaluated by naturally-occurring carbon 14 amounts in evolved CO2 based on the ISO 14855-2 method. *International Journal of Molecular Sciences* **2009**, *10* (10), 4267–4283. DOI: 10.3390/ijms10104267.

145. Anankaphong, H.; Pentrakoon, D.; Junkasem, J., Effect of rubberwood content on biodegradability of poly(butylene succinate) biocomposites. *International Journal of Polymer Science* **2015**, *2015*, 19–21. DOI: 10.1155/2015/368341.

146. Ganesh Kumar, A.; Anjana, K.; Hinduja, M.; Sujitha, K.; Dharani, G., Review on plastic wastes in marine environment – Biodegradation and biotechnological solutions. *Marine Pollution Bulletin* **2020**, *150*, 110733. DOI: 10.1016/j.marpolbul.2019.110733.

147. Iram, D.; Riaz, R. A.; Iqbal, R. K., Usage of potential micro-organisms for degradation of plastics. *Open Journal of Environmental Biology* **2019**, *4* (1), 007–0015. DOI: 10.17352/ojeb.000010.

148. Brannigan, R. P.; Dove, A. P., Synthesis, properties and biomedical applications of hydrolytically degradable materials based on aliphatic polyesters and polycarbonates. *Biomaterials Science* **2017**, *5* (1), 9–21. DOI: 10.1039/c6bm00584e.

149. Armentano, I.; Gigli, M.; Morena, F.; Argentati, C.; Torre, L.; Martino, S., Recent advances in nanocomposites based on aliphatic polyesters: Design, synthesis, and applications in regenerative medicine. *Applied Sciences (Switzerland)* **2018**, *8* (9), 1452. DOI: 10.3390/app8091452.

150. Gualandi, C.; Soccio, M.; Govoni, M.; Valente, S.; Lotti, N.; Munari, A.; Giordano, E.; Pasquinelli, G.; Focarete, M. L., Poly(butylene/diethylene glycol succinate) multiblock copolyester as a candidate biomaterial for soft tissue engineering: Solid-state properties, degradability, and biocompatibility. *Journal of Bioactive and Compatible Polymers* **2012**, *27* (3), 244–264. DOI: 10.1177/0883911512440536.

151. Huang, A.; Peng, X.; Geng, L.; Zhang, L.; Huang, K.; Chen, B.; Gu, Z.; Kuang, T., Electrospun poly (butylene succinate)/cellulose nanocrystals bio-nanocomposite scaffolds for tissue engineering: Preparation, characterization and in vitro evaluation. *Polymer Testing* **2018**, *71*, 101–109. DOI: 10.1016/j.polymertesting.2018.08.027.

152. Zhang, Y.; Yuan, W.; Liu, Y., Synthesis and characterization of bio-based poly(butylene succinate-co-10-hydroxydecanoate). *Journal of Elastomers & Plastics* **2018**, *50* (4), 325–338. DOI: 10.1177/0095244317723181.

153. Sheikholeslami, S. N.; Rafizadeh, M.; Taromi, F. A.; Shirali, H.; Jabbari, E., Material properties of degradable Poly(butylene succinate-co-fumarate) copolymer networks synthesized by polycondensation of pre-homopolyesters. *Polymer* **2016**, *98*, 70–79. DOI: 10.1016/j.polymer.2016.06.012.

154. Morales-Huerta, J. C.; Ciulik, C. B.; De Ilarduya, A. M.; Muñoz-Guerra, S., Fully bio-based aromatic-aliphatic copolyesters: Poly(butylene furandicarboxylate-co-succinate)s obtained by ring opening polymerization. *Polymer Chemistry* **2017**, *8* (4), 748–760. DOI: 10.1039/c6py01879c.

155. Hu, X.; Gao, Z.; Wang, Z.; Su, T.; Yang, L.; Li, P., Enzymatic degradation of poly(butylene succinate) by cutinase cloned from Fusarium solani. *Polymer Degradation and Stability* **2016**, *134*, 211–219. DOI: 10.1016/j.polymdegradstab.2016.10.012.

156. Pan, W.; Bai, Z.; Su, T.; Wang, Z., Enzymatic degradation of poly(butylene succinate) with different molecular weights by cutinase. *International Journal of Biological Macromolecules* **2018**, *111*, 1040–1046. DOI: 10.1016/j.ijbiomac.2018.01.107.

157. Bai, Z.; Liu, Y.; Su, T.; Wang, Z., Effect of hydroxyl monomers on the Enzymatic degradation of poly(ethylene succinate), poly(butylene succinate), and poly(hexylene succinate). *Polymers* **2018**, *10* (1), 90. DOI: 10.3390/polym10010090.

158. Shi, K.; Su, T.; Wang, Z., Comparison of poly(butylene succinate) biodegradation by Fusarium solani cutinase and Candida antarctica lipase. *Polymer Degradation and Stability* **2019**, *164*, 55–60. DOI: 10.1016/j.polymdegradstab.2019.04.005.

159. Li, S. L.; Wu, F.; Wang, Y. Z.; Zeng, J. B., Biobased Thermoplastic Poly(ester urethane) Elastomers Consisting of Poly(butylene succinate) and Poly(propylene succinate). *Industrial & Engineering Chemistry Research* **2015**, *54* (24), 6258–6268. DOI: 10.1021/acs.iecr.5b00637.

160. Hwang, S. Y.; Jin, X. Y.; Yoo, E. S.; Im, S. S., Synthesis, physical properties and enzymatic degradation of poly (oxyethylene-b-butylene succinate) ionomers. *Polymer* **2011**, *52* (13), 2784–2791. DOI: 10.1016/j.polymer.2011.04.065.

161. Yang, J.; Tian, W.; Li, Q.; Li, Y.; Cao, A., Novel biodegradable aliphatic poly(butylene succinate-co-cyclic carbonate)s bearing functionalizable carbonate building blocks: II. Enzymatic biodegradation and in vitro biocompatibility assay. *Biomacromolecules* **2004**, *5* (6), 2258–2268. DOI: 10.1021/bm049705+.

162. Huang, X.; Li, C.; Zheng, L.; Zhang, D.; Guan, G.; Xiao, Y., Synthesis, characterization and properties of biodegradable poly(butylene succinate)-block-poly(propylene glycol)segmented copolyesters. *Polymer International* **2009**, *58* (8), 893–899. DOI: 10.1002/pi.2609.

163. Han, J.; Shi, J.; Xie, Z.; Xu, J.; Guo, B., Synthesis, properties of biodegradable poly(butylene succinate-co-butylene 2-methylsuccinate) and application for sustainable release. *Materials* **2019**, *12* (9), 1507–1524. DOI: 10.3390/ma12091507.

164. Kong, X.; Qi, H.; Curtis, J. M., Synthesis and characterization of high-molecular weight aliphatic polyesters from monomers derived from renewable resources. *Journal of Applied Polymer Science* **2014**, *131* (15), 4–10. DOI: 10.1002/app.40579.

165. Kang, Z. H.; Wang, C. L., Novel poly(butylenes succinate-block-1,3-propylene sebacate): synthesis and enzymatic degradation. *Advanced Materials Research* **2013**, *774–776*, 569–572. DOI: 10.4028/www.scientific.net/AMR.774-776.569.

166. Wang, L.; Zhang, M.; Lawson, T.; Kanwal, A.; Miao, Z., Poly(butylene succinate-co-salicylic acid) copolymers and their effect on promoting plant growth. *Royal Society Open Science* **2019**, *6* (7), 190504. DOI: 10.1098/rsos.190504.

167. Nikolic, M. S.; Djonlagic, J., Synthesis and characterization of biodegradable poly(butylene succinate-co-butylene adipate)s. *Polymer Degradation and Stability* **2001**, *74* (2), 263–270. DOI: 10.1016/S0141-3910(01)00156-2.

168. Song, D. K.; Sung, Y. K., Synthesis and characterization of biodegradable poly(1,4-butanediol succinate). *Journal of Applied Polymer Science* **1995**, *56*, 1381–1395. DOI: 10.1002/app.1995.070561102.

169. Ferreira, F. V.; Dufresne, A.; Pinheiro, I. F.; Souza, D. H. S.; Gouveia, R. F.; Mei, L. H. I.; Lona, L. M. F., How do cellulose nanocrystals affect the overall properties of biodegradable polymer nanocomposites: A comprehensive review. *European Polymer Journal* **2018**, *108*, 274–285. DOI: 10.1016/j.eurpolymj.2018.08.045.

170. Scott, G., "Green" polymers. *Polymer Degradation and Stability* **2000**, *68*, 1–7. DOI: 10.1016/S0141-3910(99)00182-2.

171. Nugroho, P.; Mitomo, H.; Yoshii, F.; Kume, T.; Nishimura, K., Improvement of processability of PCL and PBS blend by irradiation and its biodegradability. *Macromolecular Materials and Engineering* **2001**, *286* (5), 316–323. DOI: 10.1002/1439-2054(20010501)286:5<316::AID-MAME316>3.0.CO;2-N.

172. Haider, T. P.; Völker, C.; Kramm, J.; Landfester, K.; Wurm, F. R., Plastics of the Future? The Impact of Biodegradable Polymers on the Environment and on Society. *Angewandte Chemie - International Edition* **2019**, *58* (1), 50–62. DOI: 10.1002/anie.201805766.

173. Kim, H. S.; Yang, H. S.; Kim, H. J., Biodegradability and mechanical properties of agro-flour-filled polybutylene succinate biocomposites. *Journal of Applied Polymer Science* **2005**, *97* (4), 1513–1521. DOI: 10.1002/app.21905.

174. Huang, Z.; Qian, L.; Yin, Q.; Yu, N.; Liu, T.; Tian, D., Biodegradability studies of poly(butylene succinate) composites filled with sugarcane rind fiber. *Polymer Testing* **2018**, *66*, 319–326. DOI: 10.1016/j.polymertesting.2018.02.003.

175. Platnieks, O.; Gaidukovs, S.; Barkane, A.; Sereda, A.; Gaidukova, G.; Grase, L.; Thakur, V. K.; Filipova, I.; Fridrihsone, V.; Skute, M.; Laka, M., Bio-based poly(butylene succinate)/microcrystalline cellulose/nanofibrillated cellulose-based sustainable polymer composites: thermo-mechanical and biodegradation studies. *Polymers* **2020**, *12*, 1472. DOI: 10.3390/polym12071472.

176. Calabia, B. P.; Ninomiya, F.; Yagi, H.; Oishi, A.; Taguchi, K.; Kunioka, M.; Funabashi, M., Biodegradable poly(butylene succinate) composites reinforced by cotton fiber with silane coupling agent. *Polymers* **2013**, *5* (1), 128–141. DOI: 10.3390/polym5010128.

177. Kim, H. S.; Kim, H. J.; Lee, J. W.; Choi, I. G., Biodegradability of bio-flour filled biodegradable poly(butylene succinate) bio-composites in natural and compost soil. *Polymer Degradation and Stability* **2006**, *91* (5), 1117–1127. DOI: 10.1016/j.polymdegradstab.2005.07.002.

178. Liu, L.; Yu, J.; Cheng, L.; Yang, X., Biodegradability of poly(butylene succinate) (PBS) composite reinforced with jute fibre. *Polymer Degradation and Stability* **2009**, *94* (1), 90–94. DOI: 10.1016/j.polymdegradstab.2008.10.013.

179. Teramoto, N.; Urata, K.; Ozawa, K.; Shibata, M., Biodegradation of aliphatic polyester composites reinforced by abaca fiber. *Polymer Degradation and Stability* **2004**, *86* (3), 401–409. DOI: 10.1016/j.polymdegradstab.2004.04.026.

180. Anstey, A.; Muniyasamy, S.; Reddy, M. M.; Misra, M.; Mohanty, A., Processability and Biodegradability Evaluation of Composites from Poly(butylene succinate) (PBS) Bioplastic and Biofuel Co-products from Ontario. *Journal of Polymers and the Environment* **2014**, *22* (2), 209–218. DOI: 10.1007/s10924-013-0633-8.

181. Phua, Y. J.; Lau, N. S.; Sudesh, K.; Chow, W. S.; Mohd Ishak, Z. A., Biodegradability studies of poly(butylene succinate)/organo-montmorillonite nanocomposites under controlled compost soil conditions: Effects of clay loading and compatibiliser. *Polymer Degradation and Stability* **2012**, *97* (8), 1345–1354. DOI: 10.1016/j.polymdegradstab.2012.05.024.

182. Platnieks, O.; Sereda, A.; Gaidukovs, S.; Thakur, V. K.; Barkane, A.; Gaidukova, G.; Filipova, I.; Ogurcovs, A.; Fridrihsone, V., Adding value to poly(butylene succinate) and nanofibrillated cellulose-based sustainable nanocomposites by applying masterbatch process. *Industrial Crops and Products* **2021**, *169*, 113669. DOI: 10.1016/j.indcrop.2021.113669.

183. Platnieks, O.; Barkane, A.; Ijudina, N.; Gaidukova, G.; Thakur, V. K.; Gaidukovs, S., Sustainable tetra pak recycled cellulose/poly(butylene succinate) based woody-like composites for a circular economy. *Journal of Cleaner Production* **2020**, *270*, 122321. DOI: 10.1016/j.jclepro.2020.122321.

184. Rojas-Lema, S.; Arevalo, J.; Gomez-Caturla, J.; Garcia-Garcia, D.; Torres-Giner, S., Peroxide-induced synthesis of maleic anhydride-grafted poly(butylene succinate) and its compatibilizing effect on poly(butylene succinate)/pistachio shell flour composites. *Molecules* **2021**, *26*, 5927. DOI: 10.3390/molecules26195927.

Chapter 3

Nanostructural Organization of Thin Films Prepared by Sequential Dip-Coating Deposition of Semicrystalline Biopolymers

---

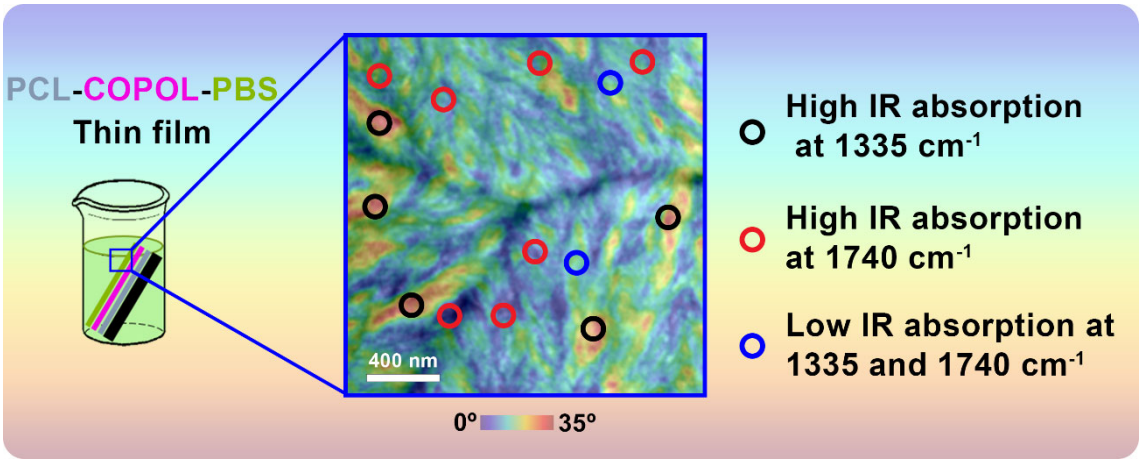

3.1. Introduction

Poly(ε-caprolactone) (PCL) and poly(butylene succinate) (PBS) are fully biodegradable aliphatic polyesters. They have attracted a great deal of attention for the development of biodegradable packaging and biomedical applications, such as implant devices, tissue scaffolds and wound dressings.[1] The blending of biodegradable polyesters is considered one of the most promising ways to obtain sustainable materials with enhanced and tailored properties. PCL/PBS blends have been prepared by melt blending or solution mixing methods attempting to improve the properties of the individual polymers. Regardless of the preparation method used, PCL/PBS blends are immiscible, as evidenced by composition independent T_gs and a biphasic melt, which leads to poor interfacial adhesion and macrophase separation.[2] Nevertheless, earlier reports on PBS/PCL blends have indicated that a noticeable improvement in the mechanical properties of PBS/PCL blends could be obtained. These results were explained by considering possible interactions between the ester groups of the neat polymers through hydrogen bonds.[3] Although bulk properties of these two polymers and their blends have been extensively studied,[4–7] not much information about the structure and morphology of their thin and ultrathin films has been reported.

Thin polymer films obtained from deposition of polymer blends in solution has been widely reported in literature as a bottom up method to produce patterned surfaces arising from different phenomena such as dewetting and phase separation.[8] The preparation of thin polymer films through sequential deposition of polymer aqueous solutions, known as layer-by-layer (LbL) method has been widely investigated to achieve nanostructured films and coatings through the incorporation of successive polymer layers that interact with each other electrostatically, H-bonded or covalently.[9–11] In contrast, the preparation of thin polymer films through sequential deposition of different polymers in organic solutions is less addressed in literature. Such method of preparation allows to deposit first a polymer layer on a substrate to have an ordered structure followed by the deposition of a second layer of a different polymer (or organic molecule)

in order to minimize their intermixing. Such approach has been employed mostly for the preparation of thin films applied as electronic devices and energy conversion set-ups.[12–14]

The morphology of polymer thin films deposited by spin-coating is mostly driven by the composition of the polymer solution and post-treatments such as thermal or solvent annealing are employed as a mean to modulate their final morphology. During the annealing process, surface segregation is induced by preferential wetting of one component in polymer blends and block copolymer thin films.[15] This phenomenon known as surface wetting induced surface segregation results in changes of the surface chemical composition of thin films and influences crystallization for crystalline block copolymer thin films and blends.[16–19] On the other hand, for thin films obtained by dip-coating, the final film morphology depends to a high extent on the experimental conditions, such as withdrawal speed, nature of the solvent, solution concentration and geometry of the reservoir and it can be modulated without the need of additional post annealing techniques.[20–22] Within this context, dip-coating constitutes one effective process for the fabrication of thin polymer films, with extensive application in small-scale fabrication for academic studies.[23] The method is based on the deposition of thin films *via* precision immersion and withdrawal of a substrate into a reservoir containing a polymer solution. Specifically, dip-coating has been extensively reported to prepare PCL thin films that can be employed as coatings for degradation prevention in biodegradable magnesium alloys and blend coatings with PEG for their application as biomaterials.[24,25] To the best of our knowledge, the preparation and characterization of PCL/PBS thin polymer films have not been described in the literature.

In this Chapter, thin films of PCL, PBS and a random copolyester (PBS-*ran*-PCL) were prepared by sequential dipping steps of a silicon substrate into chloroform solutions of the respective polymers, previously synthesized by some of us.[26] The use of poly(butylene succinate-*ran*-ε-caprolactone) (PBS-*ran*-PCL) copolymer layers together with PCL and/or PBS is expected to improve

miscibility, interfacial adhesion and the resultant mechanical properties of PCL/PBS blends as previously reported.[27] A nearly symmetric copolymer was chosen for this study, as this has a better chance of interacting with neat PCL and neat PBS, hence it would have a better chance to promote adhesion between a layer of neat PBS and a layer of neat PCL. Copolymer compositions different to approximately 50/50 would be more compatible with either PBS or PCL depending on the composition. The resulting morphology was observed by atomic force microscopy (AFM), and it was related to the thickness and composition of the films. The presence of PCL or PBS crystals was explored by Grazing-Incidence X-ray Scattering at Wide Angle (GIWAXS). Previous studies carried out on blend thin films prepared by dip-coating have employed selective dissolution of one of the polymers in order to be able to assign the polymer phases observed in AFM images.[22] For the films under study here, it is not possible to selectively eliminate one polymer as the three polymers dissolve in common solvents. Therefore, scattering-type Scanning Near-field Optical Microscopy (s-SNOM) and Fourier-Transform Infrared nanospectroscopy (nano-FTIR) were employed in selected samples to image the local distribution of the three polymers in the films under study. The information obtained allows us to correlate the dip-coating processing employed for the preparation of the samples to the structure and morphology exhibited by PCL/PBS thin films.

3.2. Experimental Part

3.2.1. Materials

Poly(butylene succinate) (PBS), poly(ε-caprolactone) (PCL) and a poly(butylene succinate-*ran*-ε-caprolactone) random copolyester, designated as COPOL, were synthesized according to a method reported elsewhere.[26] Table 3.1 reports the average molecular weight and composition for the polymers under study.

Table 3.1. Molecular characterization data.[a]

Polymer	Composition (BS/CL mol/mol)	M_w (g/mol)	M_w/M_n
PBS	(100/0)	21,470	2.9
PCL	(0/100)	17,400	3.2
COPOL	(51/49)	23,500	3.1

[a] Data taken from Ref.[26]

3.2.2. Thin films preparation

Solutions of PCL, PBS and COPOL were prepared by dissolving the appropriate mass of polymer in $CHCl_3$ to obtain concentrations of 1 mg/mL and 2 mg/mL. Thin films of PCL, PBS, and COPOL were prepared by dip-coating silicon wafers (40 x 9 x 0.5 mm^3), previously washed out from impurities with a piranha solution (60:40 H_2SO_4:H_2O_2), into the corresponding $CHCl_3$ solutions during 2 minutes. The film drying time for pristine thin films of PCL, PBS, and COPOL was determined by visualization of the height position of the drying line after withdrawing sample, located by a sharp colour. The evaporation speed, calculated by considering that the solution height was maintained at 30 mm, was ~3 $mm \cdot s^{-1}$ in all cases. It is important to note that concentrations of the polymers in the dipping solutions higher than 2 mg/mL led to the formation of stripes on the surface of the film, perpendicularly to the withdrawal direction (Figure 3.1).

This phenomenon, named "stick-slip motion" has been observed and described for films prepared by dip-coating, and it is the result of the deposition of high concentrations of the polymer in the upper part of the meniscus giving rise to the formation of local thickness heterogeneities.[22]

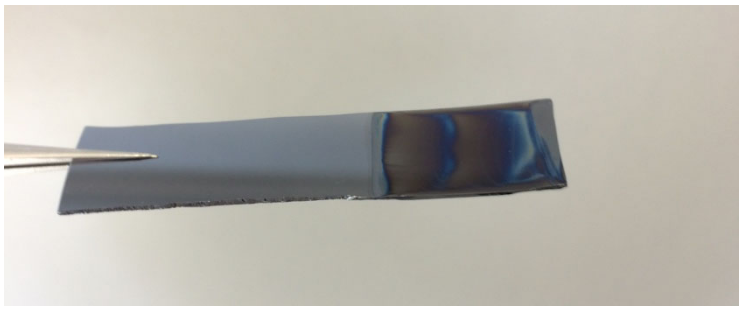

Figure 3.1. Image corresponding to a silicon substrate coated with a PBS solution in chloroform at 5 mg/mL. (Not considered for the current study. Note that only polymer films prepared from chloroform solutions of the polymers at 1 and 2 mg/mL were considered).

For the preparation of films containing PBS, PCL, and COPOL, Si wafers were sequentially immersed in $CHCl_3$ solutions of PCL, COPOL, and PBS at 1 and 2 mg/mL (series I and II in Table 3.2, respectively). A schematic representation of the process employed for the preparation of the samples is shown in Scheme 3.1. The immersion time was 2 min with an air-drying step of 20 s in between dipping steps.

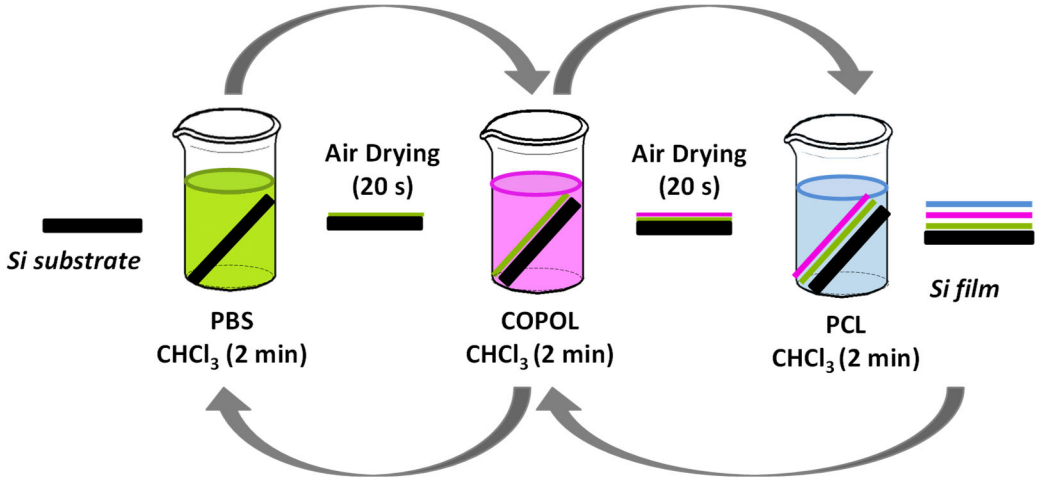

Scheme 3.1. Schematic representation of the method of preparation of the films.

Films corresponding to series I were 3-layer films prepared from $CHCl_3$ solutions of PCL, COPOL, and PBS at 1 mg/mL. The difference among them was the order employed for the deposition of the polymers. For the film designated as 3-layer (PBS)_1, the last deposited layer was PBS (i.e., the layers were deposited in the following order: PCL, COPOL and PBS), and for the film designated as 3-layer (PCL)_1, the last deposited layer was PCL (i.e., the layers were deposited in the following order: PBS, COPOL and PCL).

Films corresponding to series II were prepared from $CHCl_3$ solutions of PCL, COPOL, and PBS at 2 mg/mL. Two films were prepared with different number of layers (3 and 13) in order to determine the effect of the number of layers on the morphology of the resulting films. In both cases, the last deposited layer was PBS. The 3-layer film was designated as 3-layer (PBS)_2, whereas the 13-layer film was designated as 13-layer (PBS)_2.

Table 3.2. Nomenclature employed for all the samples under study.

Sample	*C* (mg/mL)[a]	Number of layers	Last deposited layer
Series I			
3-layer (PBS)_1	1	3	PBS
3-layer (PCL)_1	1	3	PCL
Series II			
3-layer (PBS)_2	2	3	PBS
13-layer (PBS)_2	2	13	PBS

[a] Concentration of the dipping solutions.

3.2.3. Proton Nuclear Magnetic Resonance (^{1}H-NMR)

Thin polymer films were dissolved in 1 mL of deuterated chloroform and ^{1}H-NMR spectra were taken in a Varian System 500 MHz NMR equipment.

3.2.4. Atomic Force Microscopy (AFM)

The morphology and thickness of the layers were observed by AFM (Multimode Scanning Probe Microscope, Veeco/Bruker), employing a di NanoScope IVa Controller with the conventional height mode (tapping mode, normal AFM) at a nominal force constant of 42 N/m and 320 kHz resonant frequency. The AFM samples (9 x 9 x 0.5 mm^3) were cut from the previously prepared films on silicon wafer substrates. Film thicknesses were measured by AFM by the scratch method and the results were compared to those obtained from the analysis of the AFM height profiles. WSxM5.0 software was employed for the visualization and analysis of the AFM images.

3.2.5. Grazing-Incidence X-ray Scattering at Wide Angle (GIWAXS)

Grazing-Incidence X-ray Scattering at Wide Angle (GIWAXS) was measured using synchrotron radiation at the NCD-SWEET beamline at the ALBA Synchrotron (Cerdanyola del Vallès, Barcelona, Spain). The sample was inclined to achieve different incidence angles, ranging from 0.1º to 0.3º between the sample surface and the X-ray beam. The X-ray wavelength used was 1 Å. The scattering intensity was collected by a Rayonix detector of 960 × 2880 pixels (pixel size 88.54 μm), placed at 145.6 mm from the sample. Patterns acquired with an exposition time of 5 s were corrected for background scattering and analyzed by the Fit2D software.[28]

3.2.6. Scattering-type Scanning Near-field Optical Microscopy (s-SNOM) and Fourier-Transform Infrared nanospectroscopy (nano-FTIR)

s-SNOM, based on the AFM technique, is carried out with a metallized tip which is illuminated with a monochromatic infrared laser radiation concentrated at the vertex of the tip, acting as an antenna. s-SNOM yields infrared amplitude and phase infrared images at nanoscale resolution and allows to obtain maps of the chemical properties of the surface of the sample. Nano-FTIR is based on s-SNOM, where the tip is illuminated with a broadband infrared radiation. The tip-

scattered light is recorded with an asymmetric Fourier transform spectrometer at a fixed sample position, yielding amplitude- and phase-resolved infrared spectra.[29–31]

A commercial s-SNOM/nano-FTIR setup (NeaSNOM, Neaspec GmbH, Germany) was employed for measuring s-SNOM phase images and nano-FTIR phase spectra using gold-coated commercial Si tips (Nanosensors, PPP-NCSTAu) with a mechanical resonance frequency ~135 kHz for tapping mode atomic force microscope (AFM). s-SNOM imaging was collected directly on thin film samples prepared in silicon wafers by means of a microscope equipped with a MIRcat laser (MIRcat Mid-IR laser, Daylight Solutions, USA), at a laser power of 3 mW, and a tapping amplitude of 50 nm. The acquisition time of one s-SNOM image was 11 minutes. For nano-FTIR, a broadband infrared laser continuum was employed with an average output power of ~600 μW covering a spectral range from 2200 to 650 cm^{-1}. All nano-FTIR spectra were recorded with a spectral resolution of 17 cm^{-1} and a tapping amplitude of 80 nm. Reported nano-FTIR spectra are averages of 10 full spectra.

3.3. Results and Discussion

3.3.1. Determination of the composition of the films

The process of sequential dip-coating employed for producing the films takes place through sequential immersion of a silicon substrate onto chloroform solutions of each of the polymers as shown in Scheme 3.1. Given the fact that chloroform is a solvent for PCL, PBS and COPOL, as a first step, we set to determine the (BS/CL) ratio for all the samples under study. For comparison, the spectra corresponding to neat PBS, PCL and COPOL (see chemical structures in Figure 3.2) are also included in Figure 3.3 and the peaks are assigned according to literature.[26]

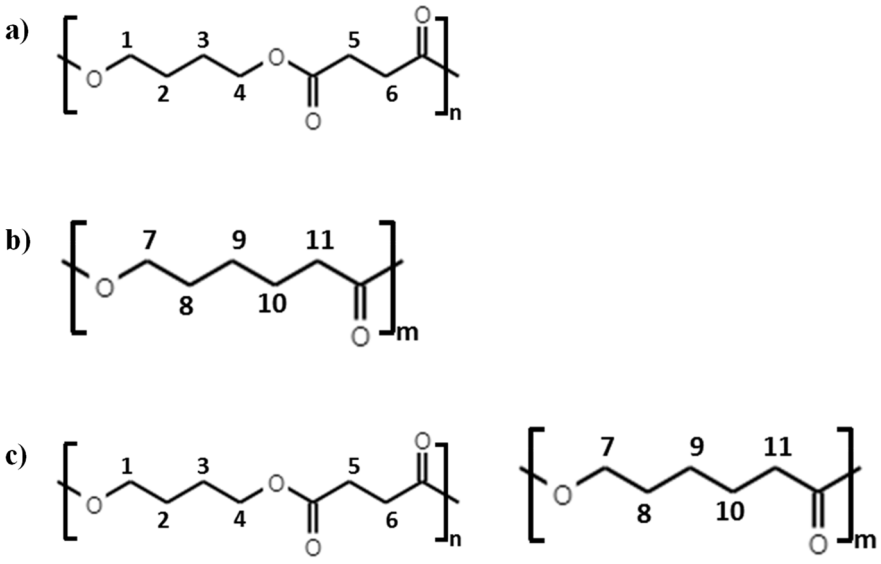

Figure 3.2. Chemical structures of pure polymers **a)** PBS, and **b)** PCL; and **c)** random copolymer PBS-*ran*-PCL, COPOL.

The triplet signal centered at 4.06 ppm can be assigned to the methylene proton resonance of CH_2 (7) in PCL and the multiplet signal centered at 4.12 ppm corresponds to the proton resonances of CH_2 (1,4) in PBS, indicated in Figures 3.2a-b. For COPOL, it was not possible to obtain separate signals corresponding to PBS and PCL sequences within this ppm region. In the films, the presence of a resonance peak at 4.08 ppm that can be assigned to COPOL (marked with an arrow in Figure 3.3) is observed, most notably for films

corresponding to series II, which confirms the presence of the three components for all the samples under study. Nevertheless, a quantitative determination is not possible due to the overlapping of the ^{1}H-NMR signals of the COPOL with those corresponding to the pristine polymers, PBS and PCL.

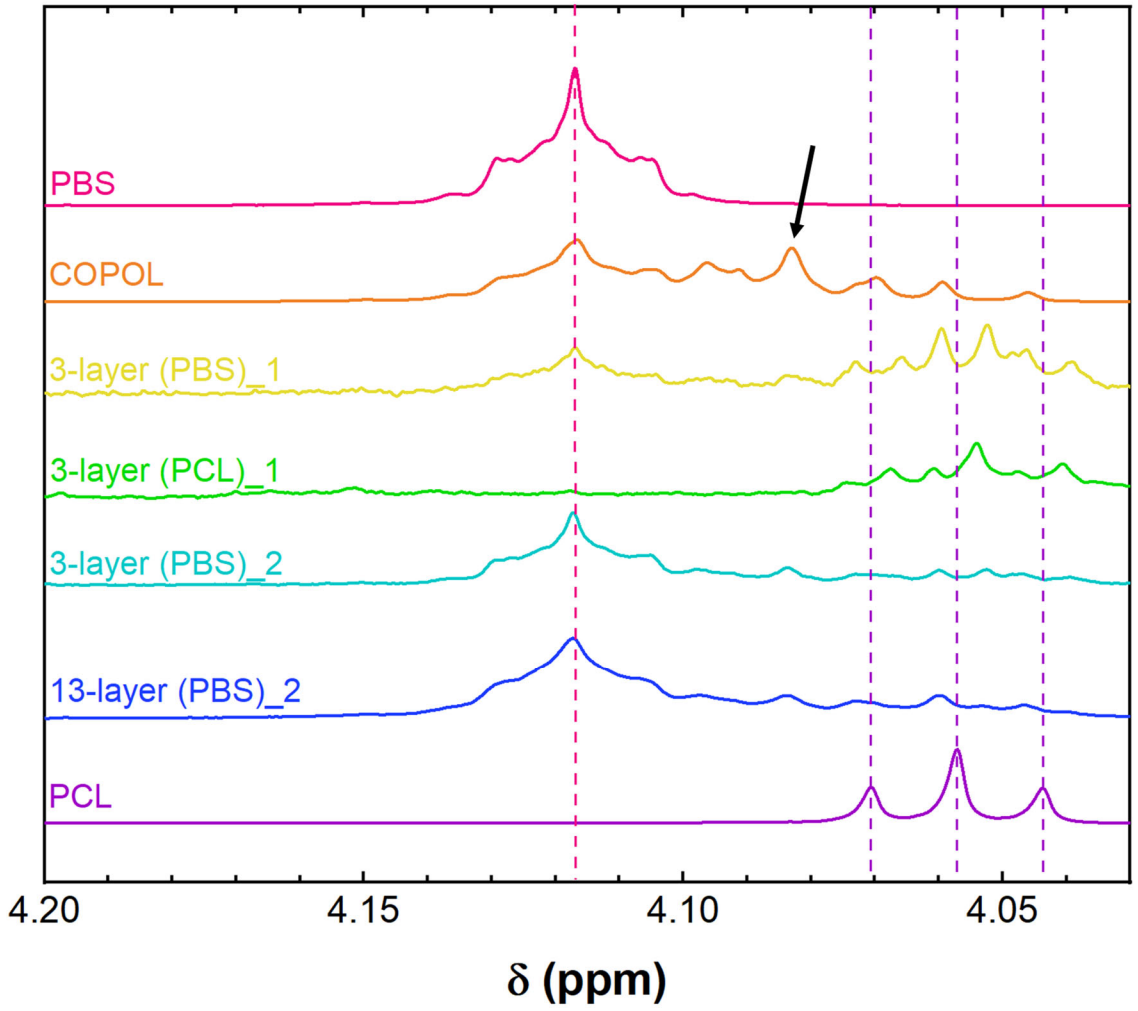

Figure 3.3. ^{1}H-NMR spectra in the 4.00-4.20 ppm region of films corresponding to series I, 3-layer (PBS)_1 and 3-layer (PCL)_1, and series II, 3-layer (PBS)_2 and 13-layer (PBS)_2. For comparison, the spectra corresponding to neat PBS, PCL and COPOL are also included in the figure.

3.3.2. Study of the morphology and crystallinity

Figure 3.4 shows AFM height images for pristine films obtained from $CHCl_3$ solutions of PBS and PCL and films corresponding to series I prepared at polymer concentrations of 1 mg/mL, 3-layer (PBS)_1 and 3-layer (PCL)_1. All the samples under study are ultrathin films with thicknesses below 10 nm as determined by AFM by the scratch method. The results were shown to match the depth profile analyzed for each of the samples, both analysis are shown in Figure 3.5.

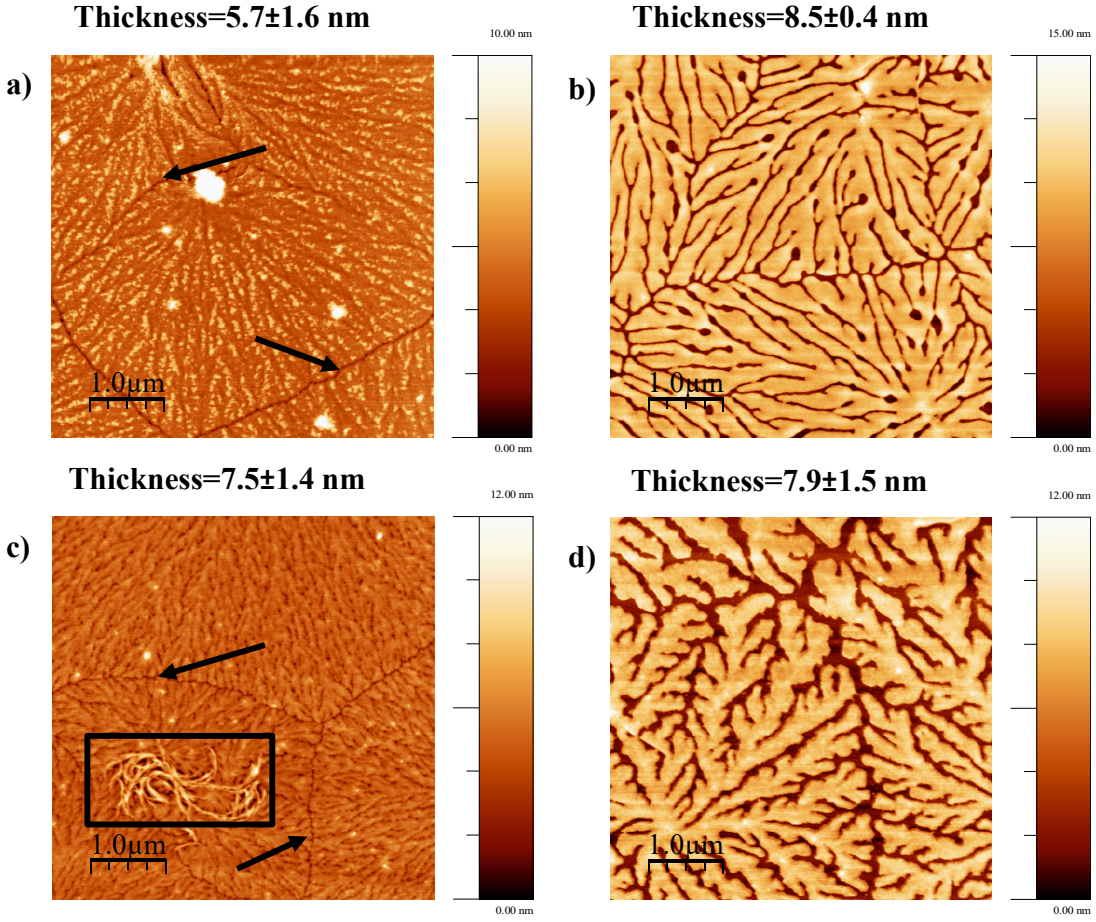

Figure 3.4. Tapping mode AFM height images of **a)** PBS films, **b)** PCL films, **c)** 3-layer (PBS)_1, and **d)** 3-layer (PCL)_1 prepared by dip-coating from $CHCl_3$ solutions at 1 mg/mL. Black arrows mark the straight boundaries observed between superstructural structures (spherulites, axialites or dendrites) which are caused by the impinging of these structures as they grow radially. The black square in Figure 3.4c marks the occurrence of new crystalline morphologies as explained in the text.

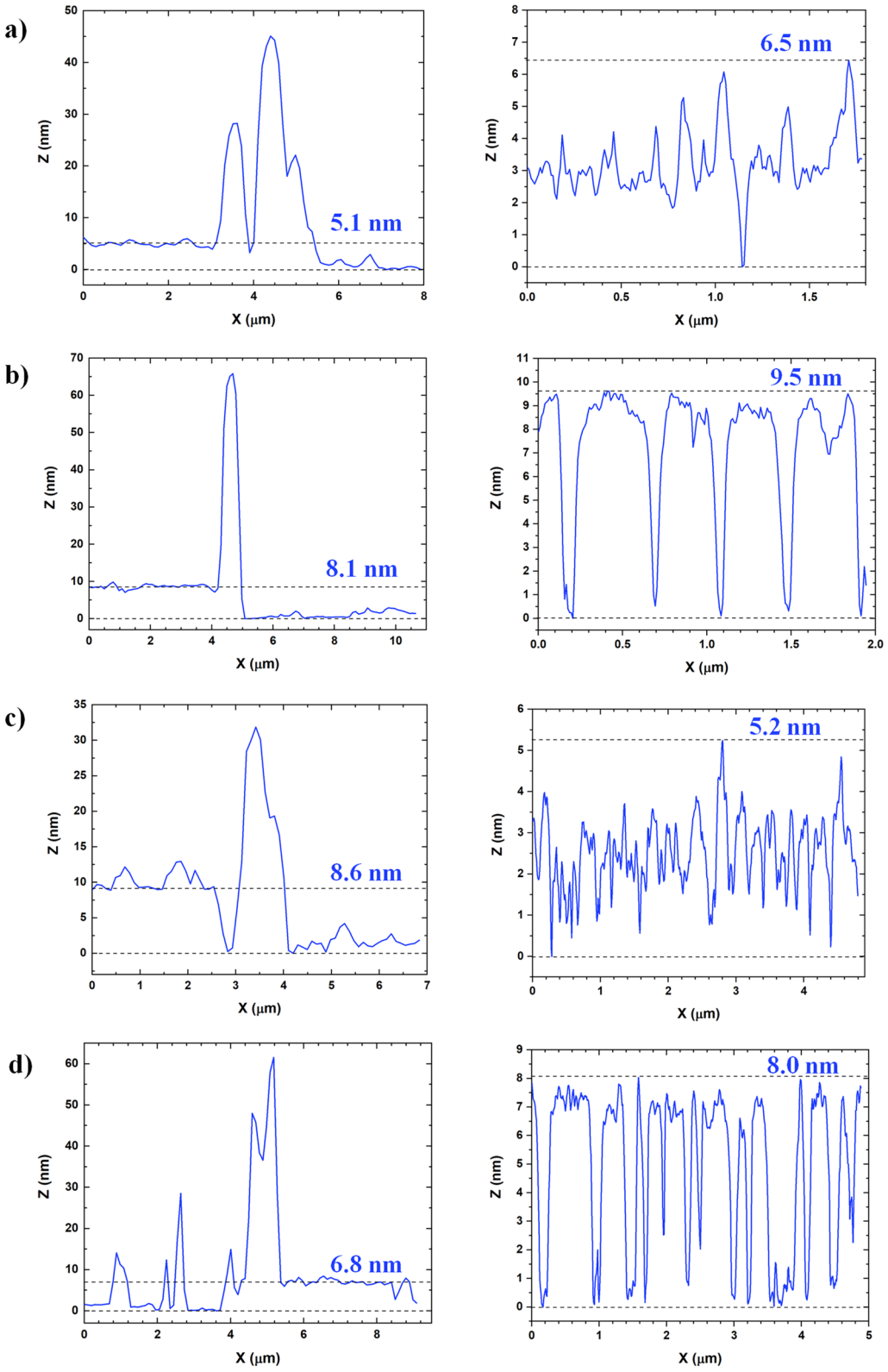

Figure 3.5. Scratch (left) and depth (right) profiles obtained from AFM height images shown in Figure 3.4 for: **a)** PBS 1 mg/mL, **b)** PCL 1 mg/mL, **c)** 3-layer (PBS)_1, and **d)** 3-layer (PCL)_1.

The morphology of PCL in ultra-thin films has been reported in the literature,[32,33] however, to the best of our knowledge, there are no studies regarding the morphology of PBS in ultra-thin films. Films obtained from $CHCl_3$ solutions of PBS at 1 mg/mL (Figure 3.4a) exhibit a semicrystalline morphology rich in edge-on lamellae radiating from central nuclei that resemble spherulitic/axialitic superstructures, whereas the morphology exhibited by PCL thin films is dendritic (Figure 3.4b). In all cases, the relatively straight boundaries between superstructural structures (spherulites, axialites or dendrites), which are caused by the impinging of these structures as they grow radially, can be clearly observed in Figure 3.4. The morphology observed in Figure 3.4b for PCL (thickness ~8 nm) is consistent with that reported for spin-coated PCL films from PCL-toluene solution for which dense-branching morphology (DBM) and dendrites were observed when $t < 2Rg$ (at thicknesses below 12 nm), related to the diffusion-limited aggregation (DLA) process.[32] The morphology corresponding to the COPOL sample consists of PBS-rich phase spherulitic/axialitic crystals (shown in Figure 3.6). Extensive previous studies by WAXS and DSC have shown that in this isodimorphic copolymer sample, only the PBS-rich phase can crystallize.[25]

Both films of series I (3-layer films described in Table 3.2) have thicknesses that are comparable within the experimental error and are also similar to those of neat components single layer films, ~7.5 nm for the films of series I and 5.7 and 8.5 nm for neat PBS and PCL respectively (at 1 mg/mL). This is as a result of the partial dissolution of the films in $CHCl_3$ during the consecutive deposition steps, since chloroform dissolves both PCL and PBS. Still, the presence of the three polymers could be ascertained through ^{1}H-NMR as shown in Figure 3.3. In general terms, the morphology observed by AFM on the film surfaces is determined by the last deposited polymer layer which confirms the sequential deposition of the polymers onto the silicon substrate. Therefore, films that were coated with PBS as last layer show a similar spherulitic/axialitic morphology to that exhibited by neat PBS films (single layer) dip-coated from chloroform solution. Correspondingly, those in which the last applied layer was

PCL display the dendritic morphology observed in neat PCL films (single layer). The morphology observed for the 3-layer (PCL)_1 sample is analogous to that reported for PS/PCL blend films with film thickness of about 15 nm, for which the crystallization of PCL leads to the formation of PCL dendritic crystals.[19] It is important to note that Figure 3.4c shows the development of a new crystalline morphology with respect to the morphology observed for pristine PBS films (Figure 3.4a). On top of the spherulitic structure, we observe curved structures (highlighted with a square in Figure 3.4c). These curved crystals have been previously reported for PLLA ultrathin films and related to edge-on lamellae,[34,35] in very thin films (thicknesses around and below 10 nm). A study of the crystal unit cell parameters and chain orientation of thin films of linear aliphatic polyesters revealed that lamellar crystal edge-on morphology seems to be the preferred configuration for aliphatic polyesters. This is related to the establishment of a molecular interaction of the carbonyl groups of the polyesters, lying on the *bc* face parallel to the substrate plane, with the outer silicon oxide layer of the substrate that controls the chain fixation to the substrate.[36]

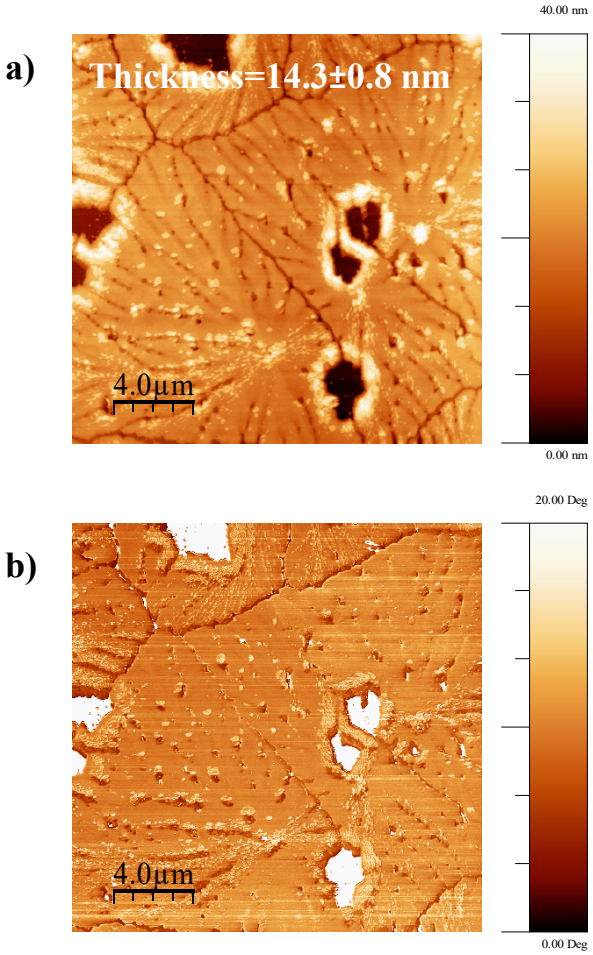

Figure 3.6. AFM images of **a)** height mode, and **b)** phase mode, corresponding to a film obtained from a chloroform solution of COPOL at 1 mg/mL.

The crystallization of the films was further investigated by GIWAXS and the diffractograms obtained using GIXRD at 0.1º incidence angle are shown in Figure 3.7. For the pristine PCL film (1 mg/mL), with thickness as low as 8.5 nm, the characteristic diffractions of (110), (111) and (200) planes are clearly distinguished in Figure 3.7a.[37] For the pristine PBS film (1 mg/mL), the GIWAXS diffractogram in Figure 3.7b showed no diffraction peaks even though a semicrystalline morphology was observed for this film in AFM images (Figure 3.4a). In contrast, a broad peak at 15.5 nm^{-1} is observed for the PBS film prepared from chloroform solutions of PBS at 2 mg/mL (Figure 3.7c), which is attributed to the diffraction of the (021) plane. Note that the peak corresponding to the diffraction of the (110) plane at 16.0 nm^{-1}, is also included within this broad peak.[38,39]

Regarding the results obtained for blend thin films, only the 3-layer (PCL)_1 sample showed the characteristic diffraction peaks of PCL, placed as the outermost layer for this sample (Figure 3.7d). For this sample, the diffraction peaks are shifted to the left with respect to the diffraction peaks observed for the pristine PCL film (Figure 3.7a). This might be a result of the different spreading of crystallites on the illuminated area.[40] As shown in Figure 3.4, the distribution of crystals appears to be more homogeneous in the case of the PCL film (Figure 3.4b) compared to the distribution of crystals observed for sample 3-layer PCL (Figure 3.4d). This might result in contributions in different positions of the diffraction centers which causes a shifting to the left of the diffraction peaks corresponding to the sample 3-layer PCL (Figure 3.7d) with respect to the sample PCL (Figure 3.7a). In contrast, neither the sample 3-layer (PBS)_1 (Figure 3.7e) nor the samples corresponding to series II, for which the outermost layer was PBS, showed diffraction peaks in GIWAXS experiments (results not shown). This is an apparent inconsistency with the AFM results shown in Figure 3.4 that clearly show an spherulitic/axialitic structure for pristine PBS films as well as for films whose last layer is PBS. In order to explain these results it is important to take into account the process of preparation of the samples through dip-coating. For this process, the evaporation rate of the solvent plays an important role on the crystallization of the polymers. Spherulite/axialite growth is the consequence of the macromolecules diffusion towards the crystal interface. Capillary flow occurring during the dip-coating process brings about a constant supply of polymer solution that contains the polymer that can crystallize.[41] In the case of the films under study here, as the evaporation rate is high (chloroform is a solvent with a high vapor pressure[42] and hence, capillary flow is high, the rapid polymer diffusion gives rise to complete spherulites/axialites due to a constant polymer supply. Still, the degree of crystallization of the PBS on the thin films under study is too low to be detected through GIWAXS experiments. Such low degree of crystallinity could be attributed to slow crystallization kinetics of PBS films casted from diluted chloroform solutions. PBS films under study here

present thicknesses below 10 nm. As it has been reported in literature, polymer chains in ultrathin films usually crystallize slowly in proximity of interfaces.[35]

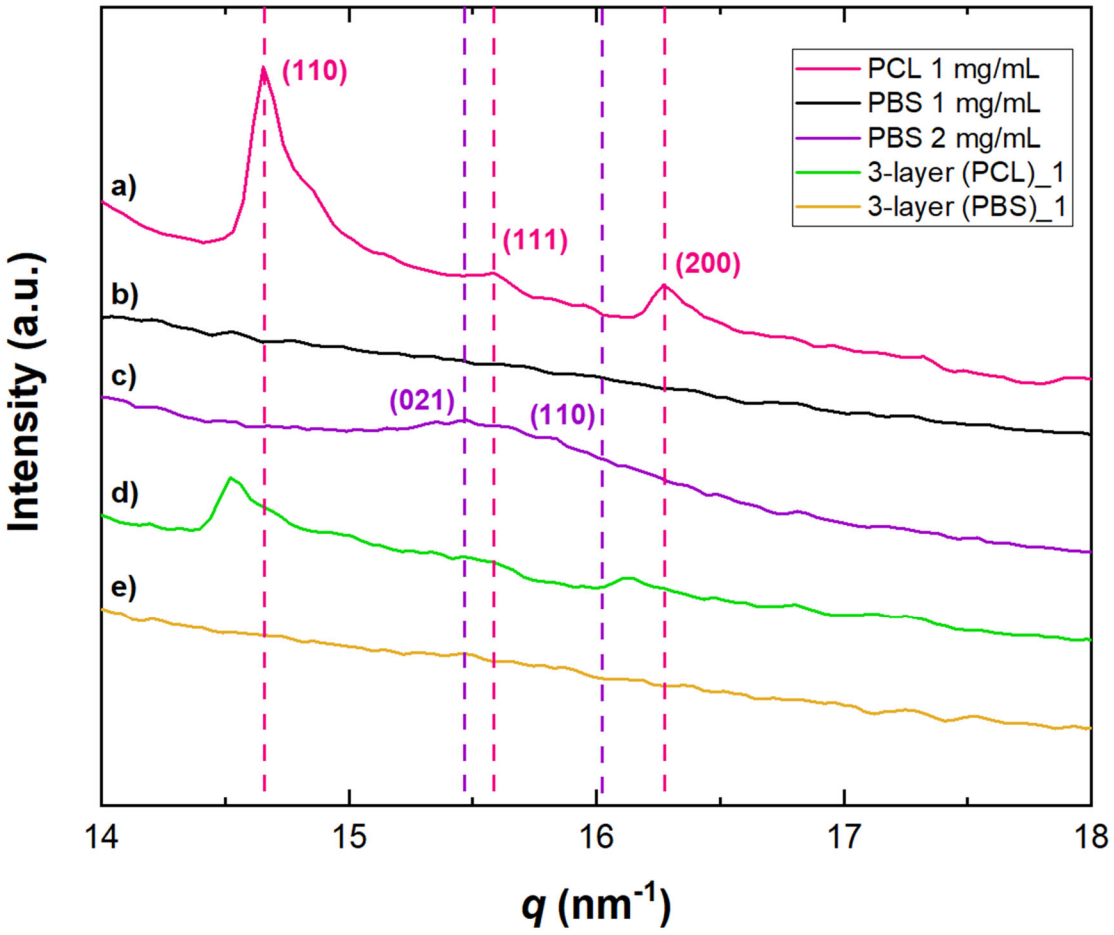

Figure 3.7. Intensity as a function of the scattering vector *q* as calculated from the corresponding GIWAXS patterns (shown in Figure 3.8): **a)** PCL 1 mg/mL, **b)** PBS 1 mg/mL, **c)** PBS 2 mg/mL, **d)** 3-layer (PCL)_1, and **e)** 3-layer (PBS)_1.

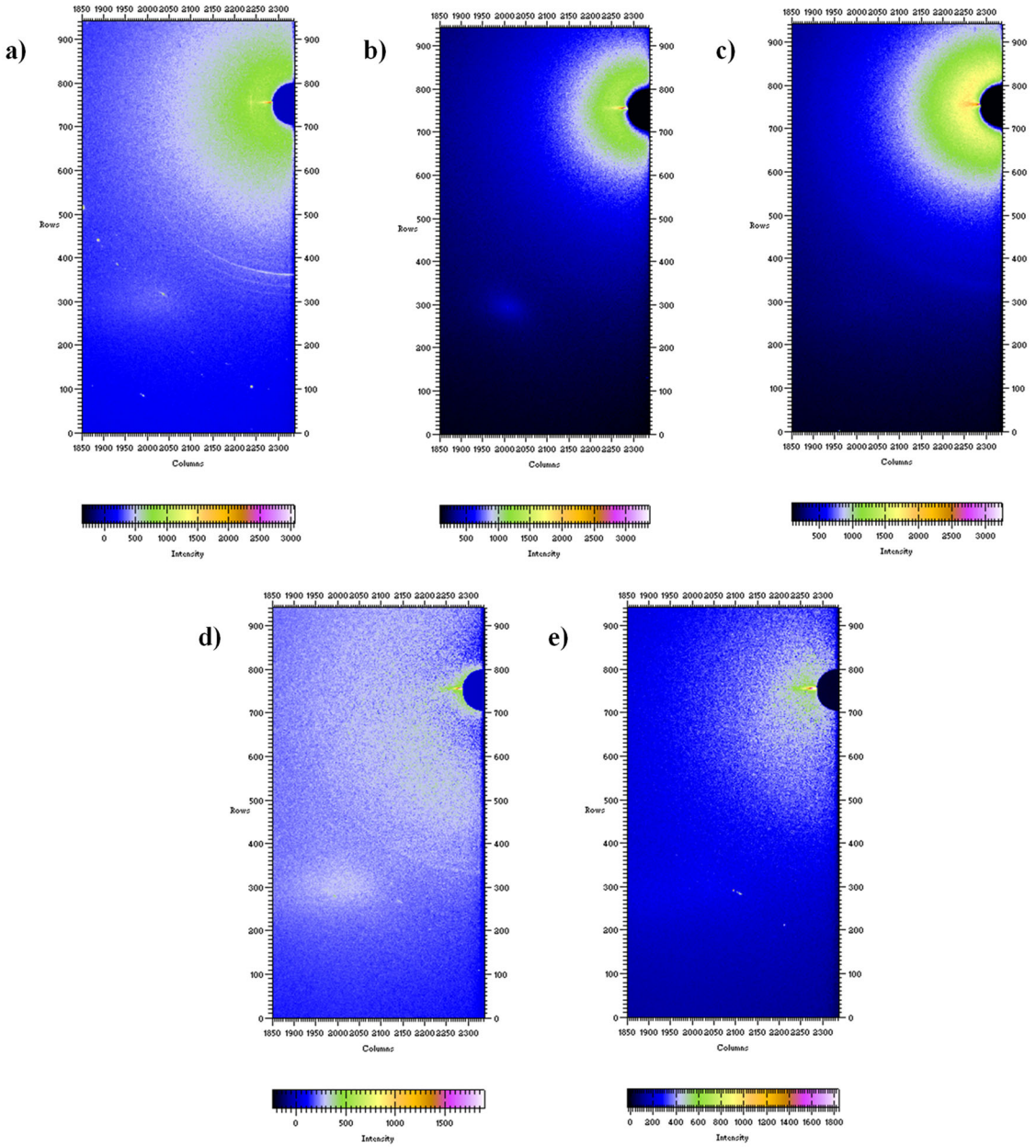

Figure 3.8. GIWAXS patterns used for the obtention of the diffractograms showed in Figure 3.7 for different samples: **a)** PCL 1 mg/mL, **b)** PBS 1 mg/mL, **c)** PBS 2 mg/mL, **d)** 3-layer (PCL)_1, and **e)** 3-layer (PBS)_1.

3.3.3. Nanoscale chemical characterization by s-SNOM and nano-FTIR techniques

The technique of infrared near-field microscopy (IR s-SNOM) and nanospectroscopy (nano-FTIR) allows for infrared imaging and spectroscopy with nanoscale spatial resolution.[43,44] It has recently been employed to investigate submicrometer chemical distribution and crystallization of polymer blend films,

as an example casted from PCL/PEG blends in THF.[45] In order to shed further light onto the chemical distribution of the three polymers, PBS, PCL and COPOL, onto the thin films prepared through sequential dip-coating, s-SNOM phase images and nano-FTIR phase spectra were recorded for samples corresponding to series II, 3-layer (PBS)_2 and 13_layer (PBS)_2. The probing depth of the nano-FTIR technique is up to 100 nm,[46,47] which is related to the oscillation amplitude of the cantilever at a fixed point on the sample. Taking into account that the films under study present thicknesses in the range from 10-25 nm, the nano-FTIR results provide information about the whole sample. By using this technique, it is possible to obtain IR absorption spectra that correlate to bulk transmission infrared spectroscopy (e.g., FTIR) as both techniques measure the amount of absorbed light.[48]

As a first step, the main FTIR bands corresponding to the individual polymers were identified from nano-FTIR spectra of pristine thin films of PCL, PBS and COPOL. Figure 3.9 shows representative spectra in the 1900-900 cm^{-1} range, in which it is possible to observe a large number of absorption bands and band overlaps (see the chemical structures in Figure 3.2). All three spectra show a C=O stretching band (at 1734 cm^{-1}) and a C-O-C stretching band (at 1174 cm^{-1} for PBS and COPOL and at 1190 cm^{-1} for PCL). However, the band at 1335 cm^{-1} band, assigned to the C-H asymmetric angular deformation, is strong in the PBS spectrum and absent in the PCL spectrum. In addition, the 1241 cm^{-1} band, assigned to the asymmetric stretching vibration of C-O-C group is very strong in the PCL spectrum and absent in the PBS spectrum. Additional FTIR bands located at 1295 and 1367 cm^{-1} are clearly visible in the FTIR spectrum corresponding to PCL which can be assigned to C-O and C-C stretching and C=O stretching in the crystalline phase, respectively.[49,50] PBS thin films under study present a low crystallinity as demonstrated through GIWAXS results, this was further demonstrated through analysis of the carbonyl region in the nano-FTIR spectra shown in Figure 3.10. According to literature, the peak in the carbonyl region in FTIR can be deconvoluted to three absorption bands that can be assigned to the stretching mode of C=O groups in the crystalline phase (1714

cm^{-1}), in the rigid amorphous fraction (1720 cm^{-1}) and the free amorphous fraction (1736 cm^{-1}).[51] The nano-FTIR spectrum corresponding to PBS film showed a broad peak in the carbonyl region with the highest intensity located at 1730 cm^{-1}, which supports the low degree of crystallinity of the PBS film under study.

The absorption bands observed for COPOL are overlapped to those observed in neat PBS and neat PCL. However, the intensity ratio of the bands at 1335 cm^{-1} and 1241 cm^{-1} increases from ~2 in the spectra corresponding to COPOL to ~8 in the spectra corresponding to PBS, a result that reflects the presence of BS and CL sequences within the COPOL sample.

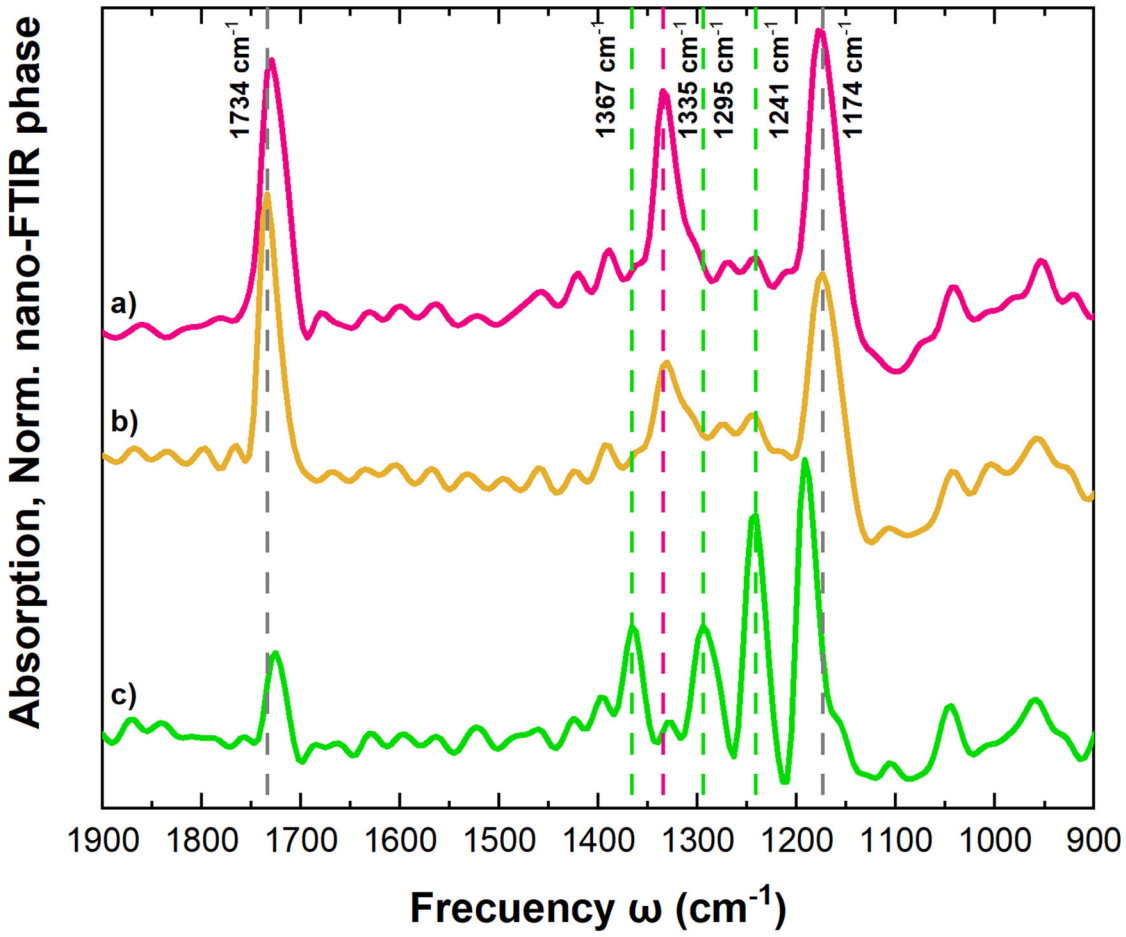

Figure 3.9. Nano-FTIR spectra of pristine films of **a)** PBS, **b)** COPOL and **c)** PCL.

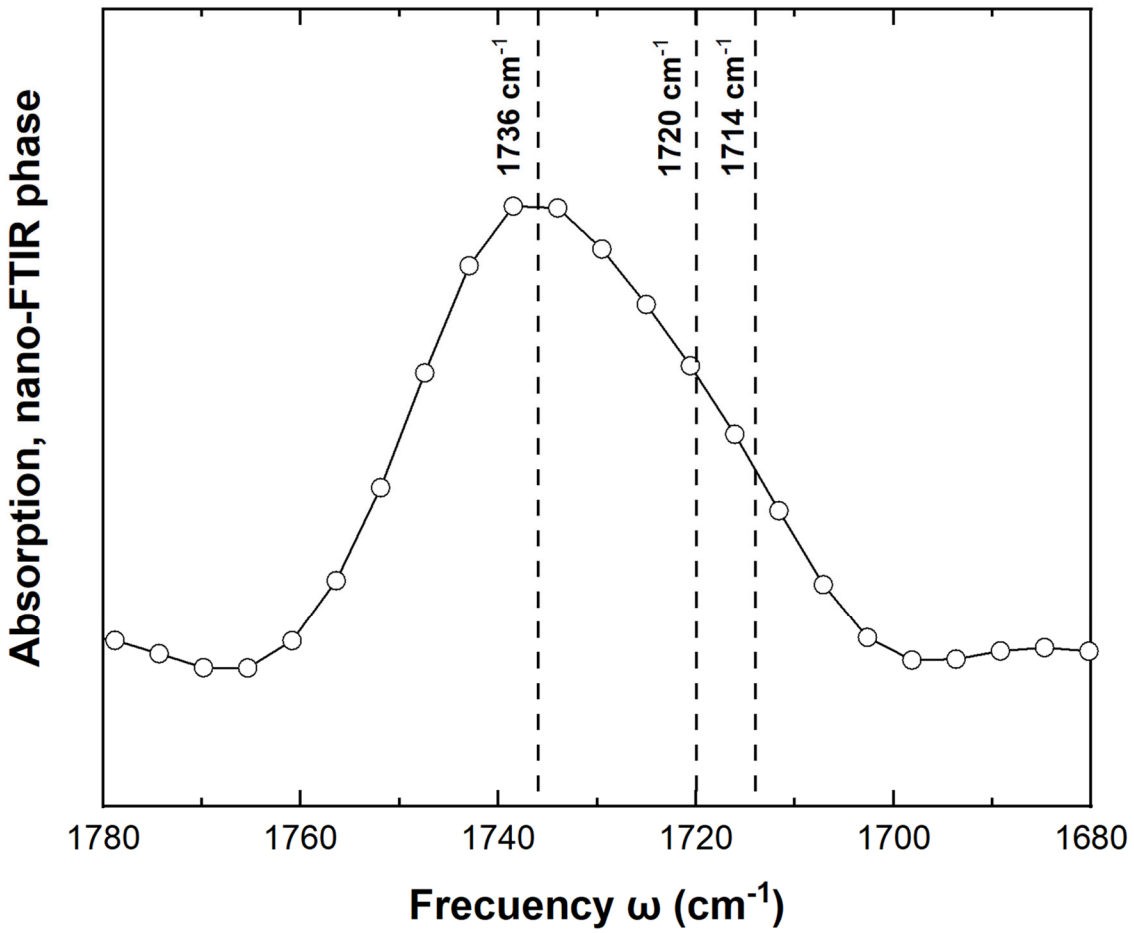

Figure 3.10. Nano-FTIR spectra of PBS in the carbonyl region.

AFM height and mechanical phase images corresponding to sample 3-layer (PBS)_2 are shown in Figure 3.11a. As can be observed, PBS crystalline superstructures (resembling spherulites or axialites) composed of PBS edge-on lamellar crystals growing from central nuclei are seen. The polygonal boundaries between these superstructures (produced by their impinging as they grow radially) are very clear in Figure 3.11a. We assume that the lamellae observed are PBS, as PBS was the last material to be deposited in the film. This was confirmed by the strong contrast observed for the absorption images at 1335 cm^{-1} (Figure 3.11b) and at 1740 cm^{-1} (Figure 3.11c), which are characteristic infrared absorption bands for PBS (see Figure 3.9). A compositional map corresponding to the sample 3-layer (PBS)_2 is shown in Figure 3.12. The image shows mainly blue areas where absorption is highest at 1740 cm^{-1} corresponding to the carbonyl region for the three polymers, PBS, PCL and COPOL and pink areas where

absorption is highest at 1335 cm^{-1}, which has been identified as a characteristic infrared absorption band for PBS. From this image, it is not possible to ascertain the presence of PCL within the sample. Hence, to further investigate the polymers' chemical distribution, several nano-FTIR spectra were recorded at determined positions within the region marked by the red square in the AFM height image in Figure 3.11a. An enlargement of this region is shown in Figure 3.13a, and the corresponding absorption image at 1335 cm^{-1} (Figure 3.13b). Several nano-FTIR spectra were recorded at different positions marked with red, black, and blue circles. The recorded individual nano-FTIR spectra show high quality and reproducibility (results not shown). The black circles correspond to spots that showed high absorption at 1335 cm^{-1}, and the red circles correspond to positions that showed high absorption at 1740 cm^{-1} (see Figure 3.11c). The blue circles correspond to positions with relatively low absorption at both IR frequencies.

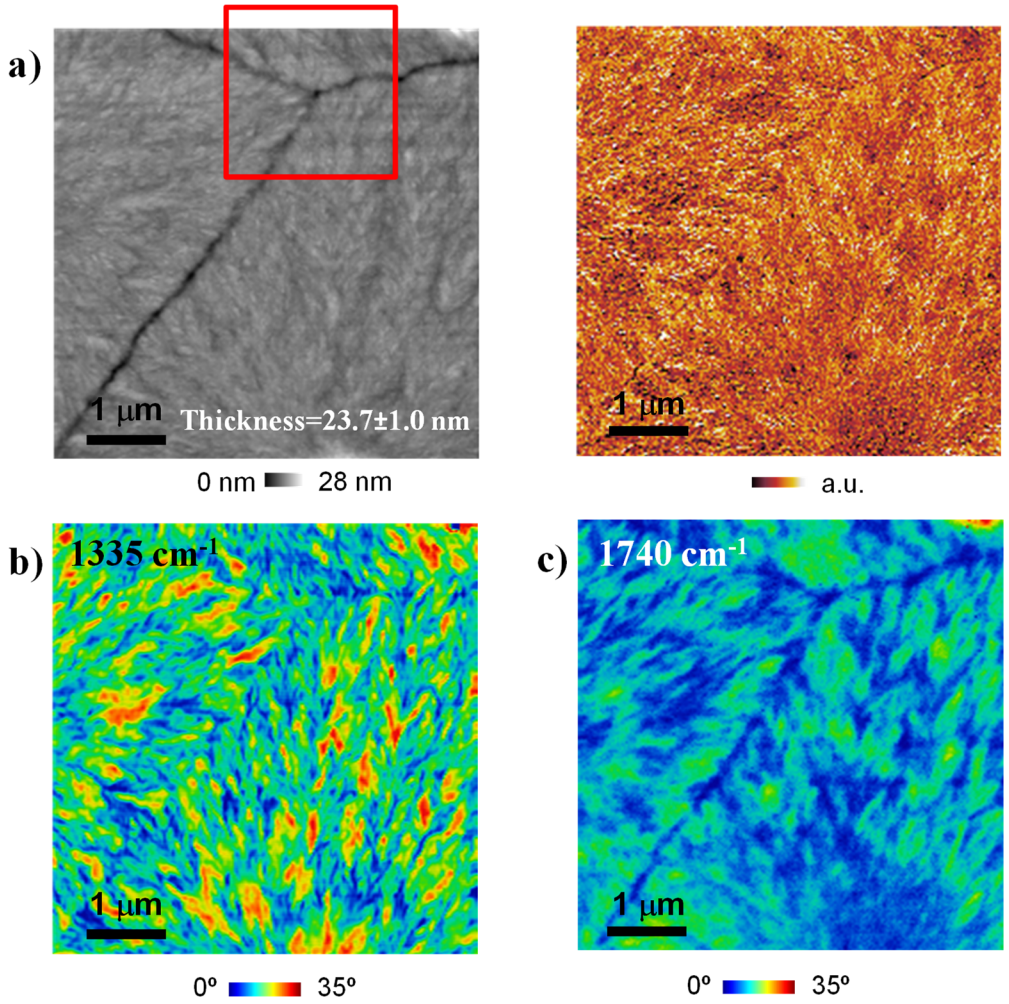

Figure 3.11. a) AFM height image (left) and mechanical phase image (right) corresponding to sample 3-layer (PBS)_2 and near-field phase (i.e. absorption) images at **b)** 1335 cm^{-1}, and **c)** 1740 cm^{-1}. The red square in Figure 3.11a marks the region employed to carry out the analysis through nano-FTIR spectroscopy (shown in Figure 3.13).

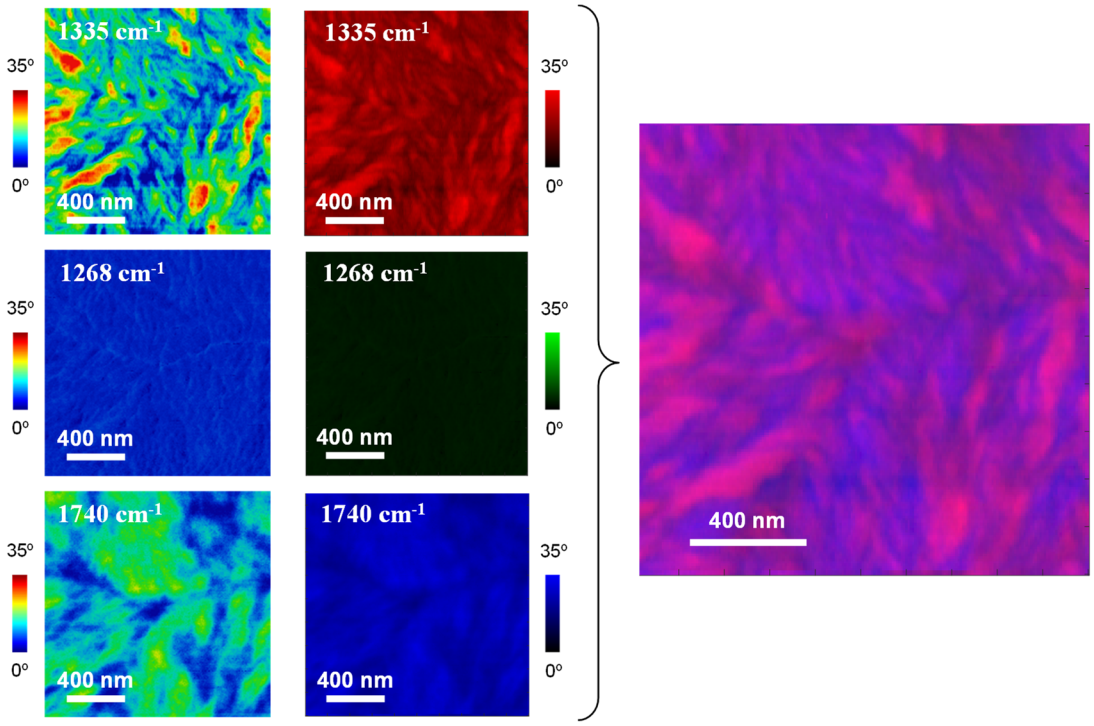

Figure 3.12. Compositional map corresponding to sample 3-layer (PBS)_2 obtained from the RGB plot of the chemical images taken at 1335, 1268 and 1740 cm^{-1}. For the generation of the 2D nano-FTIR compositional map shown on the right part of the figure, three absorption images taken at different wavelenghts of the incident radiation (1740, 1268 and 1335 cm^{-1}) were transformed to monochromatic images (red, green and blue) and combined into a single RGB figure. A RGB plot is usually employed to plot the distribution of three different components in one and the same image. The green color is not seen in the compositional map, as the absorption at 1268 cm^{-1} is comparably low.

The corresponding average nano-FTIR spectra depicted in Figure 3.13c show the characteristic C-O stretching band at 1734 cm^{-1} and the C-O-C stretching band at 1174 cm^{-1} that is overlapped for PBS, PCL, and COPOL. In addition, the three spectra show a band located at ~1335 cm^{-1} characteristic of PBS, as shown in Figure 3.9. A broad band centered at ~1268 cm^{-1} is also observed for the three samples. The intensity ratios between the peak at 1268 cm^{-1} and the peak at 1335 cm^{-1} reveal differences in the infrared absorption in different positions of the 3-layer (PBS)_2 sample and thus in the chemical distribution within the sample. The I_{1335}/I_{1268} is ~5 for the average spectrum corresponding to positions marked with black, whereas I_{1335}/I_{1268} for the average

spectra obtained from positions marked with blue and red colour decreases to ~2 for both cases, which reveals regions with higher relative content of CL sequences.

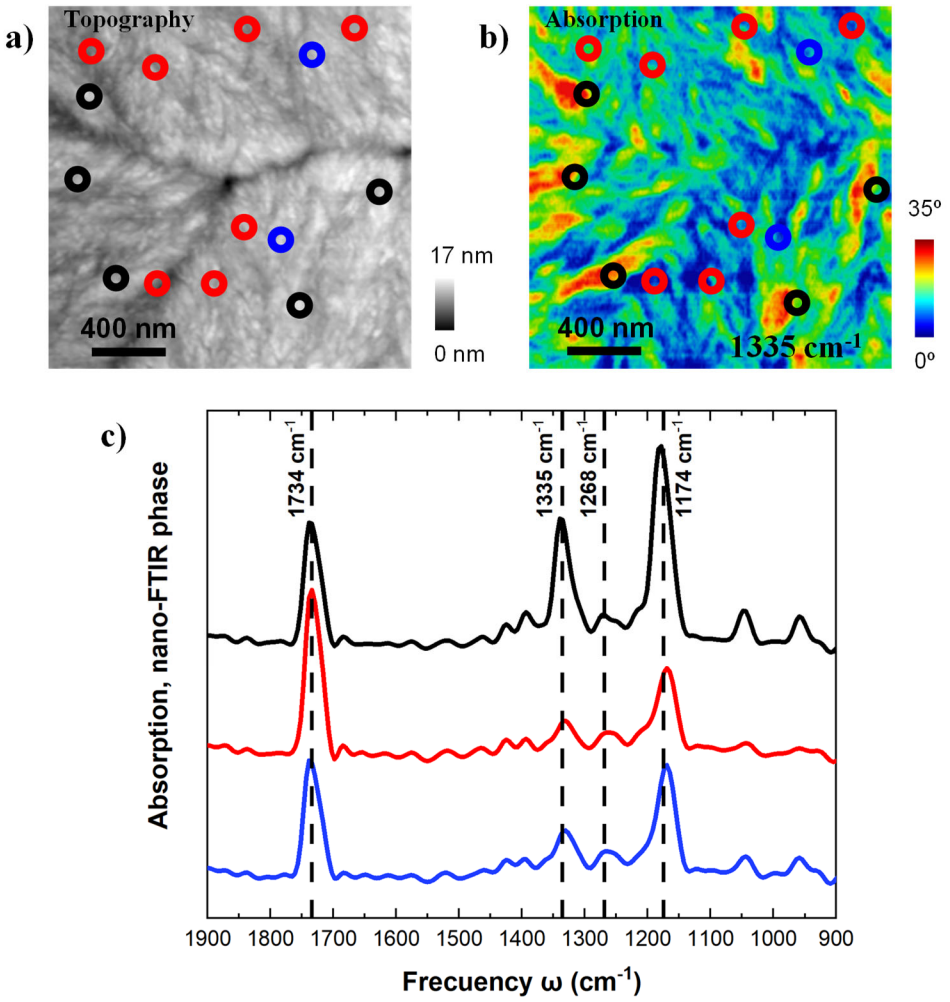

Figure 3.13. a) AFM height image, and **b)** absorption image at 1335 cm^{-1} corresponding to sample 3-layer (PBS)_2, and **c)** nano-FTIR spectra obtained by averaging spectra recorded at the positions marked by corresponding blue, red and black colors in panel b.

We now turn our attention to the results obtained for the 13-layer (PBS)_2 sample for which the total number of layers was increased from 3 to 13. The morphology observed for this sample (Figure 3.14a) is similar to the one described for sample 3-layer (PBS)_2, see Figure 3.11a. That is, the number of dipping steps employed for the preparation of the sample does not seem to have an influence on the obtained morphology.

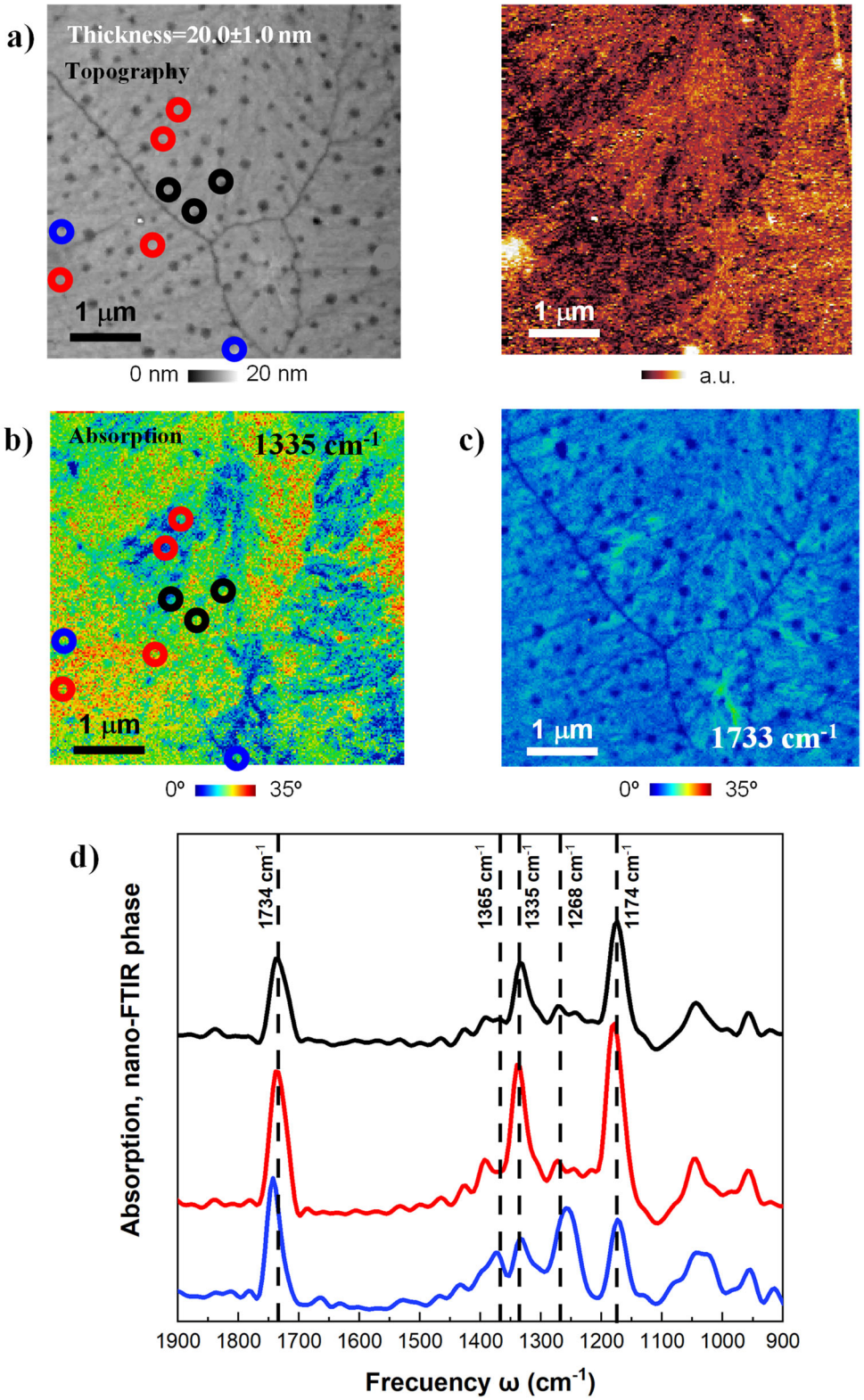

Figure 3.14. a) AFM height image (left) and mechanical phase image (right) corresponding to sample 13-layer (PBS)_2, absorption images at **b)** 1335 cm^{-1}, and **c)** 1733 cm^{-1}, and **d)** nano-FTIR spectra obtained by averaging spectra recorded at the positions marked by corresponding black, red and blue colors in panel b.

The presence of small holes on the 13-layer (PBS)_2 sample can be attributed to the rapid evaporation of chloroform during film preparation by dip-coating. As it is well known, when the solvent is rapidly evaporating, the solvent-rich films do not have enough time to level and heal surface roughness created by Marangoni instabilities. This effect and the resulting morphology could be tuned through the control of the evaporation rate during film preparation.[42] As in the case of the 3-layer (PBS)_2 sample, the absorption images taken at 1335 cm^{-1} and 1733 cm^{-1} (Figures 3.14b and 3.14c, respectively) showed high contrast, which is more clearly observed for the image taken at 1335 cm^{-1}. This is consistent with the fact that the crystalline morphology can be attributed to the last deposited polymer, that is, to PBS.

The polymer distribution was further analyzed by recording several nano-FTIR spectra at different positions marked by coloured circles in the AFM height image (Figure 3.14a, left) and the absoption image taken at 1335 cm^{-1} (Figure 3.14b). Red circles correspond to locations outside the holes and black circles correspond to locations within the holes, as seen in the AFM topography image. Both red and black spectra shown in Figure 3.14c fit nicely to the reference spectrum of PBS in agreement with the fact that the morphology observed is mostly due to PBS. In both cases, I_{1335}/I_{1268} is ~3, which indicates a similar chemical composition regarding BS/CL sequences. A close examination of the average nano-FTIR spectra obtained from regions marked with blue dots, which corresponds to positions with relatively low absorption at the IR frequency of 1335 cm^{-1}, allows to clearly distinguish a noticeable increase in the intensity of the band located at 1268 cm^{-1} with respect to the band located at 1335 cm^{-1} which is much more evident in the case of the average spectrum obtained from regions marked with blue circles. For these regions, the band located at 1365 cm^{-1}, characteristic of PCL is also clearly visible.

The results show that the increase in the number of deposited layers give rise to almost isolated PCL nanodomains within a matrix predominantly constituted of PBS. Thus it points to more segregation between BS and CL

sequences for the 13-layer (PBS)_2 sample as compared to the 3-layer (PBS)_2 sample. The final morphology obtained for these thin films could be compared to that of an immiscible blend of PCL/PBS as previously reported in literature. This could be attributed to the fact that the repetitive dipping steps employed to prepare the sample leads to the deposition of mixed solutions of the three polymers due to the partial dissolution of the films during the dipping procedure.

3.4. Conclusions

In this Chapter, sequential dip-coating of silicon substrates in chloroform solutions of PCL, PBS, and a poly (butylene succinate-*ran*-ε-caprolactone) (PBS-*ran*-PCL) copolymer has been employed to obtain thin polymer films with a varying number of layers (3 and 13). The thickness obtained for the films was, in all cases, in the range 10-25 nm regardless of the number of layers employed for their preparation, which points to partial dissolution of the films occuring during the process of preparation. The crystalline morphology observed corresponds to that of the last deposited polymer, as revealed by AFM microscopy. In the case of films for which the last deposited layer was PCL, diffraction peaks corresponding to the semicrystalline structure of PCL were detected by GIWAXS experiments. On the other hand, for films whose final layer was PBS, even if spherulitic/axialitic formation could be observed by AFM, no diffraction peaks were obtained in GIWAXS.

For films whose final layer was PBS, nano-FTIR spectroscopy provided the main evidences to determine the nanoscale organization of BS and CL sequences on 3-layer films and 13-layer films. The results showed that both samples present a heterogeneously mixed chemical composition with nanodomain regions of varying PBS and PCL content. However, in the case of 13-layer films, the analysis of the average spectra corresponding to different regions of the sample films revealed the presence of almost segregated PCL nanodomains within a PBS matrix. The results could be attributed to the fact that the partial dissolution of the film occurring during the sequential dipping steps might give rise to the deposition of a mixed solution of the three polymers resulting in a morphology that is reminiscent of that exhibited by immiscible blends.

3.5. References

1. Gigli, M.; Fabbri, M.; Lotti, N.; Gamberini, R.; Rimini, B.; Munari, A., Poly(butylene succinate)-based polyesters for biomedical applications: A review. *European Polymer Journal* **2016**, *75*, 431–460. DOI: 10.1016/j.eurpolymj.2016.01.016.

2. Gumede, T. P.; Luyt, A. S.; Müller, A. J., Review on PCL, PBS, and PCL/PBS blends containing carbon nanotubes. *Express Polymer Letters* **2018**, *12* (6), 505–529. DOI: 10.3144/expresspolymlett.2018.43.

3. John, J.; Mani, R.; Bhattacharya, M., Evaluation of compatibility and properties of biodegradable polyester blends. *Journal of Polymer Science Part A: Polymer Chemistry* **2002**, *40* (12), 2003–2014. DOI: 10.1002/pola.10297.

4. Qiu, Z.; Yang, W.; Ikehara, T.; Nishi, T., Miscibility and crystallization behavior of biodegradable blends of two aliphatic polyesters. Poly(3-hydroxybutyrate-co-hydroxyvalerate) and poly(ε-caprolactone). *Polymer* **2005**, *46* (25), 11814–11819. DOI: 10.1016/j.polymer.2005.10.058.

5. Ciulik, C.; Safari, M.; Martínez de Ilarduya, A.; Morales-Huerta, J. C.; Iturrospe, A.; Arbe, A.; Müller, A. J.; Muñoz-Guerra, S., Poly(butylene succinate-ran-ε-caprolactone) copolyesters: Enzymatic synthesis and crystalline isodimorphic character. *European Polymer Journal* **2017**, *95*, 795–808. DOI: 10.1016/j.eurpolymj.2017.05.002.

6. Pérez-Camargo, R. A.; Arandia, I.; Safari, M.; Cavallo, D.; Lotti, N.; Soccio, M.; Müller, A. J., Crystallization of isodimorphic aliphatic random copolyesters: Pseudo-eutectic behavior and double-crystalline materials. *European Polymer Journal* **2018**, *101*, 233–247. DOI: 10.1016/j.eurpolymj.2018.02.037.

7. Safari, M.; Mugica, A.; Zubitur, M.; Martínez de Ilarduya, A.; Muñoz-Guerra, S.; Müller, A. J., Controlling the Isothermal Crystallization of Isodimorphic PBS-ran-PCL Random Copolymers by Varying Composition and Supercooling. *Polymers* **2019**, *12* (1), 17. DOI: 10.3390/polym12010017.

8. Xue, L.; Zhang, J.; Han, Y., Phase separation induced ordered patterns in thin polymer blend films. *Progress in Polymer Science (Oxford)* **2012**, *37* (4), 564–594. DOI: 10.1016/j.progpolymsci.2011.09.001.

9. Criado-Gonzalez, M.; Fernandez-Gutierrez, M.; Roman, J. S.; Mijangos, C.; Hernández, R., Local and controlled release of tamoxifen from multi (layer-by-layer) alginate/chitosan complex systems. *Carbohydrate Polymers* **2019**, *206*, 428–434. DOI: 10.1016/j.carbpol.2018.11.007.

10. Gonzalez, J. S.; Mijangos, C.; Hernandez, R., Polysaccharide coating of gelatin gels for controlled BSA release. *Polymers* **2019**, *11* (4), 702. DOI: 10.3390/polym11040702.

11. Criado, M.; Rebollar, E.; Nogales, A.; Ezquerra, T. A.; Boulmedais, F.; Mijangos, C.; Hernández, R., Quantitative Nanomechanical Properties of Multilayer Films Made of Polysaccharides through Spray Assisted Layer-by-Layer Assembly. *Biomacromolecules* **2017**, *18* (1), 169–177 DOI: 10.1021/acs.biomac.6b01449.

12. Lavalle, P.; Voegel, J. C.; Vautier, D.; Senger, B.; Schaaf, P.; Ball, V., Dynamic aspects of films prepared by a sequential deposition of species: Perspectives for smart and responsive materials. *Advanced Materials* **2011**, *23* (10), 1191–1221. DOI: 10.1002/adma.201003309.

13. Weng, K.; Ye, L.; Zhu, L.; Xu, J.; Zhou, J.; Feng, X.; Lu, G.; Tan, S.; Liu, F.; Sun, Y., Optimized active layer morphology toward efficient and polymer batch insensitive organic solar cells. *Nature Communications* **2020**, *11* (1), 1–9. DOI: 10.1038/s41467-020-16621-x.

14. Hwang, H.; Lee, H.; Shafian, S.; Lee, W.; Seok, J.; Ryu, K. Y.; Ryu, D. Y.; Kim, K., Thermally stable bulk heterojunction prepared by sequential deposition of nanostructured polymer and fullerene. *Polymers* **2017**, *9* (9), 456. DOI: 10.3390/polym9090456.

15. Larrañaga, A.; Lizundia, E., A review on the thermomechanical properties and biodegradation behaviour of polyesters. *European Polymer Journal* **2019**, *121*, 109296. DOI: 10.1016/j.eurpolymj.2019.109296.

16. Stein, G. E.; Laws, T. S.; Verduzco, R., Tailoring the Attraction of Polymers toward Surfaces. *Macromolecules* **2019**, *52* (13), 4787–4802. DOI: 10.1021/acs.macromol.9b00492.

17. Yang, J.; Liang, Y.; Shi, W.; Lee, H. S.; Han, C. C., Effects of surface wetting induced segregation on crystallization behaviors of melt-miscible poly(l-lactide)-block-poly(ethylene glycol) copolymer thin film. *Polymer* **2013**, *54* (15), 3974–3981. DOI: 10.1016/j.polymer.2013.05.032.

18. Ma, M.; He, Z.; Yang, J.; Wang, Q.; Chen, F.; Wang, K.; Zhang, Q.; Deng, H.; Fu, Q., Vertical phase separation and liquid-liquid dewetting of thin PS/PCL blend films during spin coating. *Langmuir* **2011**, *27* (3), 1056–1063. DOI: 10.1021/la104003p.

19. Ma, M.; Chen, F.; Wang, K.; Zhang, Q.; Deng, H.; Li, Z.; Fu, Q., Anisotropic dewetting holes with instability fronts in ultrathin films of polystyrene/poly(□-caprolactone) blend. *Macromolecules* **2012**, *45* (11), 4932–4937. DOI: 10.1021/ma3000779.

20. Roland, S. S.; Gaspard, D.; Prud'homme, R. E.; Bazuin, C. G., Morphology Evolution in Slowly Dip-Coated Supramolecular PS-b-P4VP Thin Films. *Macromolecules* **2012**, *45* (13), 5463–5476. DOI: 10.1021/ma3007398.

21. Roland, S. S.; Pellerin, C.; Bazuin, C. G.; Prud'homme, R. E., Evolution of Small Molecule Content and Morphology with Dip-Coating Rate in Supramolecular PS−P4VP Thin Films. *Macromolecules* **2012**, *45* (19), 7694–7972. DOI: 10.1021/ma301383v.

22. Vital, A.; Vayer, M.; Tillocher, T.; Dussart, R.; Boufnichel, M.; Sinturel, C., Morphology control in thin films of PS:PLA homopolymer blends by dip-coating deposition. *Applied Surface Science* **2017**, *393*, 127–133. DOI: 10.1016/j.apsusc.2016.09.151.

23. Grosso, D., How to exploit the full potential of the dip-coating process to better control film formation. *Journal of Materials Chemistry* **2011**, *21* (43), 17033–17038. DOI: 10.1039/c1jm12837j.

24. Smith, J. R.; Lamprou, D. A., Polymer coatings for biomedical applications: A review. *Transactions of the Institute of Metal Finishing* **2014**, *92* (1), 9–19. DOI: 10.1179/0020296713Z.000000000157.

25. Visan, A. I.; Popescu-Pelin, G.; Gherasim, O.; Mihailescu, A.; Socol, M.; Zgura, I.; Chiritoiu, M.; Sima, L. E.; Antohe, F.; Ivan, L.; Vranceanu, D. M.; Cotrut, C. M.; Cristescu, R.; Socol, G., Long-term evaluation of dip-coated PCL-blend-PEG coatings in simulated conditions. *Polymers* **2020**, *12* (3), 717. DOI: 10.3390/polym12030717.

26. Safari, M.; Martínez De Ilarduya, A.; Mugica, A.; Zubitur, M.; Muñoz-Guerra, S.; Müller, A. J., Tuning the Thermal Properties and Morphology of Isodimorphic Poly[(butylene succinate)- ran-(ϵ-caprolactone)] Copolyesters by Changing Composition, Molecular Weight, and Thermal History. *Macromolecules* **2018**, *51* (23), 9589–9601. DOI: 10.1021/acs.macromol.8b01742.

27. Liu, Q.; Zhou, X. M., Preparation of Poly(butylene succinate)/poly(ε-caprolactone) Blends Compatibilized With Poly(butylene succinate-co-ε-caprolactone) Copolymer. *Journal of Macromolecular Science, Part A: Pure and Applied Chemistry* **2015**, *52* (8), 625–629. DOI: 10.1080/10601325.2015.1050634.

28. Hammersley, A. P., FIT2D: A multi-purpose data reduction, analysis and visualization program. *Journal of Applied Crystallography* **2016**, *49*, 646–652. DOI: 10.1107/S1600576716000455.

29. Govyadinov, A. A.; Amenabar, I.; Huth, F.; Scott Carney, P.; Hillenbrand, R., Quantitative measurement of local infrared absorption and dielectric function with tip-enhanced near-field microscopy. *Journal of Physical Chemistry Letters* **2013**, *4* (9), 1526–1531. DOI: 10.1021/jz400453r.

30. Amenabar, I.; Poly, S.; Goikoetxea, M.; Nuansing, W.; Lasch, P.; Hillenbrand, R., Hyperspectral infrared nanoimaging of organic samples based on Fourier transform infrared nanospectroscopy. *Nature Communications* **2017**, *8*, 14402. DOI: 10.1038/ncomms14402.

31. Amenabar, I.; Poly, S.; Nuansing, W.; Hubrich, E. H.; Govyadinov, A. A.; Huth, F.; Krutokhvostov, R.; Zhang, L.; Knez, M.; Heberle, J.; Bittner, A. M.; Hillenbrand, R., Structural analysis and mapping of individual protein complexes by infrared nanospectroscopy. *Nature Communications* **2013**, *4*, 2890. DOI: 10.1038/ncomms3890.

32. Qiao, C.; Zhao, J.; Jiang, S.; Jl, X.; Lijia, A. N.; Jiang, B., Crystalline morphology evolution in PCL thin films. *Journal of Polymer Science, Part B: Polymer Physics* **2005**, *43* (11), 1303–1309. DOI: 10.1002/polb.20422.

33. Ma, M.; He, Z.; Yang, J.; Chen, F.; Wang, K.; Zhang, Q.; Deng, H.; Fu, Q., Effect of film thickness on morphological evolution in dewetting and crystallization of polystyrene/poly(ε-caprolactone) blend films. *Langmuir* **2011**, *27* (21), 13072–13081. DOI: 10.1021/la2036289.

34. Maillard, D.; Prud'homme, R. E., Crystallization of ultrathin films of polylactides: From chain chirality to lamella curvature and twisting. *Macromolecules* **2008**, *41* (5), 1705–1712. DOI: 10.1021/ma071306u.

35. Spièce, J.; Martínez-Tong, D. E.; Sferrazza, M.; Nogales, A.; Napolitano, S., Are polymers glassier upon confinement? *Soft Matter* **2015**, *11* (31), 6179–6186. DOI: 10.1039/c5sm01229e.

36. Hernández, J. J.; Rueda, D. R.; García-Gutiérrez, M. C.; Nogales, A.; Ezquerra, T. A.; Soccio, M.; Lotti, N.; Munari, A., Structure and morphology of thin films of linear aliphatic polyesters prepared by spin-coating. *Langmuir* **2010**, *26* (13), 10731–10737. DOI: 10.1021/la100959j.

37. Yang, I.-K.; Yun Liu, C., Real-Time SAXS and WAXS Study of the Multiple Melting Behavior of Poly(e-caprolactone). *Journal of Polymer Science: Part B: Polymer Physics* **2010**, *48*, 1777–1785. DOI: 10.1002/polb.22035.

38. Safari, M.; Maiz, J.; Shi, G.; Juanes, D.; Liu, G.; Wang, D.; Mijangos, C.; Alegría, ángel; Müller, A. J., How Confinement Affects the Nucleation, Crystallization, and Dielectric Relaxation of Poly(butylene succinate) and Poly(butylene adipate) Infiltrated within Nanoporous Alumina Templates. *Langmuir* **2019**, *35* (47), 15168–15179. DOI: 10.1021/acs.langmuir.9b02215.

39. Gumede, T. P.; Luyt, A. S.; Pérez-Camargo, R. A.; Tercjak, A.; Müller, A. J., Morphology, nucleation, and isothermal crystallization kinetics of Poly(Butylene Succinate) mixed with a polycarbonate/MWCNT masterbatch. *Polymers* **2018**, *10* (4), 424. DOI: 10.3390/polym10040424.

40. Meyer, A. B., Investigation of molecular orientation in thin polymer films using X-ray scattering at grazing incidence, *University of Hamburg* **1998**.

41. Vayer, M.; Pineau, A.; Warmont, F.; Roulet, M.; Sinturel, C., Constrained crystallization of poly(L-lactic acid) in thin films prepared by dip-coating. *European Polymer Journal* **2018**, *101*, 332–340. DOI: 10.1016/j.eurpolymj.2018.03.006.

42. Strawhecker, K. E.; Kumar, S. K.; Douglas, J. F.; Karim, A., The critical role of solvent evaporation on the roughness of spin-cast polymer films. *Macromolecules* **2001**, *34* (14), 4669–4672. DOI: 10.1021/ma001440d.

43. Huth, F.; Govyadinov, A.; Amarie, S.; Nuansing, W.; Keilmann, F.; Hillenbrand, R., Nano-FTIR absorption spectroscopy of molecular fingerprints at 20 nm spatial resolution. *Nano Letters* **2012**, *12* (8), 3973–3978. DOI: 10.1021/nl301159v.

44. Richards, D.; Zayats, A., Nano-Optics and Near-Field Optical Microscopy. (Artech House) **2008**, 1–376.

45. Nguyen Tri, P.; Prud'Homme, R. E., Crystallization and Segregation Behavior at the Submicrometer Scale of PCL/PEG Blends. *Macromolecules* **2018**, *51* (18), 7266–7273. DOI: 10.1021/acs.macromol.8b01503.

46. Mester, L.; Govyadinov, A. A.; Chen, S.; Goikoetxea, M.; Hillenbrand, R., Subsurface chemical nanoidentification by nano-FTIR spectroscopy. *Nature Communications* **2020**, *11* (1), 3359. DOI: 10.1038/s41467-020-17034-6.

47. Taubner, T.; Keilmann, F.; Hillenbrand, R., Nanoscale-resolved subsurface imaging by scattering-type near-field optical microscopy. *Optics Express* **2005**, *13* (22), 8893. DOI: 10.1364/opex.13.008893.

48. Dazzi, A.; Prater, C. B., AFM-IR: Technology and applications in nanoscale infrared spectroscopy and chemical imaging. *Chemical Reviews* **2017**, *117* (7), 5146–5173. DOI: 10.1021/acs.chemrev.6b00448.

49. Monrreal-Rodríguez, A. K.; Garibay-Alvarado, J. A.; Vargas-Requena, C. L.; Reyes-López, S. Y., In vitro evaluation of poly-ε-caprolactone-hydroxypatite-alumina electrospun fibers on the fibroblast's proliferation. *Results in Materials* **2020**, *6*, 100091. DOI: 10.1016/j.rinma.2020.100091.

50. Elzein, T.; Nasser-Eddine, M.; Delaite, C.; Bistac, S.; Dumas, P., FTIR study of polycaprolactone chain organization at interfaces. *Journal of Colloid and Interface Science* **2004**, *273* (2), 381–387. DOI: 10.1016/j.jcis.2004.02.001.

51. Yao, S. F.; Chen, X. T.; Ye, H. M., Investigation of Structure and Crystallization Behavior of Poly(butylene succinate) by Fourier Transform Infrared Spectroscopy. *Journal of Physical Chemistry B* **2017**, *121* (40), 9476–9485. DOI: 10.1021/acs.jpcb.7b07954.

Chapter 4

Tunable Enzymatic Degradation of PBS Films:

Polysaccharidic Based Multilayer Coatings

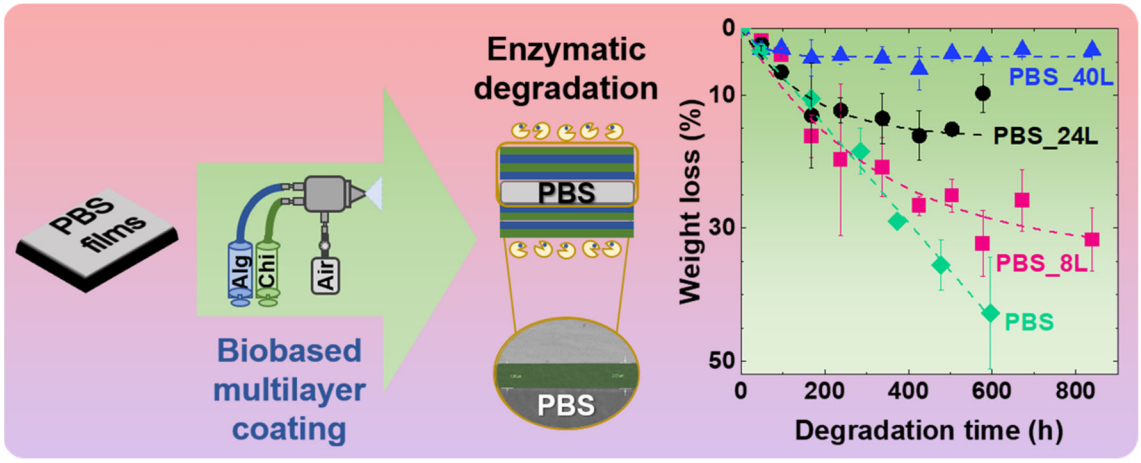

4.1. Introduction

Poly(butylene succinate) (PBS or PBSu), sometimes referred to as poly(tetramethylene succinate) (PTMS), is an aliphatic polyester that can be included in fossil-based biodegradable polymers. PBS can also be produced through biobased monomers obtained through fermentative production routes based on renewable feedstocks.[1] In soil, PBS degrades significantly faster than conventional plastics, and hence it constitutes a solution to the growing problem of accumulation of non biodegradable plastics.[2,3] Some of its potential uses include biomedical applications, packaging, and agriculture. To give a few examples, PBS has been employed to prepare polymeric mulch films to reduce plastic accumulation in soil,[4] and for the fabrication of soft packaging.[5] The biomedical applications of PBS and PBS-based materials have also been evaluated recently.[6] Moreover, in Chapter 2, an exhaustive review of the mechanical and thermal properties, crystallinity, barrier properties, and the different degradation methods of PBS and PBS-based copolymers and nanocomposites was presented.[7] Despite all the possible applications of PBS, the study of its biodegradation must be conducted carefully, as it can condition its application in different fields. To that aim, the degradation studies of PBS should be in consonance with its specific applications. For example, the hydrolytic degradation could be more related to the different biomedical applications of this polyester, whereas degradation under environmental conditions (soil burial, activated sludge, compost) could be more interesting for mulching films in agricultural applications.[8–10]

Most of the enzymatic degradation assays, which consist of a hydrolytic degradation catalyzed by an enzyme, are developed under physiological conditions (i.e., 37 ºC and pH 7-7.5).[11–13] Enzymatic degradation is more favored for PBS samples with low molecular weight and low crystallinity,[12,14] as well as at a temperature close to T_m (the PBS melting temperature is above 100 ºC), even though the self-stability of the enzymes at high temperature constitutes a drawback.[15] In literature, PBS enzymatic degradation presents a wide range of results, depending on the type of enzyme and experimental conditions. Some

authors have reported complete PBS degradation in a few hours employing different cutinases[11,16,17] and lipases,[17,18] whereas other authors observed quite low weight losses with cholesterol esterases;[19] or even negligible degradation.[12,13,20] Lipases (EC:3.1.1.3) are esterases with the ability to hydrolyze long-chain triglycerides to di- and subsequently monoglycerides.[21] Regarding the enzymatic degradation of polyesters and PBS in particular, the majority of the experiments are done with films immersed within an enzymatic solution.

Taking into consideration the high importance of focusing polymers (and, more specifically, polyesters) towards zero-waste materials, the biodegradation of PBS and its comprehension becomes a key point nowadays. In this Chapter, we report on a novel strategy to modulate the enzymatic degradation of PBS films through their combination with biobased polymers (e.g., polysaccharides) (Scheme 4.1). For this study, a lipase from *Pseudomonas cepacia* (*P. cepacia*) with a sequence composition containing 364 amino acids has been selected.[22] For such purpose, the preparation of biobased multilayer coatings, consisting of polysaccharide polyelectrolyte complexes (PPC) of alginate and chitosan deposited onto PBS films will be assessed, and the degradation of the PBS-coated films immersed in aqueous solutions containing lipase will be monitored as a function of the time. PPC have been widely investigated as good barrier materials for paperboard and other materials conducted towards sustainable packaging applications.[23–25] On this basis, PPC have been recently incorporated into biopolyester materials as a way to improve barrier properties of these packaging materials.[26,27] In addition to this, the employment of PPC in biomedical applications is also widely reported in the literature.[28,29] In particular, alginate and chitosan have been assembled into nanostructured films using layer-by-layer (LbL) assembly to be used in several biomedical applications, such as matrixes for drug delivery modulation, and iron oxide nanoparticles encapsulation for magnetic hyperthermia therapies,[30–33] due to its good stability conferred by the electrostatic interactions created among both components. However, to the best of our knowledge, the effect of PPC coatings on the biodegradation of PBS films has not

been reported so far. We hypothesize that these coatings will be able to regulate the enzymatic degradation of PBS.

Such approach could be interesting for several applications in the biomedical, agricultural or food industry fields, where degradation takes an important role. The solution proposed in this Chapter enable the facile modification of the degradation kinetics by employing biobased materials. To sum up, the present Chapter will focus on PBS enzymatic biodegradation. As a first step, the experimental conditions to carry out enzymatic degradation assays of PBS will be optimized, and thereafter, the influence of a biobased polysaccharide multilayer coating on the enzymatic degradation of PBS will be ascertained.

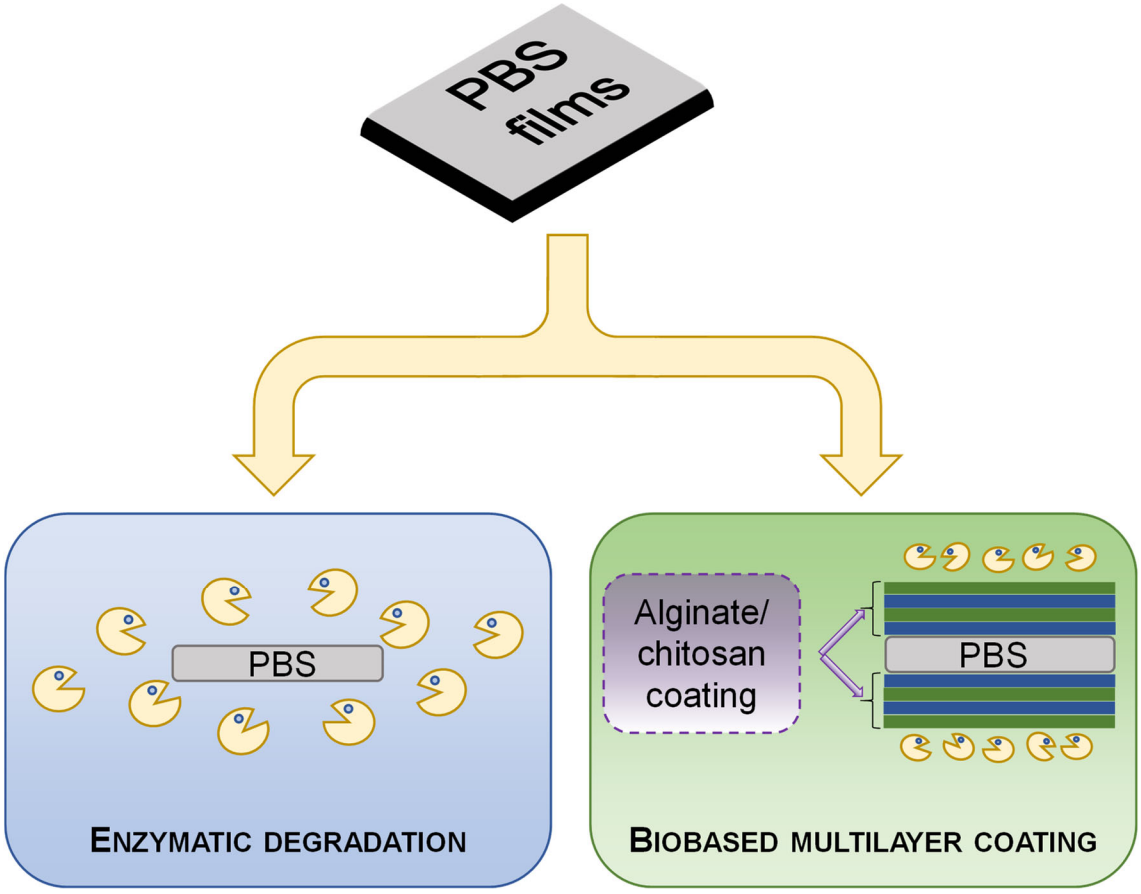

Scheme 4.1. Schematic overview of the two enzymatic biodegradation approaches proposed for PBS films: optimization of the enzymatic degradation and modulation of the biodegradation through the preparation of biobased multilayer coatings.

4.2. Experimental Part

4.2.1. Materials

Commercial poly(1,4-butylene succinate), extended with 1,6-diisocyanatohexane (Lot #MKBX5346V and referred to as PBS, M_w ~112,000 g/mol [GPC], M_n ~81,000 g/mol [GPC], M_n ~53,000 g/mol [^{1}H-NMR]), lipase from *P. cepacia* (Lot #BCBV1950, Lot #BCCG3768, Lot #BCBP8887V), phosphate buffered saline (physiologic pH of 7.2-7.4), alginic acid sodium salt from brown algae of low (Lot #SLCG0203) viscosity, chitosan (low molecular weight, Lot #BCCD9853), polyethylenimine branched (PEI), sodium acetate anhydride and Triton X-100 were purchased from Sigma-Aldrich. Calcium chloride dihydrate was acquired from Acros Organics, acetic acid glacial and 2-propanol were acquired from Scharlab and VWR, and *p*-nitrophenyl palmitate (pNPP) was provided by Alfa Aesar. Sunflower oil of alimentary grade was also employed. All reagents were used as received, except chitosan, which was purified to remove impurities following a typical methodology.[31]

4.2.2. Preparation of neat PBS hot-pressed films

Micrometric polymeric films were prepared by hot-pressing PBS pellets in a Collin 200x200 (Collin Solutions, GmbH, Germany) pneumatic press (see Scheme 4.2a). The conditions for the preparation of the films consisted of four steps done at 125 ºC: *i)* 5 minutes at 5 bars, *ii)* 2 minutes at 50 bars, *iii)* 2 minutes at 100 bars, and *iv)* a final extra cooling step (at room temperature) for 2 minutes at 100 bars. The average thickness of these films was 0.12 ± 0.02 mm, as determined by employing a digital caliper. The films were kept at room temperature for one week before starting the experiments.

4.2.3. Preparation and characterization of polyelectrolyte multilayer spray-coated PBS films

Spray-assisted layer-by-layer deposition was employed for the coating of PBS films with polysaccharide aqueous solutions following a procedure reported

elsewhere.[31,34] First, PBS films were cut into 25 x 10 mm^2 and introduced individually into a polyethylenimine (PEI) solution (1 mg/mL) for 5 minutes to confer PBS a more hydrophilic surface, as well as providing a positively charged surface, for a better deposition of the polysaccharide coating.[31–33,35] After that, the films were air-dried and washed for 2 minutes with Milli-Q water. Then, they were placed onto a metallic support for the multilayer spray-coating in the automatic equipment (ND-SP Spray Coater, Nadetech Innovations, Spain). The support with the sample was set at 135º with respect to the spray jet, in order to avoid the accumulation of alginate and chitosan solutions on the sample, which would lead to the formation of heterogeneities in the coating thickness (see Scheme 4.2b). Three different systems with varying alginate/chitosan layers (8, 24, and 40) were prepared and designated as *PBS_nL*, where *n* stands for the number of layers. For each sample, the corresponding number of layers was deposited through a consecutive deposition of alginate (2.5 mg/mL in pH 3 buffer solution) and chitosan (1 mg/mL in pH 5 buffer solution). Both sides of the PBS film were coated consecutively. Finally, samples were left drying at room temperature for 48 hours before further experiments.

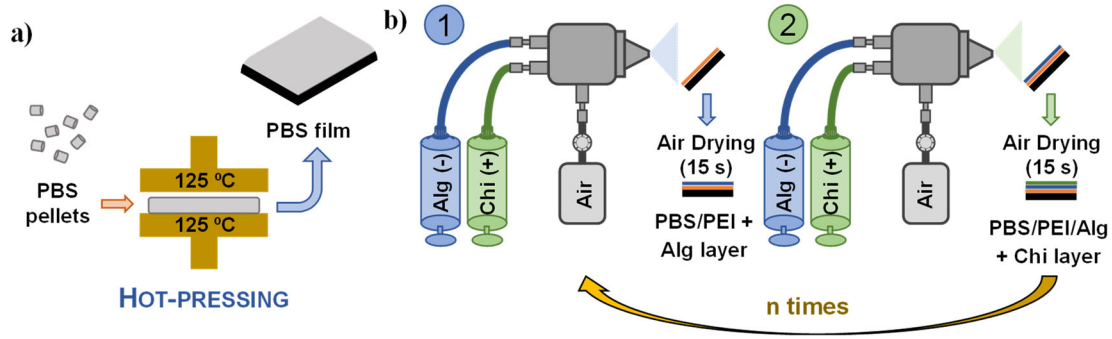

Scheme 4.2. Schematic representation of the preparation of the PBS films: **a)** hot-pressing process to obtain the PBS neat films, and **b)** spray-assisted layer-by-layer of polysaccharides for the fabrication of the Alg/Chi multilayer spray-coated PBS films. The spray-assisted LbL process was performed on both sides of the PBS film.

The thickness of the coating was assessed through Scanning Electron Microscopy (SEM) employing a Hitachi SU8000 Scanning Electron Microscope (Hitachi, Ltd., Japan) and operating at 0.8 kV. Spray-coated PBS films were

fractured in liquid nitrogen and gold-coated (Polaron SC7640 Sputter Coater, Quorum Technologies, Ltd., UK) prior to the SEM analysis. The values are presented as the average ± standard deviation of at least four positions in three different samples.

The surface wettability of the spray-coated PBS films (20 x 20 mm^2) and the neat PBS sample without coating was characterized by static Water Contact Angle (WCA) using a KSV Theta Goniometer coupled with a camera (KSV Instruments, Ltd., Finland). Water droplets of 3 μL were deposited on top of the samples, and pictures were recorded at different positions. WCA values were measured with the Software KSV CAM 200 Optical Contact Angle Meter, and results are expressed as the average ± standard deviation of at least four positions in three different samples.

4.2.4. Nanomechanical properties of PBS and alginate/chitosan coating

As a way of evaluating the mechanical behaviour of the polysaccharide coating, nanoindentation measurements were performed using a G200 Nanoindenter (KLA-Tencor Corp., USA) with a Berkovich diamond indenter. Storage modulus (E') and hardness (H) were determined using continuous stiffness measurements and a low load module (DCM). At least 30 indentation tests were produced at different locations to determine average values for each material (± standard deviation). For this purpose, alginate/chitosan coatings were deposited on two different substrates: PBS films and silicon wafers, both with dimensions 10 x 10 mm^2. For the sake of comparison, alginate and chitosan films were also tested. These polysaccharide films were obtained by pouring aqueous solutions of each polysaccharide (1 % w/v, chitosan solution also contained 1 % v/v of acetic acid) in separate Petri dishes and letting them dry in a stove set at 37 ºC for 7 days.

4.2.5. Enzymatic biodegradation by externally added lipases

a. Optimization of the experimental parameters

Enzymatic degradation assays were carried out with a lipase from *P. cepacia* at two different concentrations, 1 and 2 mg/mL. The enzymatic stock solution was prepared in phosphate buffered saline (pH 7.2-7.4). For this study, PBS films (10 x 10 mm^2) were immersed individually into 5 mL-glass vials containing 2 mL of the enzyme stock solution and placed into a thermostated chamber (Heraeus Instruments, Germany) at 37 ºC with rotational stirring (Rocker 3D Digital, IKA-Werke, GmbH & Co. KG, Germany) at 45 rpm. Experiments in the absence of stirring were also carried out to evaluate the effect of this parameter on the enzyme performance.

The samples were withdrawn at certain times, washed with distilled water, and finally weighed after complete drying at room temperature (48 hours). To control the enzymatic degradation, the weight loss of the samples was determined using the following equation (Equation 4.1).

$$W_{loss}\ (\%) = \frac{W_{initial} - W_{final}}{W_{initial}} \cdot 100 \qquad \text{(Eq. 4.1)}$$

Where W_{loss} stands for weight loss (expressed in %), $W_{initial}$ refers to the initial weight of the samples (before degradation), and W_{final} indicates the final weight of the samples after the degradation assays.

The molecular weight, crystallinity, and surface morphology of the withdrawn-dried PBS films were determined to monitor changes in these parameters as a function of the degradation time. Surface morphology was observed in a Zeta-20 Optical Profiler (KLA-Tencor Corp., USA) with a 0.50x Coupler attached at different magnifications (5x, 20x, 50x, and 100x). The determination of the number average molecular weight was carried out through Proton Nuclear Magnetic Resonance (^{1}H-NMR). Spectra were recorded in a Bruker AMX-300 Spectrometer (Bruker Corp., USA). 640 scans were recorded

from 10 mg sample solutions in 1 mL of deuterated chloroform. For M_n determination, signals from CH_2OH and CH_2COOH end groups were compared with the signals of $COOCH_2$ from samples derivatized with trifluoroacetic anhydride. Additionally, Gel Permeation Chromatography analysis (GPC) provided information on both number and weight average molecular weights. GPC were recorded in a Waters Instrument (Waters Corp., USA) equipped with RI and UV detectors. HR5E and HR2 Waters linear Styragel columns (7.8 mm × 300 mm, pore size 10^3-10^4 Å) packed with crosslinked polystyrene and protected with a precolumn were used. Samples were prepared by dissolving 1 mg of the sample in 1 mL of chloroform and using the same solvent as the eluent. Measurements were performed at 35 ºC with a flow rate of 0.5 mL/min and molecular weights were calculated against monodisperse polystyrene standards. The crystallinity of the films was further evaluated by Differential Scanning Calorimetry (DSC) in a PerkinElmer DSC 8500 with an Intracooler II (PerkinElmer, Inc., USA). For DSC analysis, PBS films were weighed and placed inside aluminum pans. Temperature sweeps with two scans were done from -30 to 160 ºC, at 10 and 20 ºC/min.

$$X_c = \frac{\Delta H_m}{\Delta H_m^0} \qquad \text{(Eq. 4.2)}$$

The crystallinity (X_c) was determined from the melting enthalpy (ΔH_m) of the peak that appeared at 110-115 ºC, which corresponds to the melting of PBS, and the equilibrium melting enthalpy (ΔH_m^0), which was considered to be 213 ± 10 J/g,[36] as detailed in Equation 4.2. DSC curves were analyzed with the Pyris Manager software (10.1 and 13.3 versions) from PerkinElmer, Inc.

b. Enzymatic degradation of PBS spray-coated films by externally added lipases

Enzymatic degradation assays were carried out with a lipase from *P. cepacia* at 2 mg/mL following the same procedure as for the neat films in Section 4.2.5.a. Then, the surface morphology changes were monitored as a function of degradation time by profilometry, as previously mentioned for the PBS neat films.

c. Method for the determination of the enzyme activity

In order to assess the performance of the lipase towards degradation, the enzymatic activity was checked before the experiment, during it, and after conducting the biodegradation. The procedure for determining the enzyme activity consisted in measuring the UV absorbance of the pNPP degradation over time at 410 nm, as detailed below.

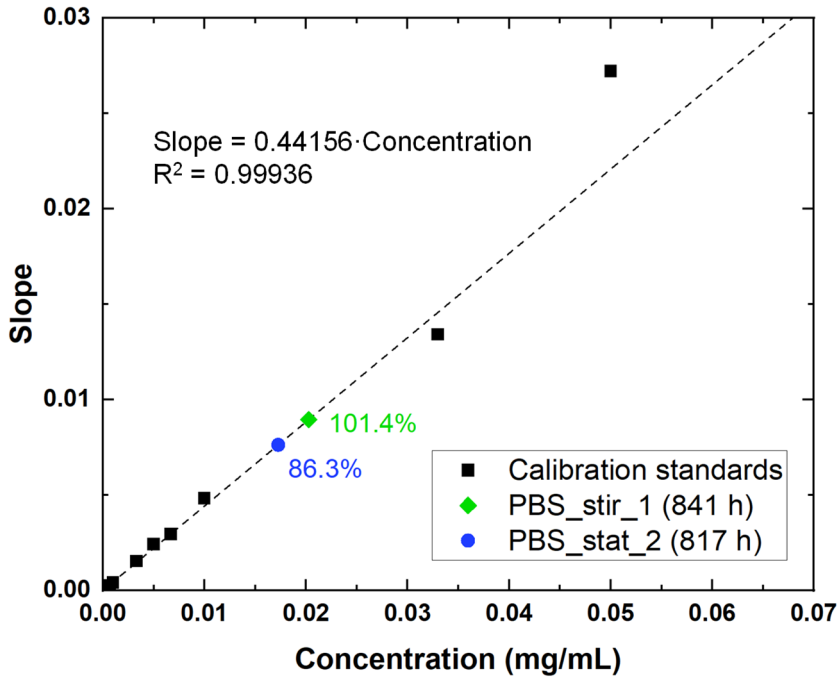

Figure 4.1. Calibration curve for lipase from *P. cepacia*, employed in PBS films degradation assays. The calibration curve (dashed black line) was obtained from experimental data (black squares) of the different slopes of the UV curves for several enzyme standards at different concentrations. Enzymatic activity was checked for two different PBS degradation experiments at the end of the assay: PBS_stat_2 and PBS_stir_1. The percentage values next to these experimental results indicate the relative activity against the calibration curve, as all these samples were measured at a theoretically concentration of 0.02 mg/mL, whereas the values in brackets shown in the legend correspond to the degradation time.

For the evaluation of the enzymatic activity, the following method reported elsewhere was used.[37,38] Firstly, a *p*-nitrophenyl palmitate (pNPP) solution was prepared at 3 mg/mL in 2-propanol, adding Triton X-100 at 0.6 % v/v with respect to phosphate buffered saline, and completing the total volume with the same

buffer, in a ratio 9:1 against 2-propanol. This solution is referred as the substrate solution. An enzyme stock solution was also prepared and from it, several standards were obtained for the preparation of a calibration curve. For the recording of the UV curves at 410 nm, 900 μL of the substrate solution were placed over 100 μL of the different enzyme standard solutions in a quartz cuvette (total volume ~1 mL). A blank was also employed with 1 mL of substrate solution. All samples/standards for the calibration curve were measured in duplicate/triplicate.

The calibration curve was obtained by the correlation between the concentration of the enzyme (the different prepared standards) and the slope of the UV curve over time, in the linear region (first stage). This curve was further employed for checking the activity of the enzyme in the biodegradation experiments. The different aliquots taken from the vials containing the enzyme solution from the biodegradation experiments revealed that the lipase remained active during the whole assay (see Figure 4.1), as evidenced by the relative activity obtained for them, ranged 86-101 %.

4.3. Results and Discussion

Many works have studied the degradation of PBS within different environments, including hydrolytic, enzymatic, compost, and soil burial. Focusing on the enzymatic degradation –the media of our study–, published results from different research groups show great variability in the extent of enzymatic degradation of PBS measured through the measurement of weight loss over time, which are related to different enzymes employed, degradation conditions (there are no standard conditions, as in other degradation tests, such as soil burial or compost) or even due to differences in PBS crystallinity. This variety of conditions results in high degradation rates for cutinases,[11,16,17,39] whereas lipases cover the whole range, from non-visible degradation[40] to total degradation.[17,18] The influence of the enzyme concentration has been a subject of study, as varying this parameter is one way to control and tune the degradation.[41] To that aim, herein one novel strategy to modulate the enzyme-induced degradation of PBS films is investigated by tuning their performance: the fabrication of polysaccharide multilayer spray-coated PBS films (Scheme 4.2b), and results will be compared with neat PBS films.

4.3.1. Effect of lipase concentration and stirring on the enzymatic degradation of PBS neat films

In a first step, the enzymatic degradation of PBS neat films was studied. For such purpose, different experimental conditions of enzyme concentration (1 and 2 mg/mL) and stirring/stationary (*stir*/*stat*) were employed, and samples were named as *PBS_stirring condition_lipase concentration* (e.g., films tested under stirring in a 2 mg/mL lipase solution are named as *PBS_stir_2*). Figure 4.2a shows the weight loss as a function of time of PBS films immersed in lipase aqueous solutions. For the PBS films immersed in an aqueous solution of lipase at 1 mg/mL (PBS_stir_1), there is a clear tendency to achieve a lower degradation extent when compared with PBS films immersed in 2 mg/mL lipase aqueous solutions. In addition, the weight loss achieved is lower for samples immersed in the lowest concentration of

lipase aqueous solution (1 mg/mL). Regarding the stirring effect, for PBS films immersed in 2 mg/mL lipase aqueous solutions, stirring seems to favor the PBS degradation slightly. An interesting effect of stirring on enzyme-degraded PBS films was related to the initial area where the degradation started. Visual observations and profilometry images revealed the lipase-induced degradation of the films subjected to stirring, starting from the central part of the film and then continuing towards the edges, showing a "hole" degradation effect (see Figure 4.3a). On the other hand, PBS films tested under stationary conditions (no stirring) showed the enzymatic degradation started from the edges towards the center and the corners exhibiting a "ring" degradation effect (Figure 4.3b). Such effect could be related to the contact achieved, as it is well-known that stirring enhances the adsorption of the enzyme on the polymer surface, promoting the degradation rate.[42] However, not related examples have been found in literature regarding this effect of stirring on degradation, as some authors reported a edge-to-center degradation for PCL discs,[43] whereas in a different publication, the observed degradation started from the surface rather from the edges.[44] It is important to note that the maximum weight loss of the sample used as a negative control in absence of enzyme (PBS_control) was around 1.5 wt%, which means that PBS films did not show any significant degradation under stirring at 37 ºC in phosphate buffered saline solution in the absence of lipase.

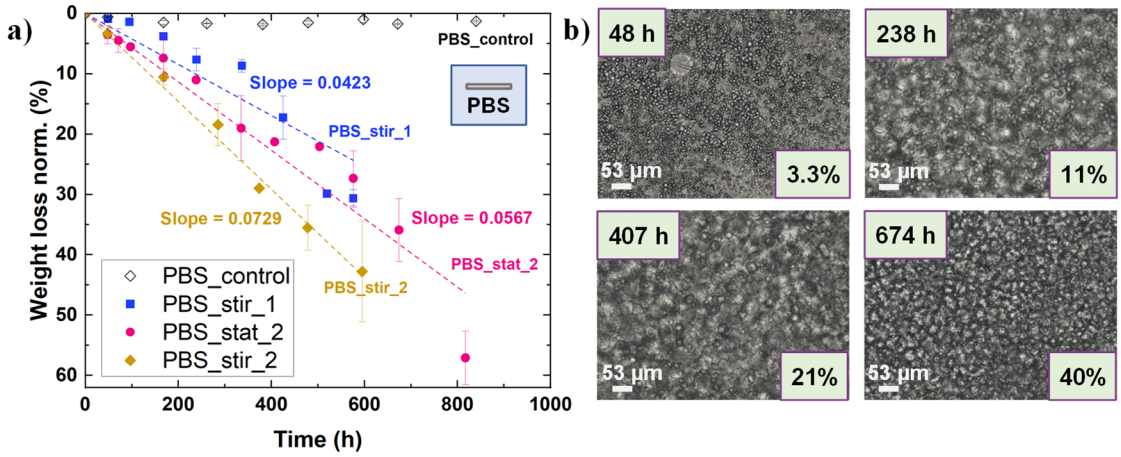

Figure 4.2. a) Determination of the weight loss for PBS films immersed in aqueous lipase solutions under different experimental conditions. For comparison, slope values are reported within the figure, which are related to degradation kinetics. Dashed lines show the linear fitting of the curves. **b)** Optical profilometry images were taken at 20x magnification for PBS_stat_2 films. In the upper left corner, the degradation time is included (in hours [h]), whereas the weight loss percentage is shown in the lower right corner.

The degradation kinetics, determined from the slope of the weight loss curves, showed a faster weight loss as the enzyme concentration increased (Figure 4.2a). Moreover, the stirring also influences the kinetics of degradation, leading to higher weight loss values for experiments performed under stirring compared to stationary conditions. Thus, the slope of the linear fit of the data showed a value of 0.0423 %/h for PBS_stir_1, whereas PBS_stir_2 and PBS_stat_2 exhibited values of 0.0729 and 0.0567 %/h, respectively. This ~70 % increase in the slope value when increasing the lipase concentration from 1 to 2 mg/mL proves the importance of selecting an appropriate enzyme concentration for the enzymatic biodegradation tests.

Optical images were taken by profilometry to analyze the surface of the degraded PBS films over time. The representative results obtained for the sample PBS_stat_2 are shown in Figure 4.2b. As appreciated in this figure, the surface is quite homogeneous after 48 hours (below 5 wt% weight loss), but after 10 days, some holes are visible even if PBS films showed a moderate weight loss (~11 wt%). These results are also in accordance with previous reports, which showed

the appearance of holes during biodegradation,[11,17] indicating that degradation takes places through surface erosion mechanism.

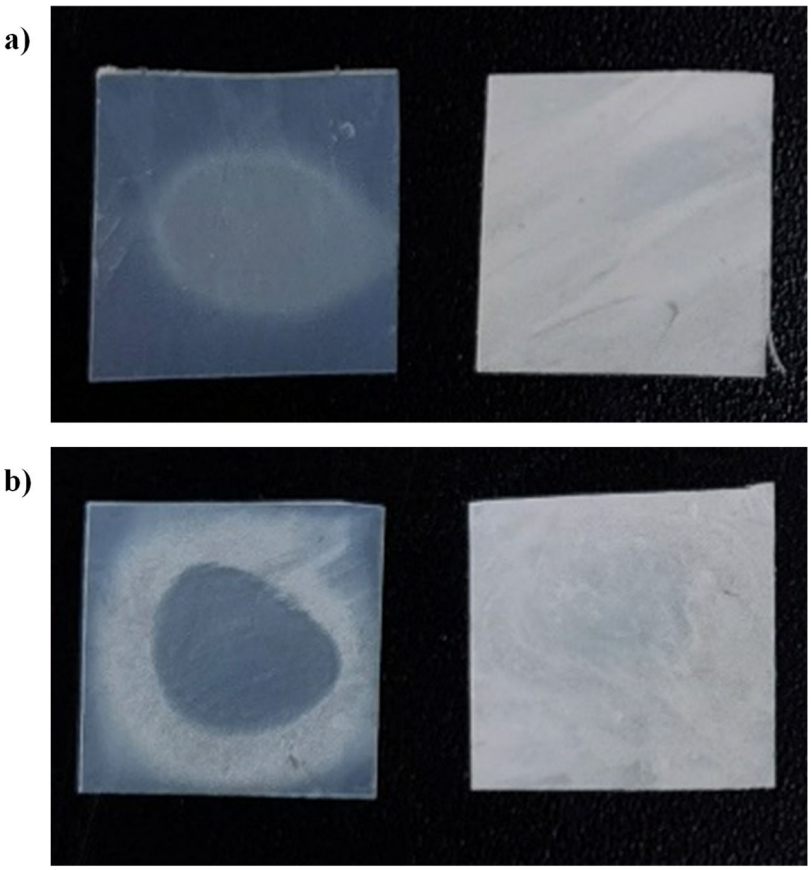

Figure 4.3. Comparison of stirring on PBS films degradation: **a)** PBS_stir_1, and **b)** PBS_stat_2. Left images correspond to 48 h of degradation, images on the right were taken at the end of degradation assays.

It is important to note that variations of crystallinity and molecular weight of the degraded samples were also monitored as a function of time, and the results are shown in Figure 4.4. Regarding PBS crystallinity, DSC analysis revealed no significant changes in the degree of crystallinity (Figure 4.4a). For PBS_stir_1 films, there was a small increase in the degree of crystallinity from 28 to 32 %, which could be due to a degradation of the amorphous part of the films.[45] Nonetheless, this trend was not observed for films studied under stationary conditions, PBS_stat_2, as the crystallinity remained almost constant. This result implies that the enzymatic degradation occurs simultaneously both in the amorphous and crystalline regions of the film, as a non-detectable change in

crystallinity was observed. In the case of PBS_stir_1 films, the degradation could be led by a more preferential attack on amorphous regions, which could explain the small increase in crystallinity. This effect could be due to the agitation of the enzymatic medium: in a static assay, the enzyme finds it easier to reach both amorphous and crystalline regions; when the experiment is carried out with stirring, the enzyme is less prone to attach to the surface, reaching preferentially the more amorphous regions, which are more susceptible to enzymatic attack because of their more porous structure. This equilibrium/slight increase was also observed in the literature on PBS films and fibers.[45,46] In an interesting study with PBS single crystals, AFM showed a preferential enzymatic attack on the crystal edges, whereas the central part remained invariable, giving credibility to a less favored affinity towards crystalline parts.[47] Likewise, the molecular weight of the films, M_n, showed a slight decrease (confirmed by both GPC and ^{1}H-NMR) throughout the course of the enzymatic degradation assay (Figure 4.4b), which suggests the bulk PBS structure remained unaltered, indicating that the degradation takes place mainly at the surface, through a surface erosion mechanism, which is in consonance with the crystallinity results provided by DSC.

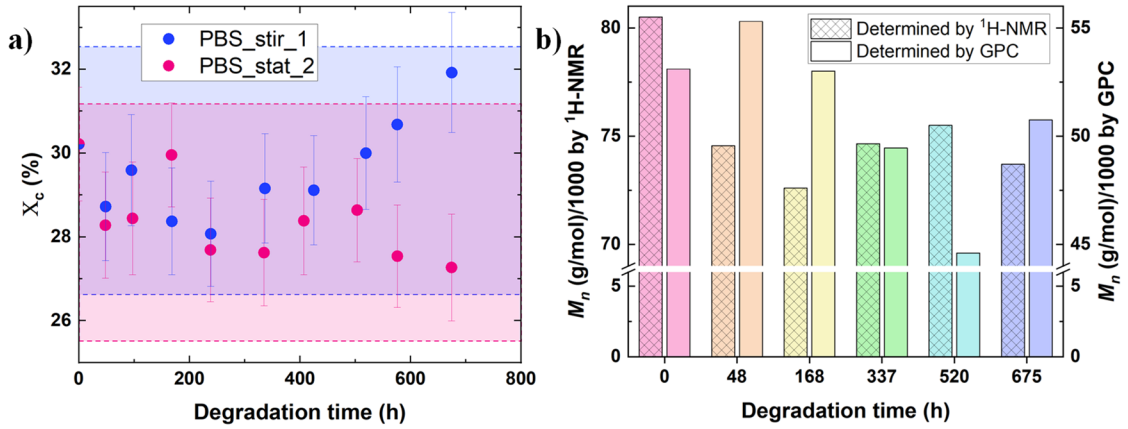

Figure 4.4. a) Changes in crystallinity of different PBS films, and **b)** Molecular weight (M_n) variation of PBS_stir_1 films (determined both by ^{1}H-NMR, left axis; and GPC, right axis). Shaded areas in Fig. 4.2a show a ± 10 % variation in X_c.

Traditionally, enzymatic degradation has been considered to follow a surface erosion mechanism, as opposed to a bulk erosion behaviour of hydrolytic degradation. For both mechanisms, crystallinity, molecular weight, and chemical

structure, among other factors, are known to influence the degradation. However, in enzymatic degradation, due to its eroding mechanism, the molecular weight of the substrate does not represent an important variation, as the low M_w products are water-soluble.[48] In fact, it has been reported that *P. cepacia* enzymatic degradation of PBS gives rise to 4-hydroxybutyl succinate as the main product (water-soluble), and traces of succinic acid and 1,4-butanediol as well.[37,46] Thus, the results obtained by GPC support that the most probable mechanism for degradation is through surface erosion, as the molecular weight of the degraded films did not change over the experiment. Nonetheless, this type of mechanism usually leads to a decrease in the size of the sample by creating visible holes or eroding the edges.[17,39] In our case, no holes nor reduction in size were observed, but only a decrease in the thickness for highly degraded films. The thicknesses for PBS_stir_1 and PBS_stat_2 films decreased from 120 ± 20 μm (non-degraded films) to 46 ± 6 μm (~62 % reduction) and 38 ± 5 μm (~68 % reduction), respectively. Similar observations were reported for PCL and PLA films.[43,49,50]

4.3.2. Modulation of the enzyme-induced degradation of PBS films through a LbL polysaccharide coating

a. Fabrication and morphological characterization of Alg/Chi multilayer spray-coated PBS films

The enzyme-induced degradation of PBS films was modulated by coating the hot-pressed neat PBS films with a polysaccharide polyelectrolyte multilayer coating composed by alginate (Alg) and chitosan (Chi), through the spray-assisted LbL technique (Scheme 4.2b). Three different samples were prepared by varying the number of Alg/Chi layers coating the PBS films, PBS_8L, PBS_24L, and PBS_40L. The thickness was determined from the SEM images of the multilayer spray-coated PBS films by measuring the cross-section of the images (Figures 4.5a-c). These observations allowed us to determine the thickness of the Alg/Chi multilayer coating over the PBS films (Figure 4.5d). The results show an increase in thickness with the number of Alg/Chi deposited layers, from ~228 nm for

PBS_8L to ~1640 nm for PBS_40L (see Table 4.1). For the sample with the highest number of deposited Alg/Chi layers, the thickness seems to increase more rapidly. This effect is more clearly appreciated when evaluating the thickness of the monolayers. For PBS_8L and PBS_24L films, each individual layer had a mean value of 28 nm/layer, whereas this parameter rose up to 41 nm/layer for PBS_40L multilayer films, with an increase of almost 50 %. This exponential behavior was previously observed in literature for Alg/Chi multilayers,[31,33] and explained for many other systems in a recent review.[30] The exponential growth of the multilayer is attributed to the high mobility of the chains within the film, occurring perpendicularly to the film growth direction but also in the plane of the film. This effect produces the diffusion of the polymer in and out of the film architecture, leading to an exponential increase in film growth. The surface wettability properties of the neat and Alg/Chi spray-coated PBS films were studied by Water Contact Angle (WCA) measurements. WCA values dropped from ~70º in the case of neat PBS films to WCA ~25º for Alg/Chi spray-coated PBS films (see Figure 4.5d), which can be attributed to the inherent hydrophilic nature of polysaccharides,[51] in contrast to the more hydrophobic character of polyesters.[52]

Table 4.1. Thickness and WCA of PBS spray-coated films as a function of the number of layers.

Sample	Description of the sample	Number of layers	Thickness of the coating (nm)	WCA (º)
Uncoated PBS	PBS	0	-	68 ± 4
PBS_8L	PBS-PEI-$(Alg-Chi)_4$	8	228 ± 39	23 ± 3
PBS_24L	PBS-PEI-$(Alg-Chi)_{12}$	24	679 ± 28	26 ± 4
PBS_40L	PBS-PEI-$(Alg-Chi)_{20}$	40	1640 ± 350	26 ± 3

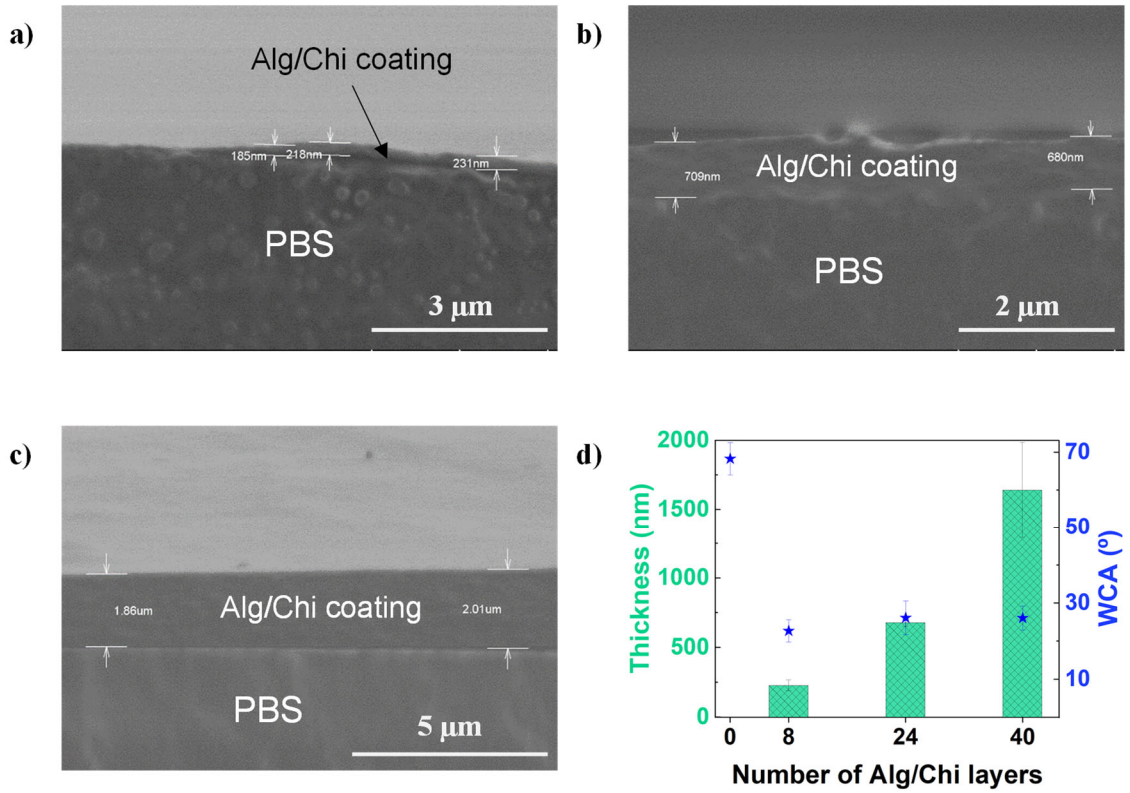

Figure 4.5. SEM images of the cross-sections of Alg/Chi coatings spray-coated on PBS films with a different number of layers **a)** PBS_8L, **b)** PBS_24L, **c)** PBS_40L. **d)** Graphical representation of the thickness *vs.* the number of Alg/Chi coating layers (left axis) and WCA *vs.* the number of Alg/Chi coating layers (right axis).

b. Nanomechanical properties of Alg/Chi multilayer spray-coated PBS films

As alginate/chitosan polyelectrolyte complexes are employed for the enhancement of the mechanical and barrier properties of PBS neat films, the nanomechanical behavior of the polysaccharide coatings was evaluated by nanoindentation. Shallow indent depths of 100 nm were chosen in order to minimize the influence of the PBS substrate. However, it is well known that compliant substrates such as PBS (E' <1 GPa) can influence the indentation response of stiffer coatings even at small indent depths, and lower apparent E' and H values can be found.[53] Hence, in order to evaluate the effect of the substrate on the intrinsic properties of the Alg/Chi coatings, silicon wafers were also used as substrates (E' ~150 GPa).

Figure 4.6 shows the E' and H values for the Alg/Chi films spray-coated on PBS and silicon. For the case of compliant PBS substrate, it is clearly seen that E' and H values rise as the number of layers increases, and constant values are approached for the thickest films (60 and 80 layers). Such behavior can be clearly attributed to the influence of PBS that produces substrate-affected E' and H values for the thinnest coatings (<60 layers). The substrate influence is also apparent in the case of silicon wafers. However, in this case, E' and H values are overestimated for the thinnest coatings because silicon is much stiffer than the deposited film. Most interesting is the observation that the E' and H values of the thickest films are the same within error, irrespective of the type of substrate. Hence, one can assume $E' = 6 \pm 2$ GPa and $H = 260 \pm 60$ MPa as the substrate-independent values for the Alg/Chi layered system. The fact that such values are in the range of those found for the neat chitosan and alginate films ($E' = 6.0 \pm 0.3$ GPa and $H = 302 \pm 24$ MPa for chitosan; $E' = 8.3 \pm 0.8$ GPa and $H = 306 \pm 52$ MPa for alginate) suggests that the evolution of the deformation field under the indenter takes place with no significant discontinuity across the different layers. In other words, the mechanical behavior of the polysaccharide coating is in agreement with significant interaction between the individual layers. This good interaction between alginate and chitosan layers ensures a durable and stable polysaccharide multilayer coating, which is important to successfully modulate PBS biodegradation.

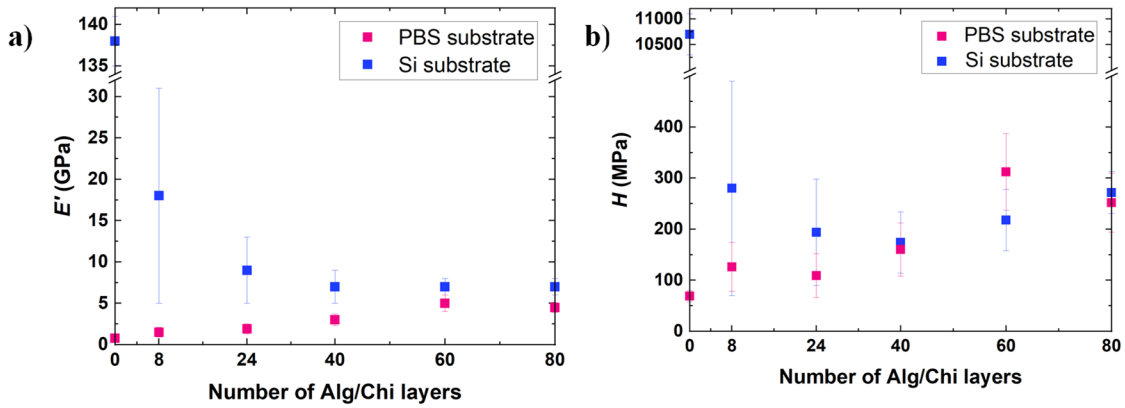

Figure 4.6. a) Storage modulus (E'), and **b)** hardness (H) values obtained by nanoindentation for Alg/Chi coatings prepared on PBS films and silicon wafers.

c. Enzymatic degradation of Alg/Chi multilayer spray-coated PBS films

We now turn our attention to the influence of the polysaccharide Alg/Chi multilayer coatings on PBS film degradation. Figure 4.7a shows the results of weight loss degradation curves corresponding to PBS spray-coated samples with a different number of Alg/Chi layers. As can be observed, the degradation seems to present a tendency directly dependent on the number of layers of the Alg/Chi coating. The higher the number of layers, the lower the degradation. This phenomenon is observed both in the weight loss reached and the degradation speed.

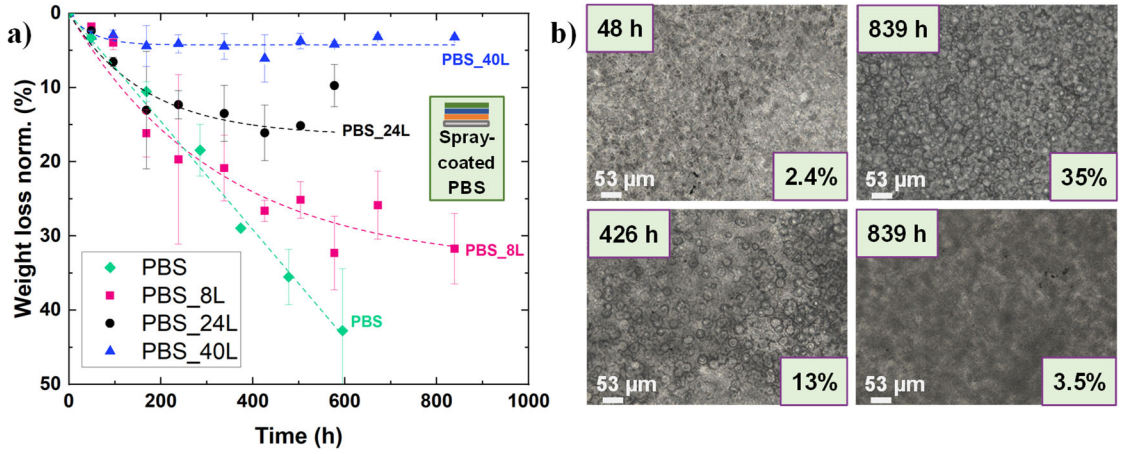

Figure 4.7. a) Determination of the weight loss for Alg/Chi spray-coated PBS films, PBS_8L, PBS_24L, and PBS_40L, immersed in a lipase aqueous solution (2 mg/mL) under stirring at 37 ºC. Neat PBS films are used as a control. Dashed lines show the fitting of the data to the proposed model (Eq. 4.3). **b)** Optical profilometry images were taken at 20x magnification for the initial steps of degradation: PBS_8L films after 48 h of degradation (top-left image), and at the end of degradation: PBS_8L after 35 days (top-right image), PBS_24L after 18 days (bottom-left), and PBS_40L after 35 days (bottom-right). In the upper left corner of each image, the degradation time is included (in hours [h]), whereas the weight loss percentage is shown in the lower right corner. The surface aspect at the beginning of degradation was similar among all the samples (initial profilometry images of PBS_24L and PBS_8L are shown in Figure 4.8).

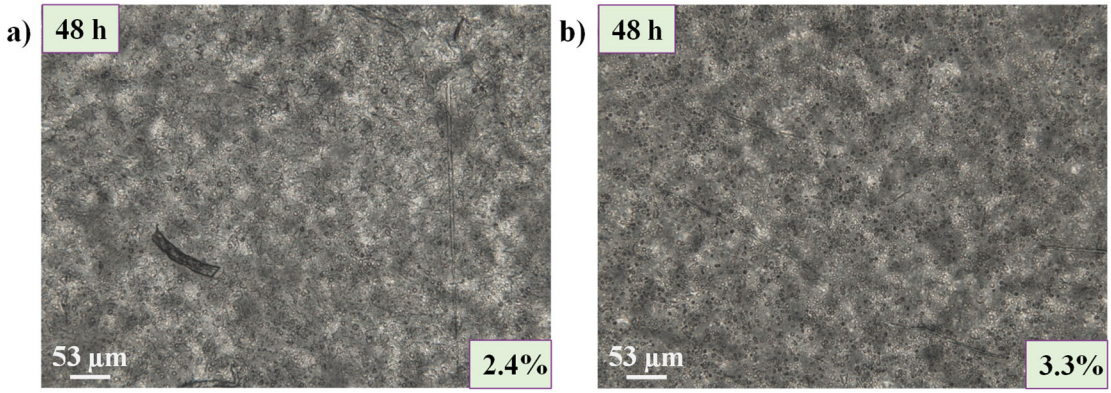

Figure 4.8. Optical profilometry images taken at 20x magnification for initial steps of degradation: **a)** PBS_24L, and **b)** PBS_40L.

Weight loss curves recorded as a function of the time can be fitted to a model to describe the degradation kinetics quantitatively. Generally, for the reactions that involve enzymes, the Michaelis-Menten' model, which describes the kinetics of enzymatic homogeneous reactions that take place in a short period of time (linear section of the reaction), is the most commonly used. For these reasons, as the biodegradation experiments are controlled by heterogeneous reactions for a long time, some corrections were needed in order to describe the whole degradation process, which includes three main steps: adsorption of the enzyme on the PBS surface, degradation of the polymer, and denaturation of the enzyme. In order to accomplish all these requirements, some authors have proposed a model for the enzymatic degradation of PLA that can be described by Equation 4.3.[54,55]

$$m_t = v_d.\tau\cdot(1- e^{-t/\tau}) \qquad \text{(Eq. 4.3)}$$

Where m_t refers to the weight loss of the sample (considered similar to W_{loss} indicated in Eq. 4.1), v_d stands for the rate of degradation, τ indicates the rate of denaturation of the enzyme (time constant), and implies that the degradation has reached a *plateau* and t is the time (expressed in hours).

The application of the modified Michaelis-Menten' model (Eq. 4.3) to the experimental data shown in Figure 4.7a allows us to extract further information on the effect of the polyelectrolyte coating on the enzymatic degradation of neat PBS films (Table 4.2).

Table 4.2. Kinetic parameters of the enzymatic degradation of Alg/Chi spray-coated PBS films. The standard deviation of the mean values is given in brackets.

Sample	v_d (%/h)	τ (h)	A (%)	R^2
PBS	0.0729 (0.0023)[a]	n.d.[b]	n.d.[b]	0.9953
PBS_8L	0.1045 (0.0164)	325 (84)	34.0	0.9420
PBS_24L	0.1003 (0.0170)	164 (40)	16.5	0.9534
PBS_40L	0.0848 (0.0221)	50 (15)	4.3	0.9375

[a] Obtained from the linear fit of the data related to the kinetics of PBS neat films degradation.

[b] These data could not be obtained for PBS neat films, as the weight loss curves did not reach a *plateau* regime; thus, the lipase is still degrading by the end of the experiment (the rate of denaturation of the enzyme, τ, will be higher than the total time of the experiment: τ > 1000 h).

Regarding the degradation rate of the films, which takes into consideration the first instants of the degradation process, it can be appreciated that this parameter increased as the number of layers of the coating decreased: 0.0848 %/h (PBS_40L) < 0.1003 %/h (PBS_24L) < 0.1045 %/h (PBS_8L). These degradation rates are slightly higher than the degradation kinetics obtained for neat PBS films. Nevertheless, concerning the rate of denaturation of the lipase, an inverse relationship with the number of layers can be observed: 50 h (PBS_40L) < 164 h (PBS_24L) < 325 h (PBS_8L). As the neat PBS films did not reach the *plateau* during the weight loss assays (i.e., the lipase continued degrading after concluding the experiment), it was not possible to determine the value for the rate of denaturation of the enzyme (τ) because the model did not apply for this case. For the Alg/Chi spray-coated PBS films, τ was reduced to an inversely proportional extent toward the number of layers of the coating. Finally, the degree of degradation at infinite time (pre-exponential term A), –calculated by multiplying the degradation rate (v_d) by the rate of denaturation of the enzyme (τ)–, was found to be maximum for PBS_8L samples, with nearly 34 % reached, whereas it decreased to values of ~4 % for PBS_40L. Overall, the Alg/Chi spray-coated PBS films reached a degradation *plateau* progressively and followed a decreasing order with the number of layers: firstly PBS_40L, then PBS_24L, and finally PBS_8L. It is hypothesized that this sort of modulation of the enzymatic degradation of PBS

films by the application of an Alg/Chi multilayer coating could be due to the hindered diffusion of the free enzyme throughout the polysaccharide coating. A similar approach was employed to modulate the drug release from polysaccharide capsules and gels produced through LbL assembly. The incorporation of additional layers hindered drug diffusion, as these added layers constituted a physical barrier to the drug diffusion.[34,56]

The stability of the Alg/Chi coating was previously checked thanks to the preparation of Alg/Chi coatings with different layers containing magnetic nanoparticles (Fe_3O_4 NPs). These coatings presented a dark-brownish tone due to these NPs, which remained present (only small cracks were observed on the surface of the films) in the degraded films up to 300 days of enzymatic biodegradation assays (see Figure 4.9). Regarding morphological changes on degraded samples, SEM images were taken of the cross-section of the films at the end of the biodegradation experiments (see Figure 4.10). In this case, the thicknesses of the degraded PBS films were reduced by the end of the experiments: a small decrease of ~20 % in the case of PBS_24L and PBS_40L films and a significant ~70 % reduction in the case of PBS_8L films (see Table 4.3). These observations were in accordance with the weight loss curves shown in Figure 4.7a. Furthermore, a partial detachment of the multilayer coating was appreciated by the end of the enzymatic biodegradation assays, related to the experimental conditions. This was evidenced both by the cross-sectional SEM images of the Alg/Chi coatings (see Figure 4.10) and the optical profilometry images of the Alg/Chi coatings (see Figure 4.7b) and the Alg/Chi with NPs coatings (see Figure 4.9).

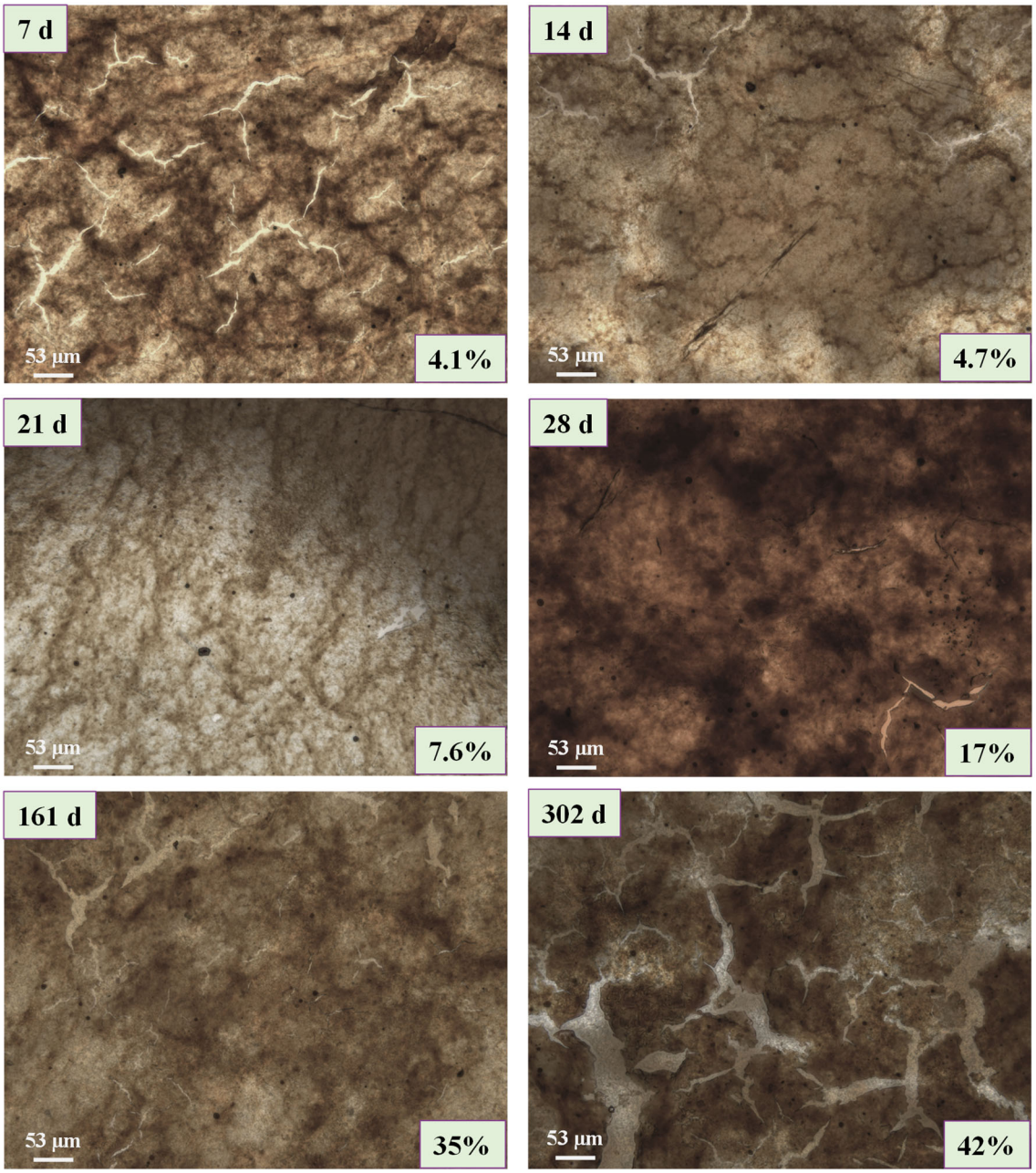

Figure 4.9. Optical profilometry images of PBS films with a Alg/Chi coating containing Fe_3O_4 nanoparticles taken at 20x magnification at different steps of degradation: 7, 14, 21, 28, 161, and 302 days. The films were prepared from Alg/Chi/NPs/Chi tetralayers (as the NPs layer was obtained throughout the preparation of a Alg ferrofluid with negative charge), up to 40 layers in total.

Table 4.3. Thickness of PBS spray-coated films as a function of the number of layers at the end of the enzymatic degradation experiments.

Sample	Description of the sample	Number of layers	Thickness before degradation (µm)	Thickness after degradation (µm)
PBS_8L	PBS-PEI-$(Alg-Chi)_4$	8	120 ± 20	38 ± 2
PBS_24L	PBS-PEI-$(Alg-Chi)_{12}$	24	120 ± 20	98 ± 1
PBS_40L	PBS-PEI-$(Alg-Chi)_{20}$	40	120 ± 20	99 ± 1

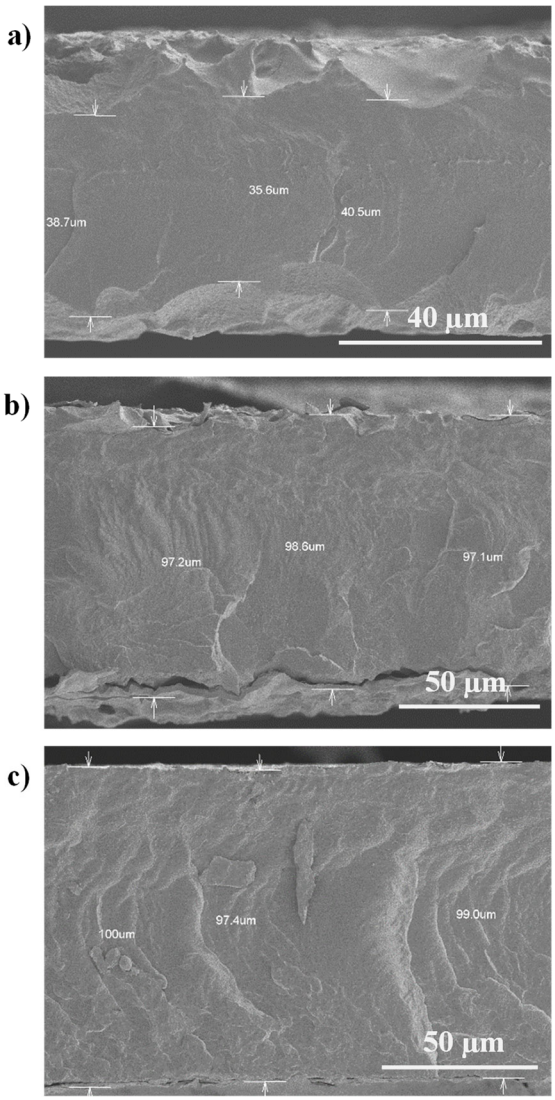

Figure 4.10. SEM images of the cross-sections of spray-coated PBS films with a different number of layers at the end of the enzymatic degradation experiments: **a)** PBS_8L, **b)** PBS_24L, and **c)** PBS_40L.

4.4. Conclusions

In this Chapter, we propose a novel strategy to modulate the enzymatic degradation of PBS films triggered by a lipase from *Pseudomonas cepacia*, which involve the enzyme-prevented degradation of PBS films by coating them with multilayer polysaccharide Alg/Chi films. For comparison, as a first step, we report a systematic study of enzymatic degradation of neat PBS films employing a lipase from *P. cepacia* in solution to ascertain the experimental parameters that influence their degradation in solution. The results showed that the increase in enzyme concentration increased the extent and the velocity of degradation of neat PBS films. Furthermore, stirring of the films within the enzymatic solution was found to favor the enzymatic biodegradation of PBS in contrast to stationary assays. Then, PBS films were coated with a different number of alginate/chitosan layers by spray-assisted LbL and subjected to enzymatic degradation experiments in solution. The extent of degradation was found to be dependent on the number of coating layers; that is, the higher the number of layers, the lower the degradation rate. The results suggest that the biobased coating constitutes an effective barrier to the diffusion of the lipase, thus proving its effectiveness in modulating the enzymatic activity as a function of the thickness coating.

To sum up, this research expands the knowledge of polyester enzymatic degradation in many ways, studying the most relevant parameters in degradation, and its modulation by applying a biobased polysaccharide multilayer coating consisting in alternating alginate/chitosan layers.

4.5. References

1. Hayes, G.; Laurel, M.; MacKinnon, D.; Zhao, T.; Houck, H. A.; Becer, C. R., Polymers without Petrochemicals: Sustainable Routes to Conventional Monomers. *Chemical Reviews* **2022**, *123* (5), 2609–2734. DOI: 10.1021/acs.chemrev.2c00354.

2. Rafiqah, S. A.; Khalina, A.; Harmaen, A. S.; Tawakkal, I. A.; Zaman, K.; Asim, M.; Nurrazi, M. N.; Lee, C. H., A review on properties and application of bio-based poly(butylene succinate). *Polymers* **2021**, *13* (9), 1436. DOI: 10.3390/polym13091436.

3. Geyer, R.; Jambeck, J. R.; Law, K. L., Production, use, and fate of all plastics ever made. *Science Advances* **2017**, *3* (7), 25–29. DOI: 10.1126/sciadv.1700782.

4. Sander, M., Biodegradation of Polymeric Mulch Films in Agricultural Soils: Concepts, Knowledge Gaps, and Future Research Directions. *Environmental Science & Technology* **2019**, *53* (5), 2304–2315. DOI: 10.1021/ACS.EST.8B05208.

5. Wu, F.; Misra, M.; Mohanty, A. K., Challenges and new opportunities on barrier performance of biodegradable polymers for sustainable packaging. *Progress in Polymer Science* **2021**, *117*, 101395. DOI: 10.1016/j.progpolymsci.2021.101395.

6. Mtibe, A.; Muniyasamy, S.; Mokhena, T. C.; Ofosu, O.; Ojijo, V.; John, M., Recent insight into the biomedical applications of polybutylene succinate and polybutylene succinate-based materials. *Express Polymer Letters* **2023**, *17* (1), 2–28. DOI: 10.3144/expresspolymlett.2023.2.

7. Peñas, M. I.; Pérez-Camargo, R. A.; Hernández, R.; Müller, A. J., A Review on Current Strategies for the Modulation of Thermomechanical, Barrier, and Biodegradation Properties of Poly (Butylene Succinate) (PBS) and Its Random Copolymers. *Polymers* **2022**, *14* (5), 1025. DOI: 10.3390/polym14051025.

8. Ayu, R. S.; Khalina, A.; Harmaen, A. S.; Zaman, K.; Mohd Nurrazi, N.; Isma, T.; Lee, C. H., Effect of empty fruit brunch reinforcement in polybutylene-succinate/modified tapioca starch blend for agricultural mulch films. *Scientific Reports* **2020**, *10* (1), 1166. DOI: 10.1038/s41598-020-58278-y.

9. Sisti, L.; Totaro, G.; Marchese, P., PBS makes its entrance into the family of biobased plastics. In: *Biodegradable and Biobased Polymers for Environmental and Biomedical Applications*. (Scrivener Publishing) **2016**, 225–286. DOI: 10.1002/9781119117360.ch7.

10. Haider, T. P.; Völker, C.; Kramm, J.; Landfester, K.; Wurm, F. R., Plastics of the Future? The Impact of Biodegradable Polymers on the Environment and on Society. *Angewandte Chemie - International Edition* **2019**, *58* (1), 50–62. DOI: 10.1002/anie.201805766.

11. Bai, Z.; Liu, Y.; Su, T.; Wang, Z., Effect of hydroxyl monomers on the Enzymatic degradation of poly(ethylene succinate), poly(butylene succinate), and poly(hexylene succinate). *Polymers* **2018**, *10* (1), 90. DOI: 10.3390/polym10010090.

12. Hwang, S. Y.; Jin, X. Y.; Yoo, E. S.; Im, S. S., Synthesis, physical properties and enzymatic degradation of poly (oxyethylene-b-butylene succinate) ionomers. *Polymer* **2011**, *52* (13), 2784–2791. DOI: 10.1016/j.polymer.2011.04.065.

13. Morales-Huerta, J. C.; Ciulik, C. B.; De Ilarduya, A. M.; Muñoz-Guerra, S., Fully bio-based aromatic-aliphatic copolyesters: Poly(butylene furandicarboxylate-co-succinate)s obtained by ring opening polymerization. *Polymer Chemistry* **2017**, *8* (4), 748–760. DOI: 10.1039/c6py01879c.

14. Papageorgiou, G. Z.; Bikiaris, D. N., Synthesis, cocrystallization, and enzymatic degradation of novel poly(butylene-co-propylene succinate) copolymers. *Biomacromolecules* **2007**, *8* (8), 2437–2449. DOI: 10.1021/bm0703113.

15. Kong, X.; Qi, H.; Curtis, J. M., Synthesis and characterization of high-molecular weight aliphatic polyesters from monomers derived from renewable resources. *Journal of Applied Polymer Science* **2014**, *131* (15), 4–10. DOI: 10.1002/app.40579.

16. Hu, X.; Gao, Z.; Wang, Z.; Su, T.; Yang, L.; Li, P., Enzymatic degradation of poly(butylene succinate) by cutinase cloned from Fusarium solani. *Polymer Degradation and Stability* **2016**, *134*, 211–219. DOI: 10.1016/j.polymdegradstab.2016.10.012.

17. Shi, K.; Su, T.; Wang, Z., Comparison of poly(butylene succinate) biodegradation by Fusarium solani cutinase and Candida antarctica lipase. *Polymer Degradation and Stability* **2019**, *164*, 55–60. DOI: 10.1016/j.polymdegradstab.2019.04.005.

18. Zheng, L.; Wang, Z.; Wu, S.; Li, C.; Zhang, D.; Xiao, Y., Novel poly(butylene fumarate) and poly(butylene succinate) multiblock copolymers bearing reactive carbon-carbon double bonds: Synthesis, characterization, cocrystallization, and properties. *Industrial & Engineering Chemistry Research* **2013**, *52* (18), 6147–6155. DOI: 10.1021/ie303573d.

19. Tserki, V.; Matzinos, P.; Pavlidou, E.; Vachliotis, D.; Panayiotou, C., Biodegradable aliphatic polyesters. Part I. Properties and biodegradation of poly(butylene succinate-co-butylene adipate). *Polymer Degradation and Stability* **2006**, *91* (2), 367–376. DOI: 10.1016/j.polymdegradstab.2005.04.035.

20. Li, S. L.; Wu, F.; Wang, Y. Z.; Zeng, J. B., Biobased Thermoplastic Poly(ester urethane) Elastomers Consisting of Poly(butylene succinate) and Poly(propylene succinate). *Industrial & Engineering Chemistry Research* **2015**, *54* (24), 6258–6268. DOI: 10.1021/acs.iecr.5b00637.

21. Khan, F. I.; Lan, D.; Durrani, R.; Huan, W.; Zhao, Z.; Wang, Y., The Lid Domain in Lipases: Structural and Functional Determinant of Enzymatic Properties. *Frontiers in Bioengineering and Biotechnology* **2017**, *5* (16), 1–13. DOI: 10.3389/fbioe.2017.00016.

22. UniProt, Entry #P22088·LIP_BURCE. Entry #P22088·LIP_BURCE, https://www.uniprot.org/uniprotkb/P22088/entry (last time accessed: October 26, 2022).

23. Basu, S.; Plucinski, A.; Catchmark, J. M., Sustainable barrier materials based on polysaccharide polyelectrolyte complexes. *Green Chemistry* **2017**, *19* (17), 4080–4092. DOI: 10.1039/c7gc00991g.

24. Chi, K.; Wang, H.; Catchmark, J. M., Sustainable starch-based barrier coatings for packaging applications. *Food Hydrocolloids* **2020**, *103*, 105696. DOI: 10.1016/j.foodhyd.2020.105696.

25. Mujtaba, M.; Lipponen, J.; Ojanen, M.; Puttonen, S.; Vaittinen, H., Trends and challenges in the development of bio-based barrier coating materials for paper/cardboard food packaging; a review. *Science of The Total Environment* **2022**, *851*, 158328. DOI: 10.1016/j.scitotenv.2022.158328.

26. Fabra, M. J.; Busolo, M. A.; Lopez-Rubio, A.; Lagaron, J. M., Nanostructured biolayers in food packaging. *Trends in Food Science and Technology* **2013**, *31* (1), 79–87. DOI: 10.1016/j.tifs.2013.01.004.

27. Enescu, D.; Frache, A.; Geobaldo, F., Formation and oxygen diffusion barrier properties of fish gelatin/natural sodium montmorillonite clay self-assembled multilayers onto the biopolyester surface. *RSC Advances* **2015**, *5* (75), 61465–61480. DOI: 10.1039/c5ra11283d.

28. Barroso, N.; Guaresti, O.; Pérez-Álvarez, L.; Ruiz-Rubio, L.; Gabilondo, N.; Vilas-Vilela, J. L., Self-healable hyaluronic acid/chitosan polyelectrolyte complex hydrogels and multilayers. *European Polymer Journal* **2019**, *120*, 109268. DOI: 10.1016/j.eurpolymj.2019.109268.

29. Li, X.; Shang, L.; Li, D.; Wang, W.; Chen, S.; Zhong, H.; Huang, Y.; Long, S., High-strength, strong-adhesion, and antibacterial polyelectrolyte complex hydrogel films from natural polysaccharides. *Polymer Testing* **2022**, *109*, 107547. DOI: 10.1016/j.polymertesting.2022.107547.

30. Criado-Gonzalez, M.; Mijangos, C.; Hernández, R., Polyelectrolyte multilayer films based on natural polymers: From fundamentals to Bio-Applications. *Polymers* **2021**, *13* (14), 2254. DOI: 10.3390/polym13142254.

31. Criado-Gonzalez, M.; Fernandez-Gutierrez, M.; San Roman, J.; Mijangos, C.; Hernández, R., Local and controlled release of tamoxifen from multi (layer-by-layer) alginate/chitosan complex systems. *Carbohydrate Polymers* **2019**, *206*, 428–434. DOI: 10.1016/j.carbpol.2018.11.007.

32. Criado, M.; Sanz, B.; Goya, G. F.; Mijangos, C.; Hernández, R., Magnetically responsive biopolymeric multilayer films for local hyperthermia. *Journal of Materials Chemistry B* **2017**, *5* (43), 8570–8578. DOI: 10.1039/c7tb02361h.

33. Criado, M.; Rebollar, E.; Nogales, A.; Ezquerra, T. A.; Boulmedais, F.; Mijangos, C.; Hernández, R., Quantitative Nanomechanical Properties of Multilayer Films Made of Polysaccharides through Spray Assisted Layer-by-Layer Assembly. *Biomacromolecules* **2017**, *18* (1), 169–177. DOI: 10.1021/acs.biomac.6b01449.

34. Gonzalez, J. S.; Mijangos, C.; Hernandez, R., Polysaccharide coating of gelatin gels for controlled BSA release. *Polymers* **2019**, *11* (4), 702. DOI: 10.3390/polym11040702.

35. Gnanasampanthan, T.; Beyer, C. D.; Yu, W.; Karthäuser, J. F.; Wanka, R.; Spöllmann, S.; Becker, H. W.; Aldred, N.; Clare, A. S.; Rosenhahn, A., Effect of Multilayer Termination on Nonspecific Protein Adsorption and Antifouling Activity of Alginate-Based Layer-by-Layer Coatings. *Langmuir* **2021**, *37* (19), 5950–5963. DOI: 10.1021/acs.langmuir.1c00491.

36. Arandia, I.; Zaldua, N.; Maiz, J.; Pérez-Camargo, R. A.; Mugica, A.; Zubitur, M.; Mincheva, R.; Dubois, P.; Müller, A. J., Tailoring the isothermal crystallization kinetics of isodimorphic poly(butylene succinate-ran-butylene azelate) random copolymers by changing composition. *Polymer* **2019**, *183*, 121863. DOI: 10.1016/j.polymer.2019.121863.

37. Honda, N.; Taniguchi, I.; Miyamoto, M.; Kimura, Y., Reaction mechanism of enzymatic degradation of poly(butylene succinate-co-terephthalate) (PBST) with a Lipase originated from Pseudomonas cepacia. *Macromolecular Bioscience* **2003**, *3* (3–4), 189–197. DOI: 10.1002/mabi.200390023.

38. Mondal, K.; Mehta, P.; Mehta, B. R.; Varandani, D.; Gupta, M. N., A bioconjugate of Pseudomonas cepacia lipase with alginate with enhanced catalytic efficiency. *Biochimica et Biophysica Acta - Proteins and Proteomics* **2006**, *1764* (6), 1080–1086. DOI: 10.1016/j.bbapap.2006.04.008.

39. Shi, K.; Bai, Z.; Su, T.; Wang, Z., Selective enzymatic degradation and porous morphology of poly(butylene succinate)/poly(lactic acid) blends. *International Journal of Biological Macromolecules* **2019**, *126*, 436–442. DOI: 10.1016/j.ijbiomac.2018.12.168.

40. Han, J.; Shi, J.; Xie, Z.; Xu, J.; Guo, B., Synthesis, properties of biodegradable poly(butylene succinate-co-butylene 2-methylsuccinate) and application for sustainable release. *Materials* **2019**, *12* (9), 1507–1524. DOI: 10.3390/ma12091507.

41. Lueckgen, A.; Garske, D. S.; Ellinghaus, A.; Mooney, D. J.; Duda, G. N.; Cipitria, A., Enzymatically-degradable alginate hydrogels promote cell spreading and in vivo tissue infiltration. *Biomaterials* **2019**, *217*, 119294. DOI: 10.1016/j.biomaterials.2019.119294.

42. Azevedo, H.; Reis, R., Understanding the Enzymatic Degradation of Biodegradable Polymers and Strategies to Control Their Degradation Rate. In: *Biodegradable Systems in Tissue Engineering and Regenerative Medicine*. **2004**, 177–202. DOI: 10.1201/9780203491232.ch12.

43. Murray, E.; Thompson, B. C.; Sayyar, S.; Wallace, G. G., Enzymatic degradation of graphene/polycaprolactone materials for tissue engineering. *Polymer Degradation and Stability* **2015**, *111*, 71–77. DOI: 10.1016/j.polymdegradstab.2014.10.010.

44. Wang, H.; Tong, D.; Wang, L.; Chen, L.; Yu, N.; Li, Z., A facile strategy for fabricating PCL/PEG block copolymer with excellent enzymatic degradation. *Polymer Degradation and Stability* **2017**, *140*, 64–73. DOI: 10.1016/j.polymdegradstab.2017.04.015.

45. Wcislek, A.; Olalla, A. S.; McClain, A.; Piegat, A.; Sobolewski, P.; Puskas, J.; Fray, M. El, Enzymatic degradation of poly(butylene succinate) copolyesters synthesized with the use of Candida antarctica lipase B. *Polymers* **2018**, *10* (6), 688. DOI: 10.3390/polym10060688.

46. Taniguchi, I.; Nakano, S.; Nakamura, T.; El-Salmawy, A.; Miyamoto, M.; Kimura, Y., Mechanism of enzymatic hydrolysis of poly(butylene succinate) and poly(butylene succinate-co-L-lactate) with a lipase from Pseudomonas cepacia. *Macromolecular Bioscience* **2002**, *2* (9), 447–455. DOI: 10.1002/mabi.200290002.

47. Jiang, X.; Yang, J. P.; Wang, X. H.; Zhou, J. J.; Li, L., The degradation and adsorption behaviors of enzyme on poly(butylene succinate) single crystals. *Macromolecular Bioscience* **2009**, *9* (12), 1281–1286. DOI: 10.1002/mabi.200900336.

48. Gigli, M.; Fabbri, M.; Lotti, N.; Gamberini, R.; Rimini, B.; Munari, A., Poly(butylene succinate)-based polyesters for biomedical applications: A review. *European Polymer Journal* **2016**, *75*, 431–460. DOI: 10.1016/j.eurpolymj.2016.01.016.

49. Kulkarni, A.; Reiche, J.; Hartmann, J.; Kratz, K.; Lendlein, A., Selective enzymatic degradation of poly(ε-caprolactone) containing multiblock copolymers. *European Journal of Pharmaceutics and Biopharmaceutics* **2008**, *68* (1), 46–56. DOI: 10.1016/j.ejpb.2007.05.021.

50. Shinozaki, Y.; Kikkawa, Y.; Sato, S.; Fukuoka, T.; Watanabe, T.; Yoshida, S.; Nakajima-Kambe, T.; Kitamoto, H. K., Enzymatic degradation of polyester films by a cutinase-like enzyme from Pseudozyma antarctica: Surface plasmon resonance and atomic force microscopy study. *Applied Microbiology and Biotechnology* **2013**, *97* (19), 8591–8598. DOI: 10.1007/s00253-012-4673-0.

51. Hou, X.; Xue, Z.; Xia, Y.; Qin, Y.; Zhang, G.; Liu, H.; Li, K., Effect of SiO2 nanoparticle on the physical and chemical properties of eco-friendly agar/sodium alginate nanocomposite film. *International Journal of Biological Macromolecules* **2019**, *125*, 1289–1298. DOI: 10.1016/J.IJBIOMAC.2018.09.109.

52. Genovese, L.; Lotti, N.; Gazzano, M.; Siracusa, V.; Dalla Rosa, M.; Munari, A., Novel biodegradable aliphatic copolyesters based on poly(butylene succinate) containing thioether-linkages for sustainable food packaging applications. *Polymer Degradation and Stability* **2016**, *132*, 191–201. DOI: 10.1016/j.polymdegradstab.2016.02.022.

53. Hay, J.; Crawford, B., Measuring substrate-independent modulus of thin films. *Journal of Materials Research* **2011**, *26* (6), 727–738. DOI: 10.1557/jmr.2011.8.

54. Hegyesi, N.; Zhang, Y.; Kohári, A.; Polyák, P.; Sui, X.; Pukánszky, B., Enzymatic degradation of PLA/cellulose nanocrystal composites. *Industrial Crops and Products* **2019**, *141*, 111799. DOI: 10.1016/j.indcrop.2019.111799.

55. Hegyesi, N.; Hodosi, E.; Polyák, P.; Faludi, G.; Balogh-Weiser, D.; Pukánszky, B., Controlled degradation of poly-ε-caprolactone for resorbable scaffolds. *Colloids and surfaces. B, Biointerfaces* **2020**, *186*, 110678. DOI: 10.1016/j.colsurfb.2019.110678.

56. Ye, S.; Wang, C.; Liu, X.; Tong, Z.; Ren, B.; Zeng, F., New loading process and release properties of insulin from polysaccharide microcapsules fabricated through layer-by-layer assembly. *Journal of Controlled Release* **2006**, *112* (1), 79–87. DOI: 10.1016/j.jconrel.2006.01.015.

Chapter 5

Self-Degradable Films of PBS and Their Blends with PLA and PBAT

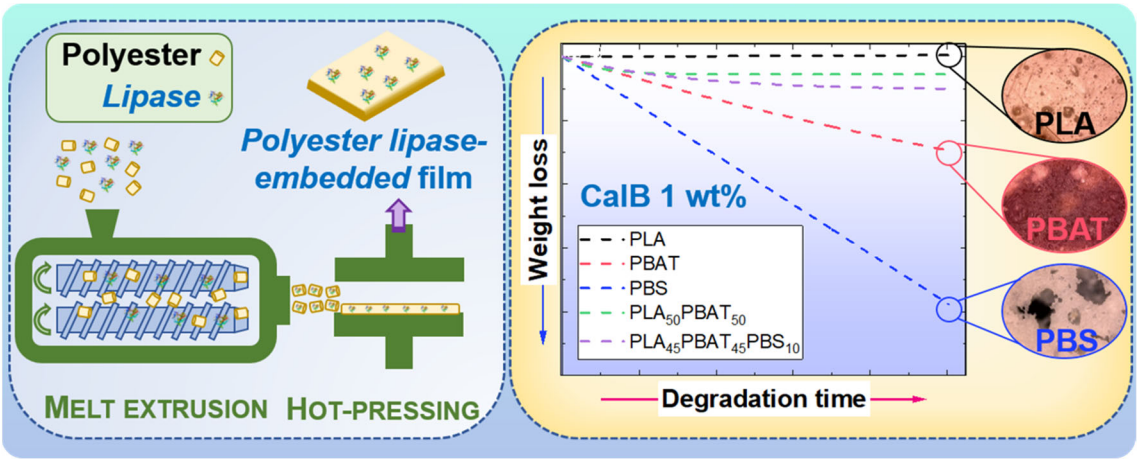

5.1. Introduction

Polyesters, and especially biopolyesters, have attracted a great deal of attention through the past years as natural substitutes to non-degradable fossil-based polymers and a good alternative to common plastics that, otherwise end up in landfills or even in the oceans.[1,2] These polymers display a wide range of mechanical, optical, thermal, and barrier properties, among others, which make biopolyesters suitable candidates for common applications in plastic materials, such as biomedical applications, packaging, and agriculture.[3] Some of the most studied biopolyesters include poly(lactic acid) (PLA), polyhydroxyalkanoates (PHA), poly(ε-caprolactone) (PCL), poly(butylene succinate) (PBS), poly(butylene adipate) (PBA), poly(butylene succinate-*co*-adipate) (PBSA) or poly(butylene adipate-*co*-terephthalate) (PBAT), among many other polyesters and copolyesters.[4] PLA and PBS are linear aliphatic polyesters with good mechanical properties in terms of rigidity (PLA is comparable to polystyrene) and are relatively inexpensive, being among the most used biopolymers in food packaging.[5] PBAT is one of the most used aliphatic-aromatic biopolyesters thanks to its adequate mechanical properties (resembling a soft thermoplastic elastomer in view of its low crystallinity degree) and biodegradability.[6]

The high importance of PLA and PBAT for packaging and PBAT and PBS-based materials for biomedical applications put these biopolyesters in the spotlight.[4,7] However, the poor thermal processability and poor ductility of PLA and PBS generate the need to improve them. Many solutions can be done, such as the preparation of copolymers, blending with other polymers,[8] or additives and fillers.[9] Another possibility is the incorporation of aromatic units into the main chain, making at the same time biodegradable materials with better material properties, due to the presence of aliphatic and aromatic groups, respectively.[1] Hence, the employment of PBAT and the preparation of binary blends with PLA and PBS turns up as a potential solution for making biopolyesters more resistant and with better properties. For instance, PLA/PBAT blends are widely employed for mulching films in agriculture,[8] as well as other interesting applications, such

as packaging, pharmaceutical or automotive industries.[10] Nonetheless, the poor compatibility of PLA/PBAT,[11] and PLA/PBS[12] binary blends encouraged the exploration of new approaches, such as the use of chain extenders or plasticizers, or the preparation of PLA/PBAT/PBS ternary blends, which has been reported to have excellent properties.[13,14] Recently, some of us have prepared PLA/PBAT/PBS ternary blends fixing the PLA/PBAT ratio (1:1) and varying the amount of PBS. Analysing the morphology, it was demonstrated that the PBS acts as a compatibilizer in the ternary blend, situating at the PLA/PBAT interface, reducing interfacial tension, preventing coalescence, thus refining the blend morphology and improving its mechanical properties.[15]

Many studies have reported interesting results regarding the biodegradation of these polyesters triggered by the action of externally-added lipases. The vast majority of them are carried out under physiological conditions (i.e., 37 ºC and pH 7-7.5).[16,17] For instance, PLA and PCL were successfully degraded by a lipase from *Aspergillus niger.*[18] Huang *et al.* studied the enzymatic degradation of PCL, PBS and PBSA films with different lipases in solution, reporting higher degradation for PCL and PBSA films.[19] Lee *et al.* investigated the degradation mechanism of PBS under the action of a lipase from *Pseudomonas cepacia* (*P. cepacia*), by studying the degradation products obtained, revealing a surface etching mechanism in the enzymatic degradation of PBS.[20] With the same lipase, Sun *et al.* reported a 35 wt% weight loss for PBS in 9 weeks.[21] However, many factors influence enzymatic degradation: type of enzyme, media (nature of the solvent, pH), temperature, agitation, and moisture, among others.[6,22]

Additionally, the substrate to be degraded has also a high importance in the results, such as the nature of the polymer (powder, film, solution), the size (nanometric, millimetric), the molecular weight distribution, the chemical nature of the polymer (aliphatic, aromatic) or the thermal properties.[10] For instance, enzymatic degradation is enhanced in semicrystalline polymers with low molecular weight,[16] under temperature conditions close to T_m. This latter

consideration might suppose a drawback for the self-stability of the enzymes, as high temperatures normally result in their denaturalization.[23]

Two main mechanisms of polymer deterioration apply to enzyme-catalysed degradation, attending to the type of erosion produced in the polymer: surface (or heterogeneous) and bulk (or homogeneous). Polymers that follow the first mechanism are degraded at the surface level only, losing the material from the surface. These samples get smaller, keeping the shape intact, whereas the molecular weight remains unchanged. On the other hand, the degradation in bulk eroding polymers affects not only the surface but also the whole sample. Although the molecular weight starts to decrease from the beginning, the dimension of the sample is maintained for a certain period of time until it finally collapses and disintegrates.[24] In general, biodegradable films are more prone to surface erosion, as the surface area/volume ratio increase as the size and thickness of the fragments decrease.[25] However, the degradation mechanism varies from one polymer to another; indeed, depending on the enzyme type, the same polymer can be degraded through different mechanisms. For instance, Shi *et al.* studied the enzymatic degradation of PBS films with a cutinase and a lipase and reported a surface erosion mechanism with cutinase, whereas the degradation using the lipase proceeded through bulk erosion.[26]

Candida antarctica lipase B (CalB) is a widely employed enzyme for polymerization reactions (esterification) in organic solvents and depolymerization (hydrolysis of esters) in aqueous media.[27] This lipase was described three decades ago as a 33 kDa secreted protein composed of 317 amino acids and a nucleophilic active site without a lid, making it highly enantioselective.[28] Previous studies have shown the best conditions for this lipase in terms of enzymatic activity, which is directly related to depolymerization and polymeric degradation: the optimum pH is in the range of 7-8, and temperature in the range of 30-40 ºC.[29,30] However, it remains stable from pH 3.5 to 9.5 in polar organic solvents and at temperatures as high as 150 ºC.[28] There are several studies in literature regarding the enzymatic degradation of PLA, PBAT and PBS, by externally-adding CalB, which reported

a wide range of results. Shinozaki *et al.* studied the enzymatic degradation of PLA films, obtaining a 50.4 % degradation in 72 h.[31] Kanwal *et al.* reported 15.7 wt% weight loss in 12 days for PBAT films.[32] In a recent publication from Hu *et al.*, a ~30 wt% weight loss was observed after 35 days-degradation of PBS films.[33]

Since the past decade, the novel approach of lipase-embedding into the polymer matrix has been developed as an alternative to externally-added lipase degradation common tests.[24] This *embedded enzymatic degradation* or *self-degradation* can have potential applications in agriculture, as many biopolyesters commonly exhibit limited environmental degradation.[34] Enzyme embedding started with the preparation of CalB-embedded PCL films via solvent-casting method from toluene, leading to complete degradation of the films in 24 h (for a CalB content of 6.5 wt%) and 17 days (1.6 wt%).[35] Later, the same PCL films with 1.6 wt% CalB inside were studied under dynamic flow conditions, reducing the time required for total degradation.[36] More recently, Jbilou *et al.* studied PBS degradation by reactive extrusion with CalB at 120 ºC without any solvent involved. Results showed a high reduction in M_n (> 90 %) in 30 minutes.[37] Iwasaki *et al.* obtained PLLA films with embedded Proteinase K by hot-pressing at 130 ºC, reaching moderate weight loss after 1 week for a block copolymer containing PLLA.[38]

As many processing techniques are heat-dependent, recent studies have shown different approaches for increasing enzyme stability: chemical modification, enzyme immobilization, or including additives.[39] Within enzyme immobilization, the encapsulation of enzymes can be a good alternative to maintain their activity, especially when high temperatures are needed. The immobilization or embedding of enzymes has been widely studied in different polysaccharide matrices,[40] including lipase-embedded alginate particles, which have been employed for the hydrolysis of oils or the synthesis of isoamyl acetate.[41,42]

In the past five years, other authors have successfully studied the self-degradation of several biopolyesters with different lipases. Huang *et al.* reported a ~15 wt% weight loss self-degradation of PLLA films by embedding an immobilized Proteinase K through melt-extrusion and hot-pressing at 200 ºC.[39] Four different lipases, including CalB, were successfully embedded through the same melt-extrusion/hot-pressing procedure, without further immobilization, into PBS (at 130 ºC), PBSA (100 ºC) and PCL (90 ºC) matrixes, reaching significant degradation for PCL (100 wt% degradation in 6 h), and PBSA films (100 wt% degradation in 96 h), and moderate degradation for PBS films (20 wt% in 504 h).[19] In a more recent publication from Huang *et al.*, the thermal embedding of a cutinase (*Humicola insolens*) into five different biopolyesters (PDLA, PBS, PBSA, PBAT and PCL) was achieved by extrusion-compression molding at temperatures as high as 175 ºC. High weight losses were obtained, especially for PCL and PBSA (complete degradation in 6 h using 0.02 wt% cutinase embedded) and PBS (complete degradation after 96 h). PBAT and PDLA reached lower weight loss (~20 wt% in 504 h). Later on, the biodegradability of these cutinase-embedded films was studied in seawater, revealing enhanced degradation, especially for PBS and PBSA enzyme-embedded films, compared to neat films.[43]

Del Re *et al.* prepared PCL and PLA films via casting with CalB, Proteinase K, and a lipase from *Burkholderia cepacia*, reporting complete degradation after 50 h when both lipases where embedded in PCL films[44] and completely depolymerizing PLA films with Proteinase K embedded inside.[45] Finally, enzyme-embedding has reached the 3D-printing field. Amano lipase was 3D-printed at 90 ºC with PCL, and degradation results evidenced a complete depolymerization in 7 days of PCL-printed samples when submitted to a buffer solution at 37 ºC. This study also demonstrated a potential use of such PCL-amano lipase printed samples for 4D-printing applications, used in combination with PLA.[46]

To sum up, this Chapter will deepen into the self-degradation of three different biopolyesters –PLA, PBAT and PBS– and their blends, addressed by the action of a lipase (CalB). For such purpose, a previous study was performed on

PBS films, through the immobilization of a lipase from *P. cepacia* into alginate particles, as a means of heat-protection. These particles were melt-extruded in combination with PBS, and self-degradable films were obtained. Moreover, a more exhaustive study was carried out with the three aforementioned biopolyesters (i.e., PLA, PBAT and PBS), through a lipase-embedding process, which has been followed to introduce CalB into the polyester matrix, turning them into self-degradable films via a melt-extrusion/hot-pressing procedure. This procedure applied on polymer blends, which has not been reported so far, will let us acquire a better comprehension of the enzymatic degradation mechanisms of the studied biopolyesters, based on their different aliphatic/aromatic nature.

5.2. Experimental Part

5.2.1. Materials

For the preparation of the lipase-embedded alginate beads, the following materials were employed: Amano lipase PS from *Burkholderia cepacia* (Lot #MKCB2061V), lipase *P. cepacia* immobilized on Immobead 150 (Lot #BCBV3782), phosphate buffered saline (physiologic pH of 7.2-7.4), alginic acid sodium salt from brown algae of high viscosity (M_w ~600,000 g/mol), sodium acetate anhydride and Triton X-100 were purchased from Sigma-Aldrich. Calcium chloride dihydrate was acquired from Acros Organics and 2-propanol were acquired from Scharlab and VWR, and *p*-nitrophenyl palmitate (pNPP) was provided by Alfa Aesar.

In the case of the blends, the following polymers were employed: a poly(lactic acid) (PLA) Ingeo™ 4043D grade (98 % L-isomer) from NatureWorks Co. Ltd., USA; a poly(butylene-*co*-adipate terephthalate) (PBAT) Ecoflex© F Blend C1200 from Polymats Co., Ltd., Thailand; and poly(butylene succinate) (PBS) BioPBS™ FZ91PM grade from PTT MCC Biochem Co., Ltd., Thailand. The initial molecular weight distribution and thermal parameters of the three biopolyesters under study are reported in Table 5.1. Three blend samples were prepared by melt blending in an internal mixer (Chareon Tut Co., Ltd., Thailand), where the mixing was performed at 190 ºC with a rotor speed of 60 rpm for 10 min.[15] The weight composition of each homopolymer in the blend was indicated with subscripts: $PLA_{50}PBAT_{50}$, $PLA_{45}PBAT_{45}PBS_{10}$, and $PLA_{30}PBAT_{30}PBS_{40}$. Lipase from *Candida sp.* recombinant, expressed in *Aspergillus niger* (CalB, ref. L3170-50ML), sodium phosphate monobasic monohydrate (ref. S9638-1KG) and dibasic heptahydrate (ref. S9390-1KG) for the preparation of the phosphate buffers (pH 7 and 8), *p*-nitrophenyl butyrate (pNPB, ref. N9876-1G), dialysis membranes (SnakeSkin Dialysis Tubing 10,000 MWCO, ref. 68100) were purchased from Sigma-Aldrich. Pluronic® F-127 (ref. P2443-250G) was acquired from Merck. Pluronic® F-127 is a hydrophilic non-ionic surfactant composed of a linear

triblock copolymer from poly(ethylene oxide) (PEO) and poly(propylene oxide) (PPO). All reagents were used as received.

Table 5.1. Initial molecular weight distribution (GPC) and thermal properties (DSC) from the homopolymers employed in this study.

Sample	M_n (x 10^4)	M_w (x 10^4)	$Đ$	T_m (ºC)	X_c (%)
PLA	9.22	18.00	2.0	149.8	2.6
PBAT	4.16	10.97	2.6	120.0	13.9
PBS	5.06	18.07	3.6	112.5	33.1

5.2.2. Preparation and enzymatic degradation of self-degradable PBS films

Self-degradable PBS films were prepared by hot-pressing, with an extrudate obtained from PBS pellets and polysaccharide particles with the embedded enzyme. Prior to the preparation of the films, the alginate particles with the embedded enzyme were prepared as follows. High M_w alginate was dissolved in deionized water (2 wt%) together with Amano lipase PS from *Burkholderia cepacia* (named *Amano lipase BC*). The amount of lipase inside the alginate beads was optimized by testing several concentrations of Amano lipase BC (0.75, 1.25, 1.75, and 2 mg/mL in 2 wt% alginate particles). Finally, the highest concentration (i.e., 2 mg/mL) was chosen for the preparation of the self-degradable PBS films, as higher concentrations of enzyme usually lead to better performance towards degradation. The beads were then fabricated using a syringe pump (Legato 200, Kd Scientific, Inc., USA) equipped with a 5 mL syringe (Inkjet Luer Solo from B.Braun, AG, Germany) and a 23 G hypodermic needle (0.6 x 25 mm 23Gx1", Nr. 16 Microlance 3 from BD, USA), by setting the flow at 800 µL/min. The alginate solution containing the enzyme was added dropwise to a 250 mL aqueous solution of calcium chloride (2 wt%). The particles, named as *AlgEmb*, were left in the $CaCl_2$ bath under stirring for at least 1 hour for hardening and then recovered and washed with distilled water. After that, the alginate beads were freeze-dried (Powerdry LL 1500, Thermo Fisher Scientific, Czech Republic), and their

morphology was observed with a Hitachi TM3030 Plus Tabletop Microscope (Hitachi, Ltd., Japan). These particles are referred to as *AlgEmbLi* from now on.

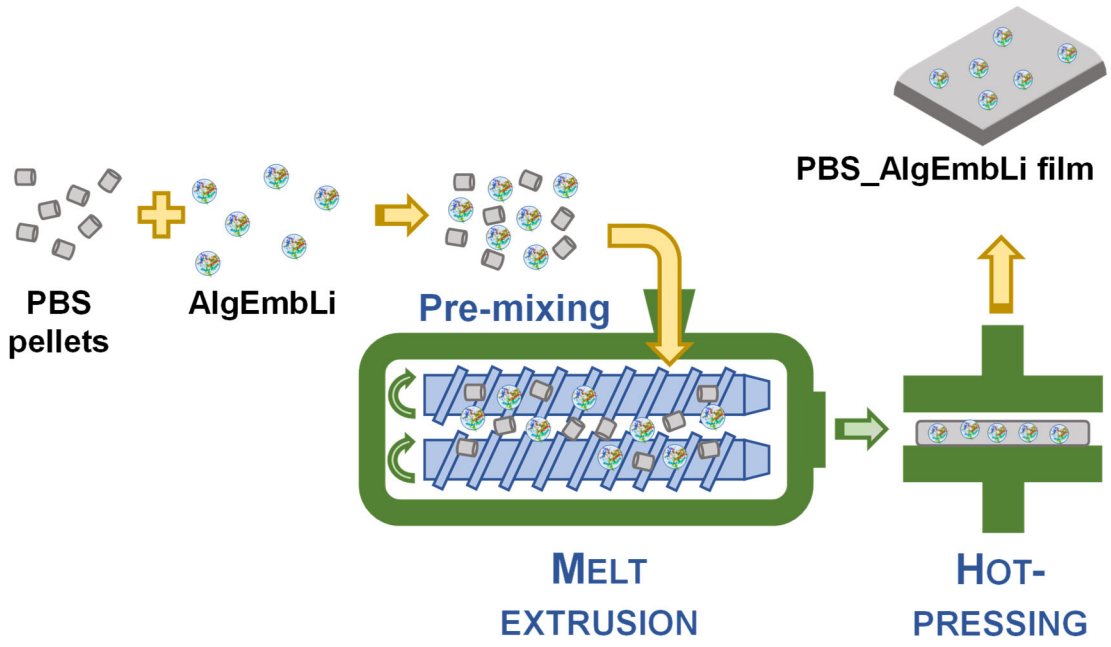

Scheme 5.1. Schematic representation of the extrusion process of PBS pellets and enzyme-embedded alginate beads (AlgEmbLi) to obtain self-degradable PBS films (PBS_AlgEmbLi).

In a second step, the joint extrusion of PBS and AlgEmbLi particles was done at a ratio of 10 wt% AlgEmbLi to PBS (see Scheme 5.1). For the extrusion process, PBS pellets (6.3 g) and the corresponding amount of AlgEmbLi beads (700 mg) were pre-mixed, introduced in an MC 15 micro compounder (Xplore Instruments BV, The Netherlands) at 125 ºC, mixed for 3 minutes at 60 rpm and extruded at 60 rpm. Finally, the films containing AlgEmbLi beads (named as PBS_AlgEmbLi) were obtained by hot-pressing at 125 ºC in a Polystat 100T (Schwabenthan-Maschinen GmbH & Co. KG, Germany) and a Collin P200E (Collin Solutions, GmbH, Germany) hydraulic presses, with the following steps: *i)* 5 minutes at 5 bars, *ii)* 2 minutes at 50 bars, *iii)* 2 minutes at 100 bars, and *iv)* a final extra cooling step (at room temperature) for 2 minutes at 100 bars. The average thickness of these films was 0.12 ± 0.02 mm, as determined by employing a digital caliper. The films were kept at room temperature for one week before starting the experiments.

Biodegradation assays were carried out in phosphate buffered saline solution (pH 7.2-7.4). For this study, the previously obtained PBS_AlgEmbLi films were cut into 10 x 10 mm^2 sized samples, immersed individually into 5 mL-glass vials containing 2 mL of the buffer solution, and placed into a thermostated chamber (Heraeus Instruments, Germany) at 37 ºC with rotational stirring (Rocker 3D Digital, IKA-Werke, GmbH & Co. KG, Germany) at 45 rpm. All the samples were weighed before starting the experiments, and the enzymatic degradation was monitored through weight loss, as indicated in the previous experiments. The samples were withdrawn at certain times, washed with distilled water, and finally weighed after a complete drying at room temperature (48 hours).

5.2.3. CalB purification, characterization, and evaluation of the enzymatic activity

The extract from *Candida antarctica* lipase B (CalB, UniProt ID #LIPB_PSEA2), provided in liquid form, was further washed following a typical methodology. Firstly, several dialysis steps were performed employing the 10 kDa membrane in a phosphate buffer medium (10 mM, pH 7). Afterwards, the liquid product was freeze-dried and preserved at -20 ºC/-80 ºC for further processes. Several batches were obtained, employing 50 mL of the liquid lipase (reactant) and obtaining ~1 g of solid neat enzyme. Additionally, and as a way to prevent the denaturation of CalB due to the high temperatures reached during the processing, 1 g of Pluronic® F-127 was dissolved in one batch of the dialysed enzymatic solution in order to achieve a ~50 % w/w CalB/Pluronic ratio. Pluronic® F-127 has been reported as a protecting agent for many lipases under high-temperature conditions or in acid/base media.[47,48]

The washed lipase was further characterized by UV-Vis in a NanoPhotometer NP80 (Implen, Germany) in order to obtain the protein content in the solid obtained after freeze-drying. A concentrated aqueous solution was prepared (~5 mg/mL) and several dilutions were done and studied at 280 nm, using a ε of 41,285 $M^{-1} \cdot cm^{-1}$. A second procedure to obtain the protein content in the enzyme was done using Bradford's method with bovine serum albumin (BSA)

standards. In this case, Bradford's reactant adheres to the hydrophobic parts of the protein, and thus, the protein content in enzymes can be determined. Several aliquots (ranging 0 to 1 mg/mL) were prepared from a concentrated solution (2 mg/mL) of BSA standard.[49] Afterwards, the absorbance at 595 nm was followed in a BioTek Synergy neo2 multi-mode reader (Agilent Technologies, Inc., USA). Finally, the purity of the protein was assessed by sodium dodecyl-sulfate polyacrylamide gel electrophoresis (SDS-PAGE), and the molecular weight of the lipase was determined. For such purpose, a few μg of enzyme were placed in different wells, and the electrophoresis process was performed at 100 V for 1-2 h.

The lipase activity was evaluated through monitoring of the release of *p*-nitrophenol (pNP) from the hydrolysis of *p*-nitrophenyl butyrate (pNPB) at the maximum peak of absorbance of pNP, 410 nm, using a multi-mode plate reader.[6] The substrate solution was prepared at 55.75 mM in absolute ethanol. In a 96-well plate, 2 μL of a lipase solution (0.20-0.25 mg/mL) were added to 200 μL of phosphate buffer solution (30 mM). Just before the measurement, 5 μL of pNPB substrate solution were added to each well, and the absorbance data were collected at 410 nm as a function of time. The experiments were performed at pH 7 and pH 8 (the media for our degradation studies) and 25 ºC. All measurements were done in triplicate. For the quantification of the enzymatic activity (*U*), the slope from the linear region of the UV curve (absorbance vs. time was obtained for each replicate and employed in the following expression (Equation 5.1).

$$U = \frac{slope \cdot V_{assay}}{\varepsilon \cdot m_{CalB}} \qquad \text{(Eq. 5.1)}$$

Where *U* stands for the enzymatic activity, the *slope* comes from the UV curves, the V_{assay} was fixed to be 207 μL, ε is the molar absorption coefficient – 7447 $M^{-1} \cdot cm^{-1}$ at pH 7 and 12,411 $M^{-1} \cdot cm^{-1}$ at pH 8–, and m_{CalB} is the CalB mass (determined from the lipase concentration, the protein content and the added volume –2 μL–).

5.2.4. Fabrication of enzyme-embedded biopolyester films: PLA, PBAT and PBS, and their blends

For the preparation of enzyme-embedded biopolyesters (i.e., PLA, PBAT, PBS, and their blends), the polyester powder (obtained by cryo-milling the pellets) and CalB powder were mixed at different CalB/polyester ratios (1, 5, and 10 wt%) and joint-extruded in a vertical double-screw MC 5 micro compounder (Xplore Instruments BV, The Netherlands). The extrusion process was performed at 125 ºC for neat PBS with CalB, and at 170 ºC for the rest of the homopolyesters (i.e., PLA and PBAT) and blends. The CalB/polyester mixture was introduced in the micro compounder, mixed for 3 minutes at 60 rpm, and extruded at 60 rpm. Finally, the enzyme-embedded polyester films were prepared by hot-pressing the extrudates in a Collin P200E (Collin Solutions, GmbH, Germany) and Polystat 100T (Schwabenthan-Maschinen GmbH & Co. KG, Germany) pneumatic presses. The processing conditions consisted of four steps: *i)* 50 seconds at 0 bars (pre-heating contact), *ii)* 10 seconds at 5 bars, *iii)* 30 seconds at 50 bars, *iv)* 30 seconds at 100 bars, and *v)* a final extra cooling step (at room temperature) for 30 minutes at 100 bars. Different temperatures were employed in steps 1-4 depending on the melting temperature of each polyester: 125 ºC for PBS, 150 ºC for PBAT, and 170 ºC for PLA and the three blends. This procedure was similar to that described in Scheme 5.1, except for the different polyesters and enzyme employed, as well as the temperature conditions.

As a way to protect CalB from the heating of the processing and its possible denaturation, a second set of samples was prepared through joint-extruding CalB/Pluronic (~50 wt% CalB) and the different polyesters at 10 wt% of CalB/Pluronic with respect to polyester, with a similar aim as that followed with AlgEmbLi particles in Section 5.2.2. The total amount of enzyme was 5 wt% in this case.

Samples were designated with their name followed by the CalB content. For example, a film prepared using the $PLA_{50}PBAT_{50}$ blend and 5 wt% CalB/polyester

will be referred to as *$PLA_{50}PBAT_{50}$_5%*. For those films prepared with Pluronic, the suffix *Plur* was added to the name of the sample (i.e., *$PLA_{50}PBAT_{50}$_5%Plur*).

The average thickness of all the enzyme-embedded prepared films was 0.13 ± 0.03 mm, as determined by employing a digital caliper. In order to minimize the possible denaturation of the enzyme and for better preservation of the films, the films were kept at 4 ºC until the beginning of the experiments.

5.2.5. Characterization of the degraded films from the enzyme-embedded biopolyesters: PLA, PBAT and PBS, and their blends

a. Analysis of the weight loss and surface morphology

Polymeric films from PLA, PBAT and PBS, and their blends (initial weight ~10 mg, 8 x 8 mm^2) were immersed individually into 4 mL-glass vials containing 1 mL of phosphate buffer solution (24 mM, pH 8) and placed into a thermostated chamber (Stuart SI500 Shaking Incubator, Cole-Parmer, USA) at 40 ºC with rotational stirring at 45 rpm. The samples were withdrawn at certain times, washed with distilled water, and finally weighed after complete drying at 50 ºC (48 hours). To control the enzymatic degradation, the weight loss of the samples was determined using the following equation (Equation 5.2).

$$W_{loss}\ (\%) = \frac{W_{initial} - W_{final}}{W_{initial}} \cdot 100 \qquad \text{(Eq. 5.2)}$$

Where W_{loss} stands for weight loss (expressed in %), $W_{initial}$ refers to the initial weight of the samples (before degradation), and W_{final} indicates the final weight of the samples after the degradation assays.

Changes in surface morphology were monitored as a function of the degradation time in an Olympus BX53M polarized light optical microscope (Evident Corp., Japan), and images were recorded with an Olympus SC50 camera at 20x magnification.

b. Analysis of the changes in molecular weights and chemical structure in degraded samples and liquid aliquots

The number and weight average molecular weights (M_n and M_w, respectively) were determined through Gel Permeation Chromatography analysis (GPC). Chromatograms were recorded in a Waters Instrument (Waters Corp., USA) equipped with RI and UV detectors. HR5E and HR2 Waters linear Styragel columns (7.8 mm × 300 mm, pore size 10^3-10^4 Å) packed with crosslinked polystyrene and protected with a precolumn were used. Samples were prepared by dissolving 3 mg of the sample in 1 mL of chloroform and using the same solvent as the eluent. Measurements were performed at 35 ºC with a flow rate of 0.5 mL/min, and molecular weights were calculated against monodisperse polystyrene standards.

The chemical composition of the degraded films was also evaluated in a Nicolet iS20 ATR-FTIR Spectrometer (Thermo Fisher Scientific, USA) equipped with a Smart iTX Accessory with Diamond Crystal. Spectra were obtained from 4000 to 400 cm^{-1}, at room temperature, with 32 scans and 4 cm^{-1} of resolution, and further analysed with OMNIC software (v. 9.13.1294).

Finally, the liquid aliquots of each vial (containing 1 mL of phosphate buffer, CalB and degradation products) were freeze-dried and further examined by Proton Nuclear Magnetic Resonance (^{1}H-NMR) in order to ascertain the possible products obtained during the degradation assays. Spectra were recorded in a Bruker AMX-300 Spectrometer (Bruker Corp., USA). 640 scans were recorded from 10 mg sample solutions in 1 mL of deuterated water. Prior to the freeze-drying of the vials, pH measurements were performed in a pH 8+ DHS pHmeter (XS Instruments, Italy) to determine possible changes in the pH of the degradation media as a means to obtain further information on the enzymatic degradation mechanism of the biopolyesters under study.

c. Analysis of the crystallinity as a function of degradation time

The crystallinity of the films as a function of degradation time was evaluated by Differential Scanning Calorimetry in a TA DSC25 equipped with an Intracooler RCS90 (TA Instruments, Inc., USA). Temperature sweeps with two scans were done from -50 to 160 ºC (PBS) or 180 ºC (PLA, PBAT, and blends), at 10 ºC/min. DSC curves were analyzed with the TRIOS software (v5.7.0.56) from TA Instruments, Inc. For the analysis of the blend films, the heating scan was performed at 60 ºC/min (to avoid PLA's cold crystallization); however, it was impossible to differentiate the melting peaks of each homopolymers. For this reason, the melting enthalpy of the whole peak (or multiple peaks) was reported for the blends.

5.3. Results and Discussion

An increasing number of recent publications in the literature report various enzymatic degradation studies on PLA, PBS, and PBAT with very different experimental conditions, which depend on the type of enzyme used. In fact, to the best of our knowledge, there are not standardized experiments regarding enzymatic degradation tests as in other degradation assays, such as soil burial or compost degradation. Results can vary significantly among studies for enzymatic degradation due to the different experimental conditions and the distinct natures of the starting polymers. Some parameters have been found to be determinants in the degradation of polyesters, such as the initial molecular weight distribution or the crystallinity.[50] The influence of enzyme concentration has been studied in externally-added enzyme tests as one of the multiple ways to control and tune the degradation.[51] Herein, the modulation of the enzyme-induced degradation of different polyester films through the preparation of self-degradable films is investigated.

5.3.1. Self-degradable PBS films containing enzyme-embedded polysaccharide beads

The morphology of the lipase-embedded alginate beads (AlgEmbLi) employed for PBS self-degradation is shown in Figure 5.1a. The particle diameters were found to be ~2 mm with smooth surfaces and some scattered regions that showed a porous morphology.

As a first step, the feasibility of employing the *P. cepacia* lipase (in free form) at the temperature conditions required to prepare the PBS films (temperature above the melting point of PBS ~115 ºC) was studied. To this aim, the enzymatic activity of the lipase was determined at different concentrations in solutions maintained at room temperature and at 125 ºC for 10 minutes. As can be observed in Figure 5.1b (left blue-shaded area of the graph), the lipase in solution loses the enzymatic activity when maintained at 125 ºC for a short time, which prevents the use of the free enzyme in the preparation of self-degradable films. In contrast, alginate beads

with embedded enzyme retain their enzymatic activity even after heating at 125 ºC, as shown in Figure 5.1b (right yellow-shaded area of the graph). For alginate beads with a lipase concentration of 1.25 and 2 mg/mL, enzymatic activity after heating was retained over 90 % with respect to initial values (~100 % for 2 mg/mL lipase concentration). Furthermore, it was also appreciated that the activity increased with the concentration of the lipase inside the alginate beads. Similar observations were obtained for Immobead commercial particles, which exhibited good behaviour towards heating, with identical activity values obtained when measured before and after heating (see Figure 5.1c). Commercially available Immobead particles, that is commercial lipase-immobilized beads, were employed in this study for comparison purposes. These particles consist on *P. cepacia* lipase immobilized on Immobead 150P, methacrylate copolymer particles (0.15-0.50 mm diameter), cross-linked and carrying oxirane groups. Regarding the effect of temperature on the enzymatic activity, similar observations to that commented in Figure 5.1b for the lab-made *AlgEmbLi* beads were shown by these particles. For instance, for a concentration of 8.5 mg, a ~15 % decrease in the enzymatic activity was obtained after heating at 100 ºC for 25 minutes, whereas other concentrations such as 12.2 mg and 4.4 mg exhibited an increase of ~6 and ~67 %, respectively. Therefore, preserving the enzyme by embedding it inside alginate beads has been proven to be necessary to maintain the enzymatic activity at levels high enough to degrade the polyester.

Then, the degradation of PBS films employed as control was compared with that of PBS films containing lipase-embedded alginate beads (PBS_AlgEmbLi). Figure 5.1d revealed that the maximum weight loss obtained for PBS_AlgEmbLi films barely achieved a 5 wt%. This could be attributed, on the one hand, to the low enzymatic activity exhibited by the lipase-embedded alginate beads (AlgEmbLi) as compared to that of the free enzyme in solution (~1 mg/mL), as seen in Figure 5.1b. In addition, it was found that the enzyme concentration (related to the enzymatic activity) of the AlgEmbLi particles was 2 orders of magnitude less (70-100 times less concentrated) than the free enzyme (i.e., in solution) employed for degradation experiments explained in Chapter 4 with the

same lipase. These results could be related to the prevention of the encapsulated enzyme to water accessibility, due to the protection of the alginate beads. Future experiments carried out in PLA, PBAT and PBS, and their blends will aim to increase the amount of embedded-lipase embedded in order to increase the extent of self-degradation of biopolyester films.

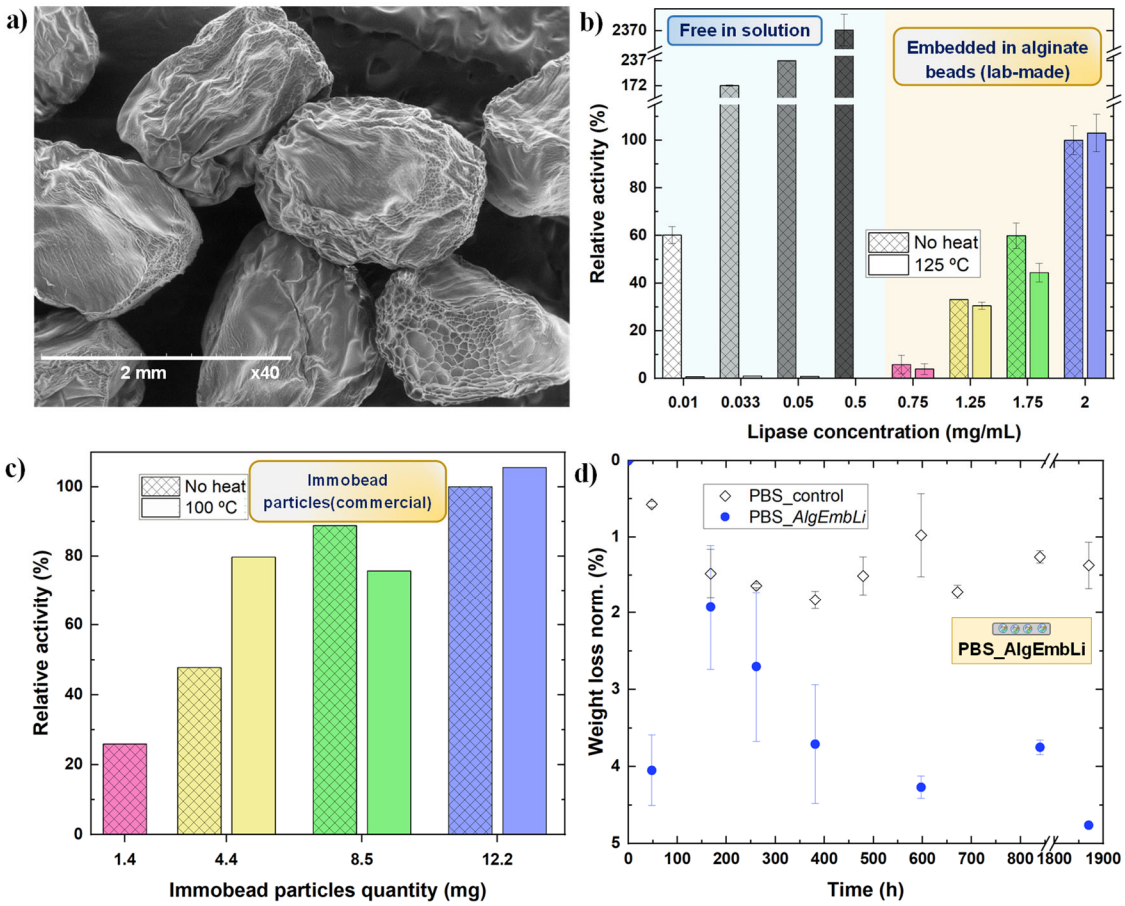

Figure 5.1. a) SEM images of the freeze-dried lipase-embedded alginate particles, AlgEmbLi, at 40x magnification. Determination of the relative enzymatic activity (with no-heating treatment and after 10 minutes at 125 ºC) of: **b)** free lipase in solution (blue-shaded area, on the left) and lab-made alginate beads with embedded lipase (AlgEmbLi, yellow-shaded area, on the right), and **c)** commercial Immobead particles. The enzymatic activity is normalized to that of the highest lipase concentration (i.e., 2 mg/mL, for embedded-lipase in alginate beads in Figure 5.1b and 12.2 mg for commercial Immobead in Figure 5.1c). **d)** Weight loss degradation curves for self-degradable PBS_AlgEmbLi films.

5.3.2. Lipase characterization and evaluation of the enzymatic activity of CalB

As multiple degradation tests were performed with six different materials (three homopolyesters and three PLA/PBAT/PBS blends), several CalB batches were washed and employed. Gel electrophoresis (SDS-PAGE) revealed the M_w of the lipase under study, which was found to be ~33 kDa, as depicted from Figure 5.2, and in agreement with literature values.[18] The protein content of each lyophilizate was evaluated by UV-Vis (absorbance at 280 nm), as well as by Bradford's method. Additionally, the enzymatic activity of each of the batches was evaluated at different pH values (7 and 8) as a way to select the best condition for degradation tests; all these parameters are included in Table 5.2.

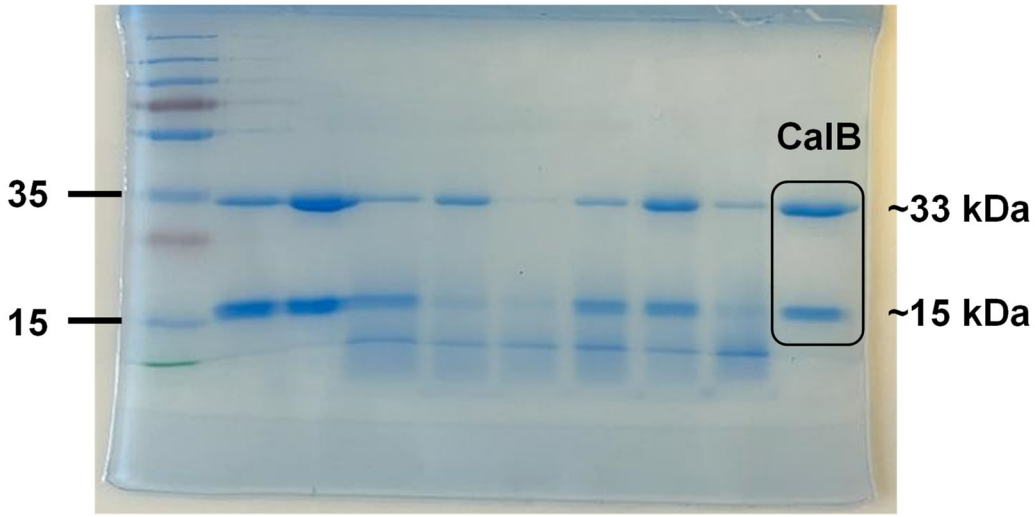

Figure 5.2. Image of the SDS-PAGE electrophoresis in a sodium dodecyl-sulfate polyacrylamide gel for the CalB under study.

Table 5.2. Description of the protein batches used in this work. CalB content of the lyophilizates was measured by UV/Bradford's, and the enzymatic activity was tracked by UV-Vis. The standard deviation of the mean values is given in brackets.

Batch#	Protein content (%)		*U* (μmol·s^{-1}·mg^{-1})	
	UV_{280}	Bradford's	pH 7	pH 8
1	47.8 (0.5)	21.4 (2.3)	0.2393 (0.0478)	0.2647 (0.0149)
2	43.7 (1.1)	n.d.	0.2488 (0.0401)	0.3329 (0.0073)
3	47.0 (1.9)	n.d.	0.1916 (0.0288)	0.2752 (0.0323)
Pluronic	37.9 (1.9)[a]	n.d.	0.1537 (0.0280)	0.2243 (0.0263)

[a] Protein content was determined taken into consideration the 50/50 CalB/Pluronic ratio.

In general, all the batches presented a protein content of 44-48 %; however, the batch containing Pluronic showed a slightly lower protein content of ~38 %. The protein content value reported from Bradford's method was significantly different from those obtained through UV-Vis at 280 nm. This method is better applied for pure proteins, and in this Chapter, the directly freeze-dried CalB was employed. For this reason, Bradford's was not further used for the protein content determination in the CalB batches studied in the current Chapter. Regarding the enzymatic activity, in all cases, CalB exhibited higher activity at pH 8 (10-46 % higher, up to ~91 % in one of the batches); mean values were 0.2743 μmol·s^{-1}·mg^{-1} at pH 8, and 0.2084 μmol·s^{-1}·mg^{-1} at pH 7. These values were as expected, justifying the selection of this pH value for the degradation experiments due to the higher enzymatic activity at pH 8.[30] Finally, the Pluronic batch presented slightly lower *U* values, probably due to the lower protein content. Similar observations are reported in literature.[47]

5.3.3. Influence of CalB content on the self-degradation of the homopolymers: PLA, PBAT and PBS

a. Analysis of the weight loss and morphological characterization of the degraded samples

Figure 5.3 depicts the results corresponding to the weight loss of the three homopolymers under study with embedded CalB at two different concentrations, 1 and 5 wt% (Figure 5.3a and Figure 5.3b, respectively). In Figure 5.3c, the results corresponding to weight loss of the 5 wt% CalB/Pluronic-embedded samples are shown for comparison purposes. Blank experiments, with neat polyester films in phosphate buffer solution (without CalB), were performed to study the hydrolytic degradation of the homopolymers, and results in Figure 5.3d showed negligible weight loss.

The Polyester_1% films (i.e., 1 wt% CalB-embedded samples) exhibited moderate weight loss for PBS_1% films (~50 wt% after 1000 hours), with a lower extent in the case of the PBAT_1% films (~16 wt% after 1000 hours), as depicted in Figure 5.3a. When the CalB content inside the films increased from 1 to 5 wt% (Figure 5.1b), the trend changed from linear to exponential. In this case, PBAT_5% films reached ~53 wt% weight loss by the end of the biodegradation test, whereas PBS_5% films exhibited complete degradation (100 wt% achieved). These results contrast with those obtained for the 5 wt% CalB/Pluronic films (Figure 5.3c), where PBAT_5%Plur films reached ~11 wt% weight loss (4.5 times lower than in PBAT_5%), and ~25 wt% for PBS_5%Plur films was obtained (~4 times less than in PBS_5% samples). In all the cases, PLA films (i.e., PLA_1%, PLA_5%, and PLA_5%Plur) did not exhibit any weight loss (0-3 wt%). Weight loss results, together with the qualitative activity evaluation of the lipase-embedded films through the reaction with pNPB –and subsequent generation of pNP– suggested that added CalB inside the polyesters maintained its activity after melt extrusion at 170 ºC without any further stabilization steps.

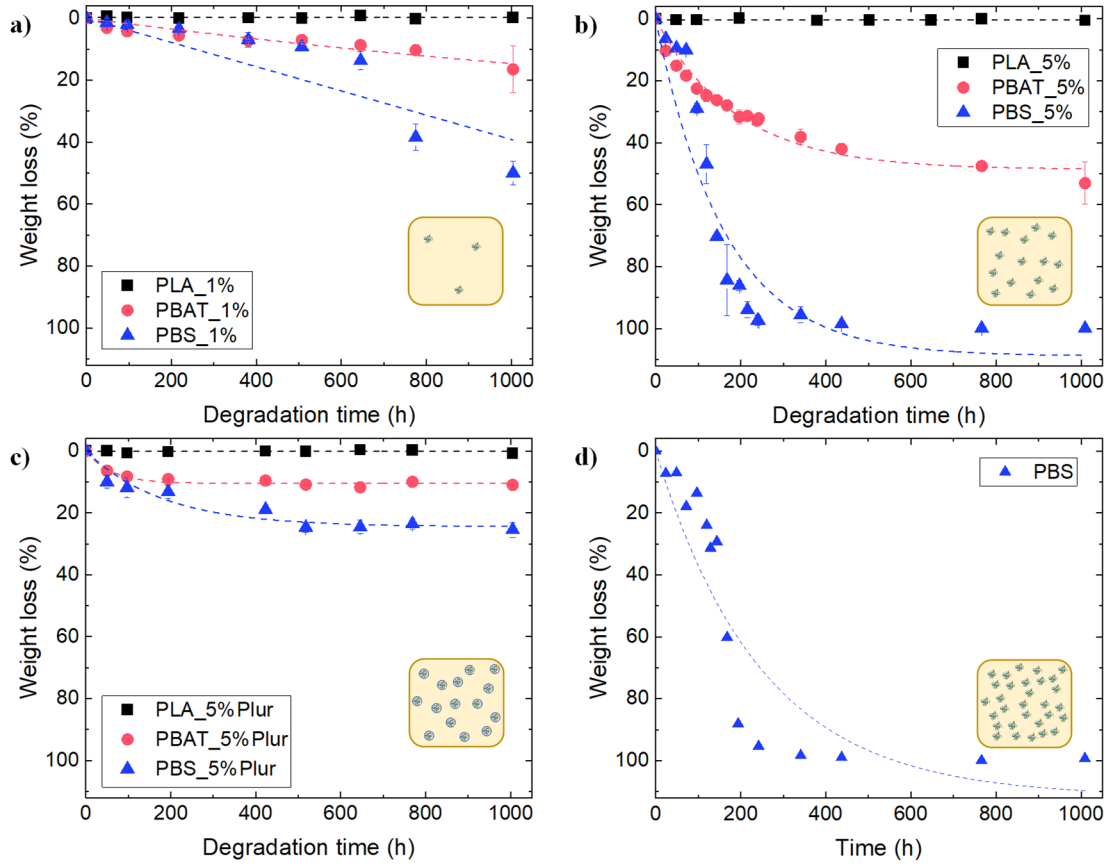

Figure 5.3. Weight loss curves for the three homopolyesters under study with increasing CalB/polyester ratio: **a)** 1 wt% CalB (Polyester_1%), **b)** 5 wt% CalB (Polyester_5%), **c)** 5 wt% CalB/Pluronic (Polyester_5%Plur), and **d)** blank experiments (without CalB). Dashed lines represent the fitting of the data to the different models: linear fitting (Figure 5.3a), and the proposed model in Equation 5.3 (Figure 5.3b-c). Each graph includes a schematic representation of each system as an inset: the yellow square represents the polyester film, whereas the embedded lipase is plotted with (embedded CalB) or (embedded CalB/Pluronic). Symbols' number is related to CalB content inside the films.

To quantify the extent of degradation and compare the different experiments, weight loss over degradation time curves were fitted to a previously employed model (also used in Chapter 4) to describe the degradation kinetics quantitatively.[22] This model, which is based on the Michaelis-Menten' model for enzymes, describes the whole biodegradation process, which is controlled by heterogeneous reactions: *i)* adsorption of the enzyme on the surface of the substrate, *ii)* degradation of the polymer and, *iii)* denaturation of the enzyme. Some authors

have proposed a modified Michaelis-Menten' model with some needed corrections for the enzymatic degradation of PLA that can be described by Equation 5.3.[52,53]

$$m_t = v_d.\tau \cdot (1 - e^{-t/\tau}) \quad \text{(Eq. 5.3)}$$

Where m_t refers to the weight loss of the sample (considered similar to W_{loss} indicated in Equation 5.2), v_d stands for the rate of degradation, τ indicates the rate of denaturation of the enzyme (time constant) and implies that the degradation has reached a *plateau* and t is the time (expressed in hours). From the product between v_d and τ, it is possible to obtain the value corresponding to the degradation at infinite time (A). This model cannot be appropriately applied for cases where weight loss does not reach a *plateau* (as for example, in the case of the Polyester_1% experiments in Figure 5.3a). For these cases, only information regarding the rate of degradation will be obtained. A linear fitting is applied to avoid this issue, where the slope is associated with the degradation's kinetics, and assumed to be similar to the degradation rate, v_d, in the modified Michaelis-Menten' model (Equation 5.3).

The application of the modified Michaelis-Menten' model (Equation 5.3) to the experimental data shown in Figure 5.3b and Figure 5.3c allows us to extract further information on the effect of the CalB concentration, as well as the effect of Pluronic, on the self-degradation of the lipase-embedded homopolyester films (Table 5.3).

Table 5.3. Kinetic parameters determined from the modified Michaelis-Menten' model for the self-degradation studies in the Polyester_5% and Polyester_5%Plur experiments, with the three homopolymers under study (PLA, PBAT, and PBS). The standard deviation of the mean values is given in brackets.

Sample	*CalB content (wt%)*	v_d (%/h)	τ (h)	*A* (%)	R^2
PLA_5%	5	0.0005 (0.0001)[a]	n.d.[b]	n.d.[b]	0.5772
PBAT_5%	5	0.2731 (0.0150)	171 (13)	46.7	0.9734
PBS_5%	5	0.6016 (0.0846)	175 (32)	105	0.9396
PLA_5%Plur	5[c]	0.0004 (0.0005)[a]	n.d.[b]	n.d.[b]	0.1551
PBAT_5%Plur	5[c]	0.1744 (0.0269)	60 (10)	10.5	0.9586
PBS_5%Plur	5[c]	0.1342 (0.0258)	182 (42)	24.4	0.9303

[a] Obtained from the linear fit of the data.

[b] These data could not be obtained, as the weight loss curves were linearly fitted due to null weight loss exhibited by PLA films.

[c] 50/50 CalB/Pluronic ratio.

In all the cases, PLA films exhibited a negligible weight loss (below 3 wt%); hence, fitting experimental data to the modified Michaelis-Menten' model was impossible, and a linear fitting was applied instead (the slope give an idea of the degradation rate, as indicated in Table 5.3). The low weight loss exhibited by PLA films with embedded CalB was unexpected, as this lipase has been reported to degrade PLA successfully. Shinozaki *et al.* reported a ~50 % degradation for PLA cast films in 72 h.[31] However, in a recent study from Rosato *et al.*, CalB –as well as other enzymes– was unable to degrade PLA, whereas it successfully depolymerised other polyesters (e.g., PBSA, and PCL).[54] Several studies have demonstrated the preferential attack of proteases (e.g., Proteinase K) on PLLA, whereas PDLA enzymatic degradation is enhanced by the action of lipases, such as CalB.[54,55] This explanation might be behind the negligible degradation observed for PLA films in our study, as the PLA employed here has a 98 % L-isomer.[56] A second reason could be related to the initial molecular weight of PLA, which almost doubled those of the other two homopolyesters (Table 5.1).

Regarding PBAT and PBS films, experimental data in Figure 5.3 were successfully modelled with the Michaelis-Menten' model, and the parameters are reported in Table 5.3. In the case of the 1 wt% CalB-embedded samples, no saturation in the weight loss curves was appreciated –similarly to all PLA samples–, and no plateau regime is reached (linear tendency), as shown in Figure 5.3a. The rate of degradation was found to be almost three times higher for the PBS films: 0.0415 %/h (PBS_1%) > 0.0154 %/h (PBAT_1%), meaning that PBS films were more degraded (according to the weight loss curves) than PBAT ones, under the selected conditions for CalB.

Similar results were found when the CalB concentration was increased up to 5 wt% (Figure 5.3b), PBS films showed a two-fold increase in the rate of degradation with respect to PBAT, being 0.6016 %/h for PBS_5% and 0.2731 %/h for PBAT_5%. On the other hand, the rate of denaturation of the lipase was found to be very similar for both homopolyesters: 171 and 175 h for PBAT_5% and PBS_5% films, respectively. This means that CalB denaturates or saturates at almost the same time. Finally, the degree of degradation at infinite time (A) was calculated to be ~47 wt% for PBAT films and >100 wt% for PBS films. This two-fold higher A value in the case of PBS_5% is attributed to the larger (double) degradation rate of these films. These degradation results are in accordance with other studies in literature, which have shown improved degradation for PBS over PBAT, when degraded under the action of CalB.[25] Although the initial molecular weight distribution of both homopolymers was similar, the initial degree of crystallinity was considerably higher for PBS than PBAT (33.1 vs. 13.9 %, respectively, as seen in Table 5.1), which would make PBAT films more prone to CalB degradation. Figure 5.4a shows the weight loss curve from the PBS_10% samples (i.e., films with 10 wt% CalB-embedded films), with comparable results with respect to PBS_5%: v_d = 0.5872 %/h for PBS_10% (0.6016 %/h for PBS_5%), τ = 182 h for PBS_10% (175 h for PBS_5%), and A ~100 % in both cases. These observations show no enhancement in the overall degradation when the CalB content was increased from 5 to 10 wt% inside the PBS films, probably due to the high lipase content.

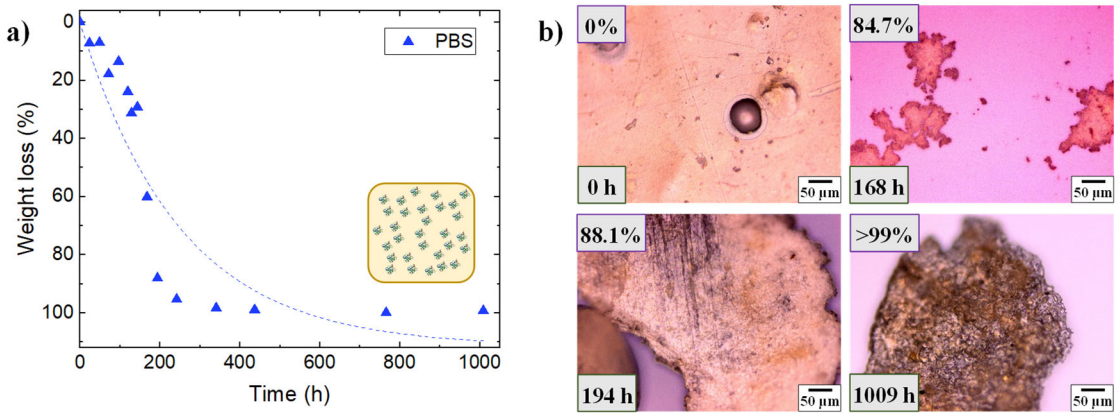

Figure 5.4. a) Weight loss curve for the PBS_10% films. Dashed lines represent the fitting of the data to the proposed model in Equation 3. A schematic representation of the system is included as an inset in the graph: the yellow square represents the polyester film, whereas the embedded CalB is plotted with . Symbols' number is related to CalB content inside the films. **b)** Optical micrographs taken at 20x magnification for the PBS_10% films. In the upper left corner, the achieved weight loss is shown, whereas the degradation time (in hours [h]) is included in the lower left corner.

If we take a look at the kinetic parameters from the Polyester_5%Plur samples (Figure 5.3c), the incorporation of Pluronic led to a reduction in degradation when compared to PBAT_5% films, as evidenced by the lower values obtained for the kinetic parameters (from the modified Michaelis-Menten' model): reduction of ~36 % in the rate of degradation, whereas the rate of denaturation dropped by ~65 %. On the other hand, PBS_5%Plur films showed a ~78 % reduction in v_d compared to PBS_5% films, with no modification in τ: 182 h for PBS_5%Plur and 175 h for PBS_5%. This behavior means that enzyme encapsulation within Pluronic does not have the same effect on the enzymatic degradation of PBS films as compared to PBAT films, as it delays the degradation by affecting only v_d, and not τ, as in the case of PBAT_5%Plur samples (where Pluronic affects both parameters). The lower weight loss exhibited by the 5 wt% CalB/Pluronic-embedded films could be related to the lower enzymatic activity exhibited by the CalB when encapsulated within Pluronic, as shown in Table 5.2. This encapsulation with Pluronic was done for heat-protecting the enzyme;

however, this procedure possibly decreases the contact between the enzyme and the polymer, thus exhibiting a lower degradation rate.

The values of the reported kinetic parameters in Table 5.3 for PBAT and PBS are in the same order of magnitude as reported in the literature for PCL degraded by the action of a lipase from *P. cepacia* (v_d = 0.004-0.156 %/h, τ = 27-586 h)[53] and PLA films with Proteinase K (v_d = 0.95-1.96 %/h, τ = 41-98 h).[52]

The surface morphology of the degraded samples was observed through optical microscopy and the results are shown in Figure 5.5. Even though PLA achieved no degradation as determined through weight loss curves depicted in Figure 5.3, some small holes could be appreciated on the surface of the films in Figure 5.5a and Figure 5.5d. Remarkably, PBS and PBAT, which presented weight losses (after 1000 h) of ~50 wt% (PBS_1%) and ~16 wt% (PBAT_1%) in the 1 wt% CalB, and 100 wt% (PBS_5%) and ~53 wt% (PBAT_5%) for the 5 wt% CalB films, did not show significant differences as to their surface morphology, at the scale shown. Small holes in PBAT films are depicted in Figure 5.5b (PBAT_1%) and Figure 5.5e (PBAT_5%) in the medium-range degradation times, turning into films with no evidence for degradation at higher times. On the contrary, PBS films presented small scattered areas at low weight loss values, turning into holes in the medium-range degradation times until the complete disappearance of the films (PBS_1% in Figure 5.5c and PBS_5% in Figure 5.5f). PBS films exhibited similar behavior with a higher content in lipase (i.e., PBS_10%), where the films presented holes on their surface that became larger with time until the total degradation of the films at times >200 h (see Figure 5.4b).

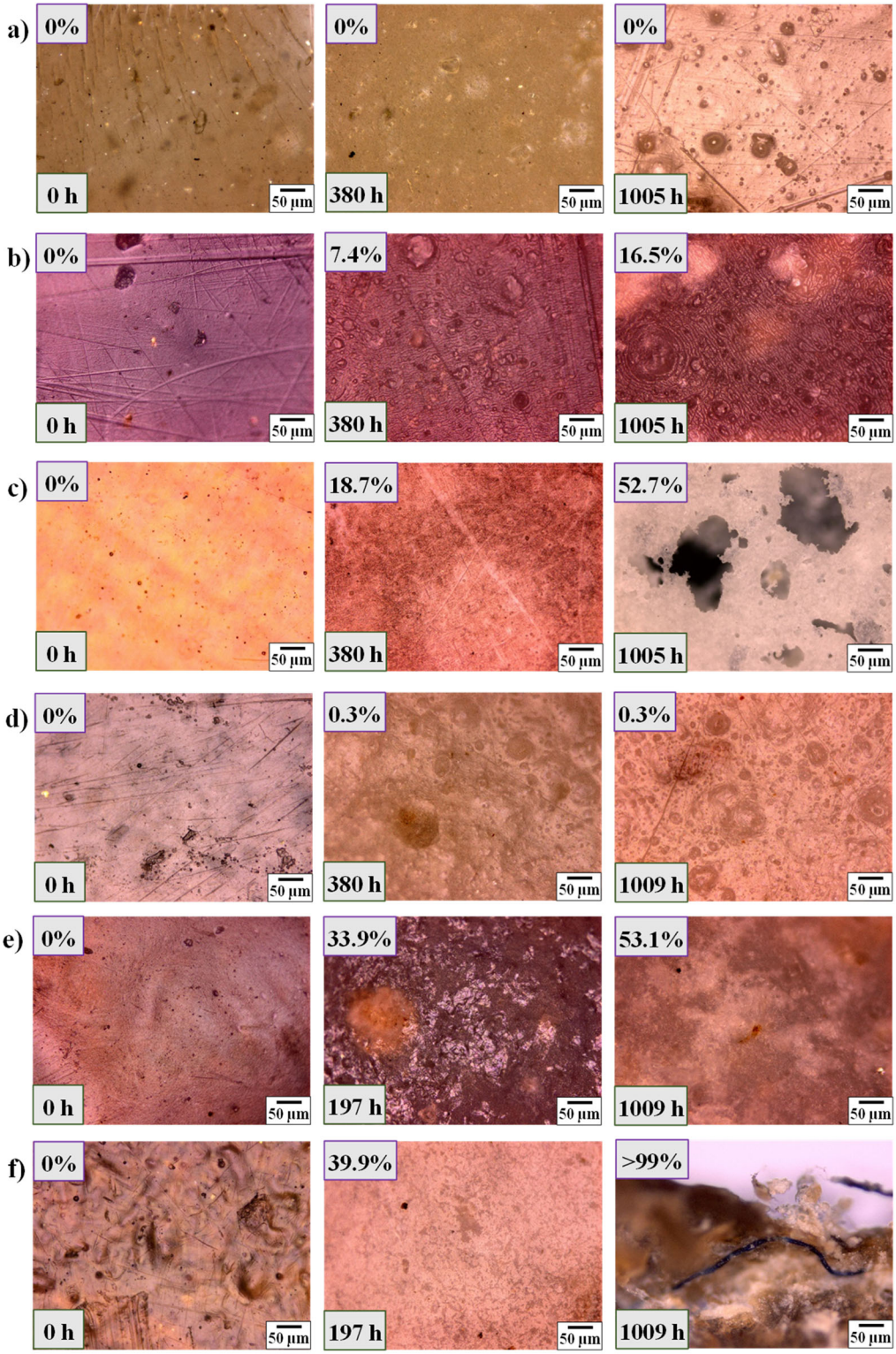

Figure 5.5. Optical micrographs taken at 20x magnification for the 1 and 5 wt% CalB-embedded polyester films: **a)** PLA_1%, **b)** PBAT_1%, **c)** PBS_1%, **d)** PLA_5%, **e)** PBAT_5%, and **f)** PBS_5%. In the upper left corner, the achieved weight loss is shown, whereas the degradation time (in hours [h]) is included in the lower left corner.

The surface morphology of the degraded samples with 5 wt% CalB/Pluronic-embedded films was observed through optical microscopy, and the results are shown in Figure 5.6. As shown in Figure 5.3c, only PBS (~25 wt%) and PBAT (~11 wt%) exhibited significant weight loss. Notwithstanding, no visual differences were appreciated from the optical micrographs in Figure 5.6b (PBAT_5%Plur) and Figure 5.6c (PBS_5%Plur), respectively. PLA samples did not exhibit any morphological variations in the surface of the films, as evidenced in Figure 5.6a.

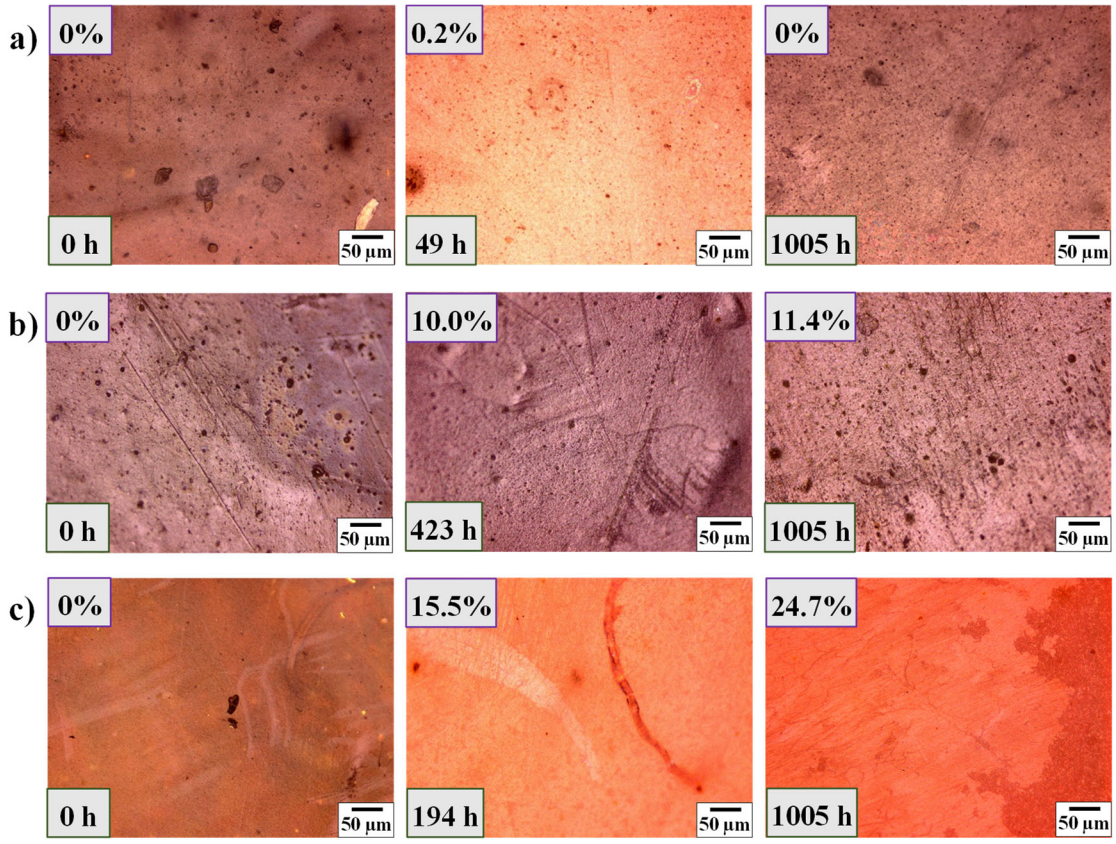

Figure 5.6. Optical micrographs taken at 20x magnification for the 5 wt% CalB/Pluronic-embedded polyester films: **a)** PLA_5%Plur, **b)** PBAT_5%Plur, and **c)** PBS_5%Plur. The achieved weight loss is shown in the upper left corner, whereas the degradation time (in hours [h]) is included in the lower left corner.

The results corresponding to PBAT_5%Plur films (Figure 5.6b) were similar to that previously seen in the PBAT_5% films (Figure 5.5e), although the achieved weight loss was ~5 times lower (~11 vs. ~53 wt%). Some small holes are appreciated, although no visible degradation is evidenced. On the other hand,

PBS_5%Plur films (Figure 5.6c) presented a completely different morphology when compared to the PBS films tested with PBS_5% films (see Figure 5.5f). Some possible degraded areas can be seen in the samples at high degradation times; however, their appearance did not resemble the large holes observed for the PBS_5% films. One possible explanation could be related to the achieved weight loss: ~25 wt% for PBS_5%Plur and 100 wt% for PBS_5% samples. Additionally, it is important to note that CalB does not degrade Pluronic –a PEO-based derivative–, and a migration of the Pluronic through the film towards the surface could also be possible. This hypothesis is aligned with the visual observations in Figure 5.6.

b. Physicochemical characterization of the degraded samples and liquid aliquots

The chemical composition of the films after degradation was monitored through FTIR spectroscopy and the results are shown in Figure 5.7. Regarding PLA films, representative peaks are located at ~1749 cm^{-1} and assigned to the C=O stretching from the ester group; at ~1081 cm^{-1}, attributed to the C-O stretching of secondary alcohol generated in the hydrolysis; at ~1178 cm^{-1}, assigned to the C-O stretching from the ester group; at ~1451 cm^{-1} corresponding to the CH_2 vibration; and at ~2996 and ~2945 cm^{-1}, assigned to the CH asymmetric stretching.[8,57] No appreciable changes are observed between the FTIR spectra corresponding to the pristine PLA films and those corresponding to degraded samples, regardless enzyme concentration (1 and 5 wt%) or the presence of Pluronic for enzyme encapsulation (Figure 5.7a). This is in agreement with the negligible weight losses observed in Figure 5.3 for PLA films.

In the case of PBAT films (Figure 5.7b), the FTIR spectra corresponding to PBAT_1% degraded films showed a decrease in the intensity from the characteristic peak of the C-O stretching of the ester group, from the esterification of a primary alcohol with adipic or terephthalic acid (1165 cm^{-1}) with respect to that corresponding to the non-degraded film, thus confirming the breakage of the ester bonds.[58] Additionally, the appearance of bands in the FTIR spectra

corresponding to the degraded film located at 1410 cm^{-1} corresponding to CH_2 angular deformation band, at ~1650 cm^{-1} corresponding to the C=O stretching of COOH end groups (from the degradation products), and the stretching peak of free C=O groups (1755 cm^{-1}) further confirmed the degradation.[1] PBAT_5% films exhibited higher variations in the bands; the peak at ~3300 cm^{-1} was assigned to the OH stretching, which additionally confirmed the degradation of PBAT films. On the other hand, PBAT_5%Plur films presented lower changes in FTIR spectra; the most noticeable is the decrease of the intensity of the band located at ~2895 cm^{-1}, which could be related to the partial solubilization of Pluronic and also confirmed the degradation.[32] There are other bands that showed a slight increase in intensity, marked in Figure 5.7 with arrows.

Finally, the FTIR spectra corresponding to degraded PBS films showed a significant decrease in the band intensity of all peaks with respect to pristine PBS films (Figure 5.7c). As in the case of PBAT, the appearance of new bands in the spectra corresponding to the degraded sample located at ~3286 cm^{-1} and ~1652 cm^{-1} assigned to OH stretching and C=O stretching of COOH end groups (from the degradation products), additionally confirmed the degradation, as well as the broad band due to hydrogen bonding. It is important to note that for the spectra of the degraded PBS films, the appearance of a peak at ~1546 cm^{-1} that can be assigned to the amide II band of CalB –N-H deformation and C-N stretching–, further confirmed the degradation of PBS films, consistent with the exposure of CalB towards the surface of the films.

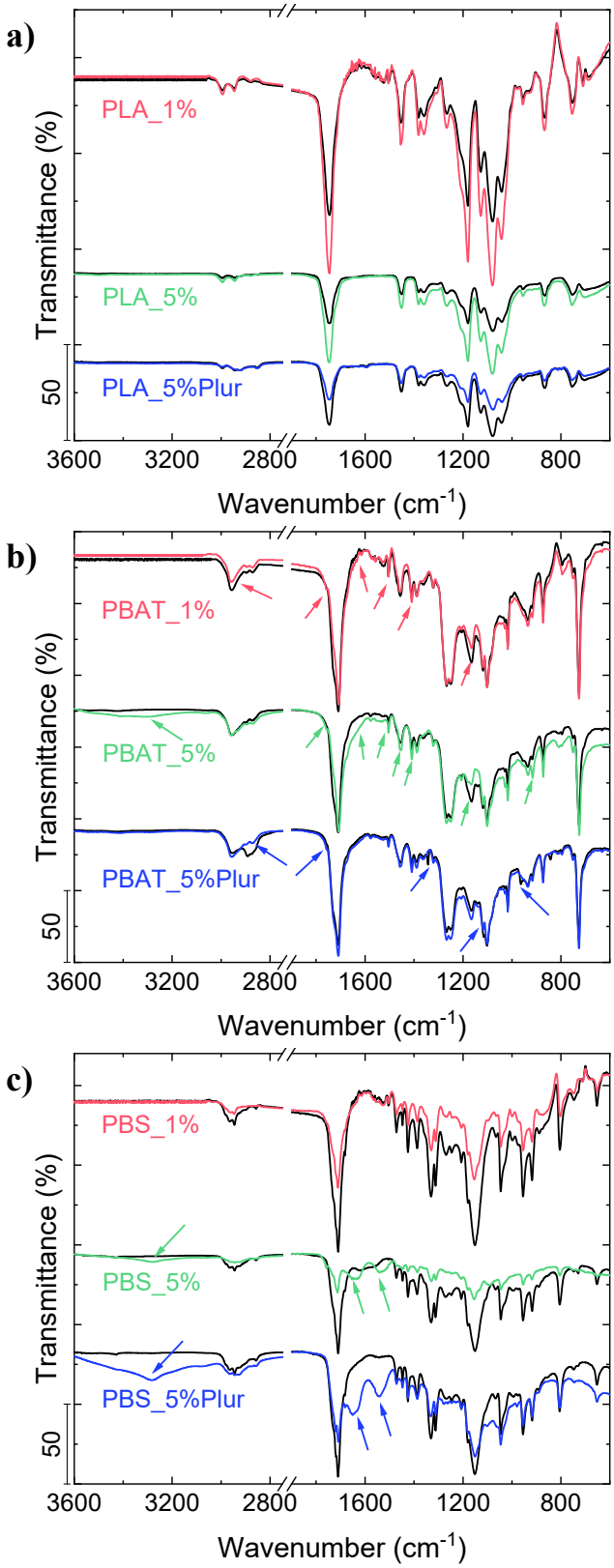

Figure 5.7. FTIR spectra corresponding to: **a)** PLA, **b)** PBAT, and **c)** PBS. Non-degraded (black) and degraded films (after 1000 h) for the 1 wt% CalB-embedded films (red), 5 wt% CalB-embedded films (green), and 5 wt% CalB/Pluronic-embedded films (blue).

The appearance of degradation products as a result of enzymatic degradation of the film was further confirmed by ^{1}H-NMR and the analysis of the pH from the degradation media (Figure 5.8). The detection of the different monomers in the liquid aliquots suggests an endo-type degradation for CalB.[57]

In the case of PLA_1%, ^{1}H-NMR spectrum exhibited the characteristic signals of lactic acid (1.46, and 3.49 ppm), as evidenced in Figure 5.8a, left. However, its low concentration (deduced from the low intensity of the peaks) did not have an effect on pH, as it maintained constant at ~8 (Figure 5.8a, right). On the other hand, ^{1}H-NMR spectra from the PBAT_1% and PBS_1% experiments (Figure 5.8a, left) showed much higher intensity for the characteristic peaks of the degradation products: 1.66 and 3.48 ppm (butanediol), 1.42 and 2.06 ppm (adipic acid), and 7.78 and 7.96 ppm (terephthalic acid) in the PBAT_1% assays; and small peaks from butanediol (1.46 and 3.49 ppm) and an intense peak from succinic acid (2.38 ppm) in the case of PBS_1%. The generation of these subproducts was in agreement with the pH of the degradation media, which was significantly reduced, as seen in Figure 5.8a, right: final pH values were ~7 (PBAT_1%) and ~4.5 (PBS_1%). This acidification process is attributed to the generation of degradation products, mainly acids, with pK_a values of 3.54 (terephthalic acid), 3.86 (lactic acid), 4.21 (succinic acid), and 4.41 (adipic acid) [59]. The lower acidification observed in PBAT_1% might be attributed to a lower generation of sub-products, as indicated by the 10-fold lower intensity of the ^{1}H-NMR peaks with respect to PBS_1% and the lower weight loss (Figure 5.3). Similar observations were obtained in a previous study with PBAT films, where enzymatic degradation by the employment of CalB slightly reduced the pH of the media.[32]

When CalB content was increased from 1 to 5 wt%, the signals from PBAT and PBS degradation subproducts were detected at a higher concentration (intensity is ten times higher than in the previous case), as evidenced in Figure 5.8b, left. These results are in accordance with the achieved weight loss (Figure 5.3), which was significantly larger, and the pH of the degradation media also

confirmed the growth in concentration of the subproducts: pH values dropped down to ~4 in PBAT_5% and PBS_5% (see Figure 5.8b, right). As in previous experiments, PLA_5% did not exhibit a pH change by the end of the assay, as almost not lactic acid residues were detected from ^{1}H-NMR spectra.

The incorporation of Pluronic to CalB led to lower degradation, which was confirmed by ^{1}H-NMR spectra, as depicted from the lower intensity peaks in Figure 5.8c, left, with no detection of adipic nor succinic acids. These results are supported by the negligible pH variation maintained in the range of the studies (pH 8 ± 0.5), as appreciated in Figure 5.8c, right. The most intense peak in PBAT_5%Plur and PBS_5%Plur was detected at 3.58 ppm and assigned to PEG from Pluronic.

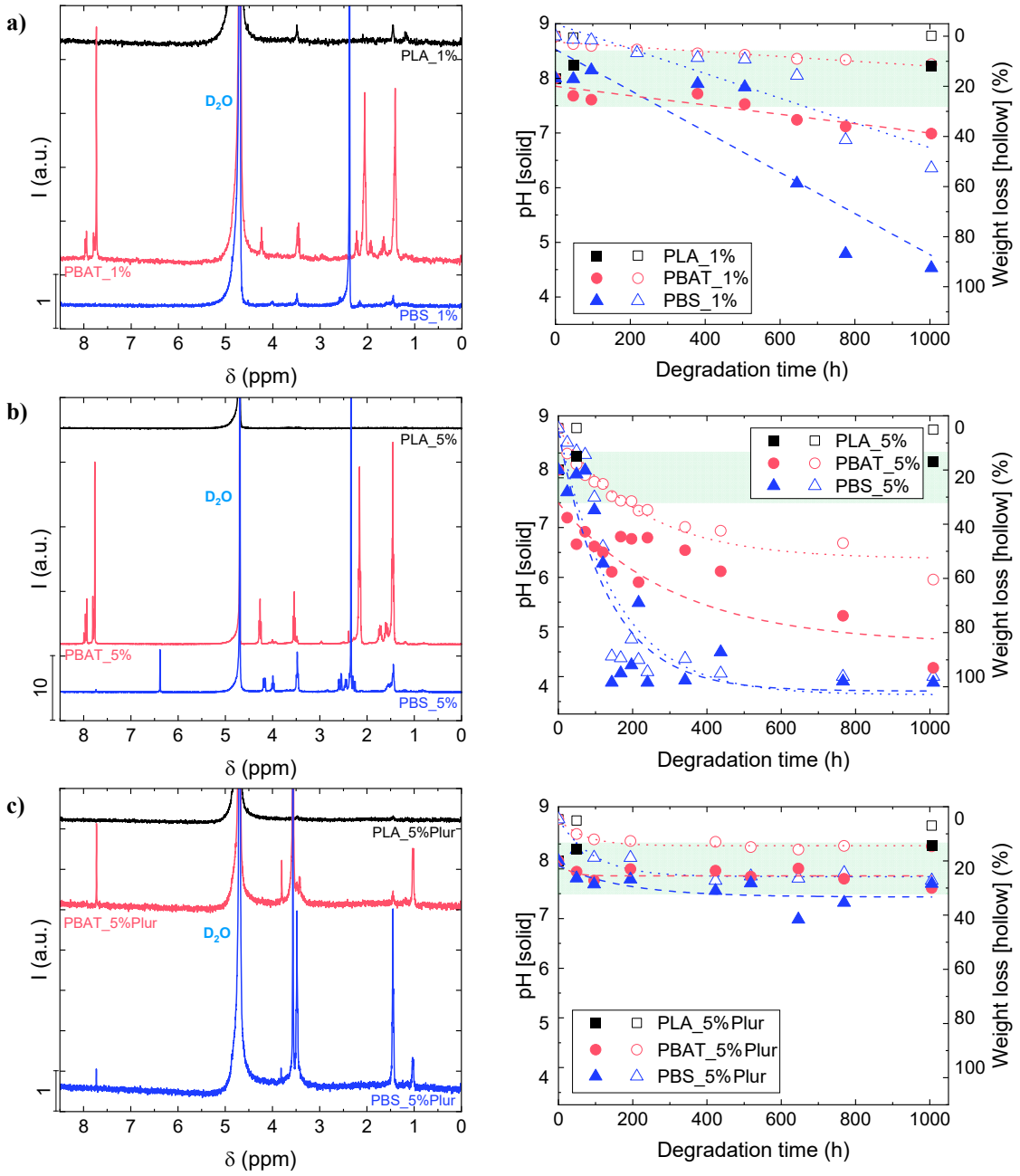

Figure 5.8. ^{1}H-NMR spectra (left) and variation in pH (right) from the liquid aliquots of: **a)** 1 wt% CalB-embedded experiments, **b)** 5 wt% CalB-embedded experiments, and **c)** 5 wt% CalB/Pluronic-embedded experiments. In the pH variation graphs (right), weight loss curves (hollow symbols) have been added for comparison purposes. The green area represents the pH value of the employed phosphate buffer (pH 8 ± 0.5).

c. Analysis of changes in molecular weight distribution over time

The molecular weight distribution over degradation time was monitored in degraded samples through GPC. In the case of the polyesters with embedded 1

wt% CalB (Figure 5.9a), there is a noticeable decrease in M_n, for the three samples under study. PLA_1% showed a decrease of ~36 % ($Đ$ maintained constant at ~2), whereas a ~66 % decrease was observed for PBAT_1% ($Đ$ increased from ~2 to ~4) and PBS_1% exhibited a ~45 % decrease ($Đ$ firstly increased from ~4 to ~5, tending to ~4 by the end of degradation). A similar observation for PBS has been reported previously in the literature, in a study in which a PBS film exhibited a significant decrease in M_n (from 45,000 to 14,000 g/mol), whereas M_w maintained almost constant, making $Đ$ increase from 1.5 to 4.1.[60] For PLA films, the moderate decrease in M_n and the fact that polydispersity does not change in the degraded samples with respect to pristine films suggests a moderate hydrolytic degradation of the films, which is reflected in a very low amount of weight loss (Figure 5.3). In contrast, for PBAT and PBS, the larger changes in M_n observed for degraded samples, together with the noticeable increase in polydispersity, are consistent with a mechanism of enzymatic degradation induced by the action of CalB. This lipase commonly acts by cutting the long polymeric chains into shorter chains, a reason that can explain the high reduction in M_n and increase in $Đ$.[57]

When CalB content was increased from 1 to 5 wt%, M_n in PLA films was not varied as much, as evidenced by Figure 5.9b: PLA_5% showed a reduction of ~22 % ($Đ$ maintained constant at ~2.5), and PBS_5% films –which exhibited total degradation in Figure 5.3b– did not present any change in M_n. Surprisingly, $Đ$ was reduced from ~8 to ~4.5 at 240 h. On the contrary, PBAT_5% reached a ~90 % decrease in M_n, up to values as low as 3000 g/mol ($Đ$ maintained constant at ~3, with a sharp increase to ~6 in the medium-range degradation times). Such reduction in $Đ$ can be attributed to the low M_n achieved at the end of degradation, making CalB cut the long chains that still remain in the polymer. Xu *et al.* reported a reduction in M_n for PBAT samples, decreasing from ~30,000 to ~10,000 g/mol,[61] similar to that observed for PBAT_1% and PBAT_5% films. These observations for PBAT_5% and PBS_5% will be commented later on.

Finally, GPC results corresponding to the sample with incorporated Pluronic (Figure 5.9c) showed a much higher reduction of M_n in PLA_5%Plur, which was

~56 %, although weight loss was null. This disagreement in degradation might be explained by the systematic cut-off of long polymeric chains into shorter ones, with no erosion on the films. On the other hand, the other two homopolymers (i.e., PBAT and PBS) presented a lower reduction in M_n: ~27 % (PBAT_5%Plur, which showed a ~11 wt% weight loss) and ~8 % (PBS_5%Plur, with a ~25 wt% weight loss). The dispersity values ($Đ$) were maintained constant at ~2.5 for both PLA_5%Plur and PBAT_5%Plur films, with a reduction from ~8 to ~4.5 in 1000 h for PBS_5%Plur films. These results could be related to their lower degradation, as shown by weight loss experiments depicted in Figure 5.3.

The behavior in PBS films with 5 wt% CalB (both alone and with Pluronic) is quite atypical and contrasted to PBS_1% films (with a more pronounced reduction in M_n and an increase in $Đ$, as seen in Figure 5.9a), as $Đ$ usually increases in enzymatic degradation assays, at the same time that M_n gets reduced.[36] The presence of a higher amount of CalB could have had a degradation effect on PBS, as reported in previous research, where a drastic decrease in M_n was found after extrusion of PBS in the presence of CalB.[37] PBS films suffered a significant decrease in the initial M_n from the reference films without embedded lipase: ~12 % in PBS_1%, and ~78 % and ~63 % for PBS_5% and PBS_5%Plur, respectively. Moreover, this effect was also appreciated for the other two studied homopolymers (i.e., PLA and PBAT) in a lower extent. For instance, PLA films suffered a reduction in M_n of ~12 % when adding 1 wt% CalB, ~38 % in PLA_5%, and ~20 % in PLA_5%Plur. In the case of PBAT films, initial M_n was not reduced in PBAT_1% (~25 % increase), and diminished by ~17 % and ~8 % for PBAT_5% and PBAT_5%Plur, respectively. The lower reduction observed in PBAT films suggests a higher resistance of this polymer towards degradation by CalB, possibly due to the presence of the terephthalate groups.[6] Hence, GPC results from PBS_5% (Figure 5.9b) and PBS_5%Plur (Figure 5.9c) are in line with the fact that only short segments are removed from the end-chains, making M_w diminish while keeping M_n constant, and thus, reducing $Đ$. This generally happens when the enzyme reaches the crystalline regions of the polymer, and it is only observed in PBS films due to the higher crystallinity of this polyester (as depicted from Table 5.1),[54] and

the larger initial degradation (higher reduction in initial M_n), possibly due to the degradation during the extrusion process.[37] Nonetheless, note that $Đ$ in PBAT_5% films started to diminish from ~6 to ~2 in the medium-range degradation times (Figure 5.9b), in a similar way to PBS_5% films.

All these observations in PBS films are in accordance with a bulk erosion mechanism, as optical micrographs revealed that the films maintained the original dimensions (at low degradation times), and the appearance of holes was also appreciated, together with a reduction in the molecular weight.[26] In the case of PBAT films, the decrease in M_n observed by GPC would also suggest a bulk erosion mechanism, despite the absence of holes in the PBAT films, which are more related to a surface erosion mechanism, as reported in previous studies.[62] The embedding of CalB inside the polyester films might be behind the change in the erosion mechanism,[63] which has been reported to enhance both surface and bulk erosion.[64]

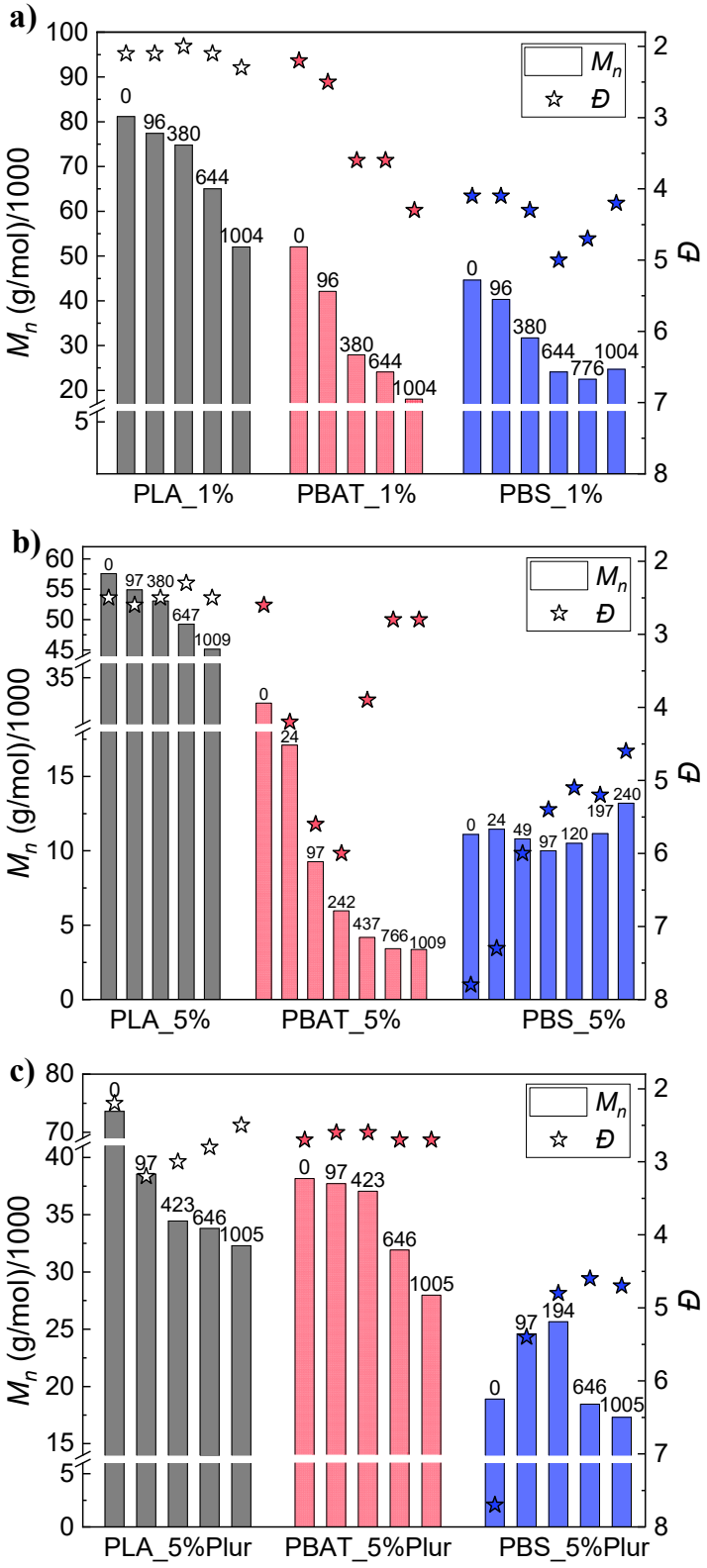

Figure 5.9. Molecular weight distribution (GPC) for the three homopolymers in: **a)** 1 wt% CalB-embedded films, **b)** 5 wt% CalB-embedded films, and **c)** 5 wt% CalB/Pluronic-embedded films. Degradation time (in hours) is indicated in the top of each bar.

d. ***Analysis of the crystallinity of the degraded samples***

Previous studies in literature have ascertained the occurrence of degradation in the case of PLA, PBAT and PBS through analysis of the crystallinity. In the case of PBAT samples, Xie *et al.* showed a small reduction from 9.5 to 5.7 %.[62] Shi *et al.* reported a small reduction in crystallinity in the case of PBS films, from 57 to 49 %.[57] Enzymes in general, and CalB in particular, usually start degrading the amorphous regions of the films, and through this process, the shorter newly-generated chains from the amorphous domains can crystallize and, thus, increase the degree of crystallinity.[57]

The 1st heating (DSC) of the degraded samples was used for the evaluation of the initial, intermediate, and final values for the crystallinity of the films (Figure 5.10). The degree of crystallinity (X_c) of the homopolymers was determined from the melting enthalpy (ΔH_m) –in the first heating scan– of the peak of each homopolymer, and the equilibrium melting enthalpy (ΔH_m^0) of each of the homopolymers, which was considered to be 93 J/g for PLA,[57] 114 J/g for PBAT,[65] and 213 J/g for PBS,[66] as detailed in Equation 5.4.

$$X_c = \frac{\Delta H_m}{\Delta H_m^0} \qquad \text{(Eq. 5.4)}$$

DSC results revealed no significant variation in crystallinity in the experiments carried out with the lowest CalB content (i.e., 1 wt% CalB), as appreciated in Figure 5.10a. Regarding PLA_1% films, X_c maintained almost invariant in the range 0-5 %, whereas in PBAT_1% and PBS_1%, the crystallinity values remained stable at ~12 and ~32 %, respectively. Surprisingly, when CalB content was increased from 1 to 5 wt% (Figure 5.10b), PLA_5% samples exhibited a higher initial X_c than previously observed (~7 %), with a growing trend by the end of the experiment (~13 %). PBAT_5% films showed a large increase in X_c, from ~10 to ~40 %, which could be related to a selective attack on the amorphous regions of PBAT, making the crystalline/amorphous ratio higher.[32] Similar behavior has been reported with PBAT mulching films in different degradation

conditions and ascribed to the faster degradation in amorphous regions by the action of microorganisms and enzymes.[67] This latter result contrasted with PBS_5% films, which showed a decreasing tendency in X_c, from values of ~35 % to ~10 %. At the very first stages of degradation, the degree of crystallinity experimented a slight increase, which could be related to a re-crystallization process. But when degradation speeds up, the enzyme also attacks the crystalline region of PBS, which is why X_c displays such a reduction.[57]

Incorporating Pluronic into the films had a clear effect on crystallinity, as PBAT_5%Plur and PBS_5%Plur samples did not exhibit any variation in the degree of crystallinity, as appreciated in Figure 5.10c. These results could be supported due to the lower degradation achieved. The slight increase observed in the initial X_c of PLA_5%, PBS_5% and PBS_5%Plur films could also be explained by the degradation during extrusion due to the higher amount of CalB.[37]

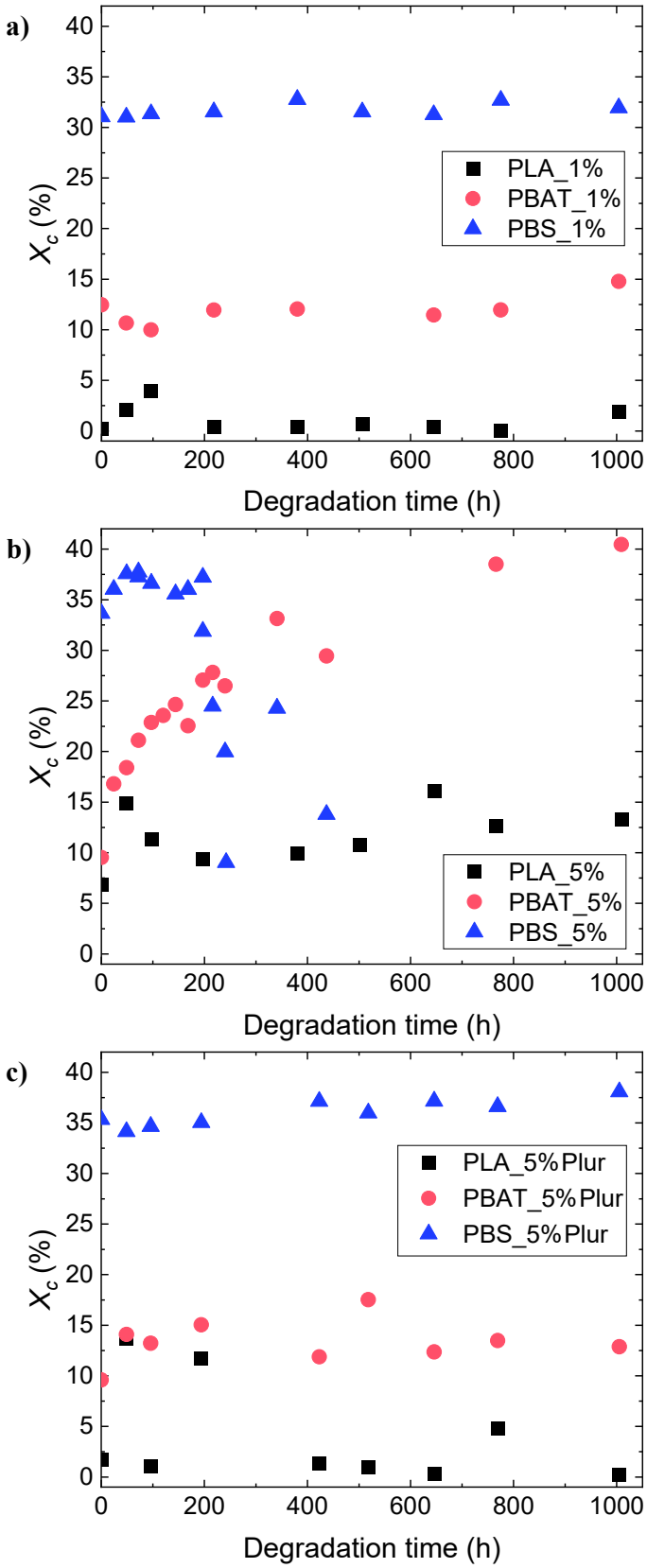

Figure 5.10. Changes in the degree of crystallinity (X_c) of the degraded samples: **a)** 1 wt% CalB-embedded experiments, **b)** 5 wt% CalB-embedded experiments, and **c)** 5 wt% CalB/Pluronic-embedded experiments.

5.3.4. Self-degradation in biopolyester blends

After studying the enzymatic self-degradation of homopolymers (i.e., PLA, PBAT, and PBS), a similar study was carried out for blends of these materials. These blends are materials with potential application for biodegradable packaging, hence the interest in them.[15] The study of the weight loss of the 1 wt% CalB-embedded films revealed very low degradation in all the blends (see Figure 5.11a, left), which were slightly higher than that exhibited by PLA_1%. When Pluronic was incorporated into the films, no change was observed from the weight loss curves (Figure 5.11b, left), showing similar results for all the blends, and in the same range as 1 wt% CalB-embedded samples (4-6 wt% weight loss).

The weight loss curves were further fitted with the modified Michaelis-Menten' model, and the results are included in Table 5.4. In this case, a 21-fold and 17-fold increase in degradation rate was obtained for $PLA_{50}PBAT_{50}$_5%Plur and $PLA_{45}PBAT_{45}PBS_{10}$_5%Plur films, respectively, with regard to the degradation kinetics from the 1 wt% CalB-embedded films (i.e., $PLA_{50}PBAT_{50}$_1% and $PLA_{45}PBAT_{45}PBS_{10}$_1%, respectively), determined from the slope of the linear fitting of the weight loss data. The v_d data from the blends presented lower values with regard to that obtained for the homopolymers PBAT_5%Plur and PBS_5%Plur (see Table 5.3). Nevertheless, the low rate of denaturation of the lipase (~50 h) resulted in a similar degradation at infinite time (A) compared to 1 wt% CalB-embedded films: ~5 wt% for $PLA_{50}PBAT_{50}$_5%Plur and $PLA_{45}PBAT_{45}PBS_{10}$_5%Plur, and ~6 wt% for $PLA_{30}PBAT_{30}PBS_{40}$_5%Plur films. In both lipase-embedding systems depicted in Figure 5.11, the polyester blends showed the same behaviour: the higher the PBS content, the faster the degradation kinetics, and the higher the weight loss achieved.

Table 5.4. Kinetic parameters determined from the modified Michaelis-Menten' model for the self-degradation studies in the 5 wt% CalB/Pluronic-embedded films, in the three blends under study. The standard deviation is given in brackets.

Sample	*CalB content (wt%)*	v_d (%/h)	τ (h)	*A* (%)	R^2
$PLA_{50}PBAT_{50}$_1%	1	0.0042 (0.0007)[a]	n.d.[b]	n.d.[b]	0.8498
$PLA_{45}PBAT_{45}PBS_{10}$_1%	1	0.0065 (0.0007)[a]	n.d.[b]	n.d.[b]	0.9206
$PLA_{30}PBAT_{30}PBS_{40}$_1%	1	n.a.	n.a.	n.a.	n.a.
$PLA_{50}PBAT_{50}$_5%Plur	5[c]	0.0902 (0.0145)	55 (9)	5.0	0.9573
$PLA_{45}PBAT_{45}PBS_{10}$_5%Plur	5[c]	0.1082 (0.0206)	45 (9)	4.9	0.9680
$PLA_{30}PBAT_{30}PBS_{40}$_5%Plur	5[c]	0.1037 (0.0086)	58 (5)	6.0	0.9899

[a] Obtained from the linear fit of the data.

[b] These parameters could not be obtained, as the weight loss curves were linearly fitted due to null weight loss exhibited by PLA films.

[c] 50/50 CalB/Pluronic ratio.

As for the case of the homopolymers, the pH of the degradation media was analyzed as a function of time, and the results showed that no changes in pH were detected, as depicted in Figure 5.11a and Figure 5.11b (left). Analysis of the chemical composition of the aliquots from degradation media through ^{1}H-NMR experiments showed the characteristic peak of terephthalic COOH groups (7.74 ppm) in both samples from 1 wt% CalB-embedded films (Figure 5.11a, right), as well as lactic acid (1.46 and 3.49 ppm) in $PLA_{50}PBAT_{50}$_1%; and adipic acid (1.42 and 2.06 ppm), butanediol (3.46 and 4.28 ppm), succinic acid (2.23 ppm), and lactic acid (3.55 ppm) in the $PLA_{45}PBAT_{45}PBS_{10}$_1% sample, with much lower intensity. On the contrary, with the incorporation of Pluronic into the films, it was not possible to appreciate the characteristic peaks of the degradation subproducts, only PEG signals from Pluronic were detected, as depicted in Figure 5.11b, right. Degradation results from the analysis of the films' weight loss from the blends, as well as ^{1}H-NMR from the liquid aliquots, evidenced minor variations among the studied blends with slightly higher degradation compared to PLA films, which

presented the lowest degradation due to its nature (predominant L-isomer). In the studied blends, the main components are PLA and PBAT at equal ratios in the three blends (50, 45 and 30 wt%), which could possibly explain the low degradation exhibited by the self-degradable films obtained from the blends.

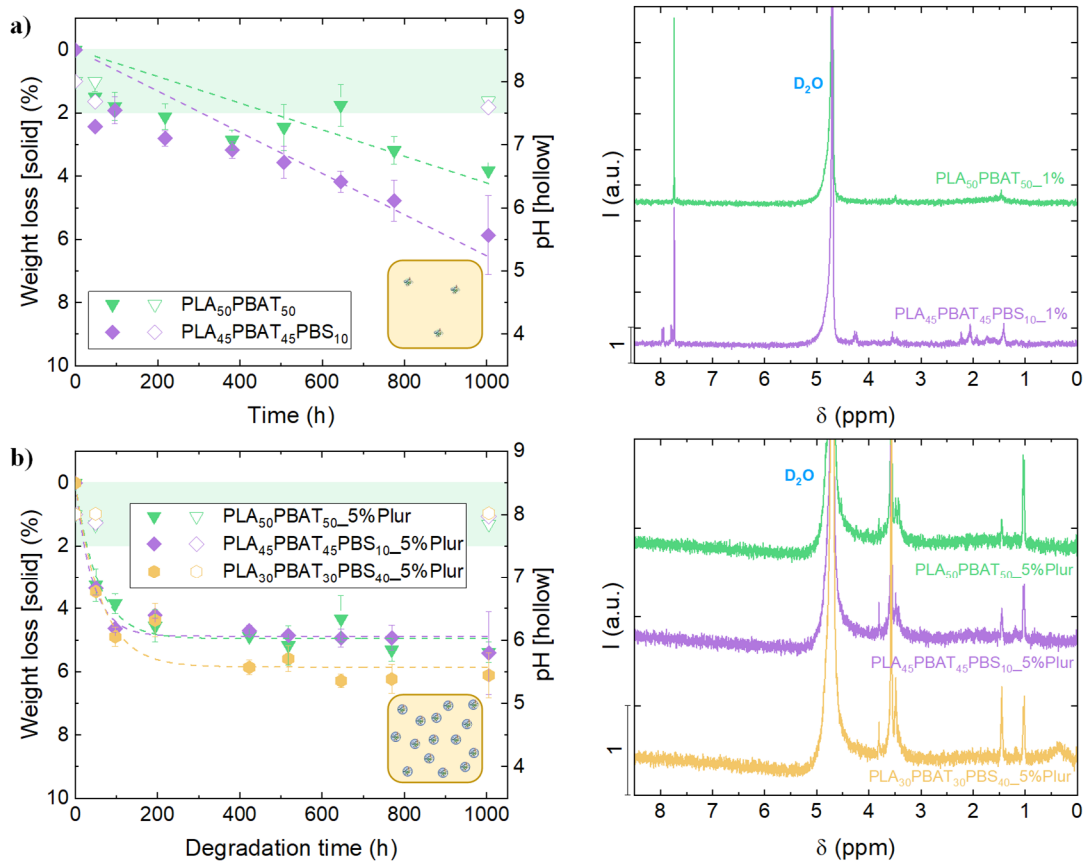

Figure 5.11. Weight loss curves for the three blends under study (solid symbols) and variation in pH of the aliquots from the degradation media (hollow symbols) in left figures, and ^{1}H-NMR spectra obtained from the liquid aliquots from the degradation media (right figures): **a)** 1 wt% CalB-embedded films, and **b)** 5 wt% CalB/Pluronic-embedded films. A schematic representation of each system is included as an inset in the left graphs: the yellow square represents the polyester film, whereas the embedded lipase is plotted with (embedded CalB) or (embedded CalB/Pluronic). Symbols' number is related to CalB content inside the films. The green area represents the pH value of the employed phosphate buffer (pH 8 ± 0.5).

The images of the degraded films are included in Figure 5.12. Control films (blank experiments) also exhibited no variation in the surface morphology, as observed in Figure 5.13 through optical microscopy.

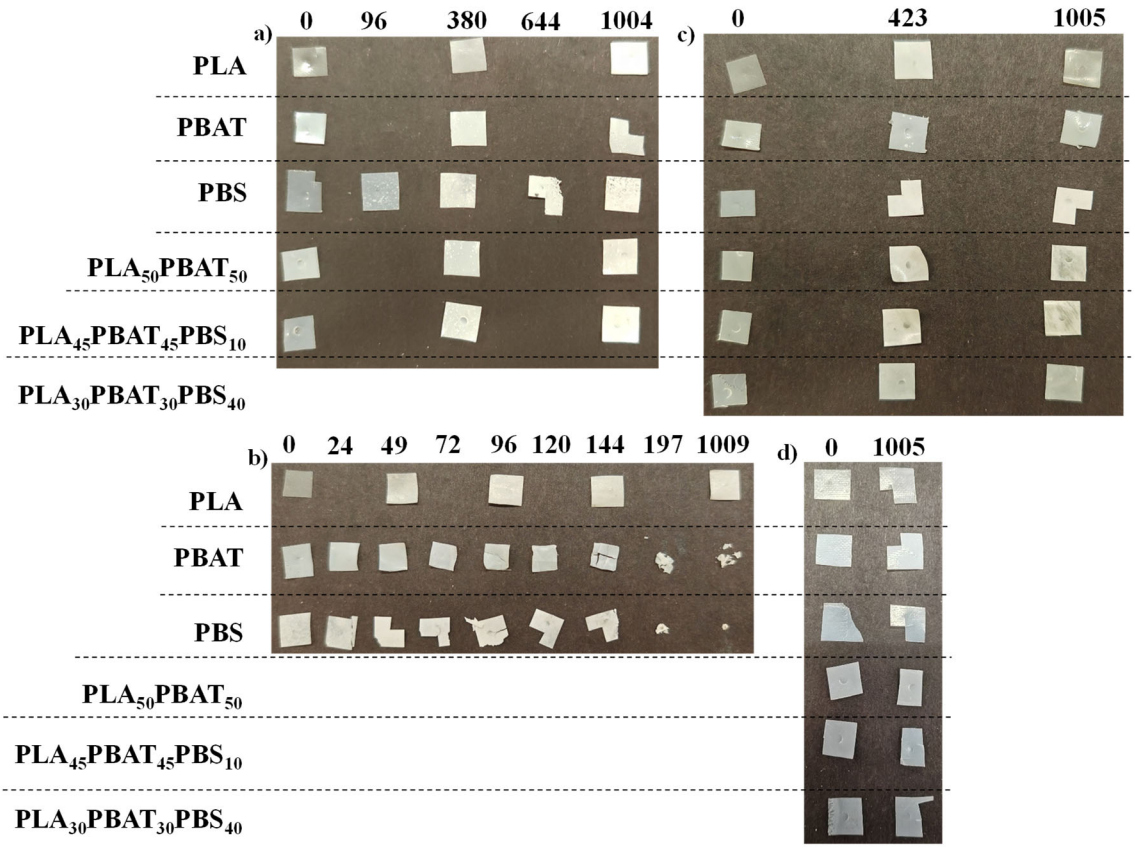

Figure 5.12. Visual aspect of the degraded films for the different experiments: **a)** 1 wt% CalB-embedded films, **b)** 5 wt% CalB-embedded films, **c)** 5 wt% CalB/Pluronic-embedded films, and **d)** blank experiments. The degradation time (in hours) is included at the top.

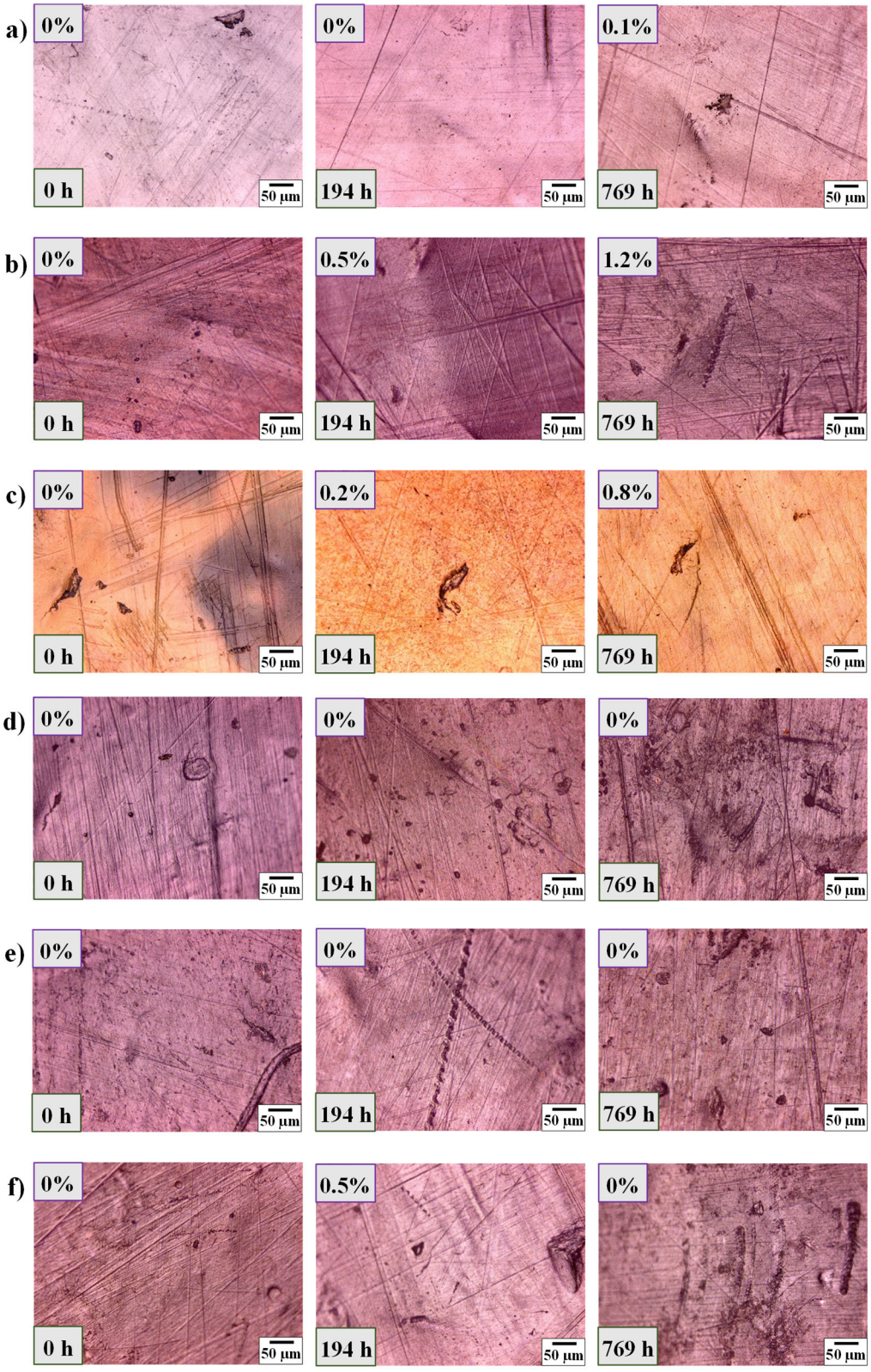

Figure 5.13. Optical micrographs taken at 20x magnification for the films in the blank experiments: **a)** PLA, **b)** PBAT, **c)** PBS, **d)** $PLA_{50}PBAT_{50}$, **e)** $PLA_{45}PBAT_{45}PBS_{10}$, and **f)** $PLA_{30}PBAT_{30}PBS_{40}$. In the upper left corner, the achieved weight loss is shown, whereas the degradation time (in hours [h]) is included in the lower left corner.

The chemical composition of the films prepared from the blends before and after degradation (1000 h) was evaluated through FTIR, and results in Figure 5.14 evidenced the low degradation of these films. The most relevant change in degraded films was the appearance of the stretching vibration of free C=O groups (~1756 cm^{-1}) and the C=C stretching as a rearrangement of the residues of the PLA ester breakage (~1682 cm^{-1}).[8] A slight reduction in the intensity of the peaks was appreciated in some samples, in accordance with the low weight loss appreciated in Figure 5.11, following the trend of the previously commented PLA samples.

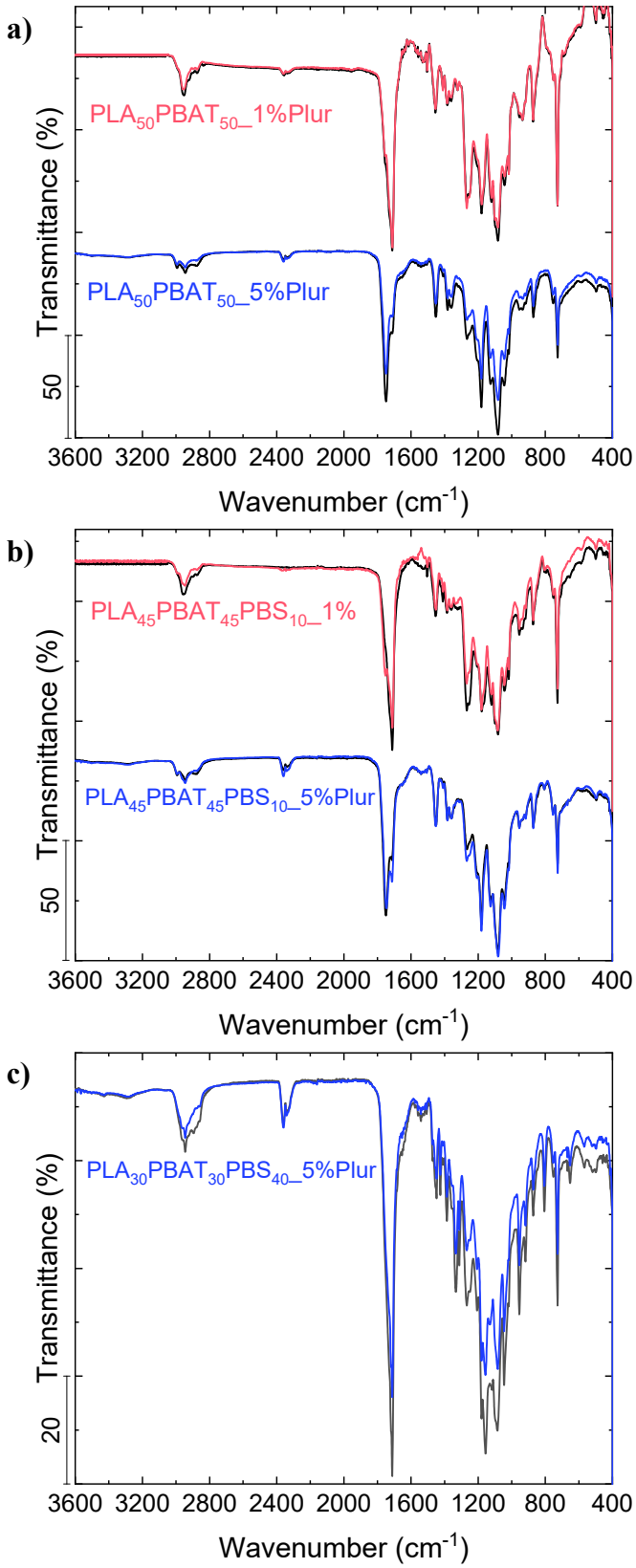

Figure 5.14. FTIR spectra of non-degraded (in black) and degraded films (after 1000 h) obtained from the three blends for the 1 wt% CalB-embedded films (red), and 5 wt% CalB/Pluronic-embedded films (blue): **a)** $PLA_{50}PBAT_{50}$, **b)** $PLA_{45}PBAT_{45}PBS_{10}$, and **c)** $PLA_{30}PBAT_{30}PBS_{40}$.

The degradation of the films was further studied through the analysis of the evolution of the molecular weight distribution over degradation time. GPC results shown in Figure 5.15 revealed a significant reduction in M_n of the three blends under study. In the case of the samples tested with 1 wt% CalB inside the films (Figure 5.15a), there is a noticeable decrease in M_n: ~25 % in $PLA_{50}PBAT_{50}$_1% and ~56 % in $PLA_{45}PBAT_{45}PBS_{10}$_1%. When Pluronic was incorporated into the 5 wt% CalB/Pluronic-embedded films, the reduction in M_n was not as high as before (Figure 5.15b): ~14 % for $PLA_{50}PBAT_{50}$_5%Plur films, ~39 % for $PLA_{45}PBAT_{45}PBS_{10}$_5%Plur samples, and ~25 % for $PLA_{30}PBAT_{30}PBS_{40}$_5%Plur films.

The polydispersity, on the other hand, was maintained constant in the 2.5-3 range; only the $PLA_{45}PBAT_{45}PBS_{10}$ blends, $PLA_{45}PBAT_{45}PBS_{10}$_1% and $PLA_{45}PBAT_{45}PBS_{10}$_5%Plur showed significant increases of $Đ$ up to values of ~4 and ~3.5, respectively. The low or negligible weight loss appreciated in many samples (Figure 5.11), as well as a moderate reduction in M_n (Figure 5.15) could be related to a hydrolytic degradation of the films. The higher degradation in $PLA_{45}PBAT_{45}PBS_{10}$_1% and $PLA_{45}PBAT_{45}PBS_{10}$_5%Plur samples (slightly higher weight loss in Figure 5.11) could be related to the presence of PBS in this blend, as this homopolymer was found to achieve higher degradation. These results would support a hydrolytic degradation mechanism induced by the catalytic action of CalB.

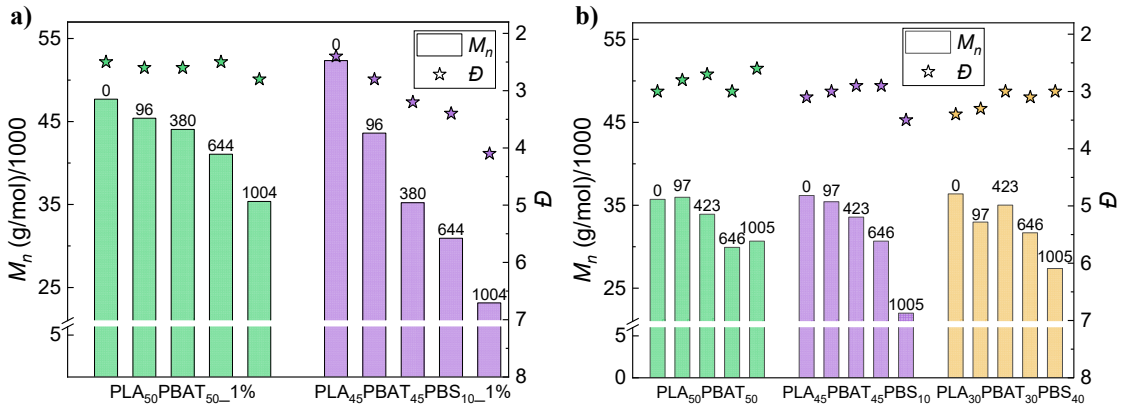

Figure 5.15. Molecular weight distribution (GPC) for the three blends under study: **a)** 1 wt% CalB-embedded films, and **b)** 5 wt% CalB/Pluronic-embedded films. Degradation time (in hours) is indicated in the top of each bar in GPC graphs (top).

1st heating (DSC) of the degraded samples revealed no variation in crystallinity for the blends (Figure 5.16). In this case, it was not possible to distinguish the melting of PLA and PBS (narrow and well defined peaks) from the wide PBAT melting peak; hence, the total melting enthalpy ($\Delta H_{m,total}$) was reported instead. In general terms, $\Delta H_{m,total}$ kept stable during the whole degradation experiment, with a slight increase in the $PLA_{45}PBAT_{45}PBS_{10}$ samples: from ~7 to ~13 J/g ($PLA_{45}PBAT_{45}PBS_{10}$_1% in Figure 5.16a), and from ~13 to ~17 J/g ($PLA_{45}PBAT_{45}PBS_{10}$_5%Plur in Figure 5.16b). Regarding $PLA_{50}PBAT_{50}$ samples, the total melting enthalpy increased from ~5 J/g to ~10 J/g when Pluronic was added to 5 wt% CalB/Pluronic-embedded films (Figure 5.16b).

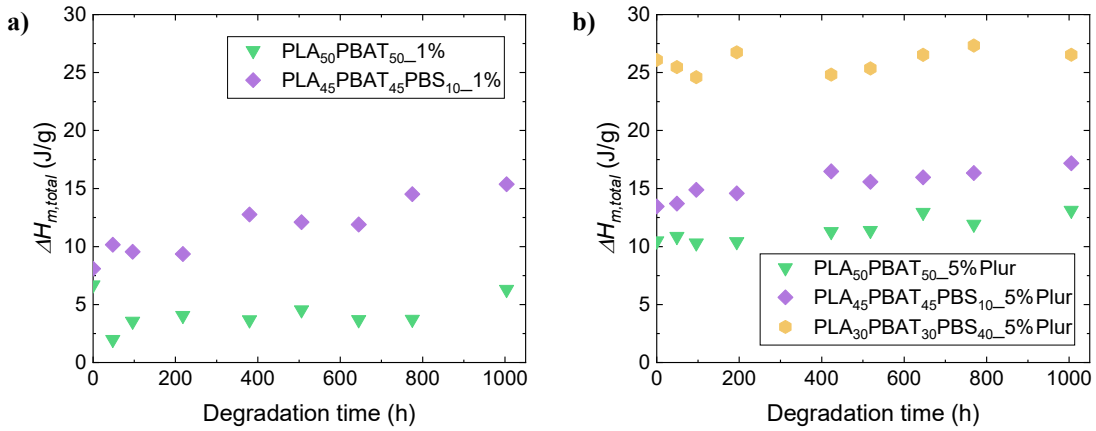

Figure 5.16. Changes in the degree of crystallinity (X_c) of the degraded samples from the three blends under study: **a)** 1 wt% CalB-embedded experiments, and **b)** 5 wt% CalB/Pluronic-embedded experiments.

5.4. Conclusions

In this Chapter, a thorough comparative investigation was conducted about the mechanism of degradation of self-degradable polyester films prepared by embedding two different lipases (Lipase from *Pseudomonas cepacia* and *Candida antarctica* lipase B, CalB) within PBS, PLA, and PBAT. The proposed lipase-embedded alginate beads were successfully employed as enzyme-heating protecting agents for PBS self-degradation. A slight degradation was observed for PBS films containing a certain amount (10 wt% with respect to PBS) of AlgEmbLi particles, whereas the control PBS samples showed minor degradation. These results were quite promising, as the enzymatic activity was about 2 orders of magnitude lower than that of previous assays.

Regarding the three studied homopolymers and their blends, the results showed that the degradation of PBAT and PBS CalB-embedded films was greatly enhanced by the increase of the CalB content inside the films (from 1 to 5 wt%). Furthermore, the incorporation of Pluronic® F-127 to CalB evidenced no real need to protect the lipase from thermal denaturation (as in the previous case with *P. cepacia*), as this study also demonstrated that lipases incorporated into these polymers maintained their activities after melt extrusion at 170 ºC without any further stabilization steps. Additionally, results from CalB/Pluronic-embedded films also supported this hypothesis: the weight loss was about 4-5 times lower when compared to films with similar content in CalB. The encapsulation of CalB within Pluronic is used as a common heat-protecting procedure; nevertheless, the encapsulation possibly decreases the contact between CalB and the polyester films, and thus, lower the degradation rate. Regarding the nature of the polyesters, CalB showed a higher preference towards PBS, as evidenced by the kinetics obtained from the modified Michaelis-Menten' model applied to weight loss curves: PBS > PBAT > PLA. PLA films did not show any degradation for all the tested conditions, which is in accordance with the high L-isomer content.

The characterization of the degraded samples revealed further information regarding the degradation mechanism of CalB. The increase in crystallinity of PBAT together with optical microscopy observations, suggest that the mechanism of self-degradation for this homopolymer is based on a surface erosion mechanism, as no holes were appreciated at the surface of PBAT films. However, the lipase-embedding procedure might have modified the degradation mechanism of PBAT films, as revealed by GPC, which suggests a bulk erosion mechanism due to the decrease in M_n. Possibly, both mechanisms are happening in PBAT degradation. PBS seems to be degraded through autocatalyzed hydrolysis, which results in drastic changes in crystallinity, surface morphology, FTIR data, and weight loss curves, which supported a bulk erosion mechanism of CalB on this polyester.

Finally, the lipase-embedding procedure was further applied to blends from these three polyesters, with increasing PBS composition. Degradation results evidenced minor variations among the studied blends, with slightly higher degradation compared to PLA films. The main components of the polymer blends under study are PLA and PBAT at equal ratios in the three blends (50, 45 and 30 wt%). Therefore, modest degradation was observed due to the nature of PLA's L-isomer. ^{1}H-NMR carried out in the liquid aliquots further supported the lack of degradation of PLA in the blends, as only terephthalic acid from PBAT was detected as a subproduct. However, the addition of PBS (10 wt%) to the second blend enhanced its degradation, possibly because of the faster degradation of PBS in the presence of CalB, as demonstrated by the higher M_n reduction. The studied lipase-embedding procedure exhibited promising results for PBS, as well as for PBAT films, when the CalB content was increased. Nonetheless, the low effectiveness of the self-degradation of PLA, together with the blends, exposed the need to select the most suitable enzyme for degrading each biopolyester, or all the components in blends. A future approach for enzymatic degradation of enzymes could lie in finding a common enzyme that degrades all the components in the blend, or in exploring a mixture of enzymes.

To sum up, this research has shed more light on the enzymatic degradation of several polyesters, and more in detail, it has deepened into the self-degradation of three biopolyesters and their blends achieved through lipase-embedding.

5.5. References

1. Aarthy, M.; Puhazhselvan, P.; Aparna, R.; George, A. S.; Gowthaman, M. K.; Ayyadurai, N.; Masaki, K.; Nakajima-Kambe, T.; Kamini, N. R., Growth associated degradation of aliphatic-aromatic copolyesters by Cryptococcus sp. MTCC 5455. *Polymer Degradation and Stability* **2018**, *152*, 20–28. DOI: 10.1016/j.polymdegradstab.2018.03.021.

2. Kim, J.; Park, S.; Jung, S.; Yun, H.; Choi, K.; Heo, G.; Jin, H. J.; Park, S.; Kwak, H. W., Biodegradation behavior of polybutylene succinate (PBS) fishing gear in marine sedimentary environments for ghost fishing prevention. *Polymer Degradation and Stability* **2023**, *216*, 110490. DOI: 10.1016/j.polymdegradstab.2023.110490.

3. Wu, F.; Misra, M.; Mohanty, A. K., Challenges and new opportunities on barrier performance of biodegradable polymers for sustainable packaging. *Progress in Polymer Science* **2021**, *117*, 101395. DOI: 10.1016/j.progpolymsci.2021.101395.

4. Wcislek, A.; Olalla, A. S.; McClain, A.; Piegat, A.; Sobolewski, P.; Puskas, J.; Fray, M. El, Enzymatic degradation of poly(butylene succinate) copolyesters synthesized with the use of Candida antarctica lipase B. *Polymers* **2018**, *10* (6), 688. DOI: 10.3390/polym10060688.

5. Phua, Y. J.; Lau, N. S.; Sudesh, K.; Chow, W. S.; Mohd Ishak, Z. A., Biodegradability studies of poly(butylene succinate)/organo-montmorillonite nanocomposites under controlled compost soil conditions: Effects of clay loading and compatibiliser. *Polymer Degradation and Stability* **2012**, *97* (8), 1345–1354. DOI: 10.1016/j.polymdegradstab.2012.05.024.

6. Kanwal, A.; Zhang, M.; Sharaf, F.; Chengtao, L., Screening and characterization of novel lipase producing Bacillus species from agricultural soil with high hydrolytic activity against PBAT poly (butylene adipate co terephthalate) co-polyesters. *Polymer Bulletin* **2022**, *79* (11), 10053–10076. DOI: 10.1007/s00289-021-03992-4.

7. Mtibe, A.; Muniyasamy, S.; Mokhena, T. C.; Ofosu, O.; Ojijo, V.; John, M., Recent insight into the biomedical applications of polybutylene succinate and polybutylene succinate-based materials. *Express Polymer Letters* **2023**, *17* (1), 2–28. DOI: 10.3144/expresspolymlett.2023.2.

8. Jia, H.; Zhang, M.; Weng, Y.; Li, C., Degradation of polylactic acid/polybutylene adipate-co-terephthalate by coculture of Pseudomonas mendocina and Actinomucor elegans. *Journal of Hazardous Materials* **2021**, *403*, 123679. DOI: 10.1016/j.jhazmat.2020.123679.

9. Gug, J.; Sobkowicz, M. J., Improvement of the mechanical behavior of bioplastic poly(lactic acid)/polyamide blends by reactive compatibilization. *Journal of Applied Polymer Science* **2016**, *133* (45), 43350. DOI: 10.1002/app.44212.

10. Ludwiczak, J.; Dmitruk, A.; Skwarski, M.; Kaczyński, P.; Makuła, P., UV resistance and biodegradation of PLA-based polymeric blends doped with PBS, PBAT, TPS. *International Journal of Polymer Analysis and Characterization* **2023**, *28* (4), 366–382. DOI: 10.1080/1023666X.2023.2218696.

11. Dong, W.; Zou, B.; Yan, Y.; Ma, P.; Chen, M., Effect of chain-extenders on the properties and hydrolytic degradation behavior of the poly(lactide)/ poly(butylene adipate-co-terephthalate) blends. *International Journal of Molecular Sciences* **2013**, *14* (10), 20189–20203. DOI: 10.3390/ijms141020189.

12. Bhatia, A.; Gupta, R. K.; Bhattacharya, S. N.; Choi, H. J., Compatibility of biodegradable poly (lactic acid) (PLA) and poly (butylene succinate) (PBS) blends for packaging application. *Korea-Australia Rheology Journal* **2007**, *19* (3), 125–131. DOI: 10.3390/ma15031132.

13. Ravati, S.; Poulin, S.; Piyakis, K.; Favis, B. D., Phase identification and interfacial transitions in ternary polymer blends by ToF-SIMS. *Polymer* **2014**, *55* (23), 6110–6123. DOI: 10.1016/j.polymer.2014.09.013.

14. Wu, F.; Misra, M.; Mohanty, A. K., Super Toughened Poly(lactic acid)-Based Ternary Blends via Enhancing Interfacial Compatibility. *ACS Omega* **2019**, *4* (1), 1955–1968. DOI: 10.1021/acsomega.8b02587.

15. Chuakhao, S.; Torres Rodríguez, J.; Lapnonkawow, S.; Kannan, G.; Müller, A. J.; Suttiruengwong, S., Formulating PBS/PLA/PBAT blends for biodegradable, compostable packaging: The crucial roles of PBS content and reactive extrusion. *Journal of Polymers and the Environment* **2023**, *XXXX* (XXX), XXX–XXX. **Manuscript submitted for publication**.

16. Hwang, S. Y.; Jin, X. Y.; Yoo, E. S.; Im, S. S., Synthesis, physical properties and enzymatic degradation of poly (oxyethylene-b-butylene succinate) ionomers. *Polymer* **2011**, *52* (13), 2784–2791. DOI: 10.1016/j.polymer.2011.04.065.

17. Morales-Huerta, J. C.; Ciulik, C. B.; De Ilarduya, A. M.; Muñoz-Guerra, S., Fully bio-based aromatic-aliphatic copolyesters: Poly(butylene furandicarboxylate-co-succinate)s obtained by ring opening polymerization. *Polymer Chemistry* **2017**, *8* (4), 748–760. DOI: 10.1039/c6py01879c.

18. Nakajima-Kambe, T.; Edwinoliver, N. G.; Maeda, H.; Thirunavukarasu, K.; Gowthaman, M. K.; Masaki, K.; Mahalingam, S.; Kamini, N. R., Purification, cloning and expression of an Aspergillus niger lipase for degradation of poly(lactic acid) and poly(ε-caprolactone). *Polymer Degradation and Stability* **2012**, *97* (2), 139–144. DOI: 10.1016/j.polymdegradstab.2011.11.009.

19. Huang, Q.; Kimura, S.; Iwata, T., Development of self-degradable aliphatic polyesters by embedding lipases via melt extrusion. *Polymer Degradation and Stability* **2021**, *190*, 109647. DOI: 10.1016/j.polymdegradstab.2021.109647.

20. Lee, C. W.; Kimura, Y.; Chung, J. Do, Mechanism of enzymatic degradation of poly(butylene succinate). *Macromolecular Research* **2008**, *16* (7), 651–658. DOI: 10.1007/BF03218575.

21. Sun, B. X.; Chuai, C. Z.; Luo, S.; Guo, Y.; Feng, X. Q., Biodegradability of poly (butylene succinate) under enzymatic degradation. *Advanced Materials Research* **2013**, *750–752*, 1318–1321. DOI: 10.4028/www.scientific.net/AMR.750-752.1318.

22. Peñas, M. I.; Criado-Gonzalez, M.; Martínez de Ilarduya, A.; Flores, A.; Raquez, J. M.; Mincheva, R.; Müller, A. J.; Hernández, R., Tunable enzymatic biodegradation of poly(butylene succinate): biobased coatings and self-degradable films. *Polymer Degradation and Stability* **2023**, *211*, 110341. DOI: 10.1016/j.polymdegradstab.2023.110341.

23. Kong, X.; Qi, H.; Curtis, J. M., Synthesis and characterization of high-molecular weight aliphatic polyesters from monomers derived from renewable resources. *Journal of Applied Polymer Science* **2014**, *131* (15), 4–10. DOI: 10.1002/app.40579.

24. Veskova, J.; Sbordone, F.; Frisch, H., Trends in Polymer Degradation Across All Scales. *Macromolecular Chemistry and Physics* **2022**, *223* (13), 1–12. DOI: 10.1002/macp.202100472.

25. Kitamoto, H.; Koitabashi, M.; Sameshima-Yamashita, Y.; Ueda, H.; Takeuchi, A.; Watanabe, T.; Sato, S.; Saika, A.; Fukuoka, T., Accelerated degradation of plastic products via yeast enzyme treatment. *Scientific Reports* **2023**, *13* (1), 1–11. DOI: 10.1038/s41598-023-29414-1.

26. Shi, K.; Su, T.; Wang, Z., Comparison of poly(butylene succinate) biodegradation by Fusarium solani cutinase and Candida antarctica lipase. *Polymer Degradation and Stability* **2019**, *164*, 55–60. DOI: 10.1016/j.polymdegradstab.2019.04.005.

27. Sarwar, M. S.; Niazi, M. B. K.; Jahan, Z.; Ahmad, T.; Hussain, A., Preparation and characterization of PVA/nanocellulose/Ag nanocomposite films for antimicrobial food packaging. *Carbohydrate Polymers* **2018**, *184*, 453–464. DOI: 10.1016/j.carbpol.2017.12.068.

28. Van Tassel, L.; Moilanen, A.; Ruddock, L. W., Efficient production of wild-type lipase B from Candida antarctica in the cytoplasm of Escherichia coli. *Protein Expression and Purification* **2020**, *165*, 105498. DOI: 10.1016/j.pep.2019.105498.

29. Yang, Y.; Wang, D.; Zhang, X.; Fang, J.; Shen, Z.; Lin, C., Transgenic rice as bioreactor for production of the Candida antarctica lipase B. *Plant Biotechnology Journal* **2014**, *12* (7), 963–970. DOI: 10.1111/pbi.12204.

30. Jang, W. Y.; Sohn, J. H.; Chang, J. H., Thermally stable and reusable silica and nano-fructusome encapsulated CalB enzyme particles for rapid enzymatic hydrolysis and acylation. *International Journal of Molecular Sciences* **2023**, *24* (12), 9838. DOI: 10.1007/s43207-023-00355-9.

31. Shinozaki, Y.; Morita, T.; Cao, X. H.; Yoshida, S.; Koitabashi, M.; Watanabe, T.; Suzuki, K.; Sameshima-Yamashita, Y.; Nakajima-Kambe, T.; Fujii, T.; Kitamoto, H. K., Biodegradable plastic-degrading enzyme from Pseudozyma antarctica: Cloning, sequencing, and characterization. *Applied Microbiology and Biotechnology* **2013**, *97* (7), 2951–2959. DOI: 10.1007/s00253-012-4188-8.

32. Kanwal, A.; Zhang, M.; Sharaf, F.; Li, C., Enzymatic degradation of poly (butylene adipate co-terephthalate) (PBAT) copolymer using lipase B from Candida antarctica (CALB) and effect of PBAT on plant growth. *Polymer Bulletin* **2022**, *79* (10), 9059–9073. DOI: 10.1007/s00289-021-03946-w.

33. Hu, H.; Luan, Q.; Li, J.; Lin, C.; Ouyang, X.; Wei, D.; Wang, J.; Zhu, J., High-Molecular-Weight and Light-Colored Disulfide-Bond-Embedded Polyesters: Accelerated Hydrolysis Triggered by Redox Responsiveness. *Biomacromolecules* **2023**, *24* (12), 5722–5736. DOI: 10.1021/acs.biomac.3c00691.

34. Maraveas, C.; Kotzabasaki, M. I.; Bartzanas, T., Intelligent Technologies, Enzyme-Embedded and Microbial Degradation of Agricultural Plastics. *AgriEngineering* **2023**, *5* (1), 85–111. DOI: 10.3390/agriengineering5010006.

35. Ganesh, M.; Dave, R. N.; L'Amoreaux, W.; Gross, R. A., Embedded enzymatic biomaterial degradation. *Macromolecules* **2009**, *42* (18), 6836–6839. DOI: 10.1021/ma901481h.

36. Ganesh, M.; Gross, R. A., Embedded enzymatic biomaterial degradation: Flow conditions & relative humidity. *Polymer* **2012**, *53* (16), 3454–3461. DOI: 10.1016/j.polymer.2012.06.017.

37. Jbilou, F.; Dole, P.; Degraeve, P.; Ladavière, C.; Joly, C., A green method for polybutylene succinate recycling: Depolymerization catalyzed by lipase B from Candida antarctica during reactive extrusion. *European Polymer Journal* **2015**, *68*, 207–215. DOI: 10.1016/j.eurpolymj.2015.04.039.

38. Iwasaki, Y.; Takemoto, K.; Tanaka, S.; Taniguchi, I., Low-Temperature Processable Block Copolymers That Preserve the Function of Blended Proteins. *Biomacromolecules* **2016**, *17* (7), 2466–2471. DOI: 10.1021/acs.biomac.6b00641.

39. Huang, Q.; Hiyama, M.; Kabe, T.; Kimura, S.; Iwata, T., Enzymatic self-biodegradation of poly(L-lactic acid) films by embedded heat-treated and immobilized Proteinase K. *Biomacromolecules* **2020**, *21* (8), 3301–3307. DOI: 10.1021/acs.biomac.0c00759.

40. Rodriguez-Abetxuko, A.; Sánchez-deAlcázar, D.; Muñumer, P.; Beloqui, A., Tunable Polymeric Scaffolds for Enzyme Immobilization. *Frontiers in Bioengineering and Biotechnology* **2020**, *8*, 830. DOI: 10.3389/fbioe.2020.00830.

41. Mondal, K.; Mehta, P.; Mehta, B. R.; Varandani, D.; Gupta, M. N., A bioconjugate of Pseudomonas cepacia lipase with alginate with enhanced catalytic efficiency. *Biochimica et Biophysica Acta - Proteins and Proteomics* **2006**, *1764* (6), 1080–1086. DOI: 10.1016/j.bbapap.2006.04.008.

42. Padilha, G. S.; Tambourgi, E. B.; Alegre, R. M., Evaluation of lipase from Burkholderia cepacia immobilized in alginate beads and application in the synthesis of banana flavor (isoamyl acetate). *Chemical Engineering Communications* **2018**, *205* (1), 23–33. DOI: 10.1080/00986445.2017.1370707.

43. Huang, Q.; Kimura, S.; Iwata, T., Thermal Embedding of Humicola insolens Cutinase: A Strategy for Improving Polyester Biodegradation in Seawater. *Biomacromolecules* **2023**, *24* (12), 5836–5846. DOI: 10.1021/acs.biomac.3c00835.

44. DelRe, C.; Chang, B.; Jayapurna, I.; Hall, A.; Wang, A.; Zolkin, K.; Xu, T., Synergistic Enzyme Mixtures to Realize Near-Complete Depolymerization in Biodegradable Polymer/Additive Blends. *Advanced Materials* **2021**, *33* (49), 2105707. DOI: 10.1002/adma.202105707.

45. DelRe, C.; Jiang, Y.; Kang, P.; Kwon, J.; Hall, A.; Jayapurna, I.; Ruan, Z.; Ma, L.; Zolkin, K.; Li, T.; Scown, C. D.; Ritchie, R. O.; Russell, T. P.; Xu, T., Near-complete depolymerization of polyesters with nano-dispersed enzymes. *Nature* **2021**, *592* (7855), 558–563. DOI: 10.1038/s41586-021-03408-3.

46. Greene, A. F.; Vaidya, A.; Collet, C.; Wade, K. R.; Patel, M.; Gaugler, M.; West, M.; Petcu, M.; Parker, K., 3D-printed enzyme-embedded plastics. *Biomacromolecules* **2021**, *22* (5), 1999–2009. DOI: 10.1021/acs.biomac.1c00105.

47. Wu, X.; Ge, J.; Zhu, J.; Zhang, Y.; Yong, Y.; Liu, Z., A general method for synthesizing enzyme-polymer conjugates in reverse emulsions using Pluronic as a reactive surfactant. *Chemical Communications* **2015**, *51* (47), 9674–9677. DOI: 10.1039/c5cc01776a.

48. Zhang, Y.; Dai, Y.; Hou, M.; Li, T.; Ge, J.; Liu, Z., Chemo-enzymatic synthesis of valrubicin using Pluronic conjugated lipase with temperature responsiveness in organic media. *RSC Advances* **2013**, *3* (45), 22963–22966. DOI: 10.1039/c3ra44879g.

49. Bradford, M. M., A Rapid and Sensitive Method for the Quantitation of Microgram Quantities of Protein Utilizing the Principle of Protein-Dye Binding. *Analytical Biochemistry* **1976**, *72*, 248–254. DOI: 10.1016/j.sbi.2014.10.005.

50. Peñas, M. I.; Pérez-Camargo, R. A.; Hernández, R.; Müller, A. J., A review on current strategies for the modulation of thermomechanical properties of poly(butylene succinate) (PBS) and its effect on the biodegradation and barrier properties. *Polymers* **2022**, *14* (05), 1025. DOI: 10.3390/polym14051025.

51. Lueckgen, A.; Garske, D. S.; Ellinghaus, A.; Mooney, D. J.; Duda, G. N.; Cipitria, A., Enzymatically-degradable alginate hydrogels promote cell spreading and in vivo tissue infiltration. *Biomaterials* **2019**, *217*, 119294. DOI: 10.1016/j.biomaterials.2019.119294.

52. Hegyesi, N.; Zhang, Y.; Kohári, A.; Polyák, P.; Sui, X.; Pukánszky, B., Enzymatic degradation of PLA/cellulose nanocrystal composites. *Industrial Crops and Products* **2019**, *141*, 111799. DOI: 10.1016/j.indcrop.2019.111799.

53. Hegyesi, N.; Hodosi, E.; Polyák, P.; Faludi, G.; Balogh-Weiser, D.; Pukánszky, B., Controlled degradation of poly-ε-caprolactone for resorbable scaffolds. *Colloids and surfaces. B, Biointerfaces* **2020**, *186*, 110678. DOI: 10.1016/j.colsurfb.2019.110678.

54. Rosato, A.; Romano, A.; Totaro, G.; Celli, A.; Fava, F.; Zanaroli, G.; Sisti, L., Enzymatic Degradation of the Most Common Aliphatic Bio-Polyesters and Evaluation of the Mechanisms Involved: An Extended Study. *Polymers* **2022**, *14* (9), 1850. DOI: 10.3390/polym14091850.

55. Shinozaki, Y.; Kikkawa, Y.; Sato, S.; Fukuoka, T.; Watanabe, T.; Yoshida, S.; Nakajima-Kambe, T.; Kitamoto, H. K., Enzymatic degradation of polyester films by a cutinase-like enzyme from Pseudozyma antarctica: Surface plasmon resonance and atomic force microscopy study. *Applied Microbiology and Biotechnology* **2013**, *97* (19), 8591–8598. DOI: 10.1007/s00253-012-4673-0.

56. Yazdaninia, A.; Khonakdar, H. A.; Jafari, S. H.; Asadi, V., Influence of trifluoropropyl-POSS nanoparticles on the microstructure, rheological, thermal and thermomechanical properties of PLA. *RSC Advances* **2016**, *6* (43), 37149–37159. DOI: 10.1039/c6ra00243a.

57. Shi, K.; Bai, Z.; Su, T.; Wang, Z., Selective enzymatic degradation and porous morphology of poly(butylene succinate)/poly(lactic acid) blends. *International Journal of Biological Macromolecules* **2019**, *126*, 436–442. DOI: 10.1016/j.ijbiomac.2018.12.168.

58. Akhir, M. A. M.; Zubir, S. A.; Mariatti, J., Effect of different starch contents on physical, morphological, mechanical, barrier, and biodegradation properties of tapioca starch and poly(butylene adipate-co-terephthalate) blend film. *Polymers for Advanced Technologies* **2023**, *34* (2), 717–730. DOI: 10.1002/pat.5922.

59. Haynes, W. M., CRC Handbook of Chemistry and Physics. (CRC Press) **2014**, 3–488.

60. Sato, S.; Saika, A.; Shinozaki, Y.; Watanabe, T.; Suzuki, K.; Sameshima-Yamashita, Y.; Fukuoka, T.; Habe, H.; Morita, T.; Kitamoto, H., Degradation profiles of biodegradable plastic films by biodegradable plastic-degrading enzymes from the yeast Pseudozyma antarctica and the fungus Paraphoma sp. B47-9. *Polymer Degradation and Stability* **2017**, *141*, 26–32. DOI: 10.1016/j.polymdegradstab.2017.05.007.

61. Xu, P. Y.; Liu, T. Y.; Huang, D.; Zhen, Z. C.; Lu, B.; Li, X.; Zheng, W. Z.; Zhang, Z. Y.; Wang, G. X.; Ji, J. H., Enhanced degradability of novel PBATCL copolyester: Study on the performance in different environment and exploration of mechanism. *European Polymer Journal* **2023**, *186*, 111834. DOI: 10.1016/j.eurpolymj.2023.111834.

62. Xie, L.; Huang, J.; Xu, H.; Feng, C.; Na, H.; Liu, F.; Xue, L.; Zhu, J., Effect of large sized reed fillers on properties and degradability of PBAT composites. *Polymer Composites* **2023**, *44* (3), 1752–1761. DOI: 10.1002/pc.27202.

63. von Burkersroda, F.; Schedl, L.; Göpferich, A., Why degradable polymers undergo surface erosion or bulk erosion. *Biomaterials* **2002**, *23* (21), 4221–4231. DOI: 10.1016/S0142-9612(02)00170-9.

64. Freije García, F.; Guadalupe, G. L., Use of Lipases as a Sustainable and Efficient Method for the Synthesis and Degradation of Polymers. *Journal of Polymers and the Environment* **2023**, *November*, 1–33. DOI: 10.1007/s10924-023-03118-z.

65. Xiao, H.; Lu, W.; Yeh, J.-T., Crystallization behavior of fully biodegradable poly(lactic acid)/poly(butylene adipate-co-terephthalate) blends. *Journal of Applied Polymer Science* **2009**, *112* (5), 3754–3763. DOI: 10.1002/app.29800.

66. Arandia, I.; Zaldua, N.; Maiz, J.; Pérez-Camargo, R. A.; Mugica, A.; Zubitur, M.; Mincheva, R.; Dubois, P.; Müller, A. J., Tailoring the isothermal crystallization kinetics of isodimorphic poly(butylene succinate-ran-butylene azelate) random copolymers by changing composition. *Polymer* **2019**, *183*, 121863. DOI: 10.1016/j.polymer.2019.121863.

67. Bo, L.; Guan, T.; Wu, G.; Ye, F.; Weng, Y., Biodegradation Behavior of Degradable Mulch with Poly (Butylene Adipate-co-Terephthalate) (PBAT) and Poly (Butylene Succinate) (PBS) in Simulation Marine Environment. *Polymers* **2022**, *14* (8), 1515. DOI: 10.3390/polym14081515.

Chapter 6

Self-Assembly of Block Copolymers in Solution:

Gels with Crystallizable Blocks

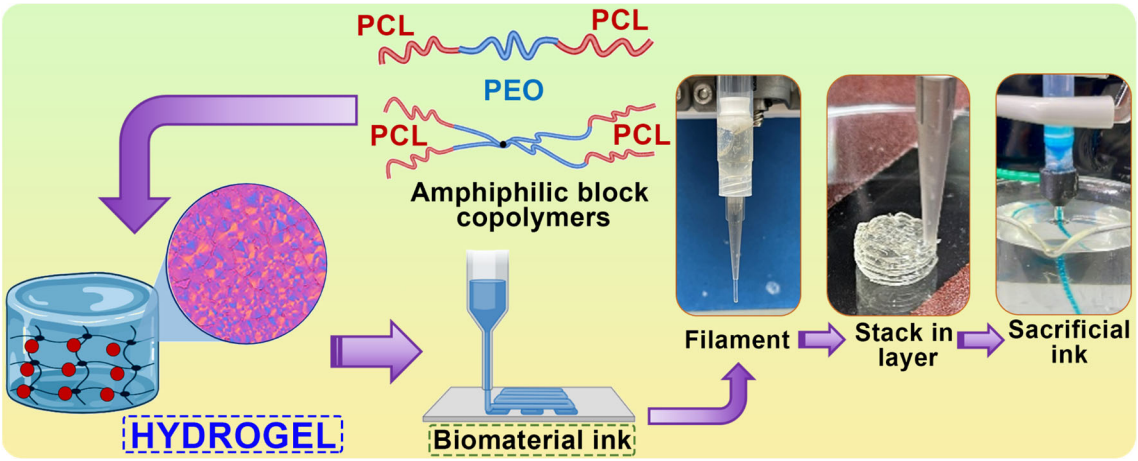

6.1. Introduction

Aqueous solutions of diblock and triblock amphiphilic copolymers based on poly(ethylene oxide) and poly(ε-caprolactone), linear PEO-*b*-PCL, and PCL-*b*-PEO-*b*-PCL can assemble in micelles whose morphology and size depend on the copolymer composition, molecular weight, and mass fraction of hydrophilic and hydrophobic blocks.[1] The use of well-defined diblock and triblock amphiphilic copolymers with a narrow molecular weight distribution structure allows them to control their self-assembly in water and hence, expand the range of applications, for example, in drug delivery devices.[2–8] Earlier results in literature have reported on thermoreversible gelation of triblock PCL-*b*-PEO-*b*-PCL copolymers due to their amphiphilic character that results in micelle formation and micelle packing at concentrations above the critical gelation concentration. Thermoreversible gelation depends to a great extent on the hydrophilic/hydrophobic ratio and temperature.[9–11]

The chain topology of the block copolymer also plays an essential role in establishing critical micelle concentration, micelle size, and aggregation number. In particular, for star block copolymers of poly(ethylene glycol) and poly(ε-caprolactone) consisting of at least three macromolecular chains (arms) radiating from a central core, experimental and theoretical results have demonstrated that the formation of micelles becomes easier for 4-arm star block copolymers than for 2 and 3-arm star block copolymers.[12] Few studies in the literature report gel formation from star block copolymers in comparison to linear block copolymers. 4-arm PEG-*b*-PCL star block copolymers were reported to self-assemble into micelles in water and form thermoreversible hydrogels at concentrations above 10 % w/v. Atomic force microscopy analyses were employed to image the morphology of aggregates, which showed a core-corona spherical structure with the micelle and a mountain-chain-like morphology with the gel that stemmed from the packing of worm-like micelle clusters.[13] More recently, the physical, mechanical, and degradation properties of hydrogels of 8-arm star copolymer with PEO blocks of 4000 and 20,000 g/mol and PCL blocks between 600 and 3500

g/mol were determined and compared to their linear analogs. Star block copolymers show better aqueous solubility and yield more homogeneous and transparent hydrogels. Also, increasing the PCL block length, as well as increasing the molecular weight, generally resulted in a larger gel window, a higher gel stiffness, and enhanced in vitro stability.[14]

PEO-*b*-PCL star block copolymers have mainly been used for the preparation of micelles to deliver pharmaceutical and biological drugs as well as for the design of imaging agents;[15] however, the formation of hydrogels from star block copolymers has been much less reported. In the present Chapter, 3 and 4-arm PEO-*b*-PCL star block copolymers were synthesized. Their gel formation was studied and compared to their linear analogs having the same PEO and PCL block molecular weights. PEO and PCL molecular weight were selected to be between 1000 and 2000 as this M_w range has been reported to yield thermoreversible gelation for linear PEO-*b*-PCL block copolymers. When the PEO block is too large, the aggregation of micelles is hampered, whereas the increase of the PCL block results in poor solubility of the copolymer in water.[10,16–18] The control of phase transitions associated with gel formation, crystallization and melting of PEO and PCL blocks was studied in detail. In fact, crystallinity-induced gelation in water can be employed to tune gelation properties and control bulk mechanical properties for hydrogels obtained from triblock copolymers with crystallizable hydrophobic blocks,[19,20] brush copolymers with crystalline side chains,[21,22] as well as for semicrystalline polymers such as polyvinyl alcohol.[23] The occurrence of crystallization within hydrogel networks obtained from block and random copolymers has been employed as a strategy in 3D extrusion (bio) printing to improve the stability and mechanical strengths of the hydrogel networks, hence improving the construction of 3D printed hydrogel structures.[24,25] Hence, the viscoelastic properties associated with gel formation were determined to tune the use of copolymers as biomaterial inks for 3D extrusion printing. In particular, we provide proof-of-concept of the feasibility of using 4-arm PEO-*b*-PCL block copolymers for direct ink printing as sacrificial biomaterial inks, which to the best of our knowledge, has not been reported before.

6.2. Experimental Part

6.2.1. Materials

Methanol (MeOH), tetrahydrofuran (THF), dichloromethane (DCM), ethyl acetate (EtOAc) and diethyl ether (Et_2O) were purchased from VWR Chemicals (HiPerSolv Chromanorm). 1,4-dioxane (anhydrous, >99.9 %), tert-butyliminotris(dimethylamino)phosphorane (*t*-BuP_1), 1-tert-butyl-2,2,4,4,4-pentakis(dimethylamino)2λ5,4λ5catenadi(phosphazene) (*t*-BuP_2) (2 M solution in THF), benzoic acid (99.5 %), calcium hydride (CaH_2, 95 %), triethylborane (Et_3B) in THF (1 M), and trifluoroacetic acid (TFAA) were purchased from Sigma-Aldrich and used as received. THF was refluxed over sodium/benzophenone before use. *ε*-caprolactone (CL, 99 %) from Sigma-Aldrich was distilled twice over CaH_2 under a dynamic vacuum. Trimethylolpropane (TMOP, >99 %) and di(trimethylolpropane) (DTMOP, 97 %) were recrystallized from EtOAc three times, dissolved in anhydrous 1,4-dioxane, cryo-evaporating the 1,4-dioxane, followed by drying under vacuum overnight. All monomers, solvents, and catalysts for polymerizations were stored under argon (Ar) in a glove box (LABmaster^{pro}SP, MBraun, Germany).

6.2.2. Synthesis of linear triblock copolymers, 3-arm and 4-arm star block copolymers

For the linear polymer samples, size exclusion chromatography (SEC) measurements equipped with a refractive index (RI) detector were conducted in THF at 35 ºC using two identical PLgel MIXED-C columns (5 μm) at a flow rate of 1.0 mL min^{-1} [(poly(ethylene oxide) standards were used to calibrate SEC for PEO samples and polystyrene standards for other samples]. ^{1}H-NMR was performed on a Bruker 500 MHz NMR spectrometer. $CDCl_3$ was used as a solvent, and the testing temperature was set to 25 ºC.

a. Linear PCL_2-b-PEO_2-b-PCL_2

6 mL difunctional initiator (H_2O, 3.0 mmol, 0.5 M in THF), 40 μL *t*-BuP_1 (0.15 mmol), 450 μL Et_3B (0.45 mmol) and 20.7 mL THF was mixed in a Schlenk flask under Ar atmosphere. The Schlenk flask was connected to a vacuum line, and 6.8 mL predried ethylene oxide (136.2 mmol) were slowly condensed into the flask at 0 ºC. The flask was kept stirring at RT until it turned to be a white solid (~6 h). The solid was heated to melt, and half of it was taken out, dissolved in a small amount of THF, and precipitated in diethyl ether two times before being dried under vacuum at 40 ºC overnight. 5.8 mL ε-caprolactone (52.6 mmol) and 225 μL *t*-BuP_2 (0.45 mmol, 2 M in THF) were added to the remaining living polymer before stirring at RT until it became a white solid. The resultant polymer was precipitated in the mixture of diethyl ether and methanol (7:3, v/v) before being dried under vacuum at 40 ºC overnight.

b. Three arms copolymer (PEO_2-b-PCL_2)$_3$

825 mg of trifunctional initiator (trimethylolpropane [TMOP], 6.15 mmol), 144 mg *t*-BuP_1 (0.615 mmol), 1.85 mL Et_3B (1.85 mmol) and 70 mL THF were mixed in a Schlenk flask under Ar atmosphere. The Schlenk flask was connected to a vacuum line, and 14 mL predried ethylene oxide (280 mmol) were slowly condensed into the flask at 0 ºC. The flask was kept under stirring at 40 ºC for 12 h. Half of the reaction mixture was removed, dissolved in a small amount of THF, and precipitated in diethyl ether twice before being dried under vacuum at 40 ºC overnight. 6.2 mL of ε-caprolactone (52.6 mmol) and 0.46 mL *t*-BuP_2 (0.923 mmol, 2 M in THF) were added to the remaining living polymer before stirring at RT until it became a white solid. The resulting polymer was precipitated in the mixture of diethyl ether and methanol (7:3, v/v) before being dried under vacuum at 40 ºC overnight.

c. Four arms copolymer (PEO_2-b-$PCL_2)_4$

1.52 g of tetrafunctional initiator {di(trimethylolpropane) [DTMOP], 6.08 mmol}, 143 mg *t*-BuP_1 (0.608 mmol), 1.82 mL Et_3B (1.82 mmol) and 70 mL THF were mixed in a Schlenk flask under Ar atmosphere. The Schlenk flask was connected to a vacuum line, and 14 mL of predried ethylene oxide (280 mmol) werw slowly condensed into the flask at 0 ºC. The flask was kept under stirring at 40 ºC for 12 h. Half of the reaction mixture was removed, dissolved in a small amount of THF, and precipitated in diethyl ether twice before being dried under vacuum at 40 ºC overnight. 6.1 mL *ε*-caprolactone (54.7 mmol) and 0.46 mL *t*-BuP_2 (0.923 mmol, 2 M in THF) were added to the remaining living polymer before stirring at RT until it became a white solid. The resulting polymer was precipitated in the mixture of diethyl ether and methanol (7:3, v/v) before being dried under vacuum at 40 ºC overnight.

6.2.3. Phase diagram determination

All block copolymers were dissolved in water at concentrations from 15 to 40 % w/v in a silicone bath maintained at 80 ºC for 30 min under magnetic stirring. Then, they were cooled in ice water for 10 min. Phase diagrams were determined via inverted vial tests and rheology. For inverted vial tests, polymer aqueous solutions in vials were placed in a Julabo ED cryostat (Julabo GmbH, Germany) at an initial temperature of 10 ºC. The heating rate was set at 2 min/ºC from 10 to 80 ºC. The samples were inspected for the formation of a stable gel (transparent and cloudy), which is determined by the inverted vial test as the point at which the sample does not flow upon tube inversion. The criterion to define the sol-gel phase transition was given by the temperature at which the vial was inverted 180º, and no flow of the sample was observed for 10 seconds. All gel samples were kept in the fridge after the measurements.

Oscillatory temperature sweeps were measured in an AR-G2 rheometer (TA Instruments, USA) using a 20 mm plate-plate geometry in the temperature range between 5-90 ºC at a heating rate of 2 ºC/min. The tests were carried out at a

constant strain of 0.5 % located within the region of linear viscoelasticity. The results were analyzed with the TRIOS software from TA Instruments.

6.2.4. Differential Scanning Calorimetry (DSC)

Thermal transitions of the gels were studied through DSC experiments carried out in a DSC 8000 (PerkinElmer, USA) equipped with an Intracooler II, using special liquid pans for gels measurements and standard aluminum pans for samples in bulk. The experimental protocol for the gels (15-25 mg) was the following: *i)* 1st heating from room temperature to 85 ºC, *ii)* cooling from 85 to 5 ºC, and *iii)* 2nd heating from 5 to 85 ºC. All gel samples were measured at a 2 ºC/min scanning rate. Measurements with the samples in bulk (5-7 mg) were performed at 20 ºC/min as indicated: *i)* cooling from 90 to -30 ºC, and *ii)* heating from -30 to 90 ºC.

6.2.5. Polarized Light Optical Microscopy (PLOM)

An Olympus BX51 polarized light optical microscope was employed to analyze the crystalline morphology of the samples in the gel form and in bulk. A Linkam THMS600 hot stage with liquid N_2 was used for accurate temperature control, and an Olympus SC50 camera was used to obtain images.

Films were prepared by melting the samples in a glass slide covered by a glass coverslip. Cooling rates of 2 and 20 ºC/min (for gels and materials in bulk, respectively) were employed to analyze morphological changes.

6.2.6. Small Angle and Wide Angle X-ray Scattering (SAXS/WAXS)

Non-isothermal simultaneous in situ SAXS/WAXS experiments were carried out at the ALBA Synchrotron Radiation Facility (Barcelona, Spain) at the beamline BL11 NCD-SWEET. DSC pans were employed as holders for copolymers in bulk, whereas hydrogels were placed inside glass capillaries. A THMS 600 Linkam (Linkam Scientific Instruments, UK) hot-stage device coupled to a liquid nitrogen cooling system was employed for the heating and cooling scans

of the samples. The non-isothermal protocol was as follows: *i)* heating from room temperature to the melt at 20 ºC/min (in the case of bulk copolymers) and at 2 ºC/min (in the case of gels) and *ii)* cooling from the melt to -20 ºC (bulk copolymers) and to 5 ºC (gel samples) at the same rates, while SAXS/WAXS data were collected simultaneously.

The X-ray energy source amounted to 12.0 keV using a channel cut Si (1 1 1) monochromator (λ = 1.03 Å). For the SAXS setup, the distance between the sample and the detector (Pilatus 1 M detector, Dectris Ltd, Switzerland, with a resolution of 3070 × 3070 pixels, pixel size of 102 μm^2) was 3652 mm with a tilt angle of 0º. Calibration was performed with silver behenate. Regarding WAXS configuration, a distance of 97.5 mm was used between the sample and the detector, with a tilt angle of 21.2º. Chromium (III) oxide was employed for calibration, using a Rayonix LX255-HS detector (Rayonix L.L.C., USA), with a resolution of 1920 × 5760 pixels; the pixel size was 44 μm^2. Scattering intensity as a function of the scattering vector, $q = 4\pi \cdot sin\theta \cdot \lambda^{-1}$ data are obtained, where λ is the X-ray wavelength, and 2θ is the scattering angle.

6.2.7. 3D extrusion printing of the hydrogels

Rheological properties were determined for selected compositions of the hydrogels to assess their printability. Two types of experiments were carried out in an AR-G2 rheometer (TA Instruments, USA): *i)* a frequency sweep from 10 to 0.01 Hz at a constant strain of 0.5 % to determine the elastic moduli and *ii)* consecutive time sweeps at 0.1 and 100 % strain to determine recovery of the elastic moduli.

Hydrogels were subjected to 3D extrusion printing tests in an adapted filament Creality Ender 3.[26] A first test was carried out to define the printing conditions where the pressure was varied from 0.6 to 1.8 bar. For the stacking test, cylinders with diameters (12 and 16 mm) were defined with a fill distance between lines of 1 mm. Printed structures were visualized through scanning electron microscopy analysis performed on a PHILIPS XL30 ESEM (Koninklijke Philips N.V.,

Netherlands) unit operated at 25 kV. The samples, previously frozen in a refrigerator and lyophilized for 24 h, were prepared by the gold coating technique using a Thermo VG Scientific Polaron SC7640 Sputter Coater (Quorum Technologies, UK) power supply in direct current at 1 kV, applying vacuum.

To determine the ability of hydrogels to be employed as sacrificial biomaterial inks, dissolution tests were carried out in the water at 37 ºC, where the mass loss was recorded at specific times. Then, two hydrogels were printed simultaneously with a coaxial nozzle (0.8 mm internal diameter, 2 mm external diameter) into a calcium chloride $CaCl_2$ solution (200 mM). A medium viscosity alginate hydrogel at 8 % w/v that crosslinks with the $CaCl_2$ solution was printed as the outer layer, whereas selected compositions of the 4-arm star copolymers were printed as the inner part.

6.3. Results and Discussion

6.3.1. Synthesis of the copolymers

The linear triblock copolymers and the 3- and 4-arm star block copolymers (Figure 6.1) were synthesized according to previous reports.[27,28] The molecular characteristics of the resulting copolymers are summarized in Table 6.1. The details of the experimental procedures and molecular characterization (^{1}H-NMR spectra, SEC traces, and MALDI-TOF spectra) are presented in Figures 6.2–6.9.

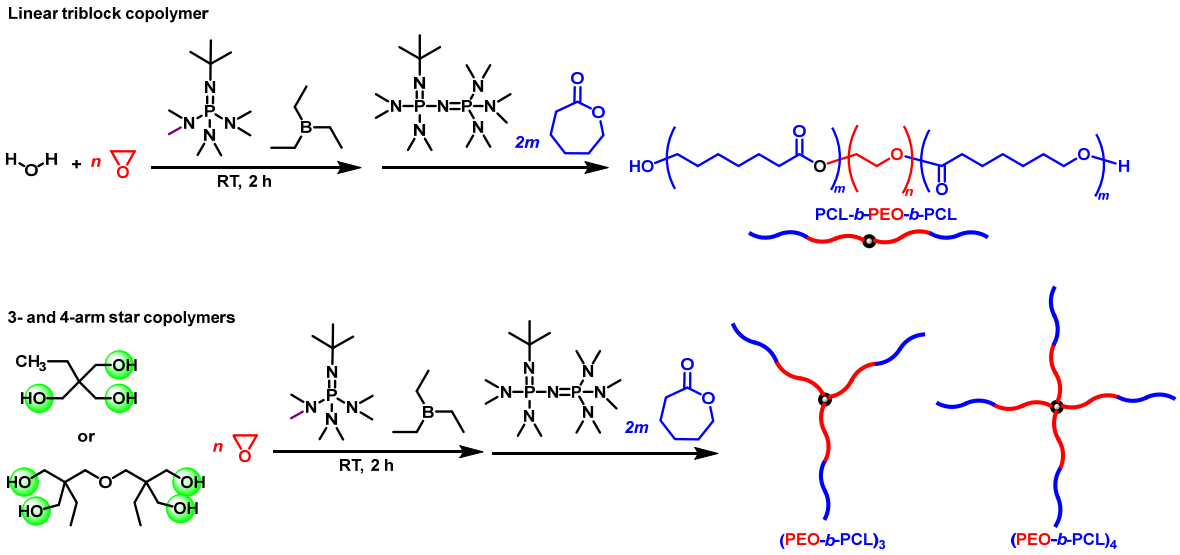

Figure 6.1. Schematic representation of the synthesis of linear triblock copolymer PCL-*b*-PEO-*b*-PCL, and 3-arm and 4-arm star block copolymers (PEO-*b*-PCL)$_x$.

Table 6.1. Molecular characteristics of the studied copolymers.

Sample	M_n (g/mol)	$M_{n,\,SEC}$ (PEO)[a]	$M_{n,\,NMR}$ (PEO)[b]	$M_{n,\,MALDI\text{-}TOF}$ (PEO)[c]	PEO/PCL[d]
Linear copolymers					
PCL_1-*b*-$PEO_{1.2}$-*b*-PCL_1	1k – 1.2k – 1k	1.1	1.2	1.2	0.6
PCL_2-*b*-$PEO_{2.1}$-*b*-PCL_2	2k – 2.1k – 2k	1.9	2.1	2.2	0.53
3-arm star copolymers					
$(PEO_{1.1}$-*b*-$PCL_{0.5})_3$	$(1.2k – 0.5k)_3$	3.1	3.6		2.4
$(PEO_{2.9}$-*b*-$PCL_1)_3$	$(4.1k – 1.4k)_3$	6.8	12.3		2.9
4-arm star copolymers					
$(PEO_{1.2}$-*b*-$PCL_1)_4$	$(1.2k – 1k)_4$	4.6	4.8		1.2
$(PEO_{2.5}$-*b*-$PCL_{1.4})_4$	$(2.5k – 1.4k)_4$	8.6	10		1.8

[a] Molecular weight by SEC (DMF, 40 ºC, PEO standards). [b] Molecular weight by ^{1}H-NMR (500 MHz, $CDCl_3$, 25 ºC) and [c] MALDI-TOF MS. [d] PEO/PCL mole fraction by ^{1}H-NMR.

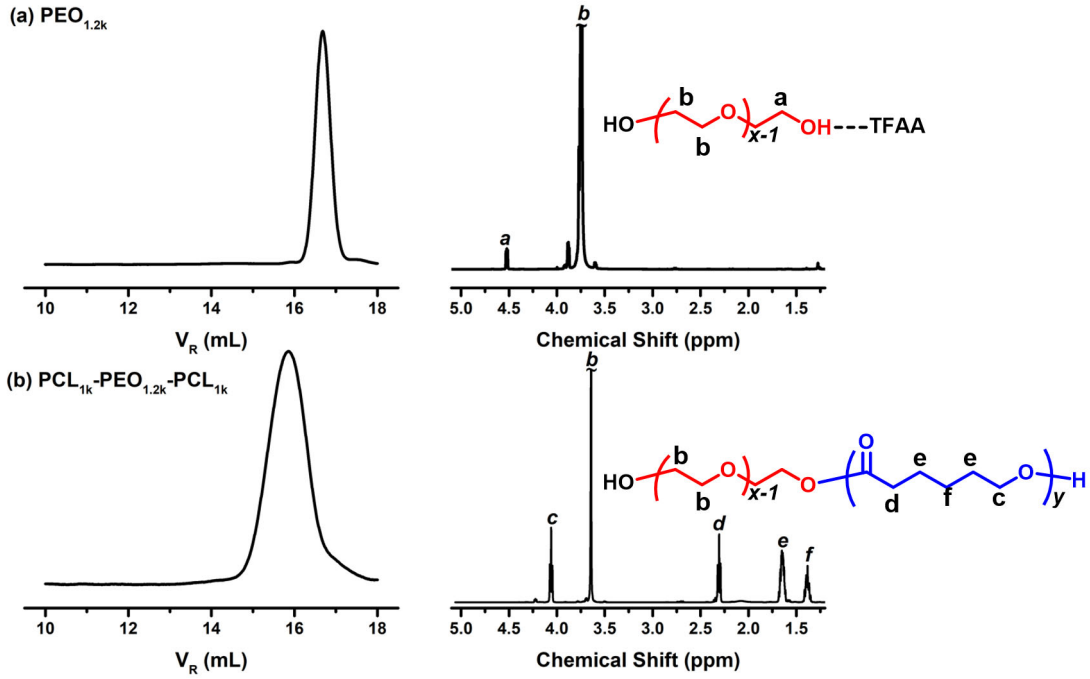

Figure 6.2. SEC traces (DMF, 40 ºC, PEO standards) and ^{1}H-NMR spectra (500 MHz, $CDCl_3$, 25 ºC) of: **a)** $PEO_{1.2}$, and **b)** PCL_1-*b*-$PEO_{1.2}$-*b*-PCL_1 linear triblock copolymer.

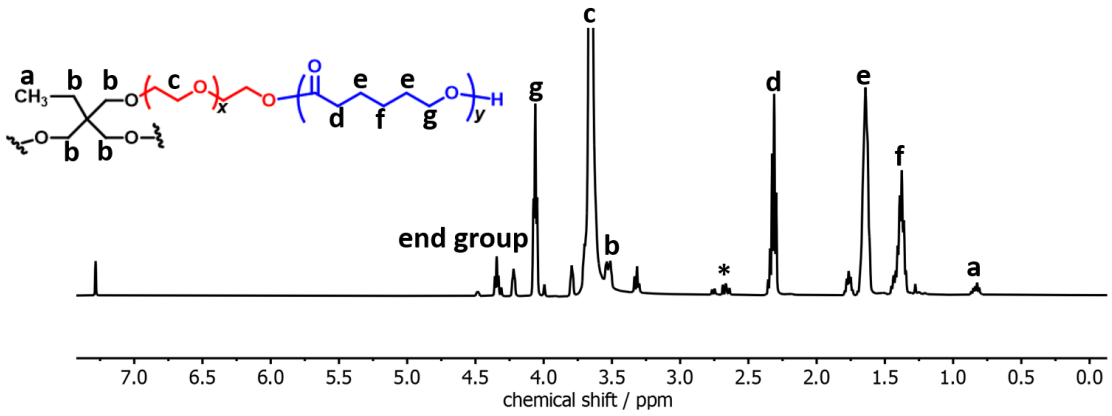

Figure 6.3. ^{1}H-NMR spectrum of $(PEO_{1.1}$-*b*-$PCL_{0.5})_3$ star block copolymer (500 MHz, $CDCl_3$, 25 ºC). * denotes an unknown impurity.

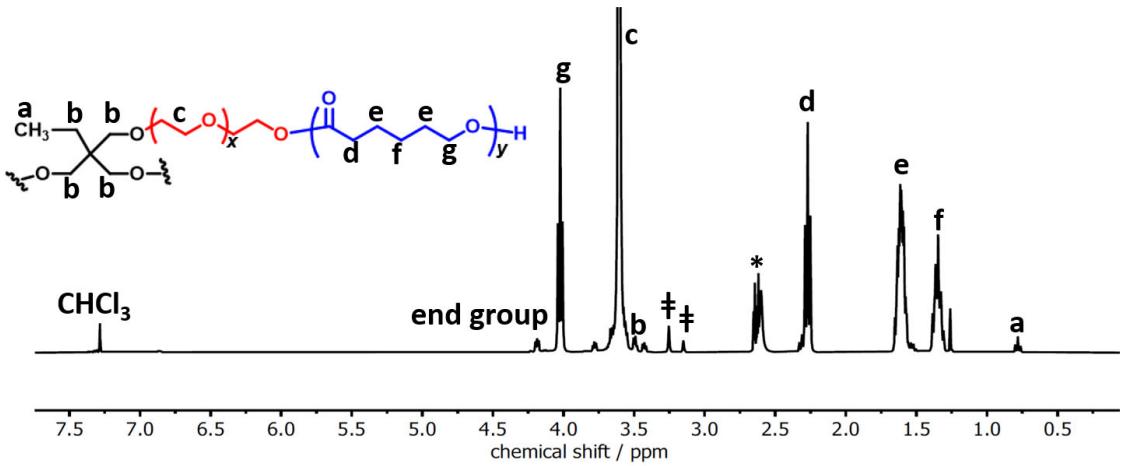

Figure 6.4. ^{1}H-NMR spectrum of $(PEO_{2.9}$-*b*-$PCL_1)_3$ star block copolymer (500 MHz, $CDCl_3$, 25 ºC). ǂ denotes the residual solvent. * denotes an unknown impurity.

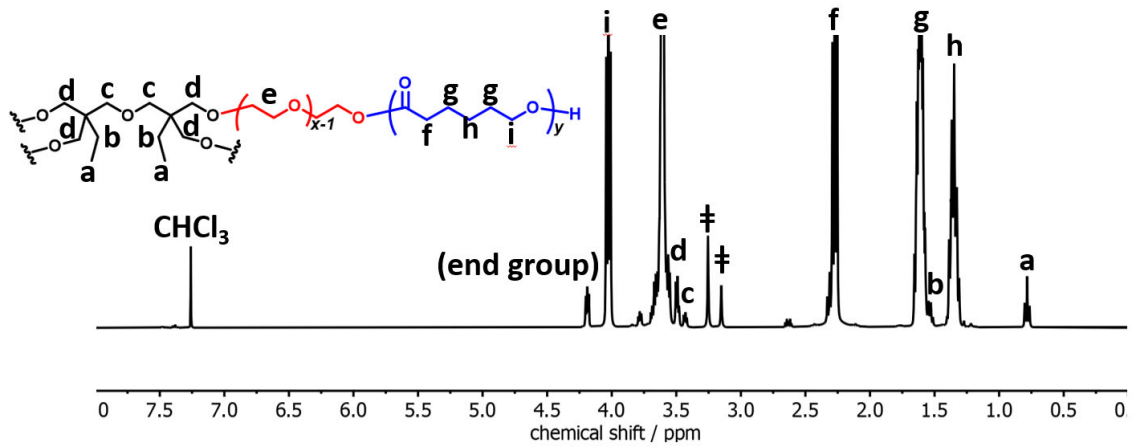

Figure 6.5. ^{1}H-NMR spectrum of $(PEO_{1.2}$-*b*-$PCL_{1})_4$ star block copolymer (500 MHz, $CDCl_3$, 25 ºC). ǂ denotes the residual solvent.

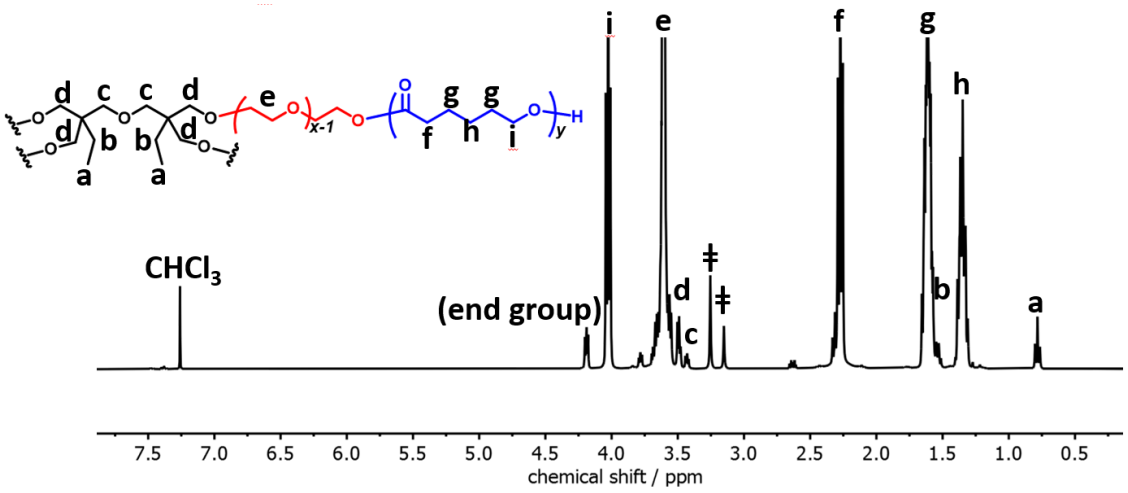

Figure 6.6. ^{1}H-NMR spectrum of $(PEO_{2.5}$-*b*-$PCL_{1.4})_4$ star block copolymer (500 MHz, $CDCl_3$, 25 ºC). ǂ denotes the residual solvent.

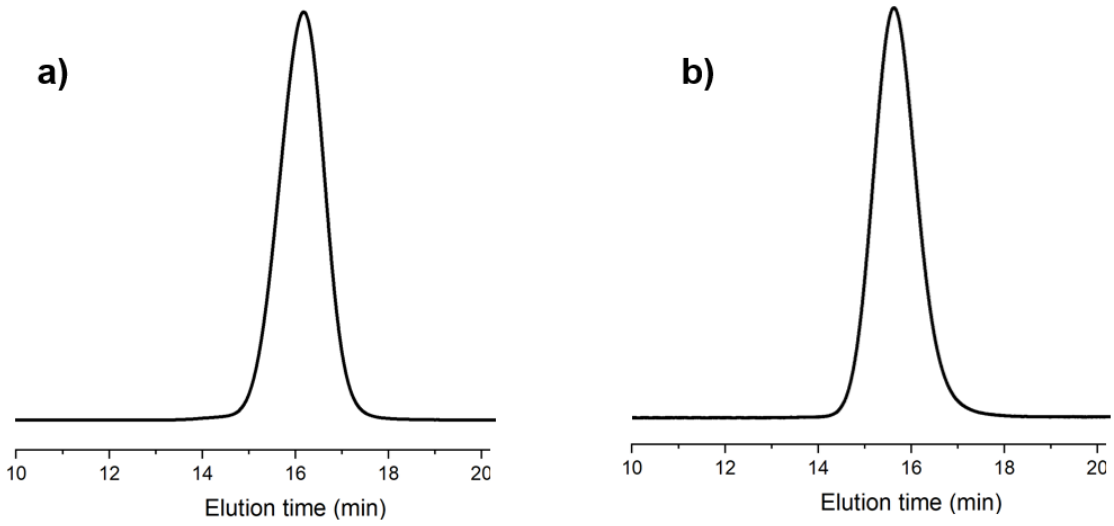

Figure 6.7. SEC traces of 3-arm star block block copolymers: **a)** $(PEO_{1.1}$-*b*-$PCL_{0.5})_3$, and **b)** $(PEO_{2.9}$-*b*-$PCL_1)_3$ (THF, 35 ºC, PS standards).

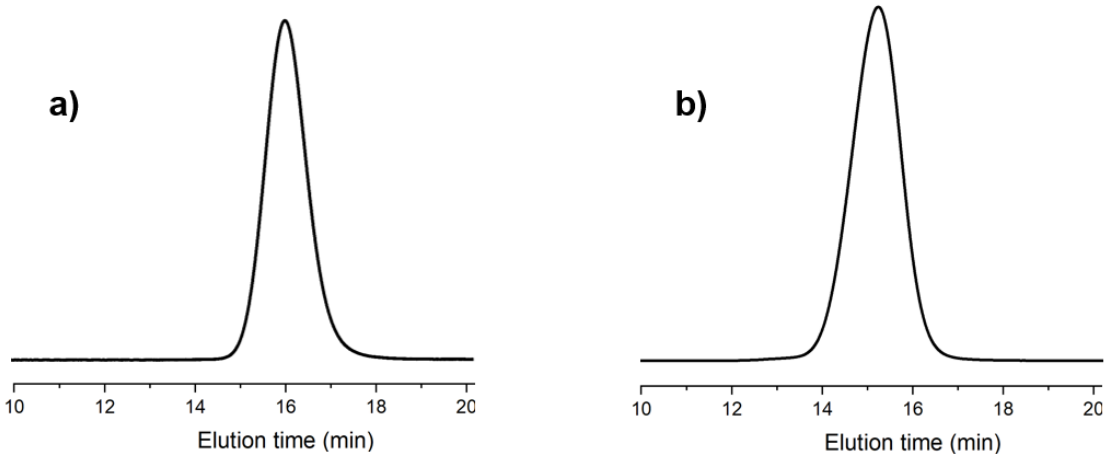

Figure 6.8. SEC traces of 4-arm star block copolymers: **a)** $(PEO_{1.2}$-*b*-$PCL_1)_4$, and **b)** $(PEO_{2.5}$-*b*-$PCL_{1.4})_4$ (THF, 35 ºC, PS standards).

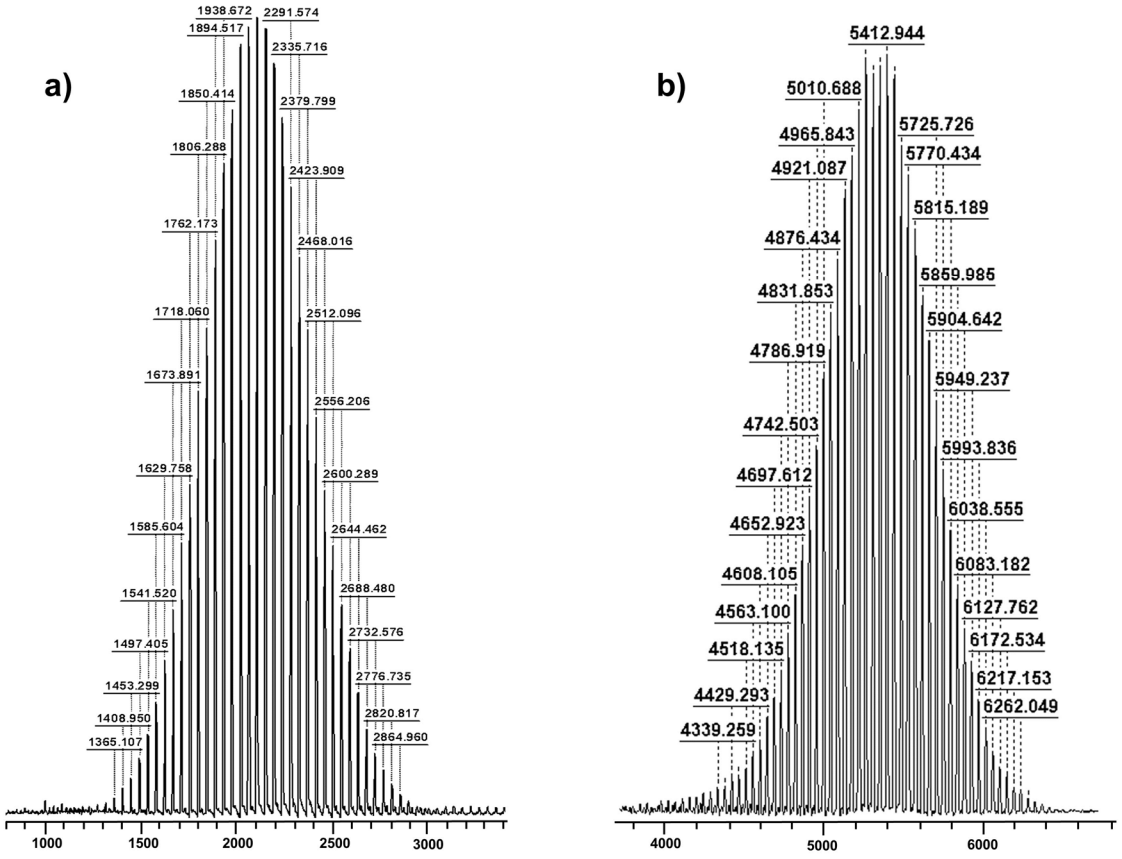

Figure 6.9. MALDI-TOF spectra of PEO precursors: **a)** $PEO_{2.1}$, and **b)** $(PEO_{2.5})_4$.

6.3.2. Determination of phase diagrams

To determine the phase diagram (temperature vs. concentration) corresponding to the aqueous solutions of the triblock copolymers under study and to evaluate the dependence of gel formation on the molecular topology, inverted vial tests were performed for aqueous solutions of polymer concentrations between 15 and 40 % w/v and at temperatures ranging from 10 to 80 ºC. The results are shown in Figure 6.10a.

Linear block copolymers, PCL_1-*b*-$PEO_{1.2}$-*b*-PCL_1 and PCL_2-*b*-$PEO_{2.1}$-*b*-PCL_2, exhibit a thermoreversible behavior with a sol-gel-sol phase transition ($T_{sol-gel-sol}$) for copolymer concentrations in the range of 15-30 % w/v. The $T_{sol-gel}$ of PCL_1-*b*-$PEO_{1.2}$-*b*-PCL_1 decreases with increasing copolymer concentration from 34 to 31 ºC, whereas the $T_{gel-sol}$ increases with concentration from 49 to 54 ºC. For the PCL_2-*b*-$PEO_{2.1}$-*b*-PCL_2 copolymer, the $T_{sol-gel}$ decreases with increasing

copolymer concentration from 64 to 52 ºC, and the $T_{gel\text{-}sol}$ increases with copolymer concentration from 74 to 80 ºC. The gel window is shifted to lower polymer concentration and higher temperatures with the increase of M_w of the PEO and PCL blocks at the same PEO/PCL ratio, as reported in similar studies.[11]

As to the 4-arm star copolymers, hydrogel formation was observed upon cooling to 0 ºC, aqueous solutions at polymer concentrations above 15 % w/v. For both samples, $(PEO_{1.2}\text{-}b\text{-}PCL_1)_4$ and $(PEO_{2.5}\text{-}b\text{-}PCL_{1.4})_4$, only one $T_{gel\text{-}sol}$ transition temperature (gel melting transition) is obtained that increases with polymer concentration. Such increase with increasing polymer concentration has been widely reported for linear and star block copolymers. It is associated with the formation of a larger number of micelles and bigger aggregates that yields more intense physical interactions in the resulting hydrogels.[14,16]

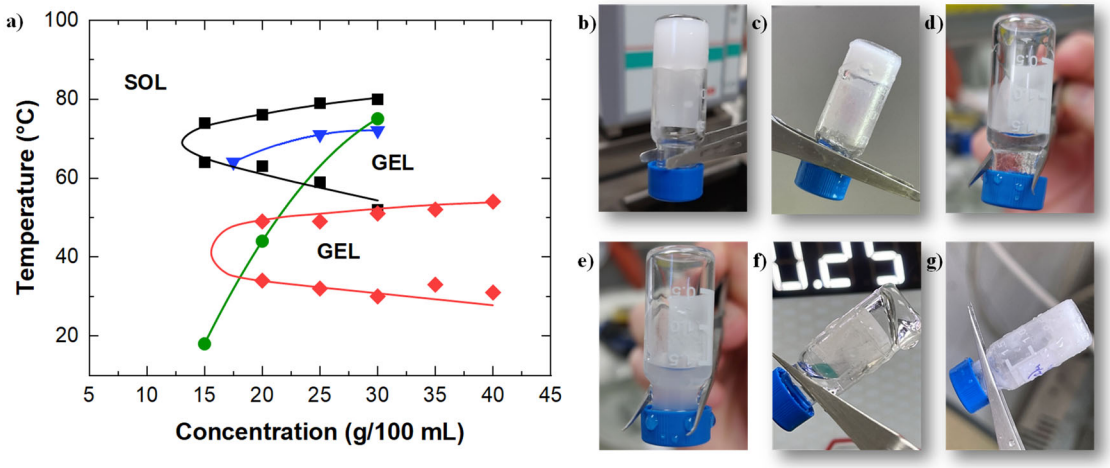

Figure 6.10. **a)** Sol-gel transition phase diagrams of block copolymers under study: ♦ $PCL_1\text{-}b\text{-}PEO_{1.2}\text{-}b\text{-}PCL_1$, ■ $PCL_2\text{-}b\text{-}PEO_{2.1}\text{-}b\text{-}PCL_2$, ▼ $(PEO_{1.2}\text{-}b\text{-}PCL_1)_4$, ● $(PEO_{2.5}\text{-}b\text{-}PCL_{1.4})_4$. 3-arm star copolymers did not show gel formation, and therefore they are not represented. Macroscopic appearance of the hydrogels at 30 % w/v: **b)** $PCL_1\text{-}b\text{-}PEO_{1.2}\text{-}b\text{-}PCL_1$, **c)** $PCL_2\text{-}b\text{-}PEO_{2.1}\text{-}b\text{-}PCL_2$, **d)** $(PEO_{1.1}\text{-}b\text{-}PCL_{0.5})_3$, **e)** $(PEO_{2.9}\text{-}b\text{-}PCL_1)_3$, **f)** $(PEO_{1.2}\text{-}b\text{-}PCL_1)_4$ and, **g)** $(PEO_{2.5}\text{-}b\text{-}PCL_{1.4})_4$. Note that solutions at 30 % w/v from 3-arm star block copolymers do not form hydrogels, remaining as transparent/translucent aqueous solutions.

It is important to note that at polymer concentrations below 25 % w/v, the $T_{gel\text{-}sol}$ temperatures are higher for $(PEO_{1.2}\text{-}b\text{-}PCL_1)_4$ hydrogels than those

corresponding to $(PEO_{2.5}$-*b*-$PCL_{1.4})_4$ hydrogels, which could be attributed to their lower total molecular weight. A shorter block length is expected to produce a smaller inter-micellar space, which should favor lattice structures with a lower coordination number and thus increase the stability of the gel phase with temperature.[29]

For linear block copolymers, it has been reported that an increase in total molecular weight causes the gel phase window to shift to higher temperatures. In contrast, the gel phase window shift observed in 4-arm star copolymers could be associated with an increase in the molecular weight of the hydrophilic PEO block in $(PEO_{2.5}$-*b*-$PCL_{1.4})_4$.[11,30] At this point, it is important to note that only hydrogels obtained from the $(PEO_{1.2}$-*b*-$PCL_1)_4$ sample were transparent whereas the rest of the hydrogels were opaque (see Figure 6.10b-g).

Aqueous solutions of $(PEO_{2.9}$-*b*-$PCL_1)_3$ and $(PEO_{1.1}$-*b*-$PCL_{0.5})_3$ 3-arm star copolymers did not form hydrogels at any concentration and temperature, remaining as transparent/translucent aqueous solutions (see Figure 6.10d-e), and hence they are not represented in Figure 6.10a. To explain these results, besides the molecular weight of each block, it is important to take into account that for amphiphilic diblock and triblock copolymers, the hydrophilic-hydrophobic ratio has been reported to be one of the main factors affecting mobility, the strength of physical interactions and the mechanism for micelle packing.[31] For our study, gel formation upon heating is favored for linear copolymers that present the lowest PEO/PCL ratio (~0.6), being the 3-arm star block copolymers that did not form hydrogels, the two samples that presented the highest PEO/PCL ratio (~2.2). Hence, the absence of gel formation in aqueous solutions of 3-arm star block copolymers could be associated with the synergy between the high proportion of the PEO hydrophilic blocks with respect to the hydrophobic PCL blocks and the decrease in the number of branches compared to 4-arm star block copolymers. Both factors possibly decreased the ability of the copolymer to form strong enough hydrophobic interactions to stabilize the gel phase.[9,32]

The behavior of the aqueous solutions of the 3-arm star copolymers, as observed in Figure 6.10d-e, and the lack of gel formation prevented any further study of these materials. The rest of the tests regarding gels were conducted exclusively with the linear and 4-arm star copolymers.

Phase diagrams obtained through inverted vial tests were further confirmed via oscillatory temperature sweeps, as shown in Figure 6.11. Gel formation for linear triblock copolymers is accompanied by an abrupt change in the storage (G') and the loss (G'') moduli, depicted as a function of temperature in Figure 6.11a. The temperature sweep corresponding to the PCL_2-*b*-$PEO_{2.1}$-*b*-PCL_2 (20 % w/v) sample shows an abrupt increase in G' starting at 47 ºC –corresponding to the sol-to-gel transition ($T_{sol\text{-}gel}$)–, followed by a decrease in both moduli at 78 ºC due to the gel-to-sol transition ($T_{gel\text{-}sol}$). For the PCL_1-*b*-$PEO_{1.2}$-*b*-PCL_1 (20 % w/v) copolymer, gel formation was recorded upon cooling from 70 ºC, as an increase in G' and G'' occurs at 58 ºC caused by the sol-to-gel transition. It is important to note that gel-to-sol transition occurring at 30 ºC could not be measured by this technique. The gel phase window is located between 50 and 75 ºC for the PCL_2-*b*-$PEO_{2.1}$-*b*-PCL_2 (20 % w/v) sample and shifts to lower temperatures for the PCL_1-*b*-$PEO_{1.2}$-*b*-PCL_1 (20 % w/v) sample. Hence, the results confirm that at the same PEO/PCL ratio, gel formation is favored for samples with lower molecular weight of the PEO and PCL blocks, as shown through inverted vial tests.

The temperature sweeps corresponding to $(PEO_{1.2}$-*b*-$PCL_1)_4$ and $(PEO_{2.5}$-*b*-$PCL_{1.4})_4$ 4-arm star block copolymers are shown in Figure 6.11b. Both samples, measured at polymer concentrations of 20 and 30 % w/v, are hydrogels formed upon cooling, as shown by the fact that G' is higher than G'' at temperatures below 20 ºC. As temperature increases, G' and G'' gradually decrease until the $T_{gel\text{-}sol}$ is reached (the $T_{gel\text{-}sol}$ temperatures are marked as dashed lines in Figure 6.11b). The $T_{gel\text{-}sol}$ is highly influenced by polymer concentration being ~50 ºC for hydrogels at 20 % w/v and ~60 ºC for hydrogels at 30 % w/v.

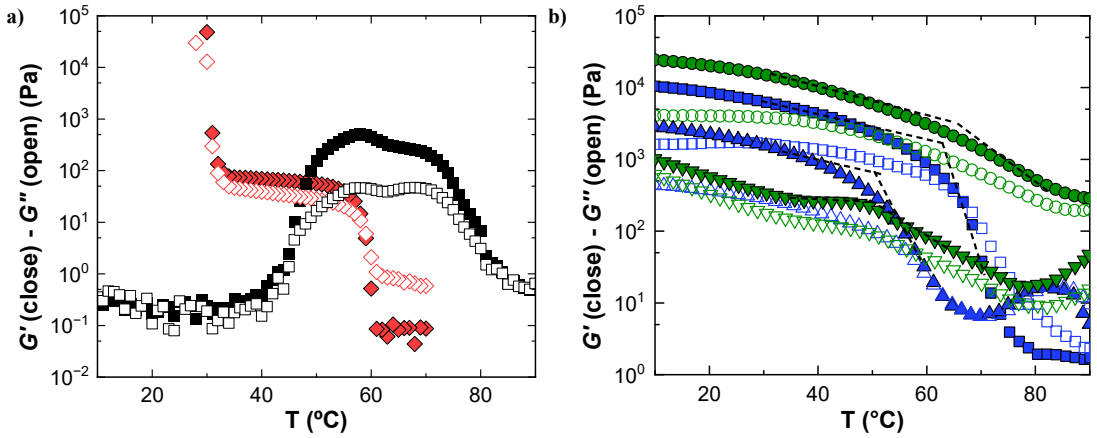

Figure 6.11. Dynamic oscillatory temperature ramp experiments showing storage, G' (close) and loss, G'' (open) moduli corresponding to **a)** linear copolymers: ♦ PCL_1-*b*-$PEO_{1.2}$-*b*-PCL_1 (20 % w/v), ■ PCL_2-*b*-$PEO_{2.1}$-*b*-PCL_2 (20 % w/v) and **b)** 4-arm star copolymers: ■ $(PEO_{1.2}$-*b*-$PCL_1)_4$ (30 % w/v), ▲ $(PEO_{1.2}$-*b*-$PCL_1)_4$ (20 % w/v), ● $(PEO_{2.5}$-*b*-$PCL_{1.4})_4$ (30 % w/v), ▼ $(PEO_{2.5}$-*b*-$PCL_{1.4})_4$ (20 % w/v). Dashed lines mark the $T_{gel\text{-}sol.}$

The results are consistent with the phase diagrams obtained through inverted vial tests depicted in Figure 6.10a and confirm sol-gel-sol behavior for linear copolymers and only a gel-to-sol transition corresponding to gel melting for 4-arm star block copolymers.

6.3.3. Structural organization and morphology of hydrogels as determined through DSC and synchrotron radiation SAXS

Earlier reports in the literature showed that the crystallization of the hydrophobic PCL blocks occurs when aqueous solutions of triblock PCL-*b*-PEO-*b*-PCL initially as a sol phase are left at room temperature for at least 1 h giving rise to the formation of opaque gels with reinforced mechanical properties with respect to "fresh" hydrogels.[10]

To investigate the occurrence of crystallization in polymer hydrogels obtained from linear and 4-arm star block copolymers, the thermal transitions of bulk copolymers determined by DSC were compared to those obtained for gels (30 % w/v composition), and the results are shown in Figure 6.12. For comparison purposes, all DSC experiments were carried out at a rate of 2 ºC/min. It is important

to note that thermal transitions corresponding to the hydrogels could not be observed when DSC experiments were performed at higher scan rates.

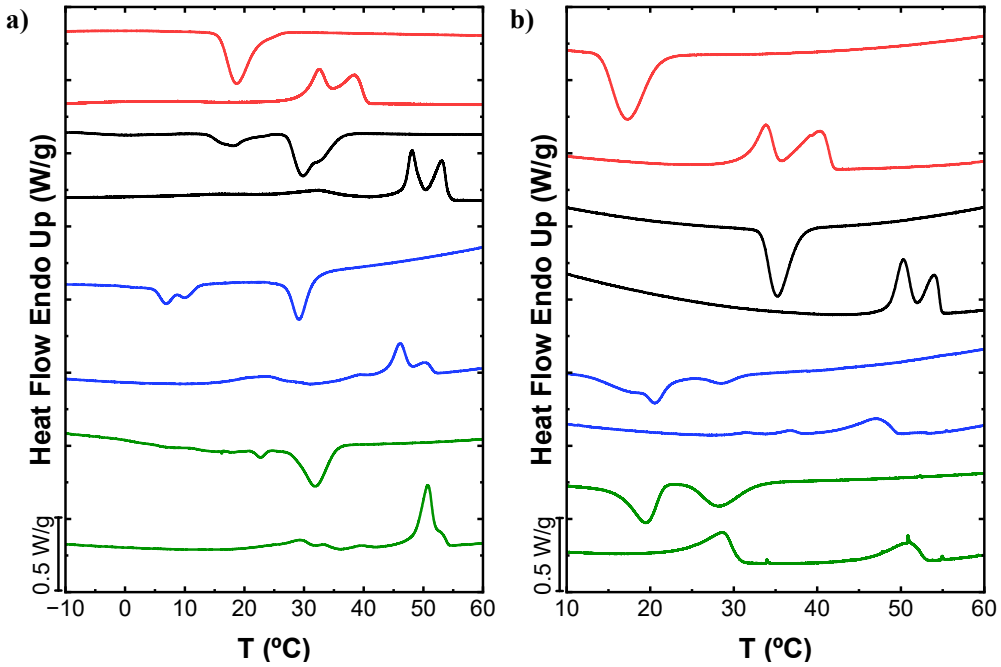

Figure 6.12. DSC cooling and 2nd heating scans at 2 ºC/min in **a)** bulk samples and **b)** gel samples (30 % w/v) for — PCL_1-*b*-$PEO_{1.2}$-*b*-PCL_1, — PCL_2-*b*-$PEO_{2.1}$-*b*-PCL_2, — $(PEO_{1.2}$-*b*-$PCL_1)_4$, — $(PEO_{2.5}$-*b*-$PCL_{1.4})_4$. The DSC traces are normalized by the mass of the polymer present in the samples.

In bulk, the PCL_1-*b*-$PEO_{1.2}$-*b*-PCL_1 linear copolymer shows a single crystallization peak at 18.8 ºC (although it also shows a shoulder at the crystallization onset at around 25 ºC) with two endothermic peaks at 32.7 and 38.7 ºC, both attributed to the melting of PCL blocks crystals (Figure 6.12a, red curves). The in-situ corresponding WAXS measurements performed at 20 ºC/min are shown in Figure 6.13a, where the presence of the PCL reflections (PCL_{110} at 15.1 nm^{-1} and PCL_{200} at 16.7 nm^{-1}) revealed that the crystallization of the PCL block started at 22 ºC during cooling from the melt. PEO block characteristic reflections are first detected at 15 and -14 ºC, as evidenced by the appearance of very small intensity peaks attributed to the PEO_{120} and $PEO_{032/112/132/212}$ reflections, which were observed at 13.8 and 16.3 nm^{-1}, respectively.[33] Given the extreme differences between the WAXS intensities corresponding to the PCL and PEO reflections, it can be deduced that in this PCL_1-*b*-$PEO_{1.2}$-*b*-PCL_1 triblock copolymer, as the PCL

block crystallizes first (with a PCL/PEO ratio of 1.66), it severely restricts the crystallization of the short PEO blocks. This is why the two endothermic peaks in Figure 6.12a for this copolymer are assigned to the melting of PCL blocks crystals, in which the melting of folded (low melting peak) and extended chains (high melting peak) lamellar crystals can account for the two melting transitions. It has been recently shown that PCL chains start to fold at M_n = 2000 g/mol.[34]

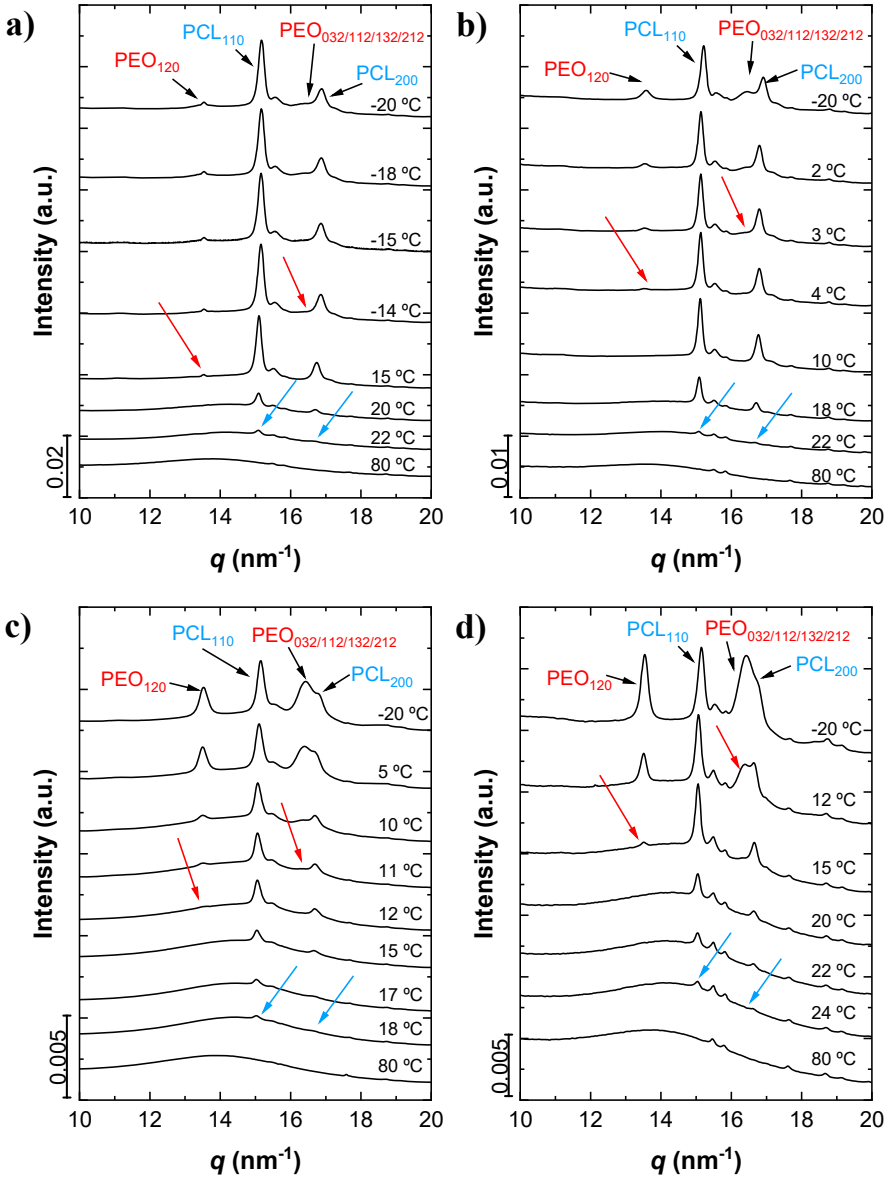

Figure 6.13. WAXS results obtained during the cooling process at 20 ºC/min for the copolymers in bulk: **a)** PCL$_1$-*b*-PEO$_{1.2}$-*b*-PCL$_1$, **b)** PCL$_2$-*b*-PEO$_{2.1}$-*b*-PCL$_2$, **c)** (PEO$_{1.2}$-*b*-PCL$_1$)$_4$ and **d)** (PEO$_{2.5}$-*b*-PCL$_{1.4}$)$_4$, showing the characteristic reflections of the PCL block in blue (PCL$_{110}$ at 15.1 nm^{-1} and PCL$_{200}$ at 16.7 nm^{-1}) and the PEO block in red (PEO$_{120}$ at 13.8 nm^{-1} and PEO$_{032/112/132/212}$ at 16.4 nm^{-1}).

The PCL_2-*b*-$PEO_{2.1}$-*b*-PCL_2 linear triblock copolymer (Figure 6.12a, black curves) showed two crystallization exotherms, at 30.1 and 18.1 ºC, corresponding to the crystallization of the PCL blocks and the PEO block, respectively. This was confirmed by WAXS results (Figure 6.13b), where the presence of the PCL_{110} and PCL_{200} reflections revealed that crystallization of the PCL blocks started at 22 ºC, whereas the crystallization of the PEO block began at 4 ºC, as evidenced by the appearance of the peaks attributed to the PEO_{110} and $PEO_{032/112/132/212}$ reflections. The differences in the crystallization temperatures detected by WAXS and DSC are due to the differences in scanning rates. Figure 6.14 shows DSC traces for the bulk materials at 20 ºC/min, for comparison purposes. Regardless of the quantitative differences in T_c values due to different cooling rates, the fact remains that the PCL blocks crystallized first and to a larger extent (as judged by the WAXS signals relative intensities) than the PEO block. Also, in DSC, the crystallization enthalpy for the PCL blocks is much higher than that of the PEO block, as shown in Table 6.2 for the materials in bulk measured at 20 ºC/min, and in Table 6.3 for the experiments measured at 2 ºC/min. The subsequent DSC heating scan showed a first very small endothermic transition at 32.7 ºC attributed to the melting of the PEO block crystals, followed by two larger melting peaks at 48.3 and 53.3 ºC corresponding to the melting of PCL block crystals.

Table 6.2. DSC cooling and heating thermal transitions of the linear and 4-arm star block copolymers, measured in bulk at 20 ºC/min. Total enthalpies are provided when transitions are overlapped.

Sample	$T_{c,\,peak}$ [ºC] PCL or PEO	ΔH_c [J/g]	$T_{m,\,peak}$ [ºC] PCL or PEO	ΔH_m [J/g]
PCL_1-*b*-$PEO_{1.2}$-*b*-PCL_1	9.1	48.8	9.0; 31.3/38.1	1.3; 49.3
PCL_2-*b*-$PEO_{2.1}$-*b*-PCL_2	7.6/16.8	60.6	33.4; 43.4/49.7	11.2; 45.1
$(PEO_{1.2}$-*b*-$PCL_1)_4$	4.9; 13.7	63.5	24.3; 42.0	63.1
$(PEO_{2.5}$-*b*-$PCL_{1.4})_4$	1.5; 16.1	72.7	40.3; 46.7	79.8

Table 6.3. DSC cooling and heating thermal transitions of the linear and 4-arm star copolymers, measured in bulk and in 30 % w/v gels at 2 ºC/min. Total enthalpies are provided when transitions are overlapped.

	Sample state	$T_{c,\,peak}$ [ºC] PCL or PEO	ΔH_c [J/g]	$T_{m,\,peak}$ [ºC] PCL or PEO	ΔH_m [J/g]
PCL_1-*b*-$PEO_{1.2}$-*b*-PCL_1	Bulk	18.8	50.2	32.7; 38.7	25.5; 23.4
	Gel 30 % w/v	17.3	60.1	33.9; 40.5	24.4; 30.2
PCL_2-*b*-$PEO_{2.1}$-*b*-PCL_2	Bulk	18.1; 30.1	12.9; 44.8	32.7; 48.3/53.3	9.2; 23.1/19.3
	Gel 30 % w/v	35.3	41.6	50.4; 54.2	24.3; 14.2
$(PEO_{1.2}$-*b*-$PCL_1)_4$	Bulk	7.0/10.1; 29.3	16.2; 30.2	23.7; 39.4/ 46.3/50.7	14.2; 33.5
	Gel 30 % w/v	20.6; 28.6	46.6	31.4/36.9; 47.1/51.6	0.9/1.4; 15.3/0.3
$(PEO_{2.5}$-*b*-$PCL_{1.4})_4$	Bulk	22.9; 32.0	17.8; 37.1	29.5/33.5; 50.9	15.1; 40.3
	Gel 30 % w/v	19.5; 28.2	29.2; 23.7	28.8; 51.0	28.3; 17.0

Regarding the 4-arm star block copolymers, the bulk $(PEO_{1.2}$-*b*-$PCL_1)_4$ exhibits two main crystallization exotherms during cooling from the melt: a first peak at 29.3 ºC corresponding to the crystallization of the PCL blocks and a second bimodal peak at 10.1 and 7.0 ºC that can be attributed to the crystallization of the PEO blocks (Figure 6.12a, blue curves). WAXS results confirmed this crystallization behaviour, since the presence of the PCL_{110} and PCL_{200} reflections evidenced that the PCL blocks were the first blocks to crystallize (18 ºC), whereas the PEO block did it at lower temperatures (12 ºC) (Figure 6.13c). The subsequent DSC heating scans show a very complex set of thermal transitions upon increasing temperature. First, there is a very small melting peak at 23.7 ºC, assigned to the melting of the PEO blocks crystals. Then there is a broad and small cold-crystallization shallow exotherm possibly due to additional PCL block crystallization during the scan. Then there are three consecutive endothermic peaks at 39.4, 46.3 and 50.7 ºC that correspond to the melting of PCL blocks crystals.

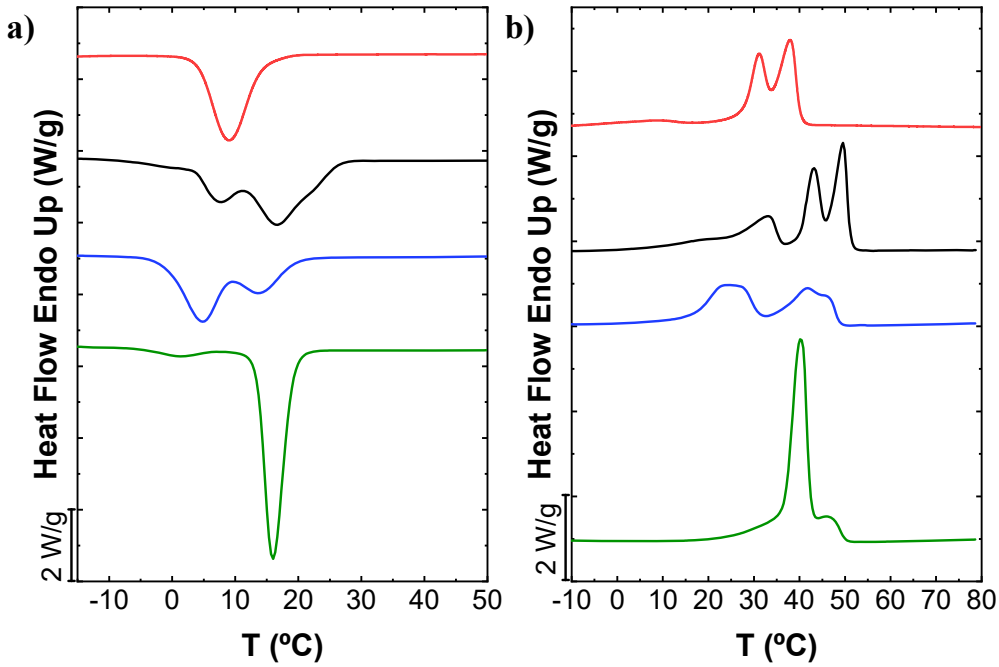

Figure 6.14. DSC **a)** cooling and **b)** heating scans at 20 ºC/min for the copolymers in bulk — PCL_1-*b*-$PEO_{1.2}$-*b*-PCL_1, — PCL_2-*b*-$PEO_{2.1}$-*b*-PCL_2, — $(PEO_{1.2}$-*b*-$PCL_1)_4$, — $(PEO_{2.5}$-*b*-$PCL_{1.4})_4$.

The bulk $(PEO_{2.5}$-*b*-$PCL_{1.4})_4$ star block copolymer shows a well-defined large crystallization peak at 32.0 ºC upon cooling from the melt, corresponding to the crystallization of the PCL blocks (Figure 6.12a, green curves), and a small peak at lower temperatures (22.9 ºC), related to the crystallization of the PEO blocks. WAXS results confirmed this crystallization behaviour (Figure 6.13d), since the presence of the PCL_{110} and PCL_{200} reflections confirmed that the PCL block was the first block to crystallize (24 ºC), whereas the peaks ascribed to the PEO block appeared at lower temperatures (15 ºC). The subsequent DSC heating scans revealed some small endothermic transitions at 29.5 and 33.5 ºC, probably due to the melting of PEO block crystals, while the main endothermic event occurring at higher temperatures is due to the melting of the PCL blocks at 50.9 ºC.

The final superstructural bulk morphology obtained by PLOM at 0 ºC of PCL_1-*b*-$PEO_{1.2}$-*b*-PCL_1 and PCL_2-*b*-$PEO_{2.1}$-*b*-PCL_2 linear triblock copolymers and $(PEO_{1.2}$-*b*-$PCL_1)_4$ and $(PEO_{2.5}$-*b*-$PCL_{1.4})_4$ 4-arm star block copolymers are shown in Figure 6.15, after cooling the samples at 20 ºC/min. All micrographs show very small spherulites. Since, in all cases, the PCL blocks are the first blocks

to crystallize in accordance with DSC results, small PCL spherulites are firstly formed. These PCL blocks spherulites can be considered templates within which the covalently bonded PEO blocks crystallize during finally forming in all cases, double crystalline spherulites, as we have demonstrated in previous works recently reviewed.[35–37]

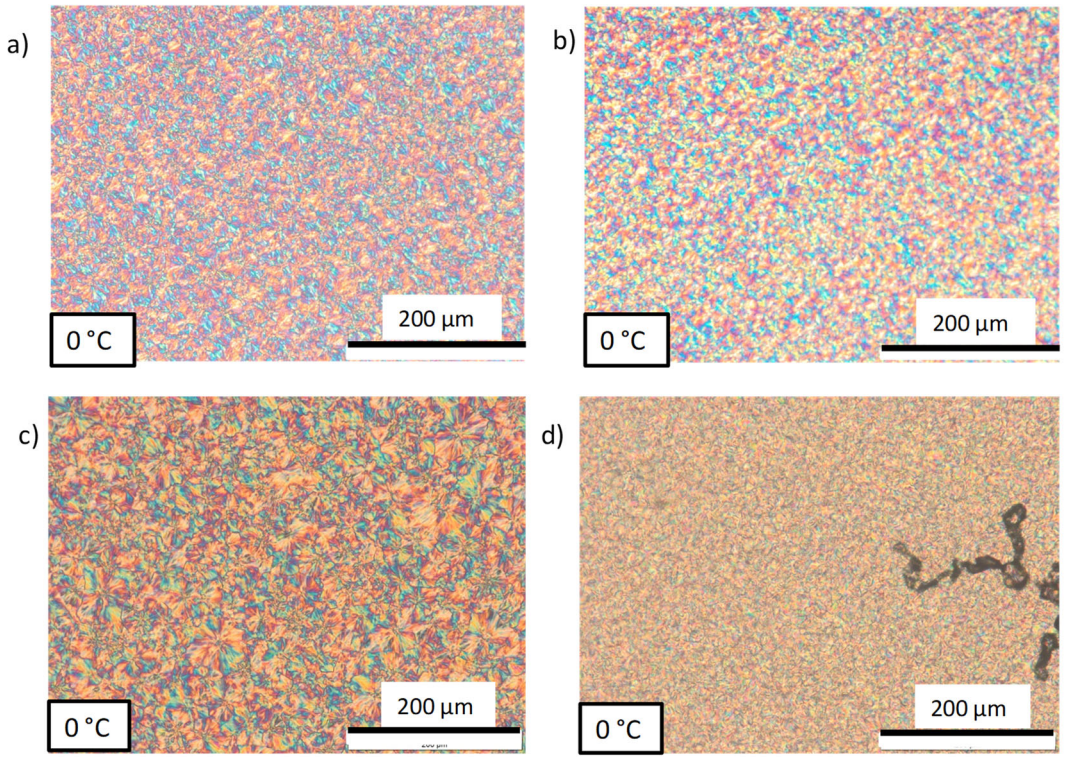

Figure 6.15. PLOM micrographs taken at 0 ºC after cooling the samples in bulk at 20 ºC/min for **a)** PCL_1-*b*-$PEO_{1.2}$-*b*-PCL_1, **b)** PCL_2-*b*-$PEO_{2.1}$-*b*-PCL_2, **c)** ($PEO_{1.2}$-*b*-PCL_1)$_4$, and **d)** ($PEO_{2.5}$-*b*-$PCL_{1.4}$)$_4$.

Now we focus on the DSC results obtained for hydrogels (30 % w/v) shown in Figure 6.12b. The 30 % w/v hydrogel from the PCL_1-*b*-$PEO_{1.2}$-*b*-PCL_1 triblock copolymer (Figure 6.12b, red curves) revealed a single exothermic peak located at 17.3 ºC, attributed to the PCL blocks crystallization. The heating scan showed two endothermic events corresponding to the melting of the PCL blocks crystals at 33.9 and 40.5 ºC (possibly due to the melting of folded and extended chains, respectively, as explained above for the same sample in bulk).

The gel formed by the PCL_2-*b*-$PEO_{2.1}$-*b*-PCL_2 triblock copolymer (Figure 6.12b, black curves) showed a single exothermic peak assigned to the PCL blocks

crystallization at 35.3 ºC; and two melting peaks located at 50.4 and 54.2 ºC corresponding to the melting of the PCL crystals, paralleling the behavior of the bulk sample but without any signals that can be attributed to the PEO crystallization or melting. As PEO is soluble in water, it is expected that it remains dissolved in the gel aqueous continuous phase during the crystallization and melting of the hydrophobic PCL component.

Regarding the hydrogels formed by the 4-arm star block copolymers, the gel from $(PEO_{1.2}$-*b*-$PCL_1)_4$ (Figure 6.12b, blue curves) exhibited two exothermic peaks during cooling at 28.6 and 20.6 ºC, which could be assigned to the crystallization of the PCL and PEO blocks, respectively. In the subsequent DSC heating scan, this gel showed two bimodal endothermic peaks: the first one at 31.4 and 36.9 ºC, which could correspond to the melting of the PEO blocks crystals, and a second one located at 47.1 and 51.6 ºC, due to the melting of PCL blocks crystals.

The $(PEO_{2.5}$-*b*-$PCL_{1.4})_4$ hydrogel (Figure 6.12b, green curves) exhibited two exothermic peaks during cooling, one corresponding to the crystallization of the PCL blocks (28.2 ºC) and another one at lower temperatures, which was ascribed to the crystallization of the PEO blocks (19.5 ºC). During the subsequent heating, this hydrogel showed two distinct endothermic peaks due to the melting of PEO block crystals at 28.8 ºC, and the second one at higher temperatures, corresponding to the melting of the PCL blocks crystals at 51.0 ºC. The results corresponding to DSC cooling and heating scans shown in Figure 6.12 are summarized in Tables 6.2 and 6.3.

In general terms, the thermal transitions associated with PCL and PEO blocks crystallization and melting observed for 30 % w/v hydrogels of linear and 4-arm star copolymers were similar to those encountered for the same copolymers in bulk. For linear copolymers, only PCL block crystallization was detected in the DSC of the hydrogels. However, hydrogels from 4-arm star copolymers, did show crystallization and melting of both PEO and PCL blocks. This is an unexpected

behavior as PEO blocks are hydrophilic and water-soluble; therefore, no crystallization was expected for these blocks. It is possible that PEO block crystallization is occurring in the star block copolymers due to their peculiar topology, whereupon PCL blocks crystallization, the PEO blocks are partially shielded from the water phase and can therefore crystallize. Our results thus suggest that there should be differences in the micellar organization within the gels of linear and star block copolymers, and this aspect will be further evaluated by SAXS measurements.

The morphology of the hydrogels formed from 30 % w/v aqueous solutions of the copolymers was also studied by PLOM and included in Figure 6.16. For the 30 % w/v as-prepared hydrogels from the linear triblock copolymers, a birefringent superstructural morphology (resembling ill-defined spherulites) was observed (Figures 6.16a and 6.16c). After subsequent heating and cooling from 60 to 5 ºC, better-defined small spherulites (with Maltese crosses and a negative sign in the case of PCL_1-*b*-$PEO_{1.2}$-*b*-PCL_1, see Figure 6.16b) could be observed (Figures 6.16b and 6.16d), which should contain only PCL blocks lamellae. For the PCL_1-*b*-$PEO_{1.2}$-*b*-PCL_1 hydrogel, the appearance of spherulites was first seen at 29 ºC (after having been previously melted at 37 ºC), whereas the PCL_2-*b*-$PEO_{2.1}$-*b*-PCL_2 gel exhibited the first spherulites at 38 ºC (after having been previously melted at 49 ºC). In the case of the hydrogels prepared from the 4-arm star copolymers, the superstructural texture was too fine to be detected by PLOM at 5 ºC (Figures 6.16e-f), indicating that these materials probably form sub-micron double crystalline spherulites, as in these cases, both PCL and PEO blocks can crystallize according to the DSC results of Figure 6.12b.

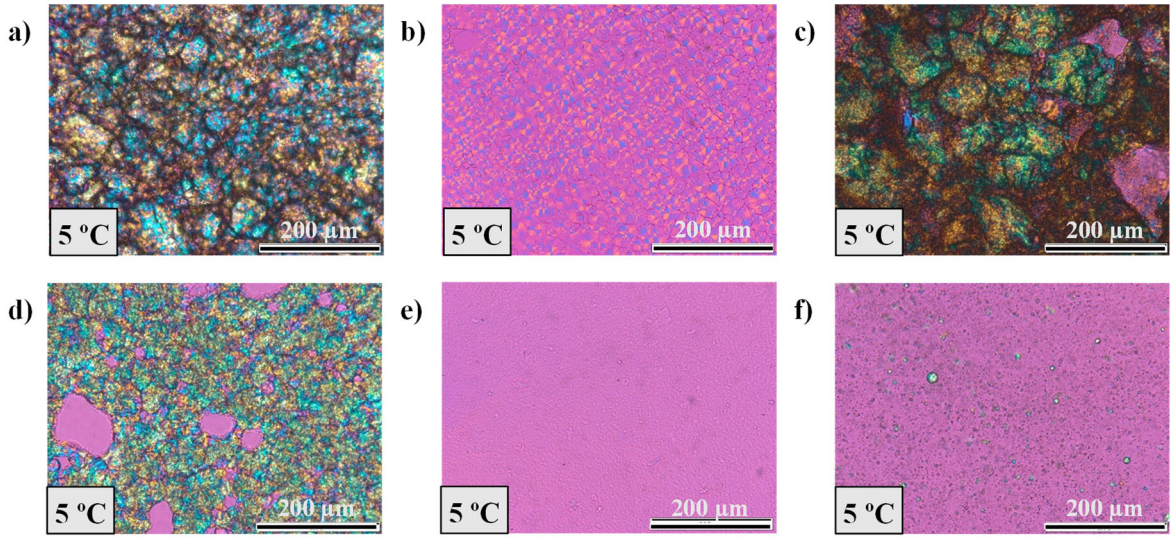

Figure 6.16. PLOM micrographs taken at 5 ºC after cooling the 30 % w/v at 2 ºC/min for **a)** PCL_1-*b*-$PEO_{1.2}$-*b*-PCL_1 (before heating/cooling steps), **b)** PCL_1-*b*-$PEO_{1.2}$-*b*-PCL_1, **c)** PCL_2-*b*-$PEO_{2.1}$-*b*-PCL_2 (before heating/cooling steps), **d)** PCL_2-*b*-$PEO_{2.1}$-*b*-PCL_2, **e)** $(PEO_{1.2}$-*b*-$PCL_1)_4$, and **f)** $(PEO_{2.5}$-*b*-$PCL_{1.4})_4$.

Synchrotron radiation SAXS constitutes a powerful tool to determine the self-assembly and network structure of polymer hydrogels.[38,39] The results corresponding to 30 % w/v hydrogels of linear triblock copolymers are shown in Figures 6.17a and 6.17b. It must be noted that these experiments were performed on gel samples that had been prepared by previously cooling to 5 ºC and stored at that temperature for two months, before they were measured at the synchrotron during heating from 5 ºC until 80 ºC at 2 ºC/min.

The SAXS profiles exhibit a broad scattering peak (denoted as P_1 in the figure) located at q = 0.35 nm^{-1} for both PCL_1-*b*-$PEO_{1.2}$-*b*-PCL_1 and PCL_2-*b*-$PEO_{2.1}$-*b*-PCL_2. In the case of PCL_1-*b*-$PEO_{1.2}$-*b*-PCL_1, the correlation peak (P_1) is more clear (in fact, it would seem that a second-order minor reflection, P_2, can be observed at q = 0.71 nm^{-1}) and substantially decreases with the temperature above 35 ºC and at 42 ºC, it tends to disappear, coinciding with the end of the PCL block crystals melting (i.e., 43 ºC, see Figure 6.12b). For PCL_2-*b*-$PEO_{2.1}$-*b*-PCL_2, the P_1 peak is less defined and broad (without any traces of a second-order peak) and tends to disappear at higher temperatures (above 51 ºC), also in agreement with the end of the PCL blocks melting endotherm in Figure 6.12b (i.e., 55 ºC), although

it is not as straightforward as in the case of the other gel formed by the PCL_1-*b*-$PEO_{1.2}$-*b*-PCL_1 sample. The position of the SAXS correlation peak (P_1) corresponds to a long period of approximately 18.0 nm for both PCL_1-*b*-$PEO_{1.2}$-*b*-PCL_1 and PCL_2-*b*-$PEO_{2.1}$-*b*-PCL_2 that reflects the average spacing between hydrophobic and semicrystalline aggregates formed by PCL domains. A possible schematic representation of the hydrogel microstructure is given in the inset of the figures in analogy with semicrystalline stereocomplexed physical hydrogels reported elsewhere.[40]

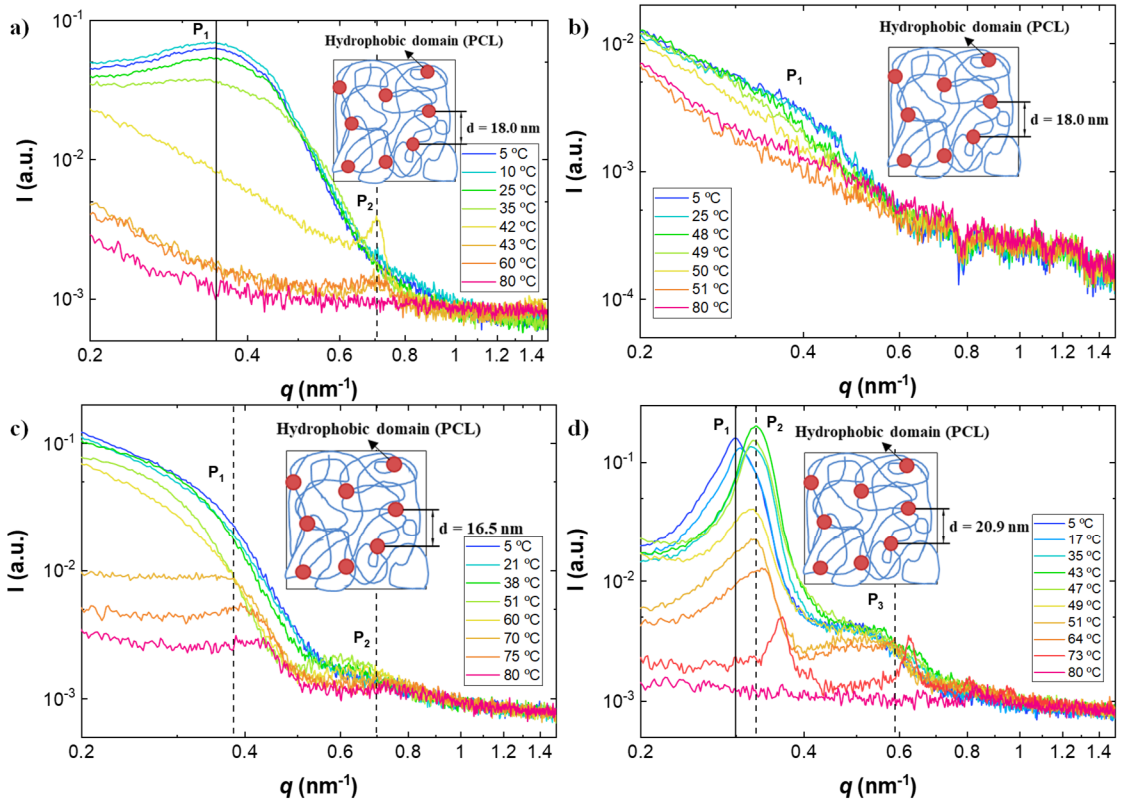

Figure 6.17. SAXS diffractograms obtained during the heating at 2 ºC/min of the 30 % w/v gels: **a)** PCL_1-*b*-$PEO_{1.2}$-*b*-PCL_1, **b)** PCL_2-*b*-$PEO_{2.1}$-*b*-PCL_2, **c)** $(PEO_{1.2}$-*b*-$PCL_1)_4$, and **d)** $(PEO_{2.5}$-*b*-$PCL_{1.4})_4$.

As to star block copolymers, the 30 % w/v hydrogel from $(PEO_{1.2}$-*b*-$PCL_1)_4$, shows a broad knee-like feature around q = 0.4 nm^{-1} (P_1) in the SAXS scattering profile (Figure 6.17c) assigned to the long spacing L between crystalline domains of PCL that disappears at temperatures above 60 ºC in agreement with DSC results (Figure 6.12b). Interestingly, at temperatures above 60 ºC, two scattering peaks at

q = 0.38 nm^{-1} (P_1) and q = 0.70 nm^{-1} (P_2) are observed, which could be attributed to micellar ordering upon heating as it will be confirmed by SAXS experiments obtained during cooling discussed below. Figure 6.17d shows the scattering profile corresponding to the 30 % w/v hydrogel of $(PEO_{2.5}$-*b*-$PCL_{1.4})_4$. At 5 ºC, the scattering profile presents a broad scattering peak constituted by two overlapped peaks at q = 0.30 nm^{-1} (P_1) and q = 0.32 nm^{-1} (P_2) followed by a broad scattering peak at q ~0.5 nm^{-1} (P_3). Upon heating to 28 ºC, the scattering peak at q = 0.30 nm^{-1} corresponding to a long distance of 20.9 nm disappears, which is coincident with the melting point of the PEO blocks crystals shown by DSC (Figure 6.12b). The SAXS curves recorded in the temperature range from 28 to 51 ºC show the occurrence of two scattering peaks at approximately q = 0.32 nm^{-1} (P_2) and q ~0.59 nm^{-1} (P_3), which could correspond to first and second-order diffraction peaks respectively. Both peaks disappear at temperatures above 51 ºC, and according to DSC results for this sample (Figure 6.12b), the melting temperature observed for PCL blocks crystals corresponds to 54 ºC. The results are reminiscent of the structure Kepola et al. proposed for a different block copolymer star network.[41] In that system, self-assembly leads to a lamellar structure perpendicular to the sheets, which gives rise to a secondary assembly in water in which the hydrophobic cores in the micelles organize in 2D to produce lamellae.

To shed further light into the microstructure of hydrogels from 4-arm star copolymers, SAXS diffractograms were recorded upon cooling of 30 % w/v aqueous solutions of $(PEO_{1.2}$-*b*-$PCL_1)_4$, and $(PEO_{2.5}$-*b*-$PCL_{1.4})_4$, and the results are shown in Figure 6.18. Information about SAXS experiments performed on linear triblock copolymers is shown in Figure 6.19. The SAXS profiles show the occurrence of well-defined scattering peaks that can be attributed to the micellar organization and crystallization of the blocks within the gels. As is well known, as the concentration is increased in semidilute or concentrated block copolymer solutions, chains begin to overlap, and this can lead to the formation of a liquid crystalline phase such as a cubic phase of spherical micelles, a hexagonal phase of rodlike micelles, a lamellar phase or a bicontinuous cubic phase.[42]

The results obtained for the $(PEO_{1.2}$-*b*-$PCL_1)_4$ gel (Figure 6.18a) show the appearance of two broad scattering peaks at 80 ºC located at q = 0.44 and q = 0.80 nm^{-1}, which could be attributed to micellar formation in analogy to the SAXS scattering curves obtained during heating where similar reflections appeared at temperatures above 60 ºC (Figure 6.17c). It is important to note that the sol-gel transition for this material is located at ~75 ºC as determined through inverted vial tests (Figure 6.10a), which would be consistent with the results obtained. At 50 ºC, the SAXS pattern in Figure 6.18a shows two reflections located at approximately q = 0.32 nm^{-1} (P_1) and q = 0.60 nm^{-1} (P_2), which could be interpreted as the formation of a lamellar morphology arising from the organization of the PCL hydrophobic cores in two dimensions, before crystallization. According to Figure 6.12b, the PCL blocks start to crystallize below 35 ºC, and the two SAXS reflections slightly shift positions. Figures 6.17c and 6.18a do not show similar SAXS patterns at low temperatures (below 20 ºC), because even though they correspond to the same samples, they have different thermal histories. In the first case, the samples were stored at 5 ºC for several days before heating them (giving ample time for gel structuring and blocks crystallization to saturation) and in the second time, the samples were measured in situ during cooling from the sol state.

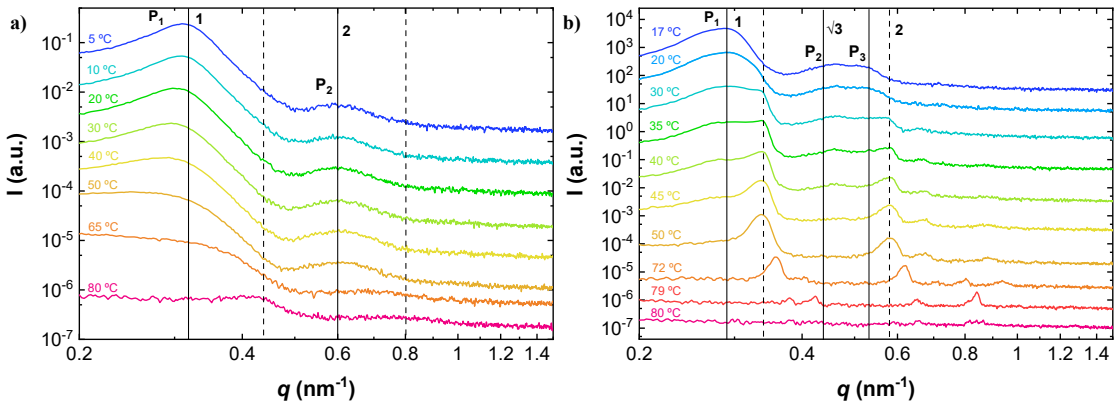

Figure 6.18. SAXS diffractograms measured at 2 ºC/min during the cooling process for the 30 % w/v gels: **a)** $(PEO_{1.2}$-*b*-$PCL_1)_4$, and **b)** $(PEO_{2.5}$-*b*-$PCL_{1.4})_4$. For easier visualization, scattering curves obtained at different temperatures have been vertically shifted. Dashed lines correspond to scattering peaks at 60 ºC whereas solid lines correspond to scattering peaks at 5 ºC (for the $(PEO_{1.2}$-*b*-$PCL_1)_4$ sample) and 17 ºC (for the $(PEO_{2.5}$-*b*-$PCL_{1.4})_4$ sample).

The $(PEO_{2.5}$-*b*-$PCL_{1.4})_4$ 30 % w/v aqueous solution (Figure 6.18b) shows a different scattering profile. At 80 ºC, no significant scattering was observed. However, upon cooling the solution, some ordering takes place. At lower temperatures, two peaks start to appear at q values of ~0.4 and ~0.6 nm^{-1}, and shift towards lower q values when temperature decreases. Eventually, at 50 ºC two well-defined reflections appeared at q = 0.34 nm^{-1} and q = 0.58 nm^{-1}, which are progressively transformed in shape as temperature decreases, as new reflections appear on the left-hand side of each peak. The structure of the solution at 50 ºC does not seem to correspond to highly ordered lamellae, as the reflections are not in the expected ratio of 1:2:3:4. It may correspond to distorted or not very well ordered lamellae, as the reflections observed are broad, i.e., to a pseudo-lamellar structure.

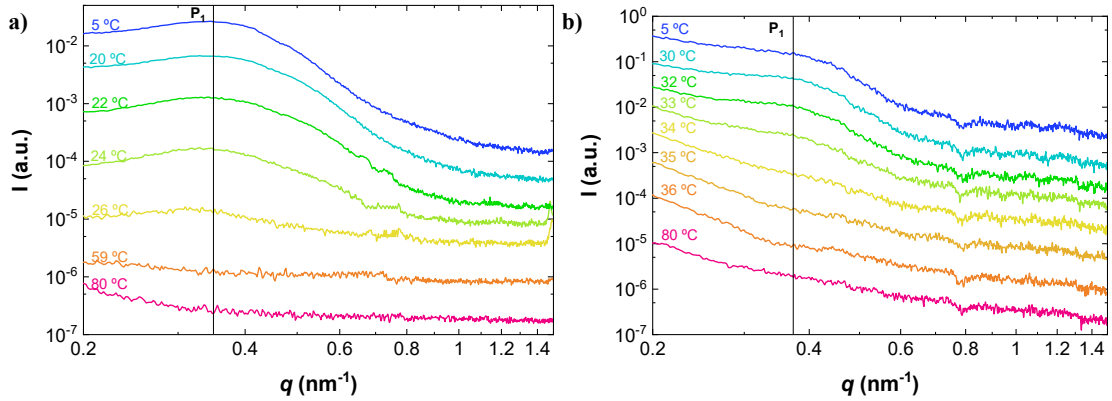

Figure 6.19. SAXS diffractograms measured at 2 ºC/min during the cooling process for the 30 % w/v gels from the linear triblock copolymers: **a)** PCL_1-*b*-$PEO_{1.2}$-*b*-PCL_1, and **b)** PCL_2-*b*-$PEO_{2.1}$-*b*-PCL_2.

At 45 ºC, a broad shoulder can be observed at q = 0.29 nm^{-1} (P_1) in Figure 6.18b that increases in intensity and shifts to lower q with the decrease in temperature. At the same time, a broad shoulder constituted of two overlapped peaks at q = 0.44 nm^{-1} (P_2) and q = 0.53 nm^{-1} (P_3) is observed within the same temperature range. The three peaks observed are in agreement with a hexagonal cylinder-like structure with the relative q-ratios 1:√3:2. Once again, we note that the reflections are quite broad; hence the degree of ordering of these cylinders is not very high. A similar structure has been proposed for a 4-arm PEO-*b*-PPO star

block copolymer, where PPO self-assembly gives rise to micelles that combine 2D lamellar sheets into hexagonal cylindrical structures.[43] Hence, our results suggest a thermally induced transition from a pseudo-lamellar structure to a hexagonal cylindrical structure upon cooling. DSC results in Figure 6.12b showed the occurrence of crystallization of the PCL blocks at temperatures below 35 ºC and of the PEO blocks at temperatures below 23 ºC. The fact that the PCL blocks crystallize first, followed by the PEO crystallization might be related to the thermally induced transition from pseudo-lamellar to hexagonal assembly observed for the ($PEO_{2.5}$-*b*-$PCL_{1.4}$) hydrogel and points to an influence of the crystallinity of the PEO and the PCL blocks on the micellar arrangement on the hydrogel. A schematic and highly idealized representation of the structure proposed for the hydrogels of 4-arm star block copolymers is shown in Figure 6.20. More experiments are currently in progress to further elucidate the micellar organization of the linear and star block copolymers in dilute solutions.

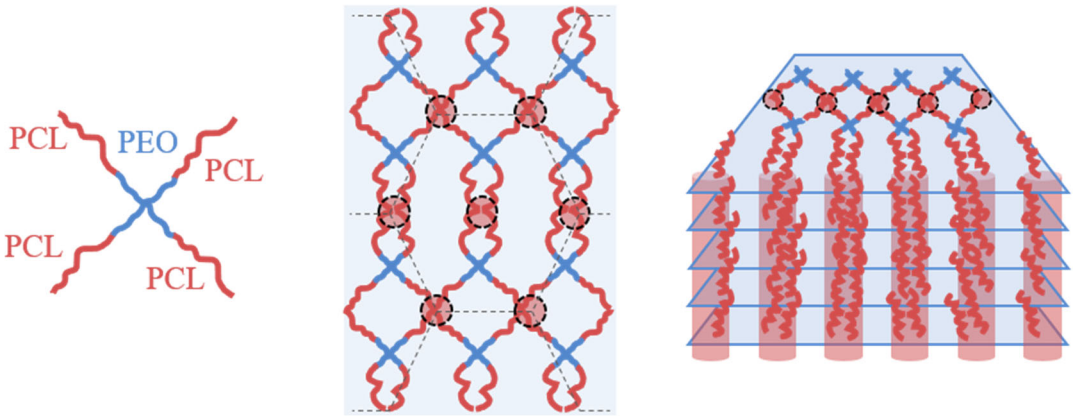

Figure 6.20. Schematic structure corresponding to 30 % w/v hydrogels of ($PEO_{1.2}$-*b*-PCL_1)$_4$, and ($PEO_{2.5}$-*b*-$PCL_{1.4}$)$_4$ where it can be observed how PCL cores organize into a 2D lamellar structures. For sample ($PEO_{2.5}$-*b*-$PCL_{1.4}$)$_4$, a thermally induced transition at temperatures below 45 ºC is observed, the PCL polymer blocks assemble adjacent lamellas in cylinder-like PCL domains, which organize themselves perpendicular to the sheets in a hexagonal pattern.

6.3.4. 3D extrusion printing of 4-arm star block copolymers. Proof-of-concept of their employment as sacrificial biomaterial inks

3D extrusion printing is based on the design of prototypes through the deposition of a material layer by layer. It is a technology widely employed in biomedicine to manufacture polymer scaffolds for tissue engineering. To that aim, hydrogels are used as biomaterial inks that can be smoothly extruded and deposited on a surface giving rise to polymer scaffolds with high shape fidelity. However, their swelling after being extruded, their lower mechanical resistance, and the difficulty in generating hollow structures remain a current challenge for their employment in 3D extrusion (bio)printing. To that aim, sacrificial biomaterial inks with suitable mechanical properties and a rapid degradation profile can be employed to provide mechanical support and improve the printability of multicomponent biomaterial inks. Sacrificial inks can be eliminated through simple dissolution in physiological conditions, hence facilitating the formation of hollow tubular structures.[44–49]

Taking into account that 4-arm star block copolymers are hydrogels at room temperature, as shown through inverted vial tests and rheological experiments shown in Figures 6.10a and 6.11b, they were further investigated for their potential employment as biomaterial inks in 3D extrusion (bio)printing. Figure 6.21a shows the results of oscillatory rheological experiments that determined the gels storage moduli at room temperature as a function of frequency for 20 and 30 % w/v hydrogels. Except for the $(PEO_{2.5}\text{-}b\text{-}PCL_{1.4})_4$ sample at a polymer concentration of 20 % w/v, all the samples presented the characteristic behaviour of a gel, where the elastic and the loss moduli were practically independent of the frequency, being G' higher than G″ over the entire tested frequency range. G' increased from 2700 to 10,100 Pa for the $(PEO_{1.2}\text{-}b\text{-}PCL_1)_4$ hydrogel when the polymer concentration increased from 20 to 30 % w/v. As to the hydrogels obtained from $(PEO_{2.5}\text{-}b\text{-}PCL_{1.4})_4$, G' was 24000 Pa for a polymer concentration of 30 % w/v. At 20 % w/v, G' and G'' are very dependent on frequency even if G' was higher than G'', which is characteristic of a weak gel. From the results obtained, it is clear that the elastic

moduli are highly dependent on polymer concentration, which is a characteristic behaviour of physical hydrogels.

Polymer hydrogels employed as biomaterial inks for 3D extrusion printing must exhibit shear thinning and self-healing properties that manifest in the instantaneous response of the gel modulus to changes in the applied strain.[50] Cyclic shear-thinning experiments corresponding to 30 % w/v hydrogels from 4-arm star block copolymers, $(PEO_{1.2}$-*b*-$PCL_1)_4$ and $(PEO_{2.5}$-*b*-$PCL_{1.4})_4$ are shown in Figure 6.21b. In this experiment, gels were subjected to three cycles of low (0.1 %) and two cycles of high (100 %) strains for 200 s. Both hydrogels showed a marked decrease in G' moduli at high strains and immediate recovery at low strains for each cyclic test. The $(PEO_{2.5}$-*b*-$PCL_{1.4})_4$ sample , being a stronger gel, presents G' values of 31,000 and 3000 Pa at 0.1 % and 100 % strain, respectively, whereas for $(PEO_{1.2}$-*b*-$PCL_1)_4$ G' decreases to 11000 and 1100 for 0.1 and 100 % strain, respectively. It is important to note that even if the sample $(PEO_{2.5}$-*b*-$PCL_{1.4})_4$ presented a higher elastic modulus than the sample $(PEO_{1.2}$-*b*-$PCL_1)_4$, it also exhibited higher mechanical hysteresis between strain cycles, losing 64 % of the initial value of G' when subjected to large strains, whereas the $(PEO_{1.2}$-*b*-$PCL_1)_4$ sample displayed minimal mechanical hysteresis between strain cycles. The results showed that both samples are suitable as biomaterial inks for 3D extrusion printing because they can be extruded during printing and maintain sufficient mechanical integrity necessary to support printed layers.

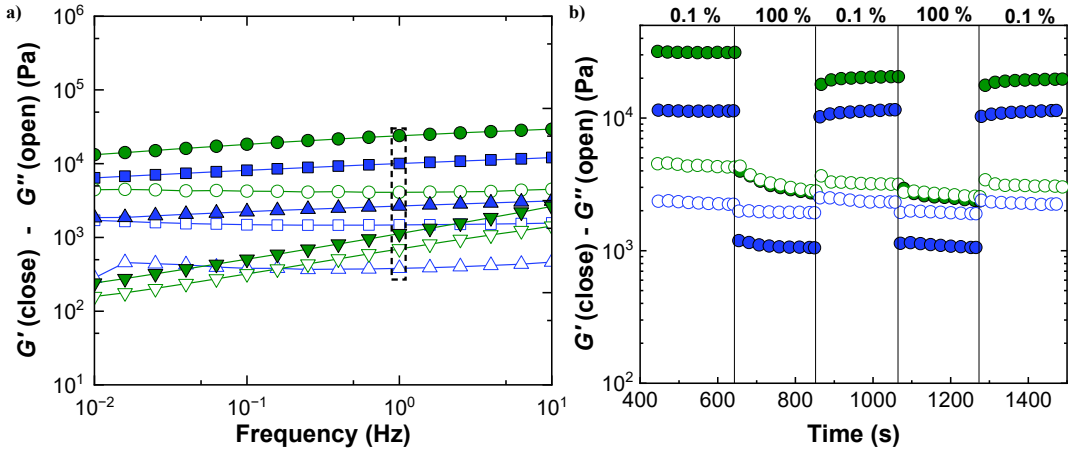

Figure 6.21. a) Dynamic oscillatory frequency sweep experiments showing storage, G' (close) and loss, G'' (open) moduli for: ■ $(PEO_{1.2}$-*b*-$PCL_1)_4$ (30 % w/v), ▲ $(PEO_{1.2}$-*b*-$PCL_1)_4$ (20 % w/v), ● $(PEO_{2.5}$-*b*-$PCL_{1.4})_4$ (30 % w/v), ▼ $(PEO_{2.5}$-*b*-$PCL_{1.4})_4$ (20 % w/v). The dashed rectangle remarks the G' and G'' values at 1 Hz. **b)** Cyclic shear-thinning experiment showing G' (close) and G'' (open) response and recovery to high (100 %) and low (0.1 %) oscillatory strains: ● $(PEO_{1.2}$-*b*-$PCL_1)_4$ (30 % w/v), ● $(PEO_{2.5}$-*b*-$PCL_{1.4})_4$ (30 % w/v).

Next, the ability to obtain 3D printed structures from 4-arm star block copolymers was demonstrated through the extrusion of 30 % w/v hydrogels formed upon cooling $(PEO_{1.2}$-*b*-$PCL_{1.4})_4$ and $(PEO_{2.5}$-*b*-$PCL_{1.4})_4$ aqueous solutions. As can be observed in Figure 6.22a, cylindrical shape structures were obtained through the stacking of 5 layers (1.1 mm height) and 4 layers (0.8 mm height) for $(PEO_{1.2}$-*b*-$PCL_{1.4})_4$ and $(PEO_{2.5}$-*b*-$PCL_{1.4})_4$, respectively. The SEM images of lyophilized 3D printed structures (Figure 6.22b, right) confirmed that both samples stacked correctly in well-differentiated layers that preserved their shape over time after printing, where individual filaments were well-defined and showed a smooth surface with no porosity at the macroscale (Figure 6.22b, left). Further magnification of the images corresponding to individual filaments allowed to observe a porous morphology with pore size in the micron range (Figure 6.22b, right).

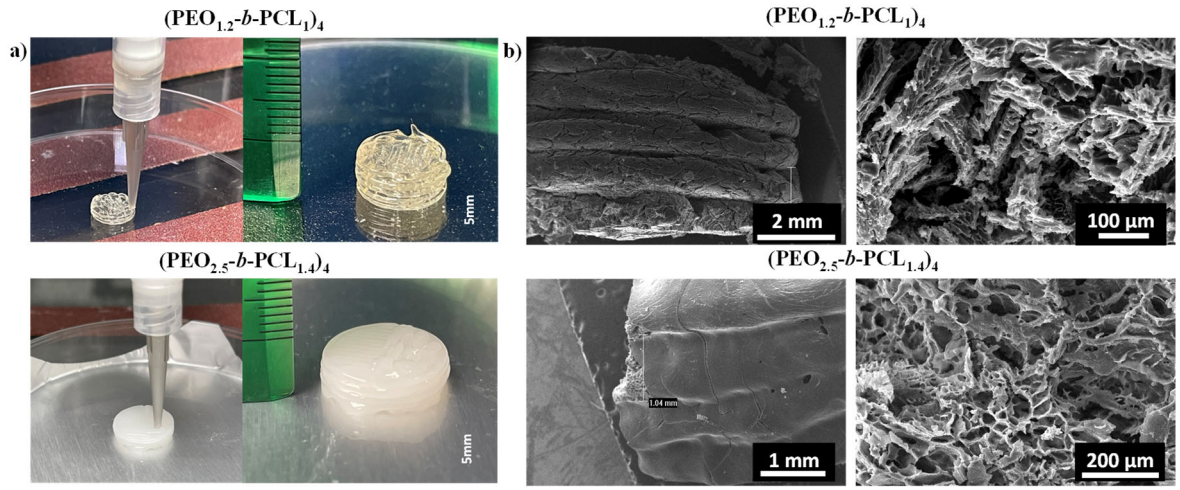

Figure 6.22. a) Extrusion-based printing setup (nozzle: conical; 1.2 mm inner diameter; speed: 1 mm/min; 1 mm layer height) (left) and printed structures showing 5-layer stacking scaffolds of 30 % w/v $(PEO_{1.2}$-*b*-$PCL_1)_4$ hydrogels (right, up) and 6-layer stacking scaffolds of 30 % w/v $(PEO_{2.5}$-*b*-$PCL_{1.4})_4$ hydrogels (right, down) and, **b)** SEM images corresponding to 30 % w/v 4-arm star copolymer hydrogels: stacking layers obtained through layer by layer 3D extrusion printing (left) and porous morphology in the micron size (right).

Dissolution tests carried out in the water at 37 ºC showed full dissolution of the $(PEO_{2.5}$-*b*-$PCL_{1.4})_4$ hydrogel after 15 minutes, whereas the hydrogel of $(PEO_{1.2}$-*b*-$PCL_1)_4$ dissolved after 60 minutes (Figure 6.23a). Hence, this latter sample was selected for a proof-of-concept for its employment as sacrificial biomaterial ink. Figure 6.23b shows the setup employed for constructing concentric tubes through coaxial printing consisting of the printing of an aqueous solution of alginate as an outer layer and a $(PEO_{1.2}$-*b*-$PCL_1)_4$ hydrogel as the inner layer. Dissolution of the inner part of the concentric tube yielded hollow alginate tubes that can be observed in Figure 6.23c, and hence, the potential employment of 4-arm star block copolymers as sacrificial biomaterial inks was demonstrated.

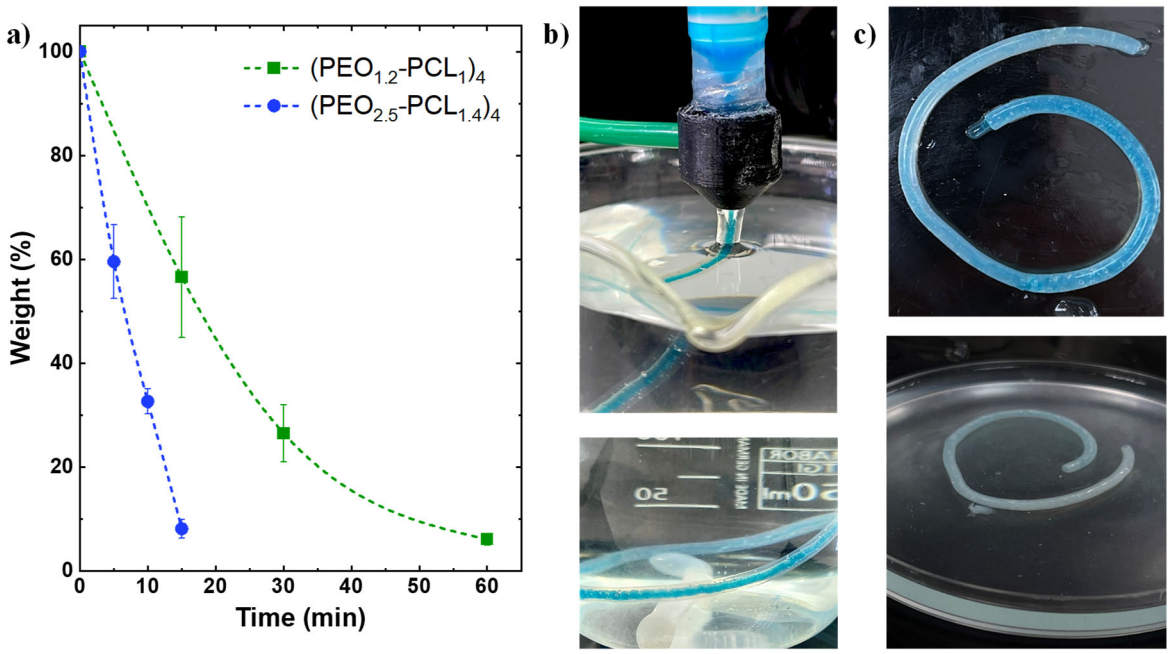

Figure 6.23. a) Dissolution tests of 30 % w/v hydrogels of ● $(PEO_{1.2}$-*b*-$PCL_1)_4$ and ■ $(PEO_{2.5}$-*b*-$PCL_{1.4})_4$ carried out in water at 37 ºC, **b)** coaxial printing of a concentric tube consisting of an alginate hydrogel (outer tube/transparent) and a hydrogel of $(PEO_{1.2}$-*b*-$PCL_1)_4$ (inner tube/blue) and, **c)** dissolution of the inner tubular structure, by immersion in water at 37 ºC for 1 h.

6.4. Conclusions

In this Chapter, hydrogel formation from aqueous solutions of model block copolymers of poly(ε-caprolactone) (PCL) and poly(ethylene oxide) (PEO) was evaluated as a function of chain topology (linear and 3 and 4 arms star copolymers) with block copolymer molecular weights of PEO and PCL of ~1000 and ~2000 g/mol. Upon heating, linear PCL-*b*-PEO-*b*-PCL triblock copolymers present a $T_{sol\text{-}gel}$ followed by a $T_{gel\text{-}sol}$, a characteristic behaviour of micellar physical hydrogels already reported in the literature that marks the formation of a gel through micellar packing and its subsequent melting with temperature. In contrast, 4-arm star block copolymers form hydrogels upon cooling to 0 ºC characterized by a single $T_{gel\text{-}sol}$ depending on polymer concentration in the gel. The 3-arm star block copolymer sample did not form hydrogels on the range of temperatures and concentrations under study. The results were attributed mainly to the PEO/PCL ratio that increases in the order: linear < 4-arm < 3-arm star block copolymers.

The use of synchrotron *in situ* WAXS, SAXS, and DSC was found to be essential to determine the crystalline organization of each of the blocks within hydrogels obtained from linear and 4-arm star block copolymers through comparison with results obtained in the bulk copolymers. Interestingly, the results showed the occurrence of PEO and PCL blocks crystallization within hydrogels obtained from 4-arm star copolymers, whereas hydrogels of linear triblock copolymers only showed PCL block crystallization. The occurrence of PEO and PCL crystallization on hydrogels of 4-arm star block copolymers might lie on the base of gel formation upon cooling of aqueous solutions of these copolymers. It is suggested that both hydrogels from 4-arm block copolymers organize into a lamellar structure upon cooling. The increase in the molecular weight of the PEO block leads to further organization of the lamellar structure into hexagonal cylinders upon cooling. More experiments are now in progress to elucidate micelle self-assembly in aqueous solutions of the linear and star block copolymers under study.

Finally, 3D printed structures with high shape fidelity and well-stacked layers could be obtained from 30 % w/v hydrogels of 4-arm shape block copolymers through 3D direct ink printing. A proof of concept on the suitability of using a $(PEO_{1.2}$-*b*-$PCL_1)_4$ hydrogel as sacrificial biomaterial ink was provided. Rapid dissolution of this hydrogel together with a high elastic modulus, allowed the construction of hollow tubular structures through 3D direct coaxial extrusion printing. To sum up, the research exposed in this Chapter expands the knowledge of the self-assembly of block copolymers with crystallizable blocks to form hydrogels, studying their structural organization as a function of copolymer architecture and paving their way to their application as polymer biomaterial inks for 3D direct printing.

6.5. References

1. Perin, F.; Motta, A.; Maniglio, D., Amphiphilic copolymers in biomedical applications: Synthesis routes and property control. *Materials Science and Engineering C* **2021**, *123*, 111952. DOI: 10.1016/j.msec.2021.111952.

2. Kulkarni, B.; Qutub, S.; Ladelta, V.; Khashab, N. M.; Hadjichristidis, N., AIE-Based Fluorescent Triblock Copolymer Micelles for Simultaneous Drug Delivery and Intracellular Imaging. *Biomacromolecules* **2021**, *22* (12), 5243–5255. DOI: 10.1021/acs.biomac.1c01165.

3. Shi, J.; Yu, L.; Ding, J., PEG-based thermosensitive and biodegradable hydrogels. *Acta Biomaterialia* **2021**, *128*, 42–59. DOI: 10.1016/j.actbio.2021.04.009.

4. Chen, X.; Zhang, J.; Wu, K.; Wu, X.; Tang, J.; Cui, S.; Cao, D.; Liu, R.; Peng, C.; Yu, L.; Ding, J., Visualizing the In Vivo Evolution of an Injectable and Thermosensitive Hydrogel Using Tri-Modal Bioimaging. *Small Methods* **2020**, *4* (9), 1–11. DOI: 10.1002/smtd.202000310.

5. Yang, X.; Chen, X.; Wang, Y.; Xu, G.; Yu, L.; Ding, J., Sustained release of lipophilic gemcitabine from an injectable polymeric hydrogel for synergistically enhancing tumor chemoradiotherapy. *Chemical Engineering Journal* **2020**, *396*, 125320. DOI: 10.1016/j.cej.2020.125320.

6. Wu, K.; Chen, X.; Gu, S.; Cui, S.; Yang, X.; Yu, L.; Ding, J., Decisive Influence of Hydrophobic Side Chains of Polyesters on Thermoinduced Gelation of Triblock Copolymer Aqueous Solutions. *Macromolecules* **2021**, *54* (16), 7421–7433. DOI: 10.1021/acs.macromol.1c00959.

7. Wang, Y.; Yang, X.; Chen, X.; Wang, X.; Wang, Y.; Wang, H.; Chen, Z.; Cao, D.; Yu, L.; Ding, J., Sustained Release of Nitric Oxide and Cascade Generation of Reactive Nitrogen/Oxygen Species via an Injectable Hydrogel for Tumor Synergistic Therapy. *Advanced Functional Materials* **2022**, *32* (36), 2206554. DOI: 10.1002/adfm.202206554.

8. Chen, X.; Wang, H.; Shi, J.; Chen, Z.; Wang, Y.; Gu, S.; Fu, Y.; Huang, J.; Ding, J.; Yu, L., An injectable and active hydrogel induces mutually enhanced mild magnetic hyperthermia and ferroptosis. *Biomaterials* **2023**, *298*, 122139. DOI: 10.1016/j.biomaterials.2023.122139.

9. Bae, S. J.; Suh, J. M.; Sohn, Y. S.; Bae, Y. H.; Kim, S. W.; Jeong, B., Thermogelling poly(caprolactone-b-ethylene glycol-b-caprolactone) aqueous solutions. *Macromolecules* **2005**, *38* (12), 5260–5265. DOI: 10.1021/ma050489m.

10. Bae, S. J.; Joo, M. K.; Jeong, Y.; Kim, S. W.; Lee, W. K.; Sohn, Y. S.; Jeong, B., Gelation behavior of poly(ethylene glycol) and polycaprolactone triblock and multiblock copolymer aqueous solutions. *Macromolecules* **2006**, *39* (14), 4873–4879. DOI: 10.1021/ma060153s.

11. Cai, B. L.; Chang, Y. G.; Mei, J. H.; Ji, W. W.; Yi, F. P.; Yang, D. Z.; Guo, Z. L.; Ma, L. G.; Wang, K.; Ming, J. T.; Yu, Q. W.; Qian, Z. Y., Thermoreversible gel-sol behavior of biodegradable PCL-PEG-PCL triblock copolymer in aqueous solutions. *Journal of Biomedical Materials Research - Part B Applied Biomaterials* **2008**, *84* (1), 165–175. DOI: 10.1002/jbm.b.30858.

12. Kim, K. H.; Cui, G. H.; Lim, H. J.; Huh, J.; Ahn, C. H.; Jo, W. H., Synthesis and micellization of star-shaped poly(ethylene glycol)-block-poly(ε-caprolactone). *Macromolecular Chemistry and Physics* **2004**, *205* (12), 1684–1692. DOI: 10.1002/macp.200400084.

13. Lu, C.; Liu, L.; Guo, S. R.; Zhang, Y.; Li, Z.; Gu, J., Micellization and gelation of aqueous solutions of star-shaped PEG-PCL block copolymers consisting of branched 4-arm poly(ethylene glycol) and polycaprolactone blocks. *European Polymer Journal* **2007**, *43* (5), 1857–1865. DOI: 10.1016/j.eurpolymj.2007.02.039.

14. Buwalda, S. J.; Nottelet, B.; Coudane, J., Robust & thermosensitive poly(ethylene glycol)-poly(ε-caprolactone) star block copolymer hydrogels. *Polymer Degradation and Stability* **2017**, *137*, 173–183. DOI: 10.1016/j.polymdegradstab.2017.01.015.

15. Forgham, H.; Zhu, J.; Qiao, R.; Davis, T. P., Star Polymer Nanomedicines-Challenges and Future Perspectives. *ACS Applied Polymer Materials* **2022**, *4* (10), 6784–6796. DOI: 10.1021/acsapm.2c01291.

16. Kasinski, A.; Zielinska-Pisklak, M.; Kowalczyk, S.; Plichta, A.; Zgadzaj, A.; Oledzka, E.; Sobczak, M., Synthesis and characterization of new biodegradable injectable thermosensitive smart hydrogels for 5-fluorouracil delivery. *International Journal of Molecular Sciences* **2021**, *22* (15), 8330. DOI: 10.3390/ijms22158330.

17. Steinman, N. Y.; Bentolila, N. Y.; Domb, A. J., Effect of molecular weight on gelling and viscoelastic properties of poly(caprolactone)-b- poly(ethylene glycol)-b-poly(caprolactone) (PCL-PEG-PCL) hydrogels. *Polymers* **2020**, *12* (10), 2372. DOI: 10.3390/polym12102372.

18. Gjerde, N.; Zhu, K.; Knudsen, K. D.; Nyström, B., Influence of poly(ε-caprolactone) end-groups on the temperature-induced macroscopic gelation of Pluronic in aqueous media. *European Polymer Journal* **2019**, *112*, 493–503. DOI: 10.1016/j.eurpolymj.2019.01.033.

19. Sanabria-DeLong, N.; Agrawal, S. K.; Bhatia, S. R.; Tew, G. N., Controlling hydrogel properties by crystallization of hydrophobic domains. *Macromolecules* **2006**, *39* (4), 1308–1310. DOI: 10.1021/ma052243n.

20. Yin, X.; Hewitt, D. R. O.; Zheng, B.; Quah, S. P.; Stanley, C. B.; Grubbs, R. B.; Bhatia, S. R., Effect of stereochemistry on nanoscale assembly of ABA triblock copolymers with crystallizable blocks. *Polymer* **2021**, *223*, 123683. DOI: 10.1016/j.polymer.2021.123683.

21. Bej, S.; Dhayani, A.; Vemula, P.; Ramakrishnan, S., Fine-Tuning Crystallization-Induced Gelation in Amphiphilic Double-Brush Polymers. *Langmuir* **2021**, *37* (5), 1788–1798. DOI: 10.1021/acs.langmuir.0c03111.

22. Okay, O., Semicrystalline physical hydrogels with shape-memory and self-healing properties. *Journal of Materials Chemistry B* **2019**, *7* (10), 1581–1596. DOI: 10.1039/c8tb02767f.

23. Bonafé Allende, J. C.; Schmarsow, R. N.; Matxinandiarena, E.; García Schejtman, S. D.; Coronado, E. A.; Alvarez Igarzabal, C. I.; Picchio, M. L.; Müller, A. J., Crystallization-Driven Supramolecular Gelation of Poly(vinyl alcohol) by a Small Catechol Derivative. *Macromolecules* **2022**, *55* (24), 10870–10879. DOI: 10.1021/acs.macromol.2c01364.

24. Cui, Y.; Jin, R.; Zhou, Y.; Yu, M.; Ling, Y.; Wang, L. Q., Crystallization enhanced thermal-sensitive hydrogels of PCL-PEG-PCL triblock copolymer for 3D printing. *Biomedical Materials (Bristol)* **2021**, *16* (3), 035006. DOI: 10.1088/1748-605X/abc38e.

25. Fanjul-Mosteirín, N.; Aguirresarobe, R.; Sadaba, N.; Larrañaga, A.; Marin, E.; Martin, J.; Ramos-Gomez, N.; Arno, M. C.; Sardon, H.; Dove, A. P., Crystallization-Induced Gelling as a Method to 4D Print Low-Water-Content Non-isocyanate Polyurethane Hydrogels. *Chemistry of Materials* **2021**, *33* (18), 7194–7202. DOI: 10.1021/acs.chemmater.1c00913.

26. Hernández-Sosa, A.; Ramírez-Jiménez, R. A.; Rojo, L.; Boulmedais, F.; Aguilar, M. R.; Criado-Gonzalez, M.; Hernández, R., Optimization of the Rheological Properties of Self-Assembled Tripeptide/Alginate/Cellulose Hydrogels for 3D Printing. *Polymers* **2022**, *14* (11), 2229. DOI: 10.3390/polym14112229.

27. Liu, S.; Bai, T.; Ni, K.; Chen, Y.; Zhao, J.; Ling, J.; Ye, X.; Zhang, G., Biased Lewis Pairs: A General Catalytic Approach to Ether-Ester Block Copolymers with Unlimited Ordering of Sequences. *Angewandte Chemie - International Edition* **2019**, *58* (43), 15478–15487. DOI: 10.1002/anie.201908904.

28. Zhao, J.; Pahovnik, D.; Gnanou, Y.; Hadjichristidis, N., Sequential polymerization of ethylene oxide, ε-caprolactone and l-lactide: A one-pot metal-free route to tri- and pentablock terpolymers. *Polymer Chemistry* **2014**, *5* (12), 3750–3753. DOI: 10.1039/c4py00429a.

29. Li, W.; Duan, C.; Shi, A. C., Nonclassical Spherical Packing Phases Self-Assembled from AB-Type Block Copolymers. *ACS Macro Letters* **2017**, *6* (11), 1257–1262. DOI: 10.1021/acsmacrolett.7b00756.

30. Gong, C. Y.; Shi, S.; Wu, L.; Gou, M. L.; Yin, Q. Q.; Guo, Q. F.; Dong, P. W.; Zhang, F.; Luo, F.; Zhao, X.; Wei, Y. Q.; Qian, Z. Y., Biodegradable in situ gel-forming controlled drug delivery system based on thermosensitive PCL-PEG-PCL hydrogel. Part 2: Sol-gel-sol transition and drug delivery behavior. *Acta Biomaterialia* **2009**, *5* (9), 3358–3370. DOI: 10.1016/j.actbio.2009.05.025.

31. Wang, P.; Chu, W.; Zhuo, X.; Zhang, Y.; Gou, J.; Ren, T.; He, H.; Yin, T.; Tang, X., Modified PLGA-PEG-PLGA thermosensitive hydrogels with suitable thermosensitivity and properties for use in a drug delivery system. *Journal of Materials Chemistry B* **2017**, *5* (8), 1551–1565. DOI: 10.1039/c6tb02158a.

32. Cao, J.; Lu, A.; Li, C.; Cai, M.; Chen, Y.; Li, S.; Luo, X., Effect of architecture on the micellar properties of poly (e-caprolactone) containing sulfobetaines. *Colloids and Surfaces B: Biointerfaces* **2013**, *112*, 35–41. DOI: 10.1016/j.colsurfb.2013.07.038.

33. Matxinandiarena, E.; Múgica, A.; Zubitur, M.; Zhang, B.; Ladelta, V.; Zapsas, G.; Hadjichristidis, N.; Müller, A. J., The Effect of the Cooling Rate on the Morphology and Crystallization of Triple Crystalline PE -b-PEO -b-PLLA and PE -b-PCL -b-PLLA Triblock Terpolymers. *ACS Applied Polymer Materials* **2020**, *2* (11), 4952–4963. DOI: 10.1021/acsapm.0c00826.

34. Fernández-Tena, A.; Pérez-Camargo, R. A.; Coulembier, O.; Sangroniz, L.; Aranburu, N.; Guerrica-Echevarria, G.; Liu, G.; Wang, D.; Cavallo, D.; Müller, A. J., Effect of Molecular Weight on the Crystallization and Melt Memory of Poly(ε-caprolactone) (PCL). *Macromolecules* **2023**, *56* (12), 4602–4620. DOI: 10.1021/acs.macromol.3c00234.

35. Castillo, R. V.; Müller, A. J., Crystallization and morphology of biodegradable or biostable single and double crystalline block copolymers. *Progress in Polymer Science (Oxford)* **2009**, *34* (6), 516–560. DOI: 10.1016/j.progpolymsci.2009.03.002.

36. Palacios, J. K.; Mugica, A.; Zubitur, M.; Müller, A. J., Crystallization and morphology of block copolymers and terpolymers with more than one crystallizable block. In: *Crystallization in Multiphase Polymer Systems*. (Elsevier) **2018**, 123–180. DOI: 10.1016/B978-0-12-809453-2.00006-2.

37. Palacios, J. K.; Michell, R. M.; Müller, A. J., Crystallization, morphology and self-assembly of double, triple and tetra crystalline block polymers. *Polymer Testing* **2023**, *121*, 107995. DOI: 10.1016/j.polymertesting.2023.107995.

38. Agrawal, S. K.; Sanabria-DeLong, N.; Tew, G. N.; Bhatia, S. R., Structural characterization of PLA-PEO-PLA solutions and hydrogels: Crystalline vs amorphous PLA domains. *Macromolecules* **2008**, *41* (5), 1774–1784. DOI: 10.1021/ma070634r.

39. Mihajlovic, M.; Staropoli, M.; Appavou, M. S.; Wyss, H. M.; Pyckhout-Hintzen, W.; Sijbesma, R. P., Tough Supramolecular Hydrogel Based on Strong Hydrophobic Interactions in a Multiblock Segmented Copolymer. *Macromolecules* **2017**, *50* (8), 3333–3346. DOI: 10.1021/acs.macromol.7b00319.

40. Cao, H.; Chang, X.; Mao, H.; Zhou, J.; Wu, Z. L.; Shan, G.; Bao, Y.; Pan, P., Stereocomplexed physical hydrogels with high strength and tunable crystallizability. *Soft Matter* **2017**, *13* (45), 8502–8510. DOI: 10.1039/c7sm01491k.

41. Kepola, E. J.; Loizou, E.; Patrickios, C. S.; Leontidis, E.; Voutouri, C.; Stylianopoulos, T.; Schweins, R.; Gradzielski, M.; Krumm, C.; Tiller, J. C.; Kushnir, M.; Wesdemiotis, C., Amphiphilic Polymer Conetworks Based on End-Linked "core-First" Star Block Copolymers: Structure Formation with Long-Range Order. *ACS Macro Letters* **2015**, *4* (10), 1163–1168. DOI: 10.1021/acsmacrolett.5b00608.

42. Hamley, I.; Castelletto, V., Small-Angle Scattering of Block Copolymers. In: *Soft Matter Characterization*. (Springer, Dordretch) **2007**, 1021–1081. DOI: 10.1007/978-1-4020-4465-6_20.

43. Mortensen, K.; Annaka, M., Structural Study of Four-Armed Amphiphilic Star-Block Copolymers: Pristine and End-Linked Tetronic T1307. *ACS Macro Letters* **2016**, *5* (2), 224–228. DOI: 10.1021/acsmacrolett.5b00936.

44. Noh, I.; Wang, X.; Vlierberghe, S. van, Injectable Hydrogels for 3D Bioprinting. (Royal Society of Chemistry) **2021**, 1–470. DOI: 10.1039/9781839163975.

45. Chamkouri, H., A Review of Hydrogels, Their Properties and Applications in Medicine. *American Journal of Biomedical Science & Research* **2021**, *11* (6), 485–493. DOI: 10.34297/ajbsr.2021.11.001682.

46. Abdollahiyan, P.; Oroojalian, F.; Mokhtarzadeh, A.; de la Guardia, M., Hydrogel-Based 3D Bioprinting for Bone and Cartilage Tissue Engineering. *Biotechnology Journal* **2020**, *15* (12), 2000095. DOI: 10.1002/biot.202000095.

47. Brunel, L. G.; Hull, S. M.; Heilshorn, S. C., Engineered assistive materials for 3D bioprinting: support baths and sacrificial inks. *Biofabrication* **2022**, *14* (3), 032001. DOI: 10.1088/1758-5090/ac6bbe.

48. Ren, B.; Song, K.; Sanikommu, A. R.; Chai, Y.; Longmire, M. A.; Chai, W.; Murfee, W. L.; Huang, Y., Study of sacrificial ink-assisted embedded printing for 3D perfusable channel creation for biomedical applications. *Applied Physics Reviews* **2022**, *9* (1), 011408. DOI: 10.1063/5.0068329.

49. Daguano, J. K. M. B.; Giora, F. C.; Santos, K. F.; Pereira, A. B. G. C.; Souza, M. T.; Dávila, J. L.; Rodas, A. C. D.; Santos, C.; Silva, J. V. L., Shear-thinning sacrificial ink for fabrication of Biosilicate® osteoconductive scaffolds by material extrusion 3D printing. *Materials Chemistry and Physics* **2022**, *287*, 126286. DOI: 10.1016/j.matchemphys.2022.126286.

50. Zhang, M.; Vora, A.; Han, W.; Wojtecki, R. J.; Maune, H.; Le, A. B. A.; Thompson, L. E.; McClelland, G. M.; Ribet, F.; Engler, A. C.; Nelson, A., Dual-Responsive Hydrogels for Direct-Write 3D Printing. *Macromolecules* **2015**, *48* (18), 6482–6488. DOI: 10.1021/acs.macromol.5b01550.

Chapter 7

Final Remarks, Publications, and Contributions

7.1. Final Remarks

Plastic pollution is a major worldwide concern recently highlighted by the United Nations' Sustainable Development Goals. One of the possible solutions to this issue is the design and development of novel polymeric materials that accomplish the environmental sustainability criteria, with a focus set on reducing the dependence on petroleum-based materials and eliminating plastic waste. Over the past decades, the emergence of naturally-degrading biopolyesters as potential alternatives to common plastics has paved the way to achieve zero-waste materials. Nevertheless, the relative novelty of these materials and the appearance of new biopolyesters requires a deep investigation to understand their processing, structure, and properties, which is vital to design materials with enhanced properties and bringing them to the top in plastic applications. Moreover, and to fulfill the sustainability needs and the achievement of zero-waste biopolyester-based materials, these polymers' biodegradation is a key point within these objectives.

Within this context, in this thesis, novel strategies for the assembly of semicrystalline biopolyesters, mainly poly(butylene succinate) (PBS) and poly(ε-caprolactone) (PCL), and their copolymers with crystallizable blocks in bulk and in solution were proposed with a focus not only on the structure-properties relationship of the resulting polymer materials but also on their (bio)degradation triggered through enzymes.

Final remarks corresponding to each of the Chapters are summarized below:

Chapter 2 contains a deep investigation of state of the art on biopolyesters, with a focus on research carried out on PBS. In this Chapter, a brief introduction to biopolyesters, the common materials in this thesis, was exposed. After that, the focus was set on PBS, with an extensive review of the mechanical and thermal properties and crystallinity properties of PBS-based materials, with an emphasis on PBS copolymers and composites. As packaging is one of the most employed

applications of biopolyesters, barrier properties and biodegradation of PBS were also reviewed in this Chapter.

Chapter 3 shows the investigation carried out on nanostructured films formed through multilayer assembly of semicrystalline biopolyesters. Ultrathin films (film thicknesses <25 nm) were prepared from chloroform solutions of PBS, PCL and a random copolymer PBS-*ran*-PCL through dip-coating to obtain samples with a number of layers from 3 to 13. AFM microscopy revealed that the crystalline morphology corresponded to that of the last deposited polyester: spherulitc/axialitic in PBS-ending films and dendritic in PCL-ending films. GIWAXS detected diffraction peaks corresponding to the semicrystalline structure of PCL in films for which the last deposited layer was PCL, whereas no diffraction peaks were observed for those films with PBS as the last deposited layer. The nanoscale organization was evaluated through nano-FTIR spectroscopy, evidencing a heterogeneous composition with nanodomain regions of varying PBS and PCL content. In the case of the 13-layer films, the spectra revealed the presence of almost segregated PCL nanodomains within a PBS matrix, probably due to the partial dissolution of the film during the sequential dip-coating, giving rise to a mixed solution of the three polymers (i.e., PBS, PCL and the random PBS-*ran*-PCL copolymer).

Chapter 4 presents a novel strategy for modulating the enzymatic degradation of PBS films through multilayer polysaccharide films composed of alginate and chitosan (Alg/Chi). The influence of several factors affecting the enzymatic degradation of PBS by the action of a lipase from *Pseudomonas cepacia* (*P. cepacia*) were studied. PBS films were coated through spray-assisted LbL assembly with an increasing number of Alg/Chi layers. The extent of degradation was found to be dependent on the number of the coating layers: the higher the number of Alg/Chi layers, the lower the degradation. These results suggested that the employed biobased coating constituted an effective barrier to the diffusion of the lipase, proving its effectiveness in modulating the enzymatic activity as a function of the thickness of the coating.

Chapter 5 unveils the enzymatic degradation studies of self-degradable films from PBS, PBAT and PLA. The first approach was conducted on PBS films, with the embedding of lipase from *P. cepacia* into alginate particles as enzyme-heating protecting agents, resulting in minor degradation. In a second approach, PBS, PBAT and PLA were melt-extruded in combination with *Candida antarctica* lipase B (CalB), showing enhanced degradation with the increase in CalB content, with a higher preference towards PBS, as evidenced by the degradation kinetics: PBS > PBAT > PLA. The degradation mechanism of this lipase was also studied from the degraded films: PBS seemed to be degraded through a bulk erosion mechanism (evidenced by the drastic changes in crystallinity, surface morphology, FTIR intensity, and weight loss), whereas PBAT films suggested a combined mechanism of surface erosion (due to the increase in crystallinity and morphological changes) and bulk erosion (with a reduction in M_n). The high L-isomer content in PLA films could explain the negligible degradation observed for all the tested conditions. Finally, the self-degradation studies on blends showed minor degradation as compared to the homopolymers, probably due to the high content in PLA and PBAT, and PLA's nature. The incorporation of higher amounts of PBS resulted in enhanced degradation, probably related to the faster degradation of PBS.

Chapter 6 displays the last system under investigation in this thesis, that is, polymer hydrogels formed through the self-assembly of copolymers with crystallizable blocks. The hydrogel formation from aqueous solutions of poly(ethylene oxide) (PEO) and PCL block copolymers (M_n <2000 g/mol) was evaluated as a function of chain topology: linear copolymers showed a sol-to-gel and a gel-to-sol transitions when heated to 80 ºC; whereas the 3-arm star copolymers did not form hydrogels, and the 4-arm star copolymers formed hydrogels upon cooling to 0 ºC, as evidenced by a single gel-to-sol transition. These differences were attributed mainly to the PEO/PCL ratio that increases in the following order: linear < 4-arm < 3-arm star block copolymers. The crystalline organization within the hydrogels was evaluated through DSC and SAXS/WAXS,

showing the crystallization of PCL in the hydrogels from the linear copolymers, and both PEO and PCL blocks in those from the 4-arm star copolymers, which might be related to the gel formation upon cooling from the corresponding aqueous solutions. The good mechanical properties and rapid dissolution of these latter hydrogels allowed their employment in 3D printing as sacrificial biomaterials inks.

As summary, this thesis has deepened into the comprehension of the self-assembly of different biopolyesters and their combination with natural-occurring polymers, studying the morphology and mechanical properties. The preparation of combined polyester/polysaccharide materials has opened the door towards the modulation in bio(degradation) of these biopolyesters, with many potential applications in agriculture or food industry for the preparation of biodegradable mulching films or food packaging materials. As a solution to reduce plastic wastes, biodegradable materials were further explored in this thesis with the study of the enzymatic degradation of self-degradable polyesters. The *embedded enzymatic degradation*, which consists on embedding enzymes into the biopolyester matrix, has been recently explored in the past decade. This approach has provided further information on the self-degradation of polyester blends, and widened the knowledge on the degradation mechanisms of several biopolyesters triggered by the action of lipases. As a culmination, biocompatible hydrogels from aqueous solutions of copolymers with crystallizable blocks (polyester) were prepared for 3D printing purposes as a way to obtain biomaterial inks with potential applications in biomedicine.

7.2. Publications Derived from This Thesis

1. Peñas, M. I.; Ocando, C.; Penott-Chang, E.; Safari, M.; Ezquerra, T. A.; Rebollar, E.; Nogales, A.; Hernández, R.; Müller, A. J., Nanostructural organization of thin films prepared by sequential dip-coating deposition of poly(butylene succinate), poly(ε-caprolactone) and their copolyesters (PBS-*ran*-PCL). *Polymer* **2021**, *226*, 123812. **Q1, Open Access.** DOI: 10.1016/j.polymer.2021.123812.

2. Peñas, M. I.; Pérez-Camargo, R. A.; Hernández, R.; Müller, A. J., A Review on Current Strategies for the Modulation of Thermomechanical, Barrier, and Biodegradation Properties of Poly(Butylene Succinate) (PBS) and Its Random Copolymers. *Polymers* **2022**, *14* (5), 1025. **Q1, Open Access.** DOI: 10.3390/polym14051025.

3. Peñas, M. I.; Criado-González, M.; Martínez de Ilarduya, A.; Flores, A.; Raquez, J. M.; Mincheva, R.; Müller, A. J.; Hernández, R., Tunable Enzymatic Biodegradation of Poly (Butylene Succinate): Biobased Coatings and Self-Degradable Films. *Polymer Degradation and Stability* **2023**, *211*, 110341. **Q1, Open Access.** DOI: 10.1016/j.polymdegradstab.2023.110341.

4. Centeno, E.; Peñas, M. I.; Zhang, P.; Ladelta, V.; Mercado-Rico, J.; Matxinandiarena, E.; Zubitur, M.; Múgica, A.; Hadjichristidis, N.; Müller, A. J.; Hernández, R., Influence of architecture, linear or star-shaped, on gelation properties and printability of block copolymers with crystallizable blocks. *European Polymer Journal* **2023**, *201*, 112526. **Q1, Open Access.** DOI: 10.1016/j.eurpolymj.2023.112526.

5. Peñas, M. I.; Beloqui, A.; Martínez de Ilarduya, A.; Suttiruengwong, S.; Hernández, R.; Müller, A. J., Novel insights onto enzymatic degradation mechanisms on lipase-embedded aliphatic and aromatic polyesters and their blends. *Biomacromolecules*. **To be submitted.**

7.2.1. Divulgation publications

1. Peñas, M. I.; Müller, A. J.; Hernández, R., Polibutilensuccinato: ¿un biopoliéster más en el mundo de los bioplásticos? *Revista de Plásticos Modernos* **2021**, *122*, 12–20.

7.2.2. Other related publications

1. Criado-González, M.; Peñas, M. I.; Barbault, F.; Müller, A. J.; Boulmedais, F.; Hernández, R., Salt-induced Fmoc-tripeptide Supramolecular Hydrogels: A Combined Experimental and Computational Study of the Self-assembly. *Materials Today Nano*. **Submitted.**

7.3. Contributions to National and International Conferences

1. Peñas, M. I.; Penott-Chang, E.; Müller, A. J.; Hernández, R., Preparation and characterization of multi-layer systems based on biopolyesters (polybutylene succinate and polycaprolactone). *4th Young Polymer Scientists Seminar (SEJIPOL 2019)*. 29 October 2019. Institute of Polymer Science and Technology (Madrid, Spain). **Oral presentation.**

2. Peñas, M. I.; Ocando, C.; Penott-Chang, E.; Safari, M.; Ezquerra, T. A.; Rebollar, E.; Nogales, A.; Hernández, R.; Müller, A. J., Nanostructured thin films obtained by dip-coating poly(butylene succinate), poly(ε-caprolactone) and their copolyesters (PBS-*ran*-PCL). *7th ECNP Young Scientists Conference & Short Course*. 27-28 October 2019. (Lodz, Poland). **Oral presentation (online).**

3. Peñas, M. I.; Müller, A. J.; Hernández, R., Novel materials based on the multilayer assembly of biopolyesters and their combination with polysaccharides. *5th Young Polymer Scientists Seminar (SEJIPOL 2020-21)*. 26 October 2021. Institute of Polymer Science and Technology (Madrid, Spain). **Oral presentation.**

4. Peñas, M. I.; Hernández, R.; Müller, A. J., Preparation of poly(butylene succinate)-based novel materials: layer-by-layer assembly of biopolyesters and its combination with polysaccharides. *GEP-SLAP Congress 2022*. 8-12 May 2022. Kursaal (Donostia/San Sebastián, Spain). **Oral presentation.**

5. Peñas, M. I.; Criado-González, M.; Martínez de Ilarduya, A.; Flores, A.; Raquez, J. M.; Mincheva, R.; Müller, A. J.; Hernández, R., Tunable enzymatic biodegradation of poly(butylene succinate): biobased coatings and self-degradable films. *XI Congress of Young Researchers in Polymers (JIP 2023)*. 2-5 October 2023. Hotel Port Alicante City & Beach (Alicante, Spain). **Oral presentation.**